SURFACE PROPERTIES AND FLOW BEHAVIOR OF FOAMS IN RELATION TO FLUID DISPLACEMENT IN POROUS MEDIA

By

TIEN-FENG TYRONE LING

A DISSERTATION PRESENTED TO THE GRADUATE SCHOOL
OF THE UNIVERSITY OF FLORIDA IN
PARTIAL FULFILLMENT OF THE REQUIREMENTS
FOR THE DEGREE OF DOCTOR OF PHILOSOPHY

UNIVERSITY OF FLORIDA

1987

To

my parents and my wife

ACKNOWLEDGEMENTS

I wish to express my sincere appreciation to Professor Dinesh O. Shah, thesis advisor and chairman of the supervisory committee, for his excellent guidance and continuous encouragement. I also would like to convey my deep appreciation and thanks to Professor Birdwell Finlayson for his advice and concern as well as generous support. Special thanks also go to the members of the supervisory committee, Professors J.P. O'Connell, R. Narayanan, G. Westermann-Clark, G. Lyberatos, and B.M. Moudgil for their time, advice, and interest in my research activities.

I thank my colleagues in Professor Shah's group for the many hours spent in fruitful conversation and encouragement. Thanks are gratefully extented to Charles Brown, Heike Charest, Tracy Lambert, Ronald Baxley, Shirley Kelly, and Nancy Krell for their assistance and cooperation. My gratitude also extends to Thomas M. Dunthorn, Alison Jessup, and Patricia Brown for their assistance of proof reading during the preparation of this manuscript.

Above all, I wish to express my most sincere thanks to my parents, Mr. and Mrs. Kung-Po Ling, and my wife, Ling-Jean, for their many years of love, patience, and

support without which this work could not have been accomplished. I thank, too, my son, Vincent, who has given me much joy in my life.

TABLE OF CONTENTS

LIST OF TABLES

LIST OF FIGURES

Abstract of Dissertation Presented to the Graduate School of the University of Florida in Partial Fulfillment of the Requirements for the Degree of Doctor of Philosophy

SURFACE PROPERTIES AND FLOW BEHAVIOR OF FOAMS IN RELATION TO FLUID DISPLACEMENT IN POROUS MEDIA

By

TIEN-FENG TYRONE LING

December, 1987

Chairman: Dinesh O. Shah
Major Department: Chemical Engineering Department

Surface properties such as surface tension, surface viscosity, foaminess, foam quality, apparent foam viscosity, rate of drainage, bubble size distribution, etc., were investigated and correlated with fluid displacement in porous media. The effect of chain length compatibility, i.e., similarity, on surface properties of foaming solutions and fluid displacement in porous media were also studied. The foam behavior in porous media was well correlated to the surface properties of the foaming agent. The presence of long chain alcohols in the foaming agent improved fluid displacement compared to results obtained by the foaming agent alone. However, the effect of chain length compatibility was only partially observed for the

fluid displacement experiments.

Two mathematical models for foam flow through porous media were developed which can be used to predict foam viscosity and foam behavior in porous media. To better understand the foam stability, a numerical solution of the Poisson-Boltzmann equation in two dimensional bispherical coordinates was obtained and used to calculate the potential energy of interaction between two spherical bubbles. The method is completely general because neither the simplified equation (e.g., the first few terms of an expansion of the Boltzmann equation with restrictions on potential magnitude) nor other restrictive conditions (e.g., infinite flat plate model, small surface potential, univalent-salt condition, etc.) are required. Predicted potential energies were consistent with results from other models.

The effect of polymer on foam properties was also studied. The improvement of surface activity of the surfactants was due mainly to the effect of the excluded polymer volume and electrical double layers. The change of the surface properties of the polymer containing foam was dependent on the counterbalance of the rheology of the liquid films and the water content in the liquid films.

These studies have been successfully applied to enhanced oil recovery and to characterization of biological polymers. A concept of surfactant-polymer-foam flooding is proposed, including the use of nonionic surfactants to form

alcohol-free microemulsions and the injection of foam for the mobility control in heavy oil recovery. A wash-out mechanism in porous media was applied to characterize the physical properties of intraocular biological polymers.

CHAPTER I

INTRODUCTION

Foams are aggregates of gas bubbles dispersed in a relatively small amount of liquid. Bubbles separated from each other by thin liquid films vary in size from several microns to several millimeters. Foams are both unusual and intriguing in their physical properties, and have been studied by many researchers [1-9]. There is little doubt that at least some foams behave like non-Newtonian fluids, and have apparent viscosities considerably higher than those of either the gas or liquid phase [10]. Foam properties are determined by numerous factors such as the surface tension of the liquid, surface viscosity, bubble size distribution, interbubble gas diffusion, Gibbs elasticity, drainage of liquid from lamellae, adsorption/desorption of surfactant molecules at the liquid/gas interface, rheology of the adsorbed layer, external pressure, and temperature [11-15]. For the flow of foam through a porous medium, the permeability of the porous medium, the pore size, and the surface properties of the matrix, etc., must be considered as the factors related to rheological properties of foams.

Foam has been successfully used as a fracturing fluid for several years [16]. It is a very powerful tool for fluid leakoff control [17,18]. Montman [19] reported that foam cement could be used to seal underground storage caverns, insulate wellbores, and perform remedial squeeze jobs. In the meantime, CO_2 foam has been employed in gas and oil wells, high- and low-temperature reservoirs, and deep and shallow holes even though there are some limitations. A successful field application of CO_2-foam fracturing fluids in the Arkansas-Louisiana-Texas region was reported by Warnock et al. [20].

One technique for thermal oil recovery involves the injection of steam into a reservior to reduce the oil viscosity and make the oil more mobile. Foam has been suggested as a "blocking agent" in steam injection to reduce gravity override and channeling effects (Figure 1.1). The mobility of injected steam can be controlled by the generation of foam in a porous medium and the reduction of mobility is proportionately higher in the more permeable sands. The process is highly efficient since the foam first finds its way into the largest pores, in which it tends to block further flow. The smaller pores are thus invaded next, and so on until the entire permeable section has been filled with the foam. Laboratory experiments have shown that vertical sweep efficiency is much improved by the injection of foam [21]. Despite the great potential of the foam flooding process, the mechanism of the foam/oil

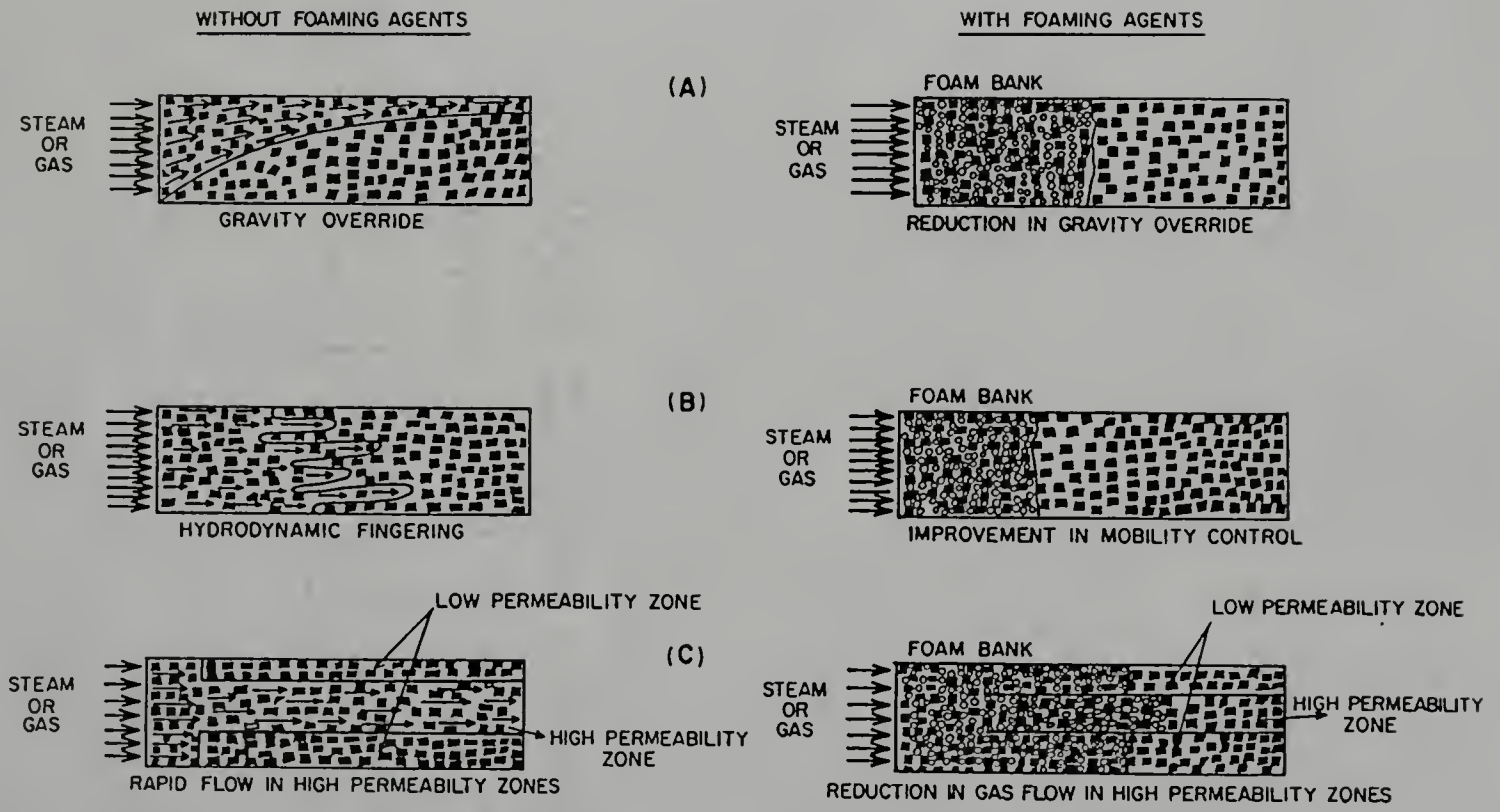

Figure 1.1. Schematic Illustration of the Effects of Foam on Transport of Steam or Gas in Porous Media.

displacement is still not fully understood. The basic principles of foam flooding have been studied for the past 25 years by many investigators [22-26]. A number of research papers have been published on foam behavior in porous media [27-31].

Sharma and coworkers [32] proposed that the molecular properties of foaming agents can influence the microscopic characteristics of the foam which in turn can affect its flow behavior in porous media and ultimately the oil recovery efficiency. However, Sharma's work gives rise to certain questions since (1) the generality of the result was questionable because only one surfactant, sodium dodecyl sulfate, with different alkyl alcohols was selected and used to study several surface properties of foaming solutions; some important foam properties such as foam quality, apparent foam viscosity, rate of drainage, etc., were not investigated, and (2) several experimental results obtained in this work were different from Sharma's. Therefore, further study of foam properties and their relationship to foam behavior in porous media was necessary for the use of foam in enhanced oil recovery. Chapters II and III present the results of laboratory studies designed to correlate the relationship between the surface properties and microscopic characteristics of foaming agents and fluid displacement in porous media. Pure (e.g., sodium dodecyl sulfate) as well as commercial surfactants (e.g., Stepanflo 40 and Suntech IVA) were selected and the

concept of chain length compatibility was applied to both systems. The foam-promoting additives (i.e., co-surfactants) used in experiments were straight, long-chain alcohols, $C_8H_{17}OH$, $C_{10}H_{21}OH$, $C_{12}H_{25}OH$, $C_{14}H_{29}OH$, and $C_{16}H_{33}OH$. The condensed notation, C_nOH (n = 8, 10, 12, 14, and 16), will be used through this work. Various surface properties such as surface tension, surface viscosity, foaminess, foam quality, apparent foam viscosity, rate of drainage, bubble size distribution, and observations of microscopic foam behavior in micromodels, were studied and are reported in these chapters. Some interesting phenomena which differed from previous studies [32-33] are discussed. The results may provide part of the answers to the following questions:

(1) Are all the surface properties of the foam consistent with the theory of chain length compatibility?

(2) Does the foam behavior in porous media correspond to the effects of chain length compatibility?

(3) Can we predict the foam behavior in porous media by only observing the surface properties of the foam outside the porous media?

(4) Is there any rule which can correlate the surface properties of the foam with the foam displacement processes?

To better understand and explain foam behavior in porous media, two mathematical models based on the Darcy's law, a modified equation of continuity, and the equation of state of the foam are developed in Chapter IV. These models

can be very important in the prediction of pressure distribution, velocity profile, and volume flow rate during foam flooding. The effects of foam viscosity, permeability of porous media, and compressibility of foam on the foam flow through porous media were studied.

Chapter V focuses on the stability of foam bubbles. The understanding of foam stability and foam breaking requires an understanding of interactions between two thin films. Two major forces, namely, the London-van der Waals force and the electrostatic repulsive force, are considered for the interactions between two films. The DLVO theory was introduced and the general Poisson-Boltzmann equation has been developed in bispherical coordinates. A general numerical solution of the Poisson-Boltzmann equation was obtained and compared with other models' results. The solution was then used to calculate the potential energy of interaction between two spherical bubbles.

It is well known [14] that the elasticity and viscosity of the foam can be improved by the addition of a proper polymer. Almost all of the cited references [34-39] deal with anionic surfactant-cationic polymer interactions in relation to the physical properties of the aqueous solutions. Little attention has been devoted to the effect of anionic surfactant-anionic polymer interactions on foam properties. In Chapter VI, the effects of adding anionic polymer on the surface properties of the foam containing an anionic surfactant were studied. Various surface properties

of mixed surfactant + polymer systems such as surface tension, foam quality, apparent foam viscosity, rate of drainage, and bubble size distribution were investigated. Interactions between similarly charged surfactant and polymer were also studied and the results support the mechanism proposed by Desai [40]. The improvement of surface activity of an anionic surfactant is due mainly to the effects of the excluded polymer volume and the electrical double layers.

The flow of fluid in porous media is encountered frequently in chemistry, biology, and engineering. It is also of interest in petroleum engineering, especially the displacement of oil with gas, water, or polymer solutions. Chapter VII gives two applications of fluid flow through porous media. One is heavy oil recovery by foam flooding, and the other is the transport mechanism of viscoelastic gels in porous media. Several methods for tertiary oil recovery such as foam flooding, polymer flooding, surfactant-polymer flooding, and surfactant-polymer-foam flooding were examined. It has been demonstrated that foam can be used as a mobility control buffer instead of using a large amount of polymer. A viscoelastic polymeric gel (Viscoat^{TM}) has been used in the intraocular surgery. To better understand the flow behavior of Viscoat in trabecular meshwork, which is a porous channel, a wash-out kinetics model is proposed. The results are compared with other viscoelastic gels (e.g., Healon^{TM}, hyaluronic acid,

etc.) and are used to explain a rise in the postoperative intraocular pressure.

Finally, Chapter VIII summarizes the results of the entire study and provides recommendations for future research in this area.

CHAPTER II

SURFACE PROPERTIES OF FOAMING AGENTS AND FOAM STABILITY

2.1 Introduction

It is essential to study the surface properties of foaming agents to understand the behavior of foam. Foam properties are determined by numerous factors such as surface tension of the solution, surface viscosity, bubble size distribution, interbubble gas diffusion, Gibbs elasticity, drainage of liquid from lamellae, adsorption/desorption of surfactant molecules at the liquid/gas interface, rheology of the adsorbed layer, external pressure, and temperature [11-15]. Several external properties exhibited by foam are foaminess, foam quality, apparent foam viscosity, foam compressibility, rate of drainage, bubble size distribution, etc. These external properties often correlate with each other and determine a foam's behavior [14,41].

The indicators of foam stability [42] are (1) time required to rupture, (2) gas diffusion rate, (3) loss of interfacial area, (4) change of bubble size distribution, and (5) drainage of interstitial liquid out of the

lamellae. The stability of a foam is directly dependent on the ability of the surfactant molecules to adsorb at the liquid/gas interface. Reduction of the surface area, and the consequent to rupture of the lamellae, requires that the adsorbed solute be returned to the bulk solution. The more strongly adsorbed the solute, the larger is the free energy contribution to the stability of the lamellae. Therefore, a slower rate of loss of interfacial area corresponds to higher foam stability. A measurement of the time required to decrease the initial foam volume by 50% is called the half-life of the foam. Since the reproducibility of this parameter is poor, this method is not employed here. The bubble size distribution and the rate of drainage are the relevant properties most readily accessible and were used in this work to study foam stability. Measurements of gas diffusion rate and loss of interfacial area require specialized equipment and hence they are not considered in this work.

Schick and Fowkes [43] showed that polar additives can lower the critical micelle concentration (CMC) of anionic surfactants and stabilize the foam. The effectiveness of the additives in reducing the CMC of sulfate- and sulfonate-type surfactants is due to the hydrogen-bonding between the additive and the surfactant molecules. Most of these additives contain hydroxyl, primary or secondary amine, carboxyl, sulfonyl groups, or combinations of these groups. They also showed that the maximum lowering of the

CMC occurs when the surfactant and the additive possess the same length of the straight hydrocarbon chain. Klevens [44] reported that an additive present in the surface film resulted in tighter packing of surfactant molecules and lower surface tension. These factors stabilize a foam by conferring high surface viscosity and low gas permeability. Moreover, an additive which can bind to surfactants in films can lead to slow-drainage or rigid interfacial films [45]. Therefore, the stability of a foam is enhanced by adding foam-promoting additives.

Although previous studies [33,46] give some evidence of the effect of chain length compatibility on foams, we raise the following questions:

(1) Do all surface properties of a foam correspond to the theory of chain length compatibility?

(2) Does foam behavior in porous media reflect the effects of the chain length compatibility on foam properties?

(3) Can we predict foam behavior in porous media by only observing the properties of the foam outside porous medium?

In this chapter the effect of chain length compatibility on the surface properties of foaming agents as well as foam stability are discussed. Furthermore, results are related later to foam behavior in a porous medium (Chapter III). Surfactants used in the experiments included sodium dodecyl sulfate (SDS) and a series of commercial surfactants, Stepanflo and Suntech IV. The polar

additives, also called co-surfactants, were alkyl alcohols, C_8OH, $C_{10}OH$, $C_{12}OH$, $C_{14}OH$, and $C_{16}OH$.

2.2 Materials and Methods

2.2.1 Materials

Several different commercial and pure surfactants were used in experiments. Stepanflo surfactants and Suntech IV were supplied by Stepan Company, Illinois, and by Sun Refining and Marketing Company, Pennsylvania, respectively. Sodium dodecyl sulfate was purchased from Research Organic Inc., Ohio. Long chain alkyl alcohols, C_nOH (n = 8, 10, 12, 14, and 16), were purchased from Sigma Chemical Company, St. Louis, Missouri. All foaming agents were used as such without further treatment. The purity of SDS and alkyl alcohols was tested using NMR and showed 99% purity. Sodium chloride was obtained from Fisher Scientific Company, New Jersey. Distilled water was used throughout experiments.

2.2.2 Methods

2.2.2.1 Surface tension

The Wilhelmy plate method [47] was used for the measurement of the static surface tension of surfactant soultions. A surfactant solution (25ml) was poured in a petri dish, and sufficient time (about two hours) was allowed for the surfactant molecules to diffuse into the

surface layer. The platinum blade was always cleaned in distilled water, then heated to a red color with a Bunsen burner before using. All measurements were carried out at room temperature and the results reported are the average values.

2.2.2.2 Surface viscosity

The surface viscosity of the surfactant solution was measured using a single knife-edge rotational viscometer [13]. Surfactant solution (20ml) was injected into the cup (diameter 5cm and depth 1cm) which was placed at the center of a turntable. About two hours were allowed for the surfactant molecules to reach equilibrium at the liquid/air interface. The bob was then slowly lowered until it was just touching the liquid surface. The angular deflections were recorded at various rotational speeds by viewing through a telescope. The rotational speeds were adjusted continuously and smoothly to the desired speed from zero to ten rpm. The equipment was enclosed in a plexiglas box and could be leveled with three adjustable screws. The surface viscosity was calculated by employing the modification of the Reiner equation [13]. Three readings were taken for each solution and the results reported are the average values. It should be noted that surface viscosity has the dimensions mass x time^{-1}, rather than mass x length^{-1} x time^{-1} as for the three dimensional or bulk viscosity, and the unit g_m/sec is usually called the surface poise.

2.2.2.3 Foaminess

A glass cylinder with 2cm diameter and 118 cm length was used for the measurement of foaminess of the foaming agents. The cylinder contained a sieve 25-50 μm in size at the bottom and had an outer jacket for water circulation to keep the temperature constant. A definite volume (50 ml) of surfactant solution was carefully injected into the cylinder along the glass wall in order to prevent the surfactant solution from foaming. The foams were produced by the injection of air at constant pressure from a compressed air cylinder. The pressure applied at the inlet of the foam generator was strictly controlled because the foaminess was very sensitive to the pressure.

Foam volumes were recorded at various time intervals. The results were reproducible within 10%. After a foam was produced an attempt was made to measure its decay. Theoretically, this would allow us to evaluate the half-life of a foam. However, it was difficult to determine the exact foam volume left in the cylinder after a certain time, the collapse often occurred in the middle of foam column, and the resulting shape was irregular. Due to the poor reproducibility of the experimental results, the half-life of foams was not studied here.

2.2.2.4 Foam quality

A home-made glass cylinder (2.7cm ID x 14.5cm L) with two slits and two valves at both ends was used for the measurement of the specific conductivity of the foam (Figure 2.1). Two electrodes were placed vertically in the two slits and were connected to a digital multimeter (model 8050A, John Fluke MFG. Co. Inc., Everett, WA.). Foam was produced in a foam generator (see Foaminess) and was pushed into the cylinder from one end while leaving the valve at the other end open. Once the foam filled up the cylinder, both valves were closed and the electrical resistance (R_f) of the foam at different time intervals was recorded. The initial time was counted as the foam was generated. During measurements, the liquid drained from the bubbles was drained out by carefully opening and closing the valve. The conductance L_f of a foam with a resistance R_f is

$$L_f = 1/R_f$$

The specific conductivity K_f of a foam is

$$L_f = K_f(A/h)$$

where A is the cross-sectional area of the cylinder and h is the distance between two electrodes.

The same technique was used for the measurement of the specific conductivity of surfactant solutions. A solution was injected directly into the cylinder using a syringe. Figure 2.1 shows the apparatus which was used for measuring foam quality as defined in section 2.3.4.

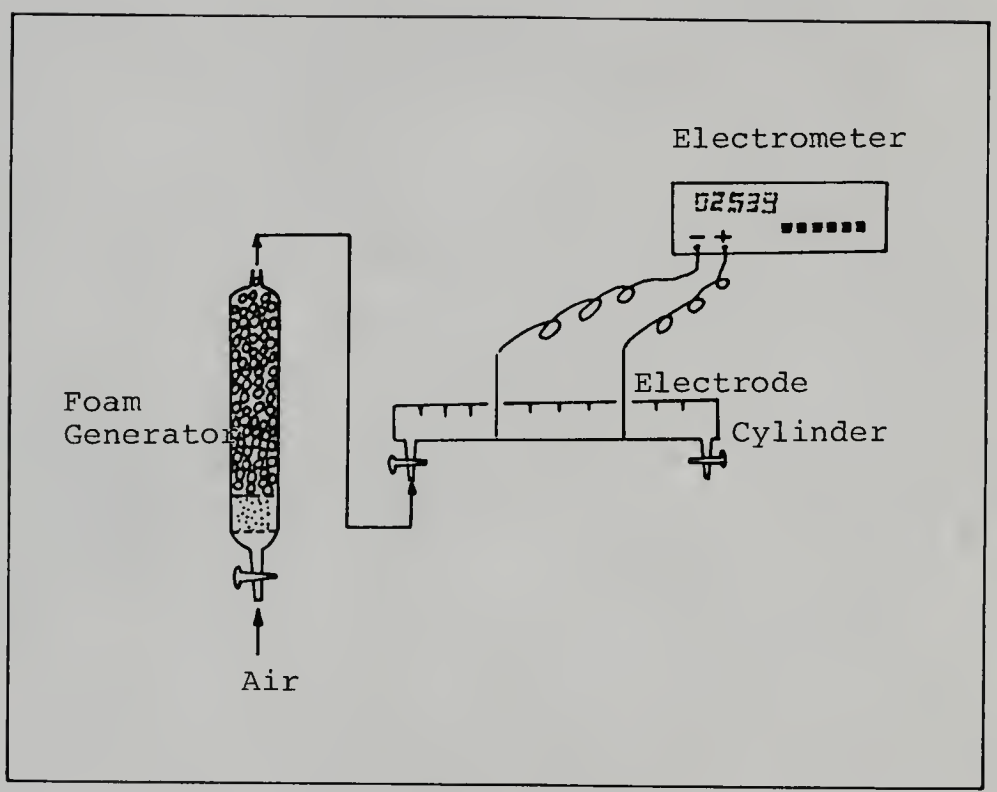

Figure 2.1. Apparatus for the Measurement of Foam Quality.

2.2.2.5 Apparent foam viscosity

The apparatus used for measuring the apparent foam viscosity is shown in Figure 2.2. The pressure drop across the capillary tube and the average volume flow rate were measured. The apparent viscosity was calculated with the Hagen-Poiseuille equation. Due to the drainage of liquid from the foam, the time elapsed for each experiment was also recorded. The initial time was counted as soon as the foam was produced. A capillary tube with 0.378 cm diameter and 125 cm length was used in the experiments. Theoretically, the smaller the diameter of the tube, the more accurate the results. In practice, foam was easy to break down (i.e., discontinuous) in a smaller diameter tube. A proper tube diameter had to be selected by trial-and-error.

2.2.2.6 Rate of drainage

A definite volume (30ml) of surfactant solution was injected into a graduated cylinder (100ml). Foam was produced by shaking the cylinder vigorously for three minutes. To keep all experiments under the same conditions, the liquid volumes were recorded at various time intervals after the liquid volume in the cylinder had reached 20ml. The initial time during which 20ml fluid accumulated was not counted. The kinetics of drainage were measured for solution collected beyond 20ml.

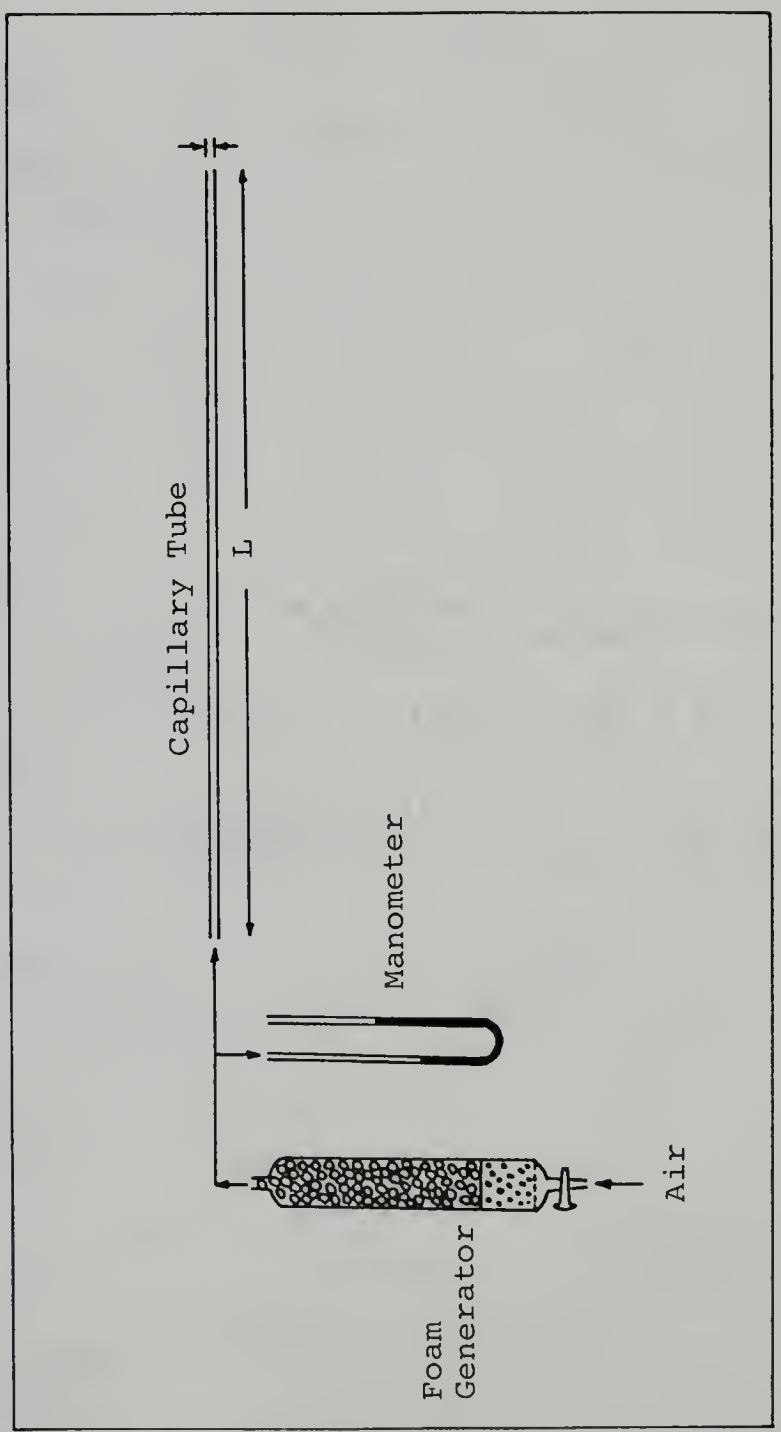

Figure 2.2. Apparatus for the Measurement of Apparent Foam Viscosity.

2.2.2.7 Bubble size distribution

A rectangular plexiglas cell (2.75"x2.75"x0.5") was used for measurements of bubble size. Ten milliliters of a surfactant solution were injected into the cell. The foam was generated by vigorously shaking the cell for three minutes. The foam was then photographed at various time intervals. The photographs were analyzed using a digital image analysis system consisting of an Image Technology model 5000 processor, an IBM personal computer, and a Sony video camera, to determine the average bubble size and bubble size distribution.

2.2.2.8 Microscopic view of foam flow in porous medium

The general foam behavior at the microscopic level was investigated using a micromodel. The experimental apparatus was designed to achieve the following major objectives:

(1) Find the mechanisms of gas flow in porous media in the presence of mixed surfactant solutions.

(2) Visually observe and study the flowing foam.

A schematic diagram of the apparatus is shown in Figure 2.3. The apparatus included a camera control unit (Sony, Model DXC-1850), video cassette recorder (Panasonic, Model NV-8950), time data generator (Panasonic, Model WJ-810), video monitor (Panasonic, Model CT-1330M), and video camera (Sony, Model DXC-1850). The micromodel had a pore neck of 50 μm and pore diameter of 100 μm. The micromodel was saturated with surfactant solution followed by air flow to

generate in-situ foam. The photographs of foam generated inside the micromodel were taken directly using the television camera attached to the microscope.

2.3 Theory

2.3.1 Surface Tension

Surface tension is a measure of the work required to increase the surface by unit area, at constant temperature, pressure, and composition [48]. It is also a measure of the attraction between molecules. In general, the surface tension decreases with increasing temperature or pressure. As the temperature is increased, the kinetic energy of liquid molecules increases, and the attractive forces between molecules are easily overcome, which in turn reduces the surface tension of the liquid. An increase in the pressure over the liquid surface will cause more gaseous molecules to come in contact with the surface. The attractions between liquid molecules and gaseous molecules neutralize part of the inward attractions of the liquid molecules. The net effect is a decrease in surface tension with increasing pressure.

At constant temperature and pressure, the surface tension of a surfactant solution decreases as the concentration of the surfactant increases until the CMC is reached. There is little effect on surface tension when the concentration is above the CMC. Therefore, the CMC of a

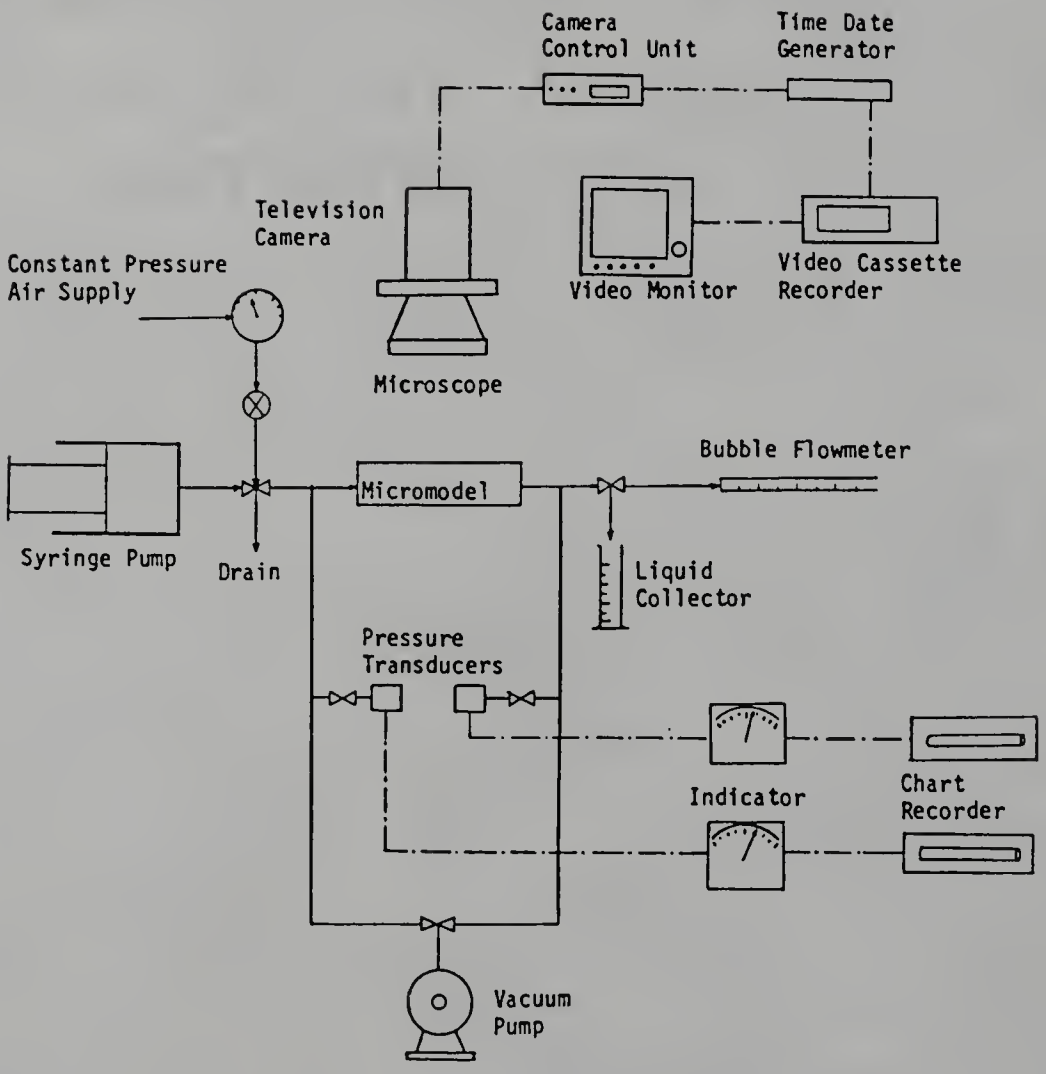

Figure 2.3. Schematic Diagram of Apparatus for Foam Flow through a Micromodel.

surfactant can be determined from the measurement of the surface tension. The CMC is an important physical property for a surfactant because it is related to many other surface properties of the surfactant.

2.3.2 Surface Viscosity

Surface viscosity is a measure of molecular interactions in monomolecular films at the interface. The study of surface viscosity is useful in connection with foam stability. Shah [49,50] has shown that the surfactant solution with high surface viscosity produces a stable film due to tight packing of the surfactant molecules. For some commercial surfactants, a similar trend was observed in the variation of surface viscosity with increasing surfactant concentration [4]. These results suggest that a high surface viscosity leads to a retardation of bulk liquid flow near the surfaces, which in turn reduces the rate of thinning of the liquid films and, consequently increases the foam stability. Surface viscosity can also damp out fluctuations that might lead to rupture of the film. Bikerman [51] pointed out that the surface viscosity may affect the foam life through its effect on foam formation if the foam is produced by the beating method.

2.3.3 Foaminess

Foaminess is a measure of the capability of a foaming agent to produce foam. The method of determination is

dynamic. If one takes a cylinder filled with surfactant solution and shakes it vigorously, then the work done on the system mainly goes into expanding the interfacial area. The work done in expanding an interface is given by γdA, where γ is the interfacial tension and dA is the increase in interfacial area. Therefore, one would expect the largest interfacial area in the system which has the minimum interfacial tension at the liquid/air interface. One might also expect that large foam volume corresponds to low interfacial tension. Actually this is not true. For instance, n-octyl alcohol does not produce much foam even though its surface tension, 27.53 dynes/cm at 20°C, is very low [52]. This implies that not only surface tension but also foam stability has to be considered for foaminess. The processes of foam generation and foam collapse, as well as their combined effects, determine the capability of a foaming agent to produce the foam. For a given foaming agent, in the pre-CMC region, foaminess generally increases with increasing surfactant concentration. The maximum foam volume is observed when the concentration is around or slightly above CMC. Further increases in surfactant concentration does not improve foaminess.

2.3.4 Foam Quality

The volumetric gas content of a foam is called foam quality and is expressed by the relationship:

foam quality = (gaseous volume)/(total foam volume)

Lemlich [3] reported that the volume fraction of liquid in the foam can be determined by measuring the specific conductivity of foam:

$$\phi_i = 3K_f/K_s \qquad (2.1)$$

where ϕ_i = the volume fraction of liquid in the foam

K_f = the specific conductivity of foam

K_s = the specific conductivity of solution.

The foam quality is equal to $1 - \phi_i$. The principle of foam conductivity is based on the view of foam as a network of interconnected films whose liquid content has the same specific conductance as the bulk solution.

Foams with a quality higher than 0.8 are termed "dry" while those with a quality lower than 0.7 are termed "wet." Raza and Marsden [53] have shown that a minimum of about 4% liquid is required to produce foams. This implies that the maximum foam quality which can be achieved is around 0.96. Any "foam" with a quality higher than 0.96 must be like a chain of bubbles separated from each other by a thin liquid film (i.e., lamella). Usually, liquid drains off very fast from wet foams; further drainage may be retarded due to the Marangoni-Gibbs effect [54]. There is an optimum range of quality in which foams exhibit uniform dispersion of the two phases and are more stable. Laboratory experiments have shown that foams may remain stable for more than a month at rest, and even longer when flowing in a low permeability porous medium ($k < 1mD$) [55]. On the other hand, the apparent viscosity of a dry foam is higher than that of a

wet foam [56]. Hence, dry foam is preferred in applications to enhanced oil recovery.

2.3.5 Apparent Foam Viscosity

It is well known that the apparent viscosity of a foam is considerably higher than that of either constituent phase. Also, foam is the only known compressible non-Newtonian fluid with both variable density and viscosity. There is almost no way to measure the foam viscosity as foam flows through a porous medium. A classical conceptual model for the fluid flow through porous media was the bundle of capillary tubes model. Therefore, an approximate method may be employed to determine the apparent foam viscosity when foam is treated as a single fluid flowing through a capillary tube. The relationship between the flow rate and pressure drop in a capillary is described by the Hagen-Poiseuille law [57]:

$$Q = (\pi R^4 \Delta P)/(8\mu L) \qquad (2.2)$$

where R = the radius of the capillary tube

ΔP = the pressure drop across the tube

Q = the average volume rate of flow

L = the length of the tube

μ = the viscosity of the fluid

The assumptions that are implied in the development of the Hagen-Poiseuille law are:

(1) the flow is laminar (Reynolds number < 2100)

(2) the density of the fluid is constant

(3) the flow is at steady state

(4) the fluid is Newtonian

(5) end effects are neglected

(6) the fluid behaves as a continuum

(7) there is no slip at the tube wall.

Based on these assumptions, it is clear that the foam flow in a capillary cannot be described by Equation (2.2). Princen [58] suggested that when the equivalent bubble radius is small compared to the capillary radius, foam exists as bulk foam instead of as a chain of bubbles. Also, if the pressure drop is small then it has little effect on the foam density. The velocity of the foam is slow at this low pressure so that it may be viewed as an incompressible, Newtonian fluid. In consequence, Equation (2.2) is appropriate for the measurement of foam viscosity in a certain low pressure range.

The liquid content of foam dominates foam density. The less liquid contained in the foam, the higher foam viscosity. On the other hand, the liquid content determines foam quality. So, the higher the foam quality, the greater the apparent foam viscosity.

2.3.6 Rate of Drainage

The rate of drainage is the rate at which liquid drains from the films of the foam bubbles. The method of determination is static. The mechanism of drainage of aqueous solutions is affected by gravity, the capillary

force [59,14], gas diffusion between adjacent bubbles of different size, and the statistical rupture of films [60]. Drainage under the influence of gravity is obvious. Drainage due to capillary forces is illustrated in Figure 2.4. It is easy to prove $P_y > P_x$ by applying the Laplace equation [54]. The mechanism of transfer of air from the smaller bubbles to the larger ones is by dissolving in, followed by diffusion through the liquid film. The rate of gas diffusion is influenced by the molecular packing of surfactant at the air/liquid interface which in turn affects the thinning of the film.

For rapid drainage, the rate of drainage may be described by the following equation [59]:

$$V = V_o\{1 - EXP[-(K_1 t+K_2)]\}$$

or $$-\ln[1 - (V/V_o)] = K_1 t + K_2$$

where V = the total volume of the liquid drained from the foam, ml

V_o = the total liquid volume in the container, ml

t = time, seconds

K_1, K_2 = the constants of the drainage process.

K_1 and K_2 are determined by curve fitting using linaer regression.

2.3.7 Bubble Size Distribution

The factors that influence the bubble size of foam are surface tension, interbubble gas diffusion, drainage due to gravity, pressure, and temperature. The rate of foam decay

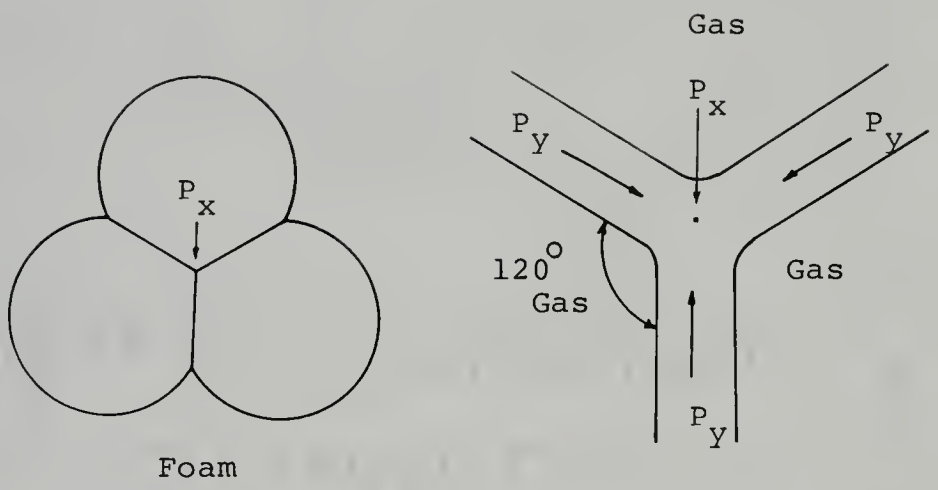

Figure 2.4. Plateau Border in a Foam.

resulting from interbubble gas diffusion and gravity drainage has been shown [60] theoretically and experimentally to be a sensitive function of the initial distribution of bubble sizes. This may explain why some foam stability tests are difficult to reproduce. The rate of gas diffusion between bubbles and the mechanism of gravity drainage can be dramatically changed by the molecular packing of surfactant at the liquid/air interface, which in turn affects the collapse of foams. The bubble size increases with elapsed time due to coalescence of bubbles and collapse of foams.

Although the experiments for bubble size distribution measurement are difficult to reproduce, the comparison of measurements of bubble size distribution are still very useful in predicting foam stability. With the aid of image analysis, the bubble size distribution and mean bubble size are especially meaningful from statistical point of view.

2.3.8 Microscopic View of Foam Flow in Micromodel

Many researchers [31,53,61-64] have studied the rheology of foam in porous media. The flow behavior of foam in a porous medium is a complex one, which cannot be correctly described in terms of the high apparent viscosity or bubble stability of the foam. There is a general agreement that foam behaves like a pseudoplastic fluid with high apparent viscosity. However, there are diverse opinons

on how foam and its components are transported through a network of pores.

Fried [65], Marsden and Khan [1], and David and Marsden [66] proposed that foam behaves as a single, homogeneous fluid: the gas and the liquid flow at the same rate. However, Raza [31] and Minssieux [27] suggested that foam cannot be described as a single fluid because the viscosity and quality of a bulk foam are quite different from those of a foam flowing through a porous medium. Foam with large and less stable bubbles is propagated inside a porous medium by the breaking and reforming of foam bubbles [26,63,65].

Micromodels permit a pore-size level study of foam flow processes. Several approaches such as capillary tubes [1,66], single layer glass bead model [67,68], and a network of etched micromodels [26,69,70] have been used for the microscopic study of foam flow. The capillary tube is the simplest micromodel which has been employed to study the rheology of foam. The single layer glass bead model and the etched network micromodel are essentialy two dimensional systems. The latter is much easier to manipulate, reproduce, and observe under a microscope. Both models can be used to study the foam drive process, fluid distributions, and mechanism of fluid displacement by foam.

In this work, the micromodel was only used as a tool for the study of microscopic foam flow in a porous medium. The observations were related to other surface properties

of the foaming agent. Details of the fabrication techniques of the micromodels can be found in literatures [67-70].

2.4 Results and Discussion

2.4.1 Surface Tension

Surface tension was measured as a function of the concentration of surfactant solutions and the results are shown in Figure 2.5 and 2.6. The surface tension of the surfactant solution decreased with the increase of surfactant concentration, and it remained constant or decreased slightly beyond the CMC. Among the surfactant solutions tested, Suntech IVA, B, and C, Suntech IVA had the lowest CMC (Figure 2.5). It seems that Suntech IVA, among the samples of Suntech IV, appears to be the most surface active agent. The surface tensions of another series of commercial surfactants, Stepanflo 20, 40, 50, 60, 70, and 80, were also measured at various concentrations (Figure 2.6). The CMCs of Stepanflo surfactants were very close. It is hard to tell which surfactant is the most surface active agent.

For the pure surfactant SDS, it was observed [32] that the surface tension was the lowest for the system consisting of SDS and dodecyl alcohol as compared to that of SDS with other long chain alcohols. Figure 2.7 shows that indeed the lowest surface tension was found when both components of the mixed surfactants had the same chain

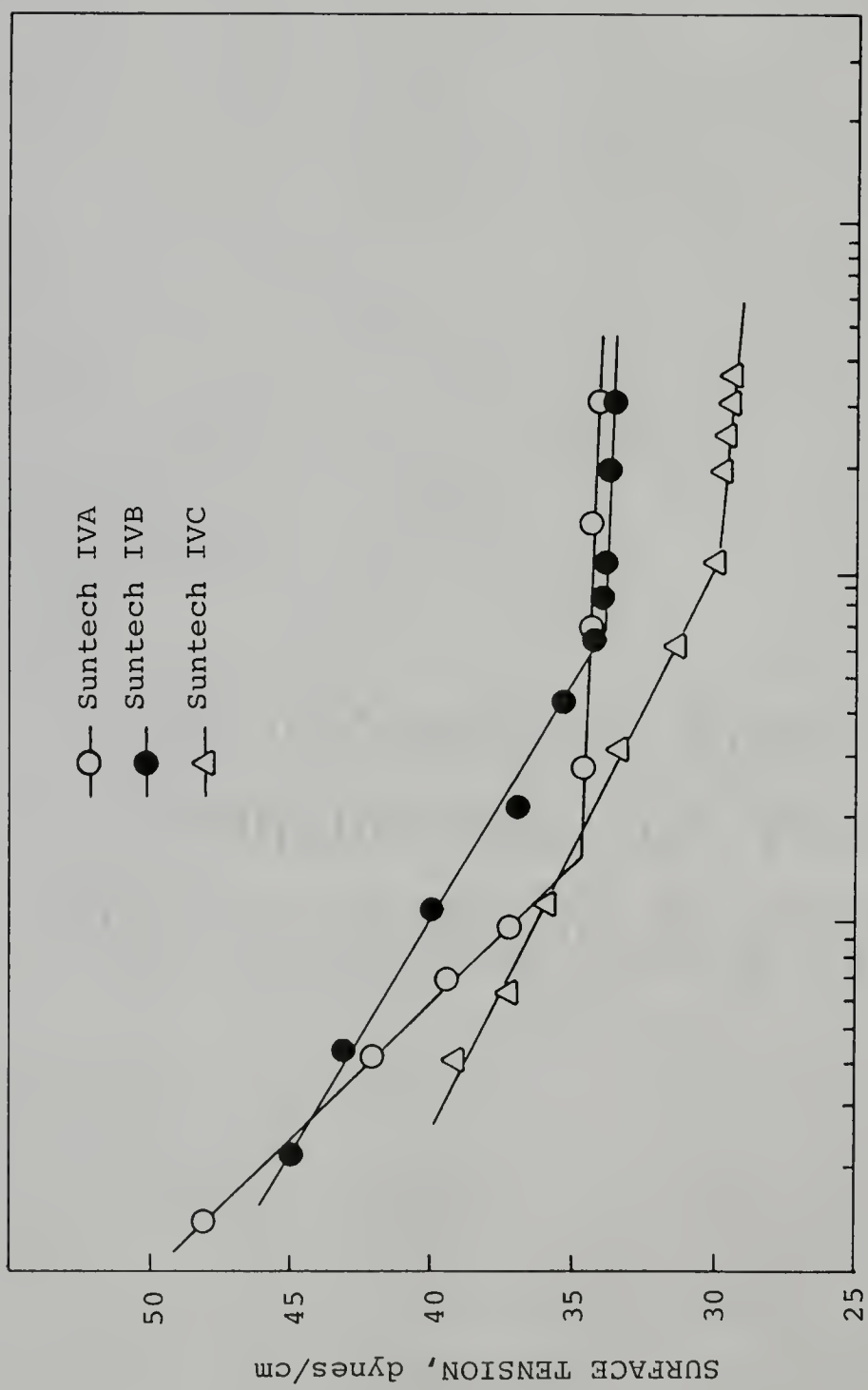

Figure 2.5. Variation in Surface Tension as a Function of the Concentration of Suntech IV Surfactants.

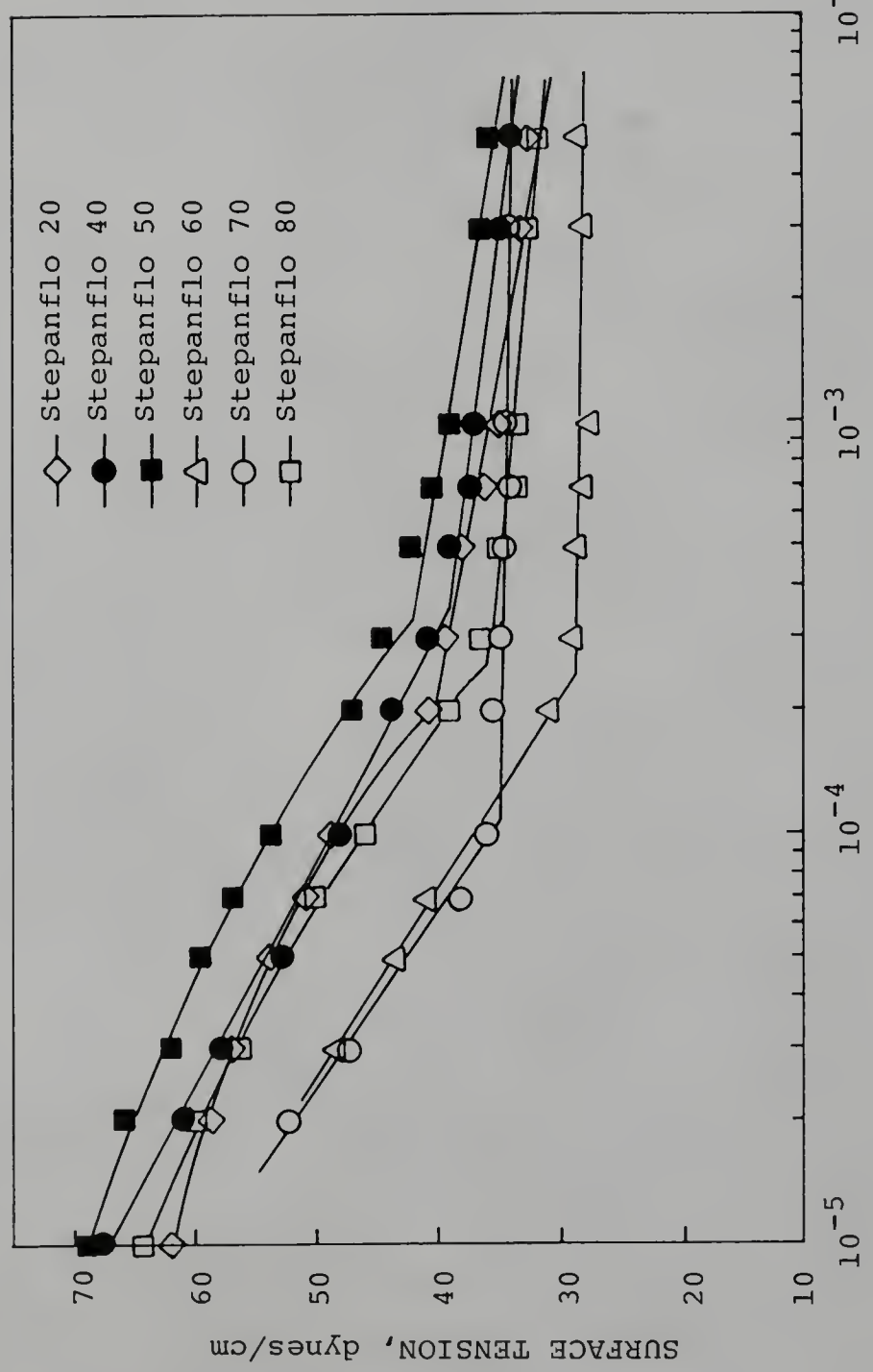

Figure 2.6. Variation in Surface Tension as a Function of the Concentration of Stepanflo Surfactants.

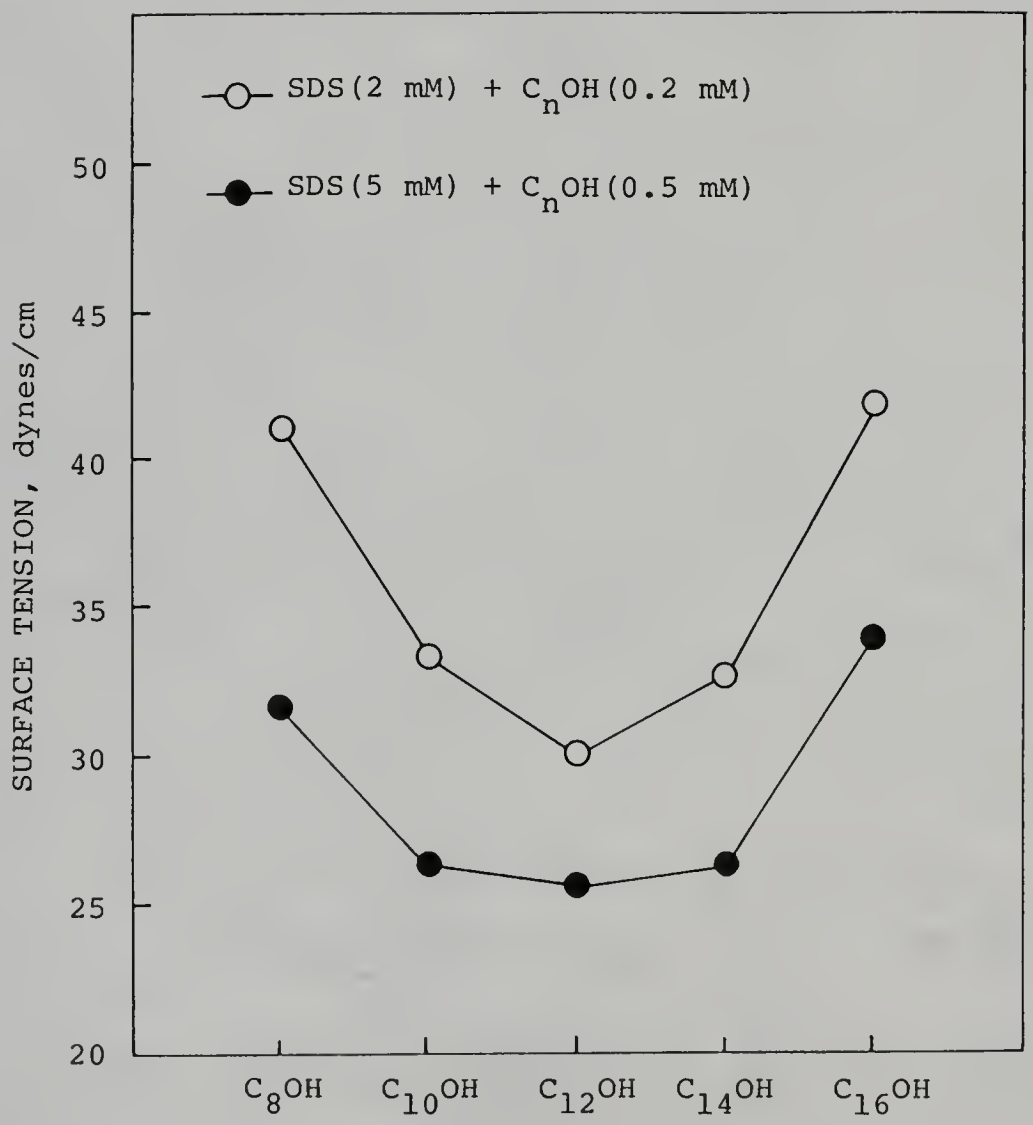

Figure 2.7. Surface Tension for Solutions of SDS and Alkyl Alcohols.

length (i.e., SDS + $C_{12}OH$). Note that at the higher concentration the surface tension was also very low for the system consisting of SDS + $C_{10}OH$ and SDS + $C_{14}OH$, respectively. The situation became complex for the mixed surfactant systems, SDS + C_nOH (n = 8, 10, 12, 14, and 16), in the presence of brine since the precipitation of mixed surfactants occurred. Sharma and Shah [33] have shown that the addition of NaCl to the mixed surfactant systems of SDS + $C_{12}OH$ results in an increase in surface tension. This increase in surface tension is presumably related to the decrease in solubility of dodecyl alcohol in the solution and the precipitation of the complex of SDS + $C_{12}OH$. The concentrations of the mixed surfactant system for the above observations were above the CMC. But for concentrations below the CMC, the surface tensions of mixed surfactant systems, SDS + C_nOH, were decreased by adding a small amount of NaCl (Figure 2.8). The main reasons were due to the salting out effect and the tight packing of surfactant molecules at the interface. Figure 2.9 shows the surface tension of mixed surfactant systems with same concentration of sodium chloride and long chain alcohols at various concentrations of SDS. Again, the lowest surface tension was found for the system consisting of SDS and dodecyl alcohol.

A commercial surfactant, Stepanflo 40, was also influenced by the addition of long chain alcohols, while, there was little effect on the surface tension of Suntech

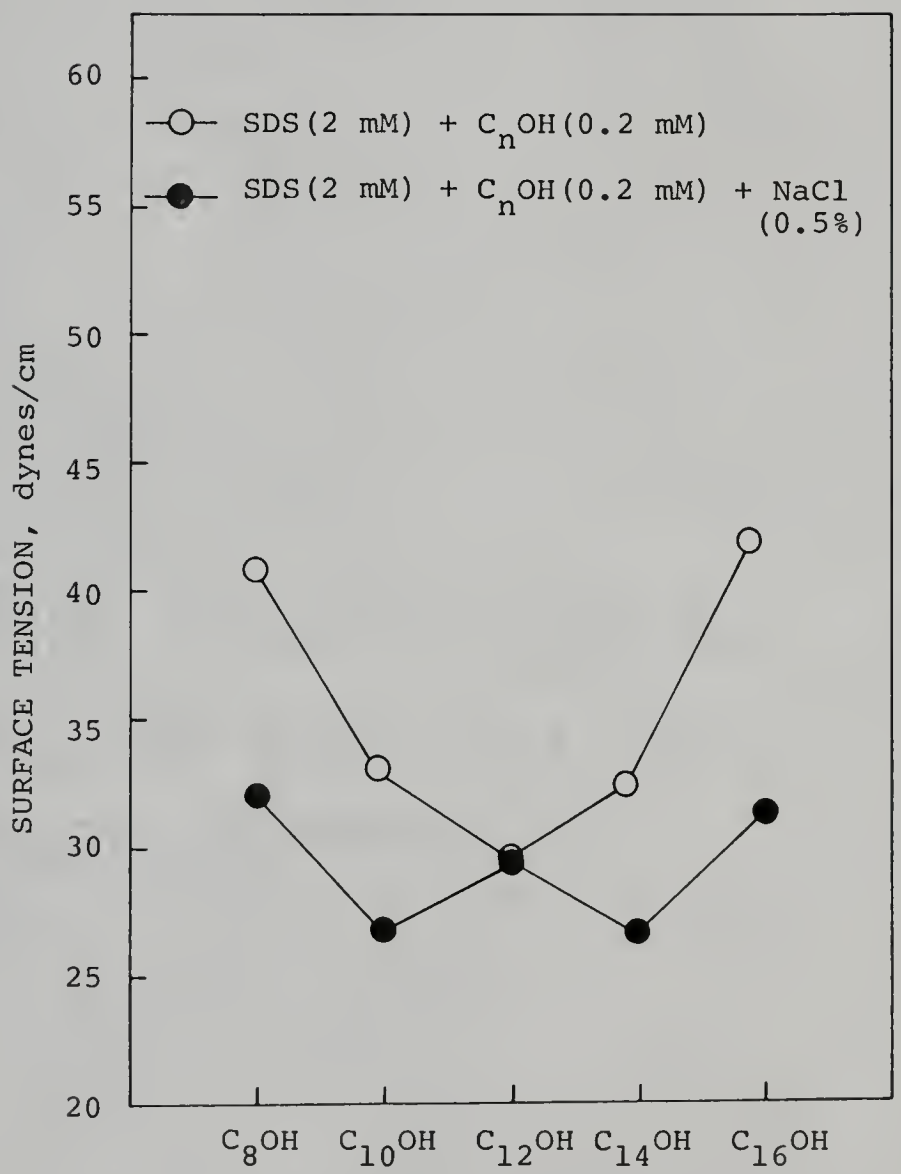

Figure 2.8. Surface Tension for Solutions of SDS + Alkyl Alcohols with and without Salt.

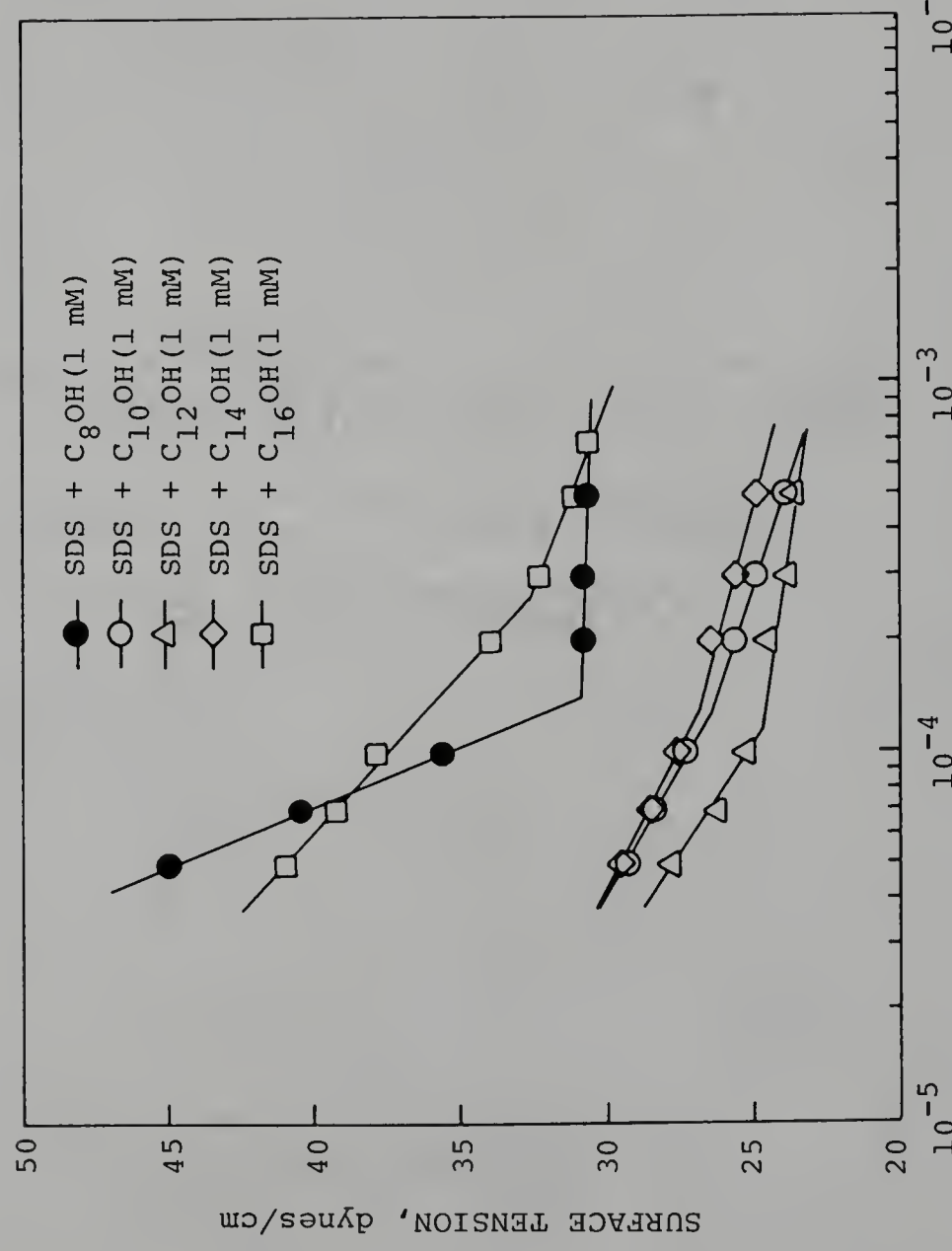

Figure 2.9. Surface Tension of Mixture of SDS + Alkyl Alcohols in 0.5% Brine as a Function of the Concentration of SDS.

IVA by adding long chain alcohols (Figure 2.10). The major components of Stepanflo 40 and Suntech IVA are C_{12} + benzene sulfonate and C_{15-17} + Toluene, respectively [71,72]. Since the number of carbon atoms in Suntech IVA molecules is from 22 to 24 and the structure of the molecules is not straight hydrocarbon chains, the addition of long chain alcohols exhibits little effect on the surface tension of mixed surfactant systems. Although the molecular structure of Stepanflo 40 is not available, the lowest surface tension was observed for the system consisting of Stepanflo 40 and dodecyl alcohol. This implies that there exists an interaction between Stepanflo 40 and alkyl alcohols. If the effect of electrolytes is considered, the situation becomes much more complicated. Generally speaking, the surface tensions of mixed surfactant systems, Stepanflo 40 + C_nOH, were significantly decreased by adding NaCl, whereas little effect on the surface tensions of Suntech IV + C_nOH was observed.

2.4.2 Surface Viscosity

A slight increase in surface viscosity was observed with increasing surfactant (i.e., Suntech IVA, B, and C) concentration, whereas beyond the CMC, the surface viscosity remained constant (Figure 2.11). It has been observed [32] that the surface viscosity is the highest when both components have the same chain length (i.e., SDS + $C_{12}OH$). Shah and co-workers [73,74] have shown that the

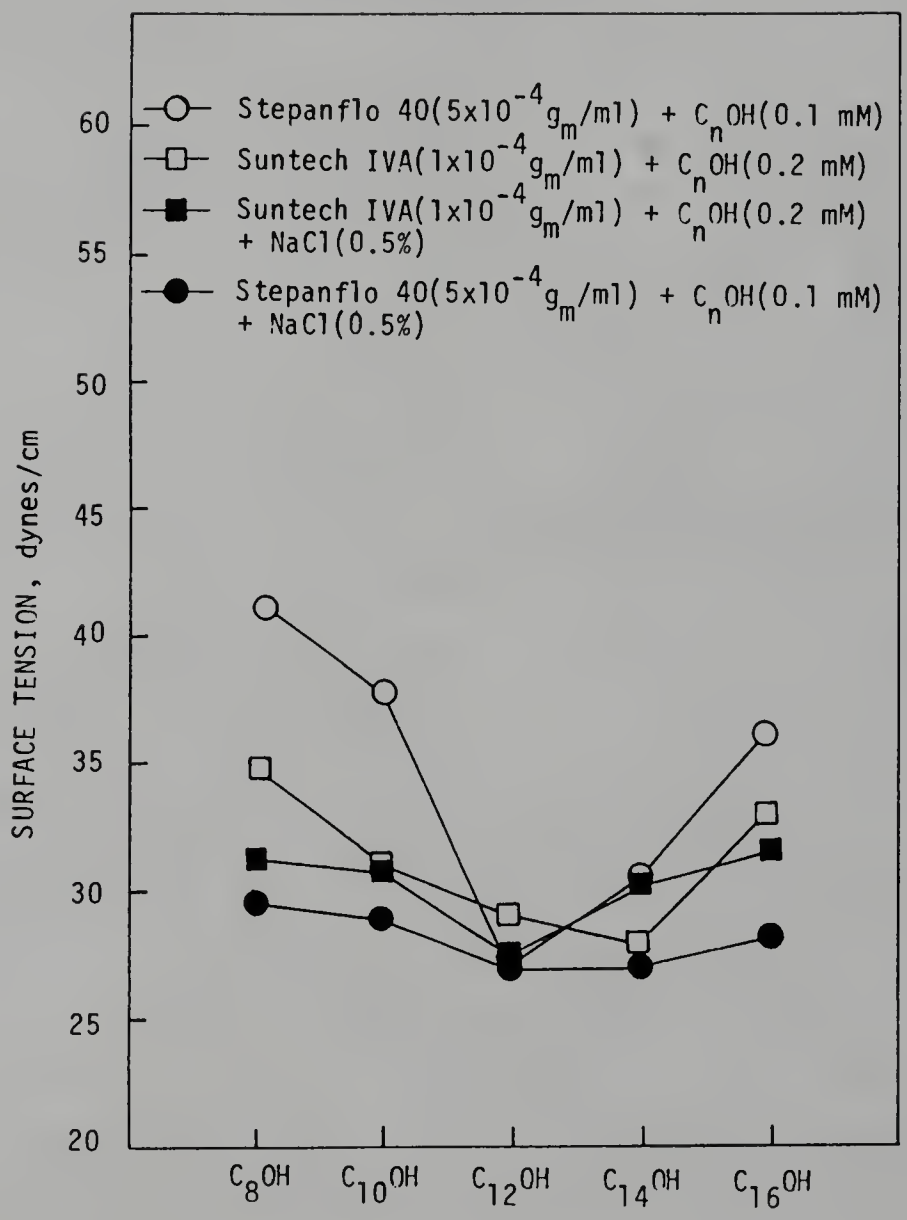

Figure 2.10. Effect of Surfactants with Different Alkyl Alcohols on Surface Tension.

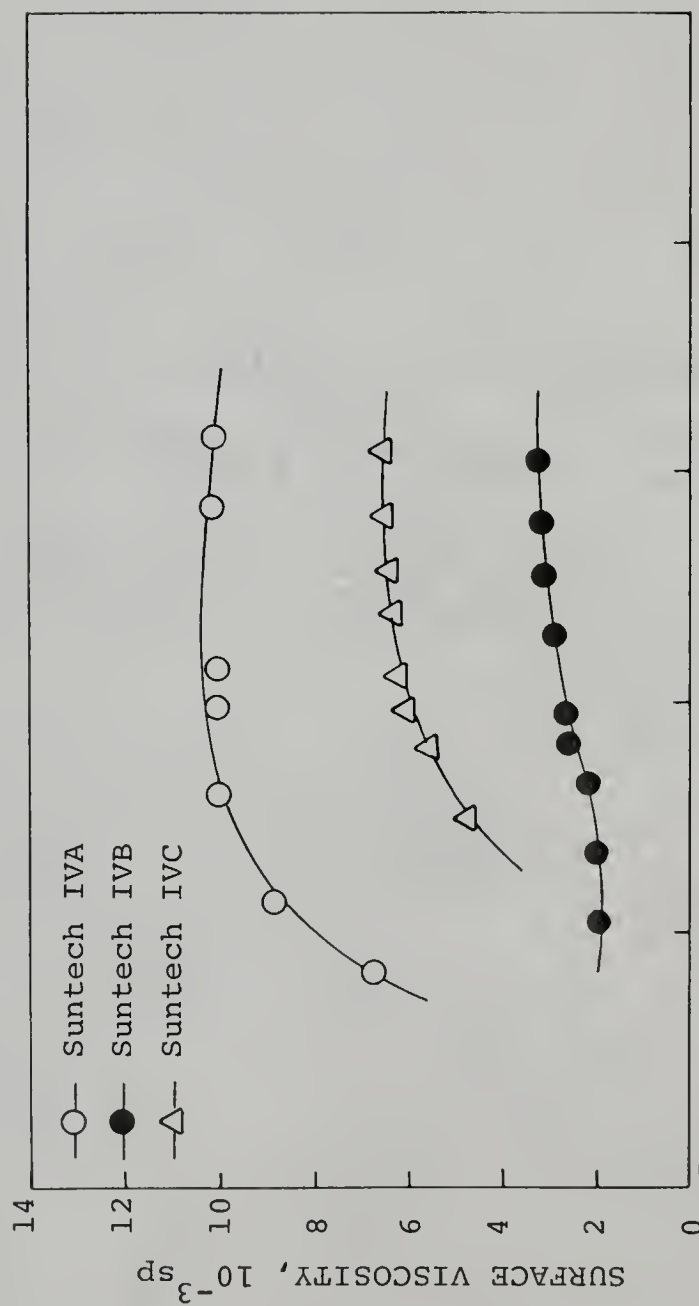

Figure 2.11. Variation in Surface Viscosity as a Function of the Concentration of Suntech IV Surfactants.

increase in foam stability of decanoic acid solutions in the presence of decanol is due to the increase in surface viscosity caused by the alcohol. These results suggest that the surfactant molecules that have similar chain length are more tightly packed at the interface as compared to molecules with dissimilar chain lengths.

2.4.3 Foaminess

Figure 2.12 shows foaminess as a function of the concentration of Suntech IVA, B, and C. As the concentration of surfactants increased, foaminess increased. Beyond a certain concentration, foaminess remained constant for all of these surfactants. However, solutions of Suntech IVA and B can produce more foam as compared to that of Suntech IVC. Usually, the lower the CMC, the more efficient the foaminess of surfactants. But this relationship is not always true. For instance, Suntech IVA had a lower CMC than that of Suntech IVB, but both surfactants possessed almost same ability to produce foam under a given condition as shown in Figure 2.12. For a series of surfactants, Stepanflo 20, 30, 40, 50, 60, 70, and 80, the highest volume of foam was found for Stepanflo 40 (Figure 2.13). Therefore, Stepanflo 40 was chosen for further study of the effect of chain length compatibility.

Figure 2.14 indicates that the highest volume of foam was found for the mixed surfactant systems of SDS + $C_{12}OH$ and Stepanflo 40 + $C_{12}OH$, respectively. There was little

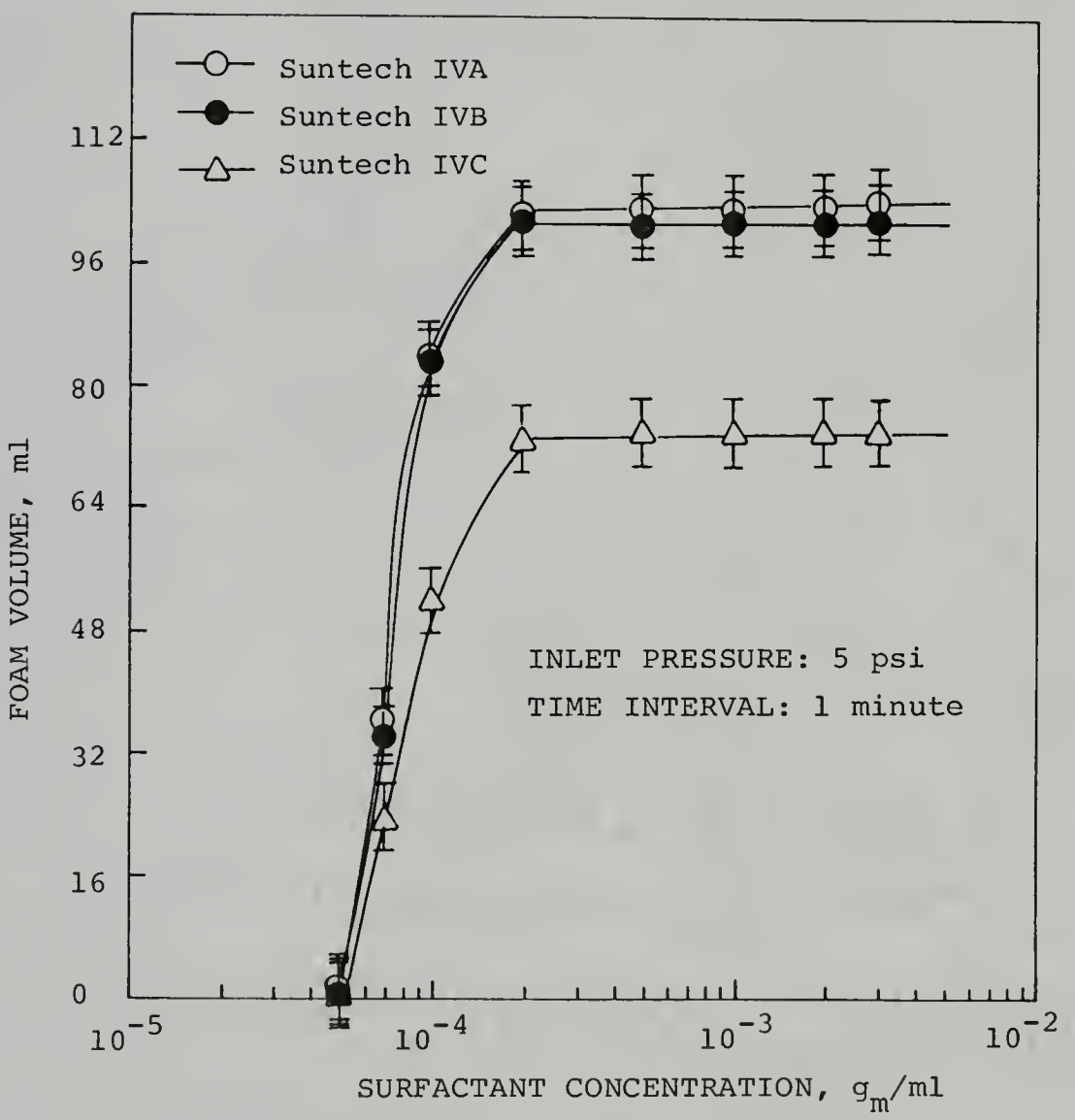

Figure 2.12. Effect of the Concentration of Suntech IV Surfactants on Foaminess.

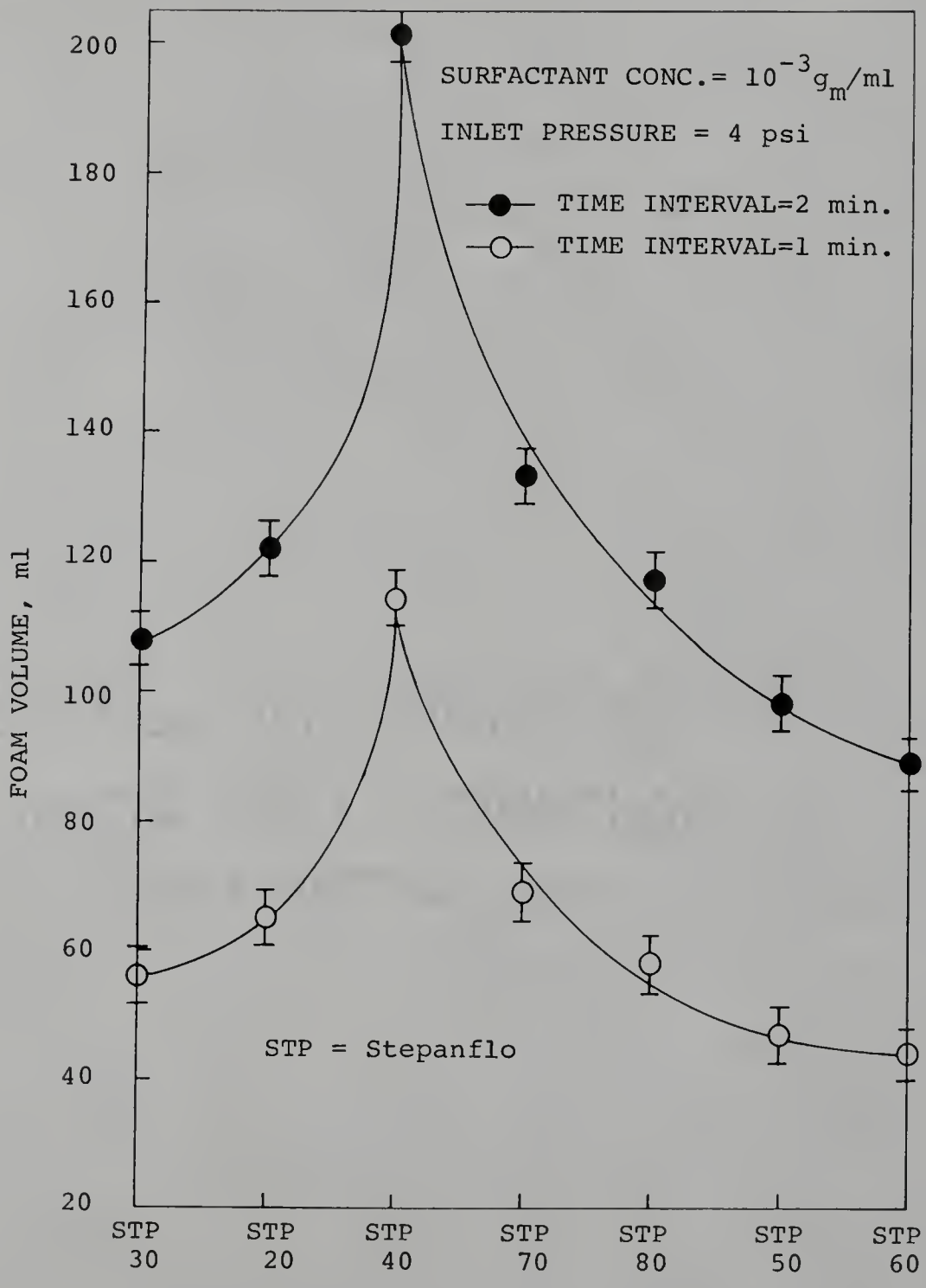

Figure 2.13. Variation in Foaminess for Stepanflo Surfactants.

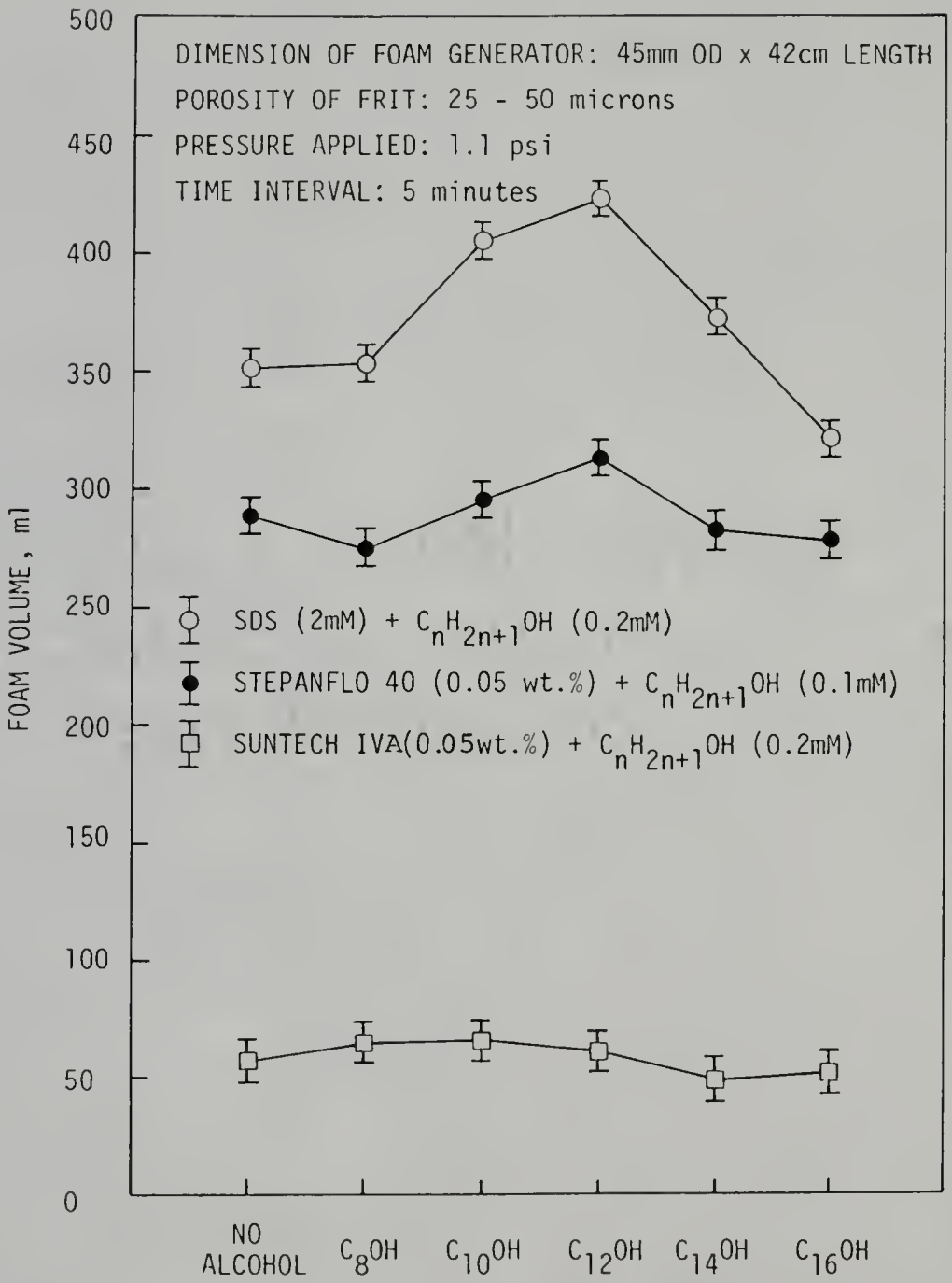

Figure 2.14. Effect of Surfactants with Different Alkyl Alcohols on Foaminess.

influence on the foaminess by the addition of long chain alcohols to Suntech IVA. It is noted that foaminess of SDS + $C_{10}OH$ was quite similar to SDS + $C_{12}OH$. It is hard to say whether SDS + $C_{12}OH$ or SDS + $C_{10}OH$ produced the maximum foam volume, since the experimental results were very sensitive to the pressure applied and the experimental error was about 10%. Similarly, foam volumes were almost the same for Stepanflo 40 + $C_{12}OH$ and Stepanflo 40 + $C_{10}OH$.

Foaminess of both pure and commercial surfactants increased with the increase of temperature [33]. At room temperature, a decrease in foaminess was observed for the mixed surfactant systems with the addition of NaCl, presumably due to the precipitation of mixed surfactants or the decrease of solubilization of alkyl alcohols in the solution. On the other hand, the effectiveness of brine in reducing foaminess decreased at higher temperature [75]. Since so many factors affect foaminess, there is still no clear relationship found between foaminess and surface properties of foaming agents.

2.4.4 Foam Quality

The foam quality of a series of Stepanflo surfactants at different time intervals (5 min., 10 min., and 20 min.) is shown in Figure 2.15. Foam quality varied with time because the static foam collapsed gradually and the liquid drained from the thin liquid films. It is clear that Stepanflo 40 had the lowest foam quality of all Stepanflo

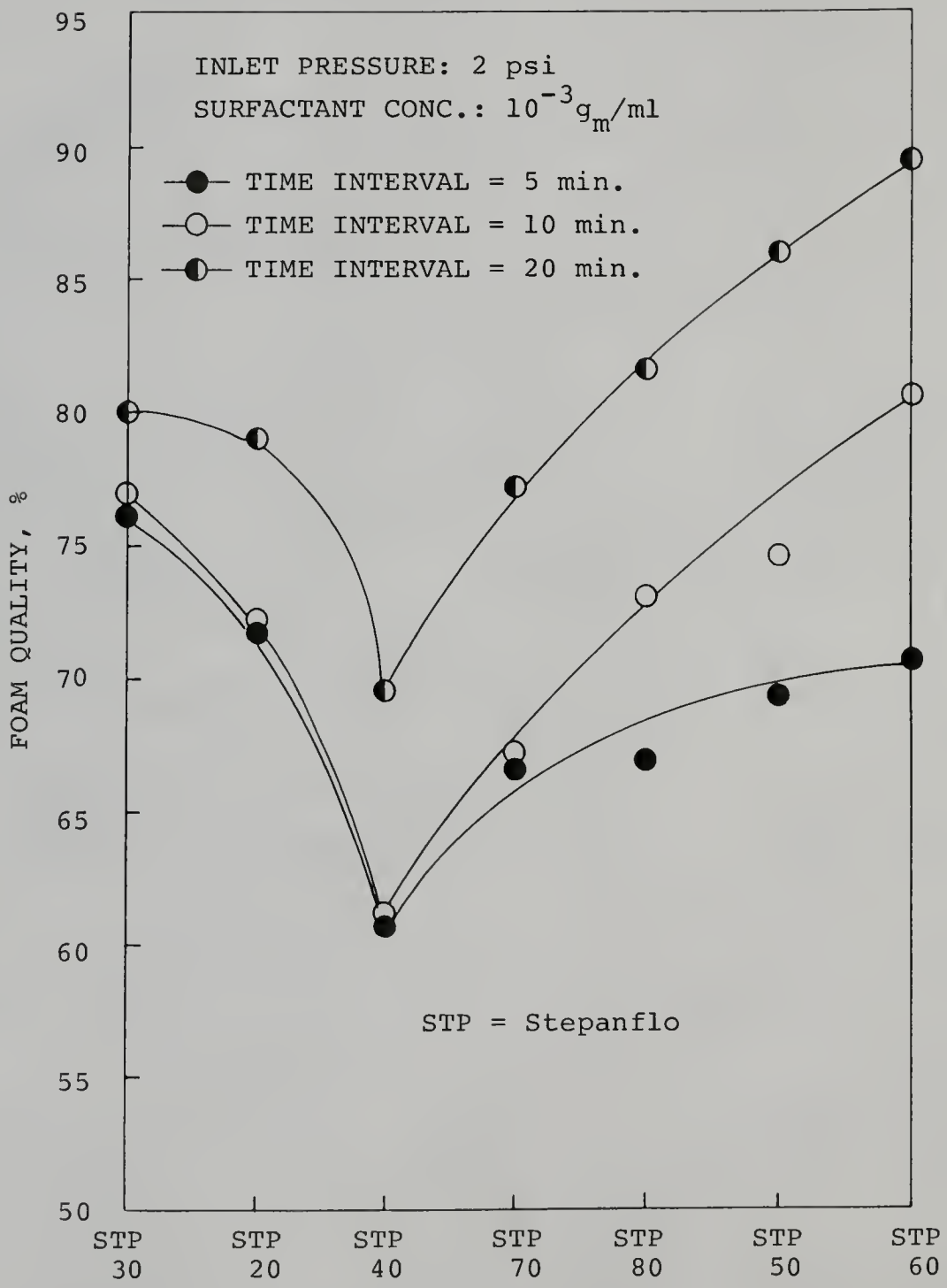

Figure 2.15. Variation in Foam Quality for Stepanflo Surfactants.

surfactants. Most of these surfactants at concentration of 0.1% g_m/ml produced "wet" foams. Figure 2.16 shows the foam quality as a function of the concentration of Stepanflo 40. The foam quality decreases with increase in concentration in the pre-CMC range. Beyond CMC, the foam quality remained constant or slightly decreased. Hence, the measurement of foam quality is one of many methods to determine the CMC of a foaming agent.

The foam quality of mixed surfactants as a function of alkyl chain length at different time intervals (5 min., 10 min., and 20 min.) is shown in Figure 2.17 and 2.18 [76]. Foams produced by these mixed surfactants were considerably "dry." For the system of SDS + C_nOH, foam quality decreased with the increase of chain length of alcohols from C_8 to C_{10}, then it increased as chain length increased further. For the mixture of Stepanflo 40 with different long chain alcohols, foam quality also decreased as hydrocarbon chain length of alcohols increased from C_8 to C_{10}. There was almost the same effect on foam quality by adding decyl or dodecyl alcohol in Stepanflo 40 solution. Interestingly, the foam generated by adding hexadecyl alcohol was even "dryer" than that without adding any alcohol. This may be due to the effect of hydrophobicity of hexadecyl alcohol.

2.4.5 Apparent Foam Viscosity

Figure 2.19 shows the apparent foam viscosity of various Stepanflo surfactants at intervals of five and ten

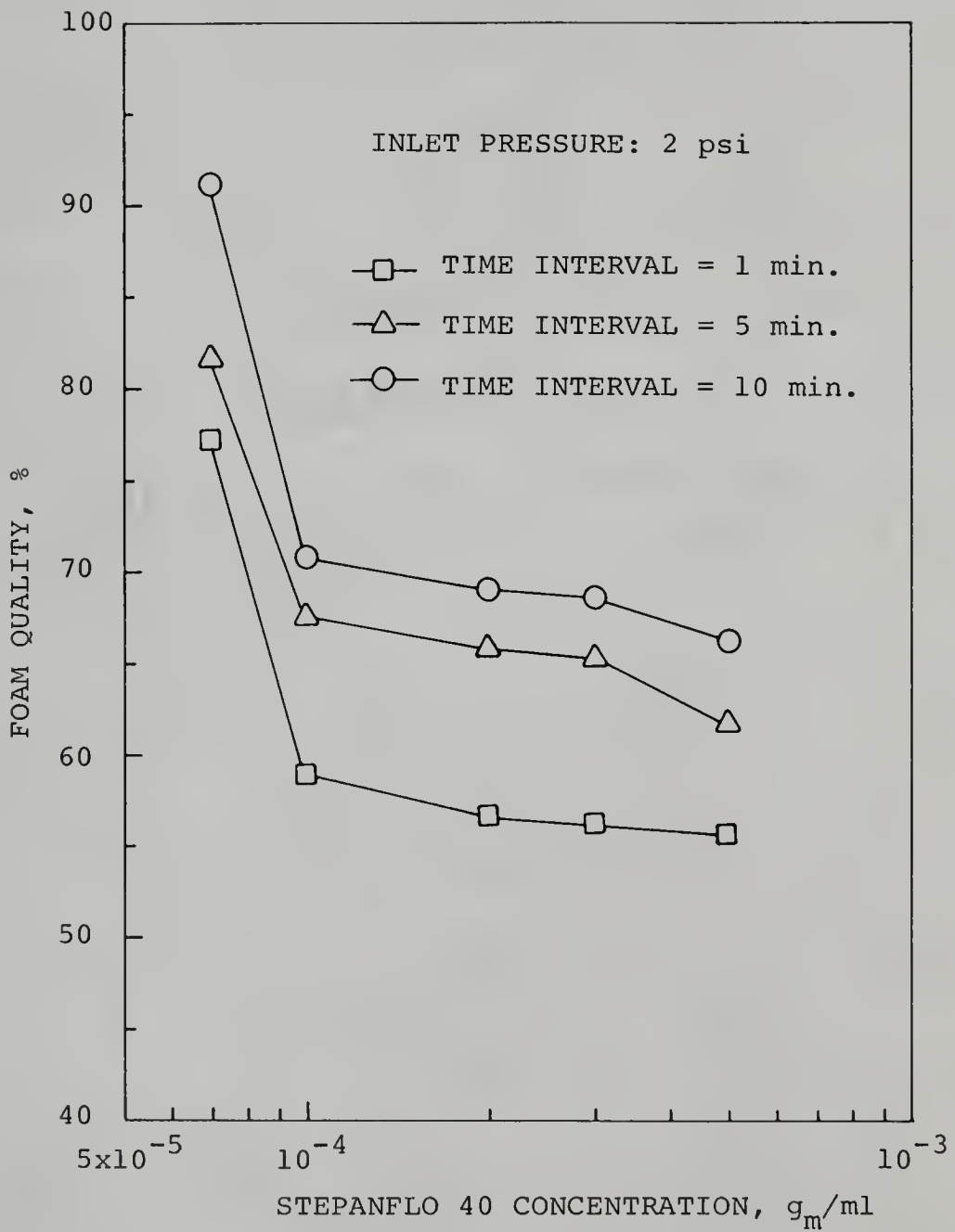

Figure 2.16. Variation in Foam Quality as a Function of the Concentration of Stepanflo 40.

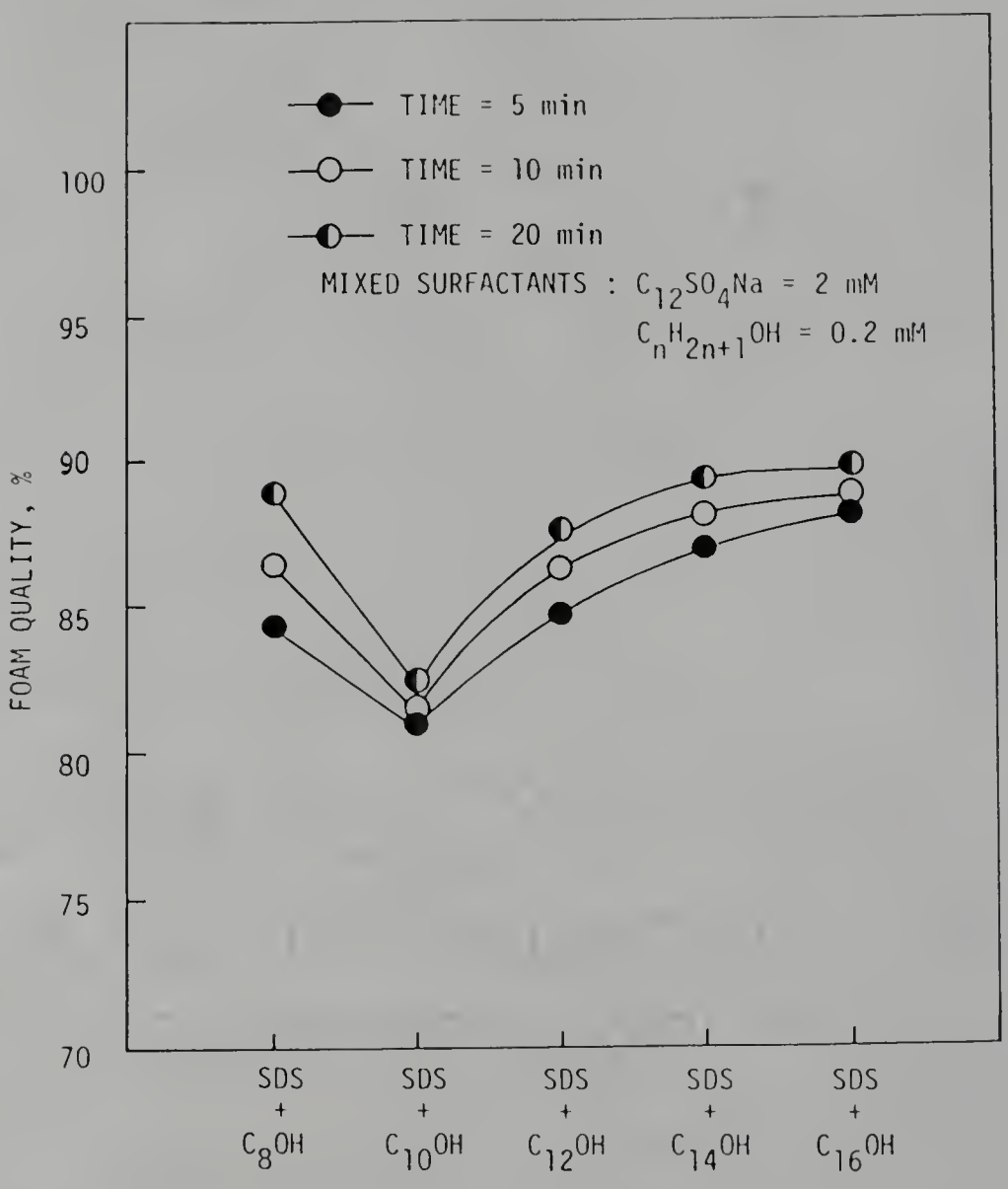

Figure 2.17. Variation in Foam Quality as a Function of SDS with Different Alkyl Alcohols.

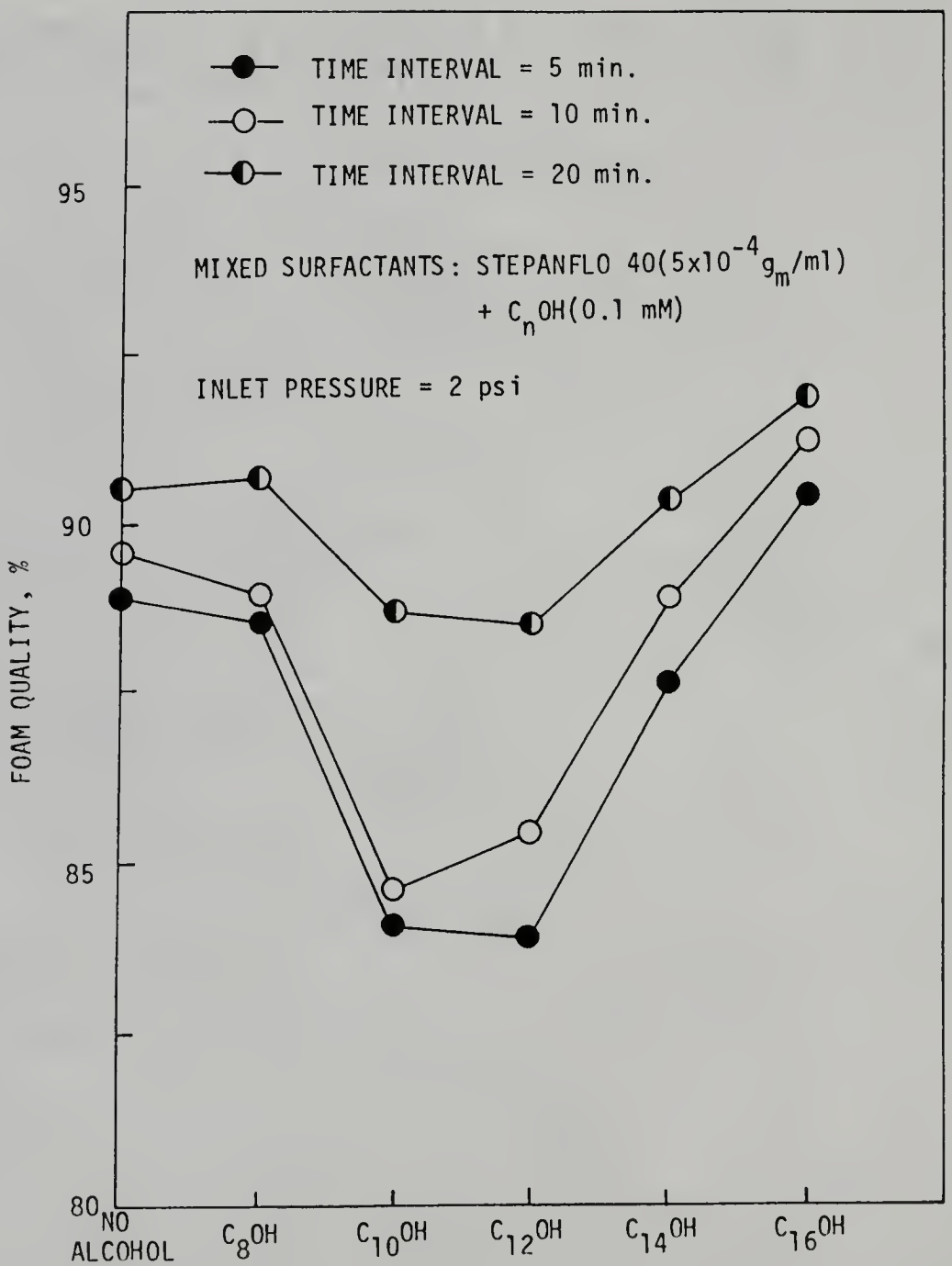

Figure 2.18. Variation in Foam Quality as a Function of Stepanflo 40 with Different Alkyl Alcohols.

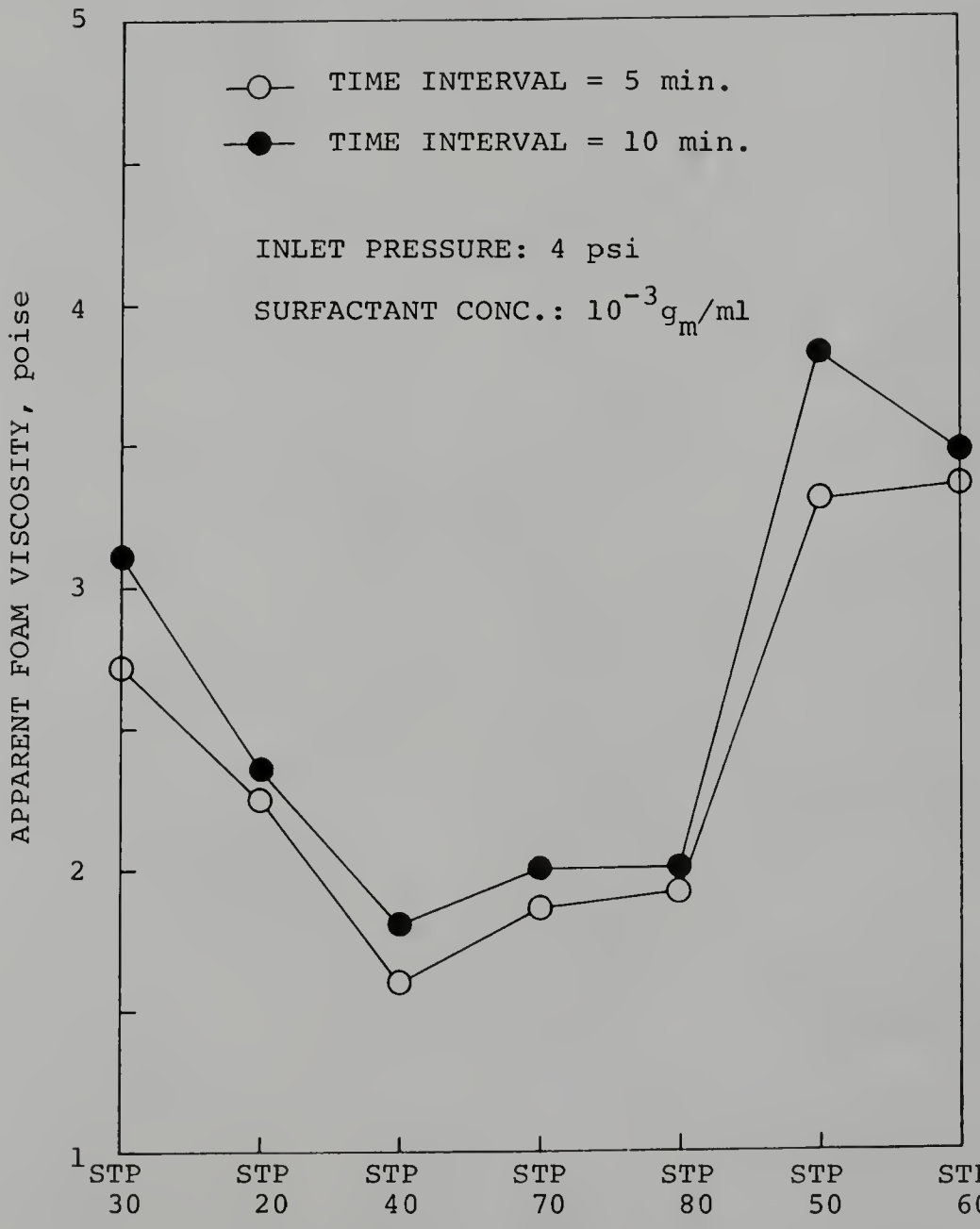

Figure 2.19. Variation in Apparent Foam Viscosity for Stepanflo Surfactants.

minutes. The lowest apparent viscosity was found for the surfactant Stepanflo 40. The combination of high foaminess, low apparent viscosity and foam quality in Stepanflo 40 produces the most uniform, stable foam of all Stepanflo surfactants. The effects of adding different chain alcohols to SDS and Stepanflo 40 solutions are illustrated in Figures 2.20 and 2.21, respectively. Among the SDS systems, the lowest apparent viscosity was observed for SDS + $C_{10}OH$, although a smiliar value was found for the SDS + $C_{12}OH$ system. A similar minimum was observed with Stepanflo 40 + $C_{10}OH$ and Stepanflo 40 + $C_{12}OH$.

The apparent foam viscosity depends on: (1) slugs of liquid between bubbles, (2) the resistance to deformation (i.e., elasticity) of the interfaces of foam bubbles passing through a capillary, and (3) the surface tension gradient that occurs when surfactant molecules are swept from the front of a bubble to the back of it. Hirasaki and Lawson [77] have shown that the transition from bulk foam to individual lamellae is a function of r_B/R_p, where r_B and R_p are the equivalent radius of the bubbles and the capillary radius, respectively. Foam exists as bulk foam when $r_B/R_p < 1.0$. They suggested that the apparent viscosity of the bulk foam, where the surface tension gradient effect is insignificant, does not change as long as the r_B/R_p ratio is kept constant. Since the radius of the capillary used in experiments is 0.378 cm and the bubbles are of the order of several microns in diameters,

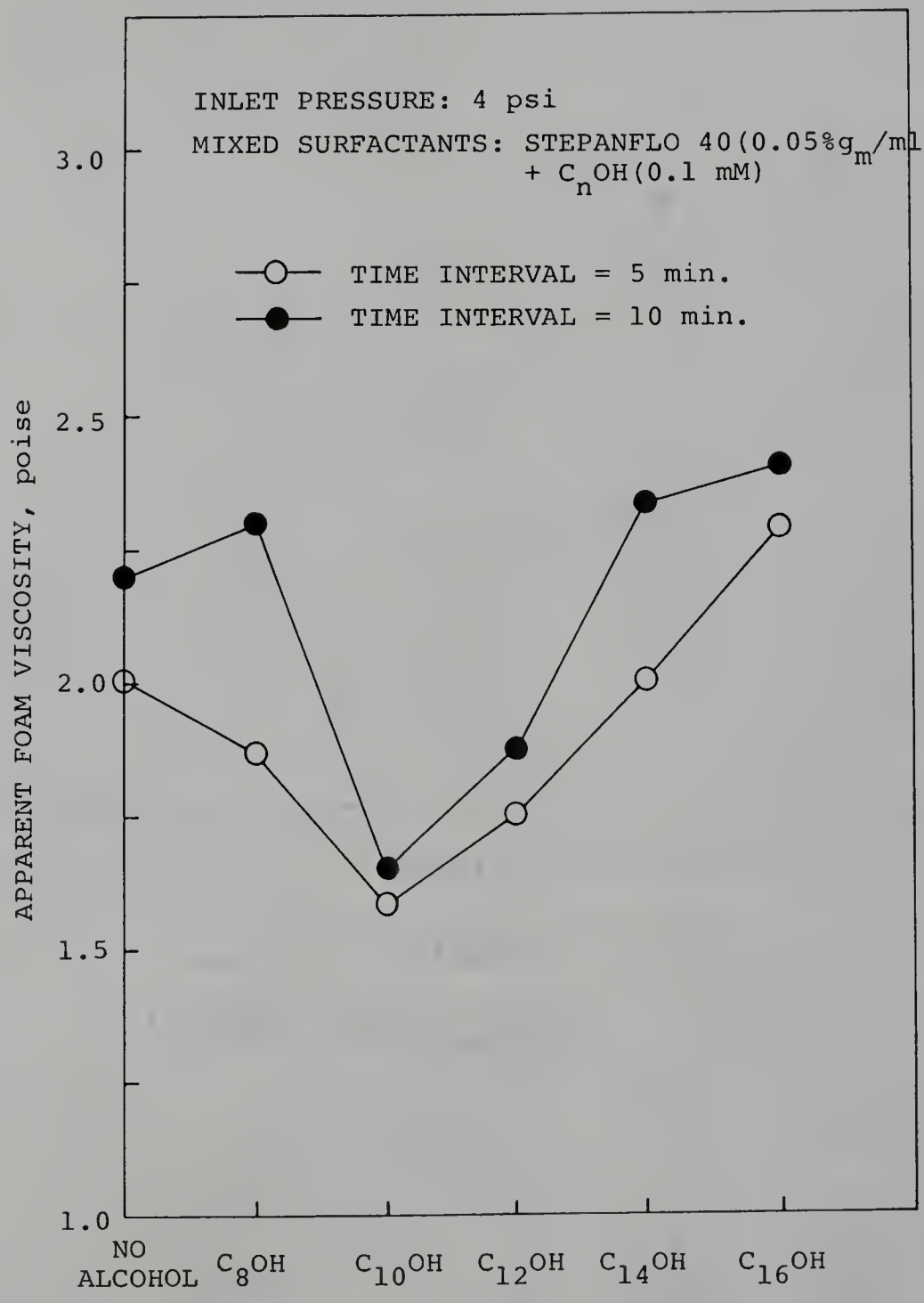

Figure 2.20. Apparent Foam Viscosity for Mixed Foaming Agents of Stepanflo 40 and Alkyl Alcohols.

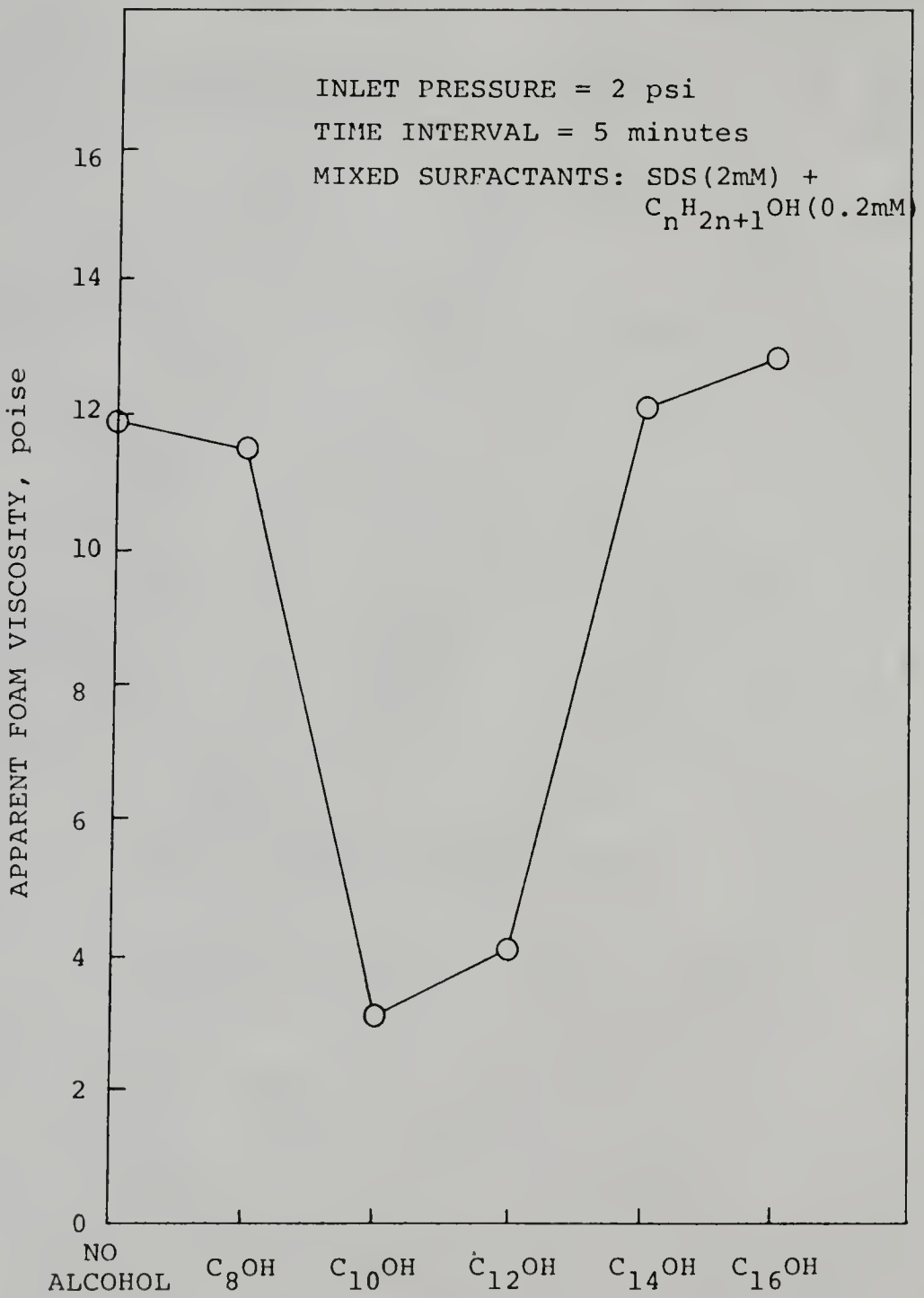

Figure 2.21. Apparent Foam Viscosity for Mixed Foaming Agents of SDS and Alkyl Alcohols.

r_B/R_p << 1.0 and the surface tension gradient effect is negligible. Therefore, the low apparent foam viscosity is expected resulting from the high liquid containing bubbles and from the low elasticity of the films. These two factors account for the low apparent foam viscosity. SDS and $C_{12}OH$ molecules are tightly packed at the interface due to chain length compatibility, which produces a more elastic film than that of SDS with $C_{10}OH$. Moreover, dodecyl alcohol is more hydrophobic than decyl alcohol. The latter can bring more water into bubble films and these water molecules can be retained by the moderate elasticity films. That is the reason why the lowest foam quality and apparent viscosity was found for the system of SDS + $C_{10}OH$.

If foam quality and apparent foam viscosity were measured in separate experiments at a series of times under the same conditions, then a plot of apparent foam viscosity vs. foam quality can be obtained as shown in Figure 2.22. It is clear that the higher the foam quality, the higher the apparent viscosity. The primary effect of the quality is to change the radius of curvature of the bubbles. When the ratio of r_B/R_p is greater than one, the foam exists more like a bubble chain where each pair of bubbles is separated by an individual lamella. This effect is much more important at high foam qualities. The surface tension gradient effect can not be ignored and tends to increase the apparent viscosity. The effects of foam quality on the apparent viscosity are mainly due to the number of bubbles

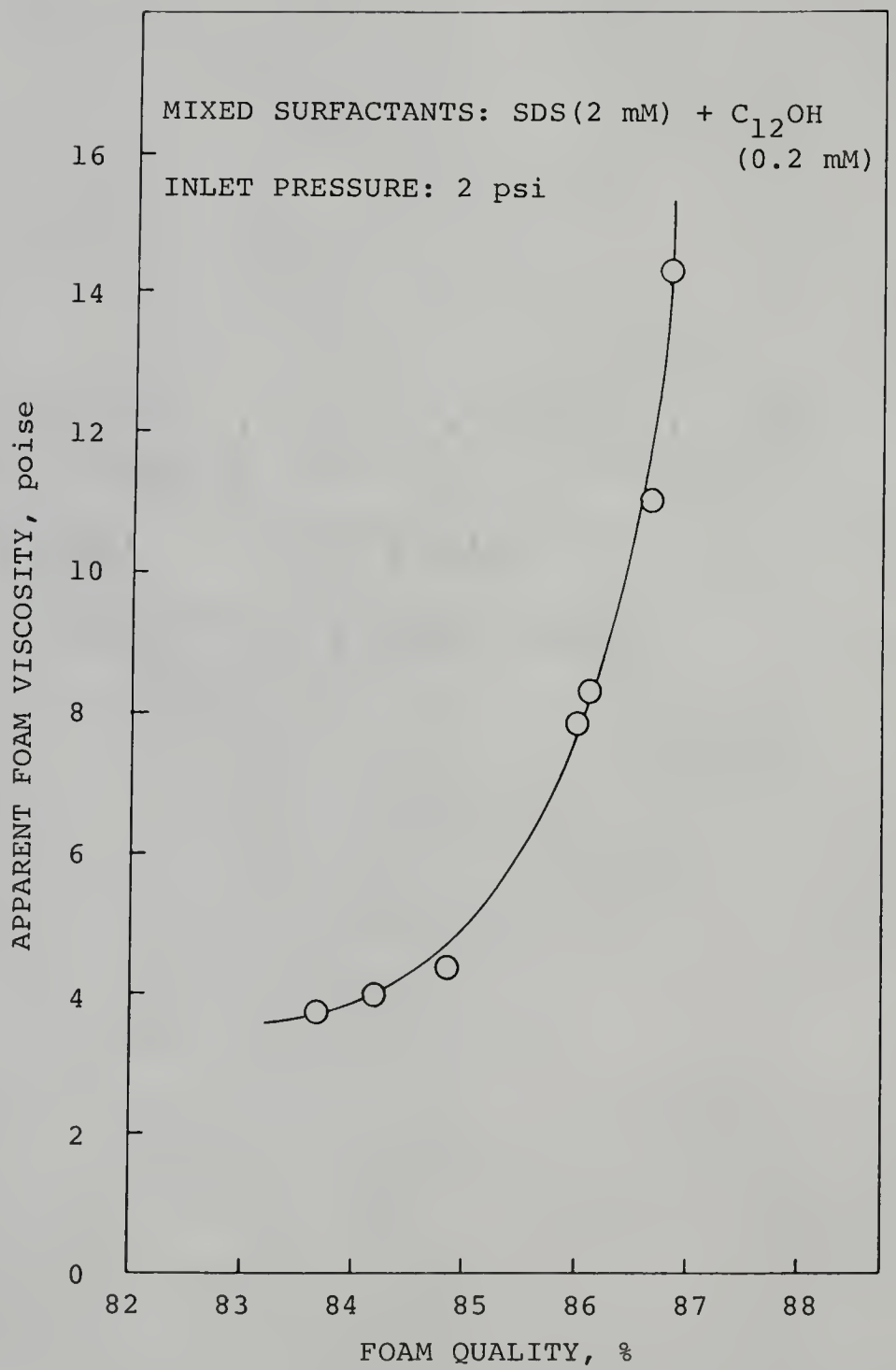

Figure 2.22. Apparent Foam Viscosity as a Function of Foam Quality.

per unit length, the radius of curvature of the gas/liquid interface, and the thickness of liquid films [77].

These results have practical significance for foam flowing through porous media. The apparent viscosity of the foam will not change with pore size if $r_B/R_p < 1.0$, but will increase with decreasing pore size if $r_B/R_p > 1.0$.

2.4.6 Rate of drainage

Figure 2.23 and 2.24 show the volume ratio of liquid drained from the foam column as a function of time. For the mixed foaming systems, SDS + C_nOH (n = 8, 10, 12, 14, and 16), the overall slowest drainage was observed for the system consisting of SDS + $C_{14}OH$ while the fastest drainage was found for the system of SDS + C_8OH. The correspondence of chain length compatibility with rate of drainage was not observed in this study. Shiao [46] also reported that chain length compatibility was not observed for the rate of drainage of mixed foaming systems of SDS with different long chain alcohols. One interesting phenomenon observed during the experiment was that a large amount of foam was easy to produce by shaking for the systems of SDS + C_8OH, SDS + $C_{10}OH$, and SDS + $C_{12}OH$, but not for the systems of SDS + $C_{14}OH$ and SDS + $C_{16}OH$.

If the same amount of liquid is distributed in the foam, then the foam with lesser volume possesses thicker liquid films. The SDS + $C_{12}OH$ solution had the highest surface viscosity, followed by SDS + $C_{14}OH$, SDS + $C_{16}OH$,

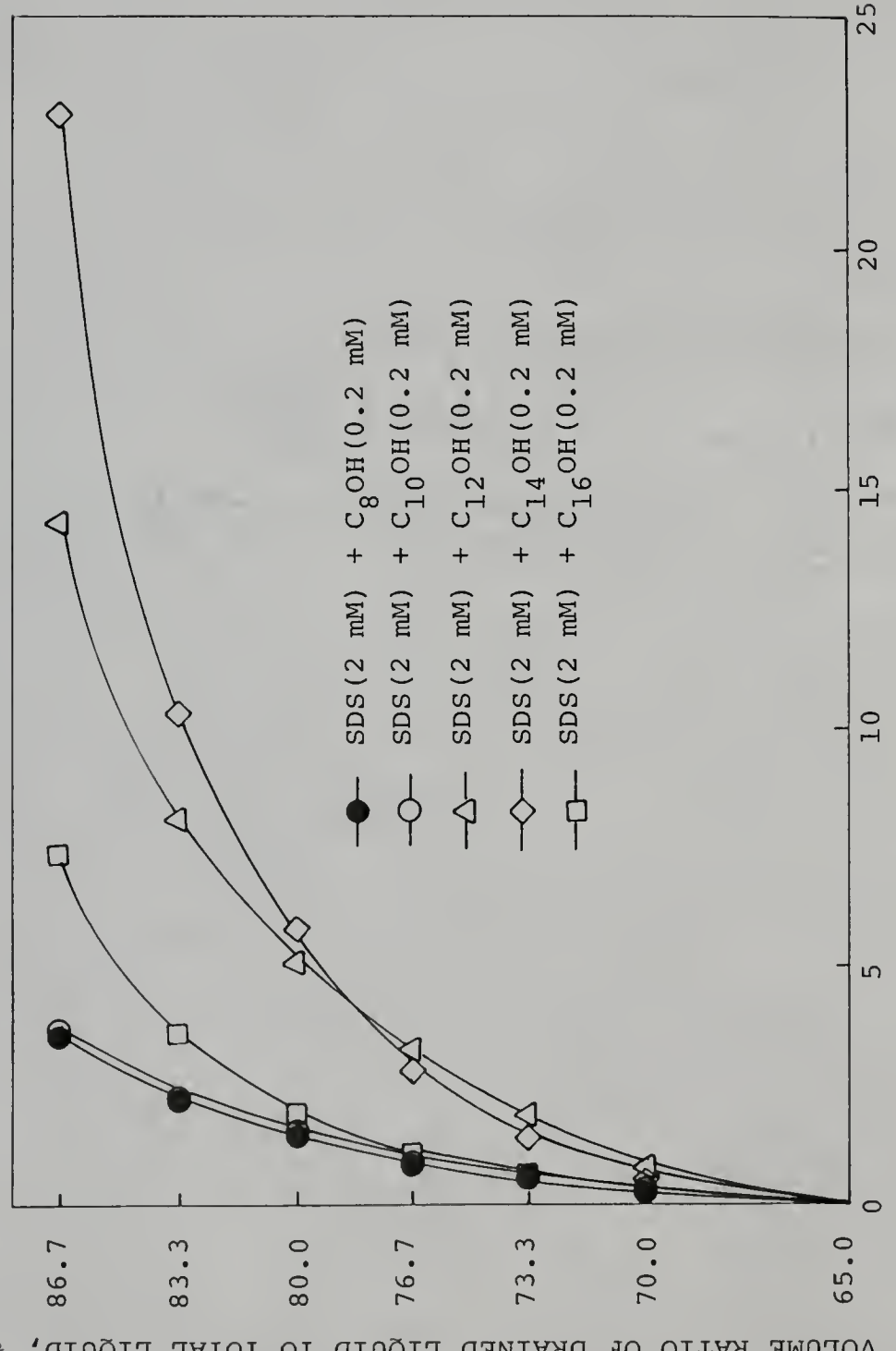

Figure 2.23. Rate of Drainage for Mixed Foaming Agents of SDS and Alkyl Alcohols.

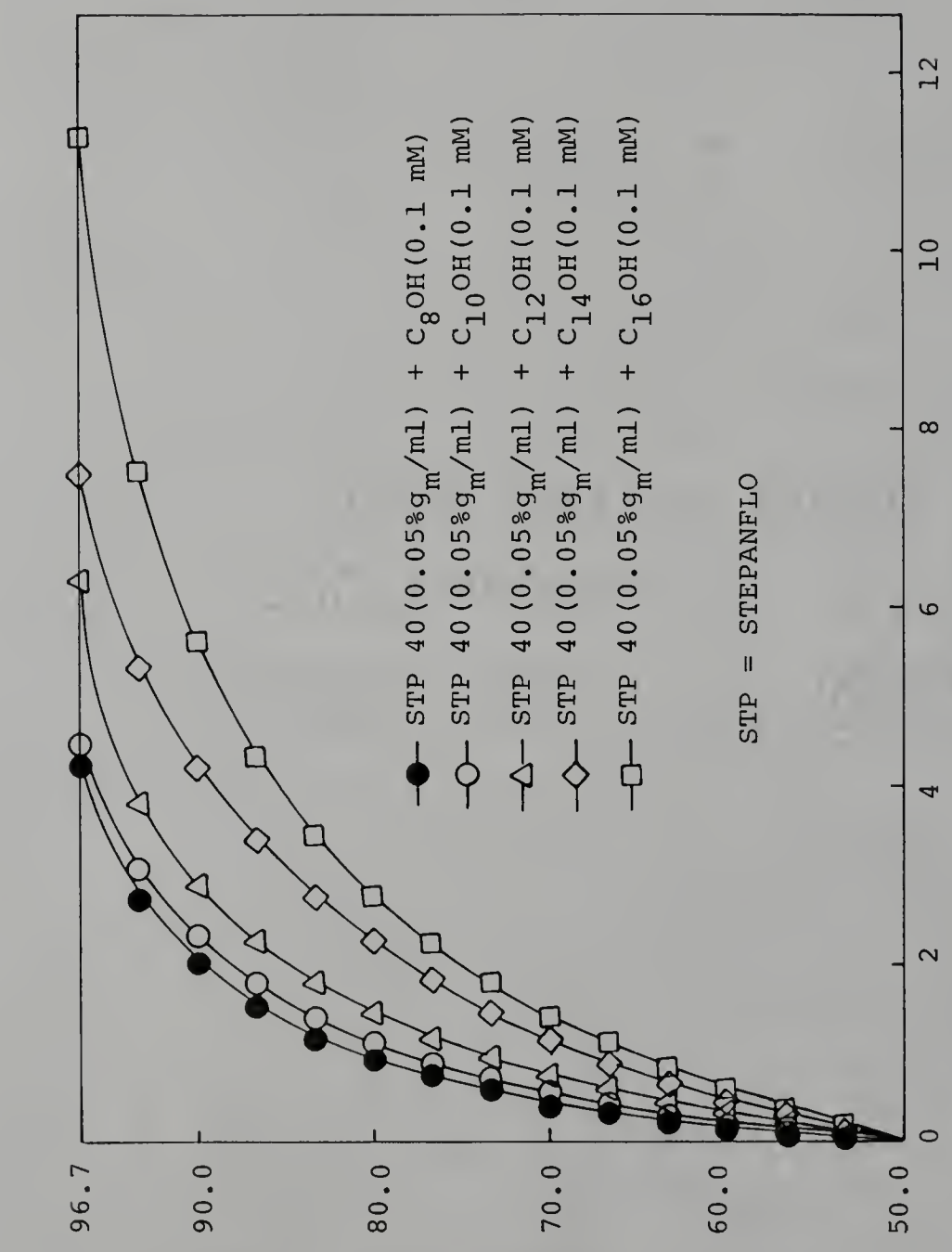

Figure 2.24. Rate of Drainage for Mixed Foaming Agents of Stepanflo 40 and Alkyl Alcohols.

SDS + $C_{10}OH$, and SDS + C_8OH [21]. As mentioned in the previous section, a high surface viscosity leads to a retardation of bulk liquid flow near the surfaces which in turn reduces the rate of drainage of the liquid films. Therefore, the slowest drainage for the first five minutes was found for the system of SDS + $C_{12}OH$ rather than SDS + $C_{14}OH$ (Figure 2.23). However, after a certain time has passed (e.g., 10 minutes or longer) and a critical thin film thickness is reached, another factor that has to be considered is the effect of Marangoni flow [42]. It has been shown [78] that the molecular interactions between dodecyl alcohol and SDS are stronger than those of tetradecyl alcohol and SDS. The thermal motion of the terminal segment of tetradecyl alcohol at the interface causes the thin film of SDS + $C_{14}OH$ to possess a higher fluidity compared to SDS + $C_{12}OH$. According to the Marangoni effect, thin film with high fluidity can easily restore the instability of the film due to a small disturbance. Thin film of SDS + $C_{12}OH$ is too rigid to resist a small disturbance and, in consequence, foam is easy to break. Hence, the slowest drainage was observed for the system of SDS + $C_{14}OH$ at the later period of drainage (Figure 2.23).

In Figure 2.24 the slowest drainage was observed for the mixed surfactants consisting of Stepanflo 40 and $C_{16}OH$. The rate of drainage and the total foam volume generated by shaking decreased with the increase of hydrocarbon chain

length of alcohols. Again this result is not compatible with the trend of the other foam surface properties described before. The argument mentioned above may be employed to explain this result, but the actual reasons are still unknown. More information about Stepanflo 40 such as major components, molecular structures, and physical properties are needed.

The rate constants, K_1 and K_2, of the drainage process were calculated by linear regression and are shown in Figure 2.25 and 2.26. The smallest value in K_1 corresponds to the slowest drainage.

2.4.7 Bubble Size Distribution

Photographs of the foams taken at different time intervals are presented in Figures 2.27-2.30. An increase in bubble size with elapsed time was observed. The bubble size increased with elapsed time due to coalescence. The bubble size increased more rapidly with elapsed time for Suntech IVC than for Suntech IVA. These results imply that the surfactant solution with low CMC and high surface viscosity produces relatively stable foam. Figure 2.31-2.33 show the histograms of bubble size distributions of Suntech IVA, B, and C after 60 minutes. These distributions were determined from Figure 2.27 using a digital image analyzer. It is clear that the number of bubbles with small radius (e.g., less than 0.1 cm) is larger for Suntech IVA than for Suntech IVB and C. The mean radii of the foam bubbles for

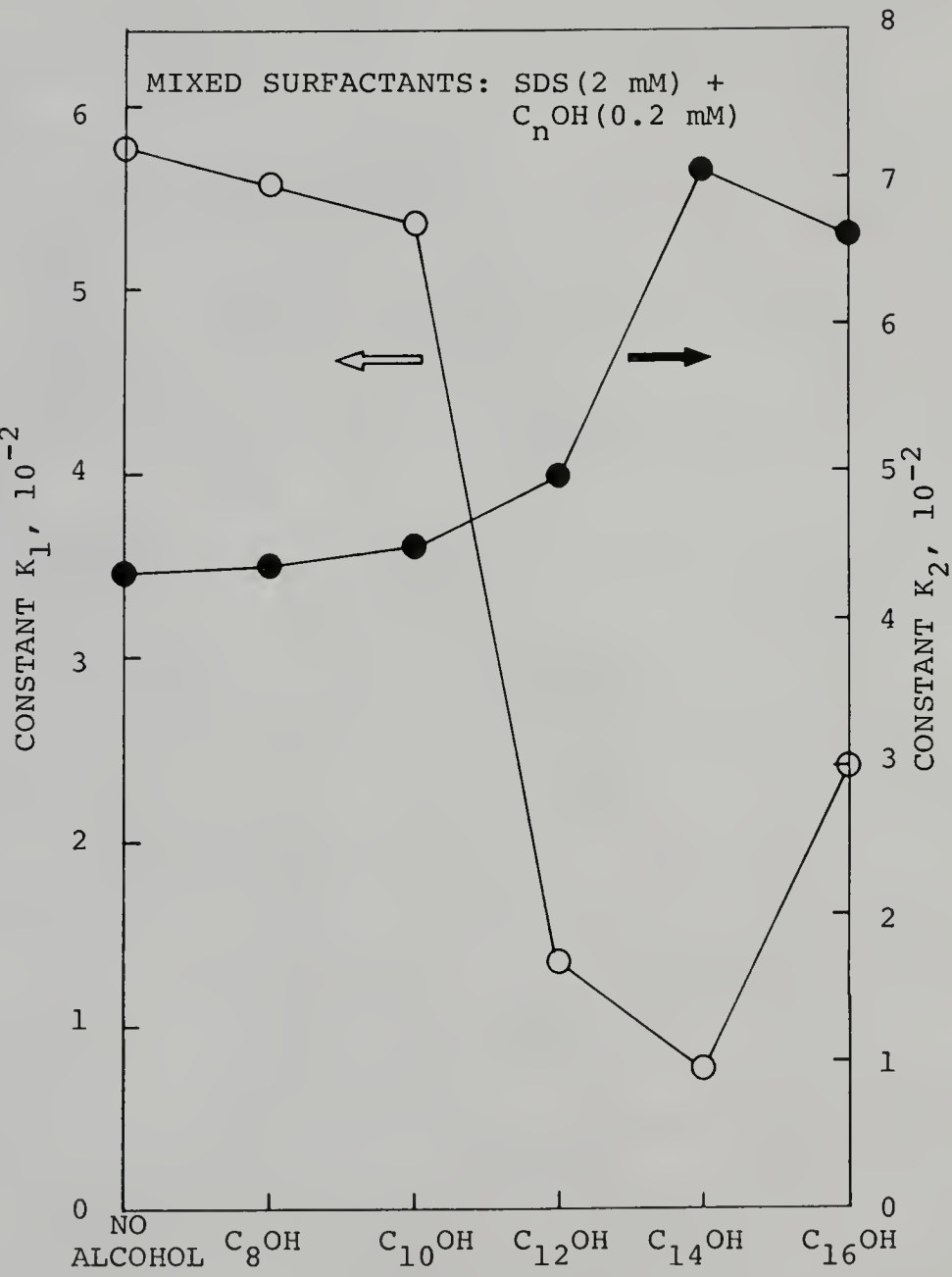

Figure 2.25. Rate Constants of Drainage Process for Mixed Faoming Agents of SDS and Alkyl Alcohols.

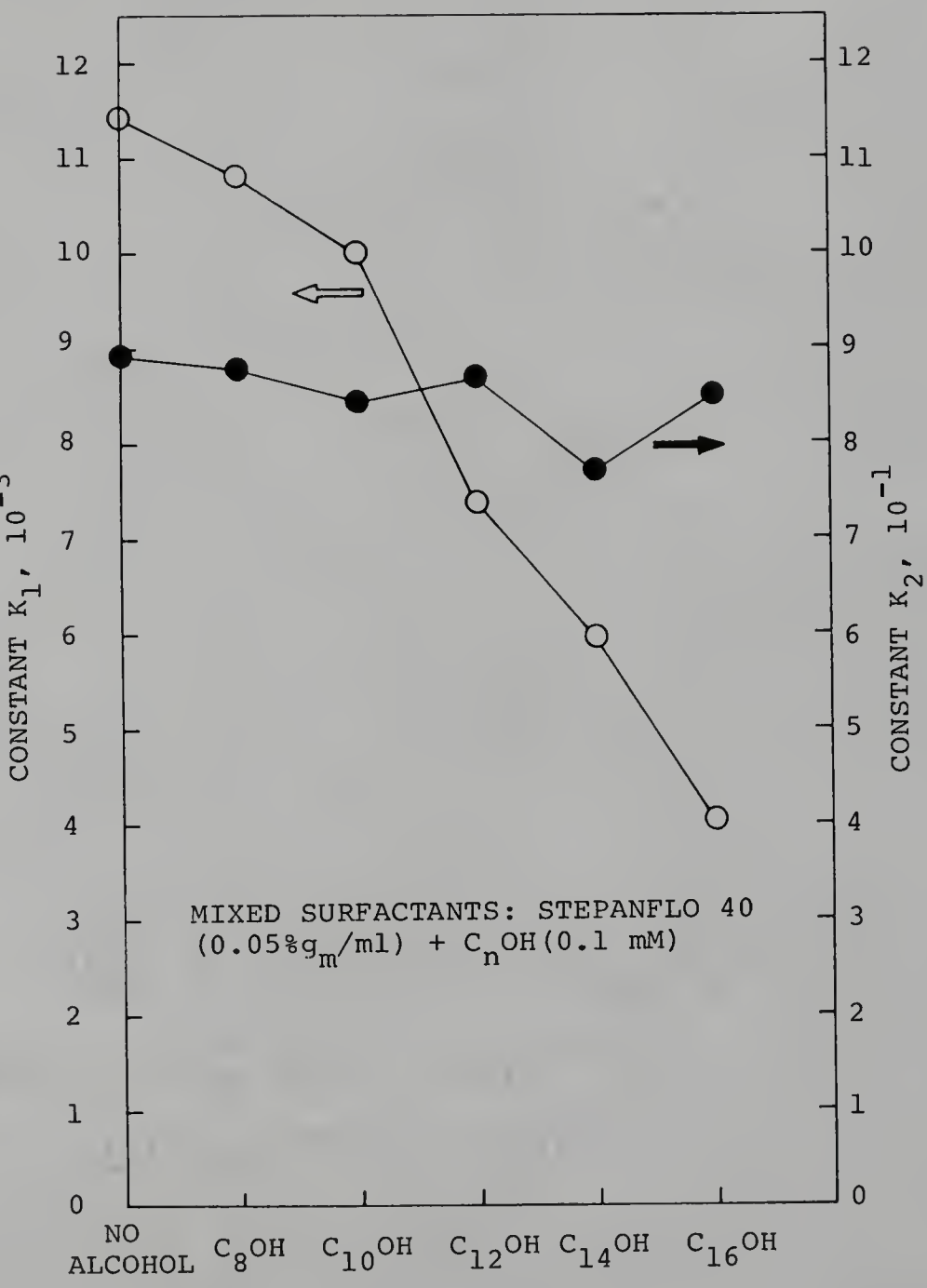

Figure 2.26. Rate Constants of Drainage Process for Mixed Foaming Agents of Stepanflo 40 and Alkyl Alcohols.

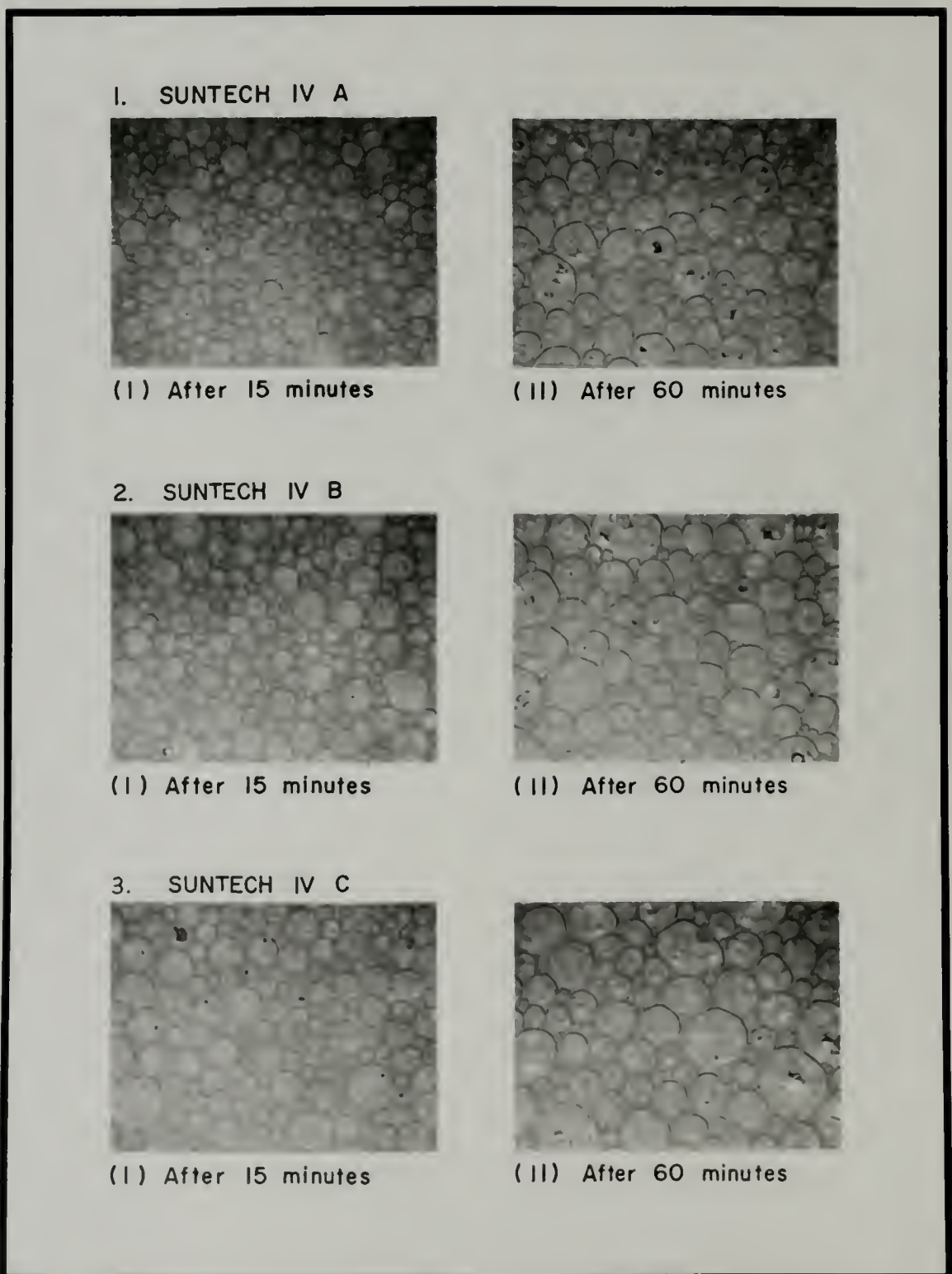

Figure 2.27. Photographs of Suntech IV Foams at Various Time Intervals after the Foams Were Produced.

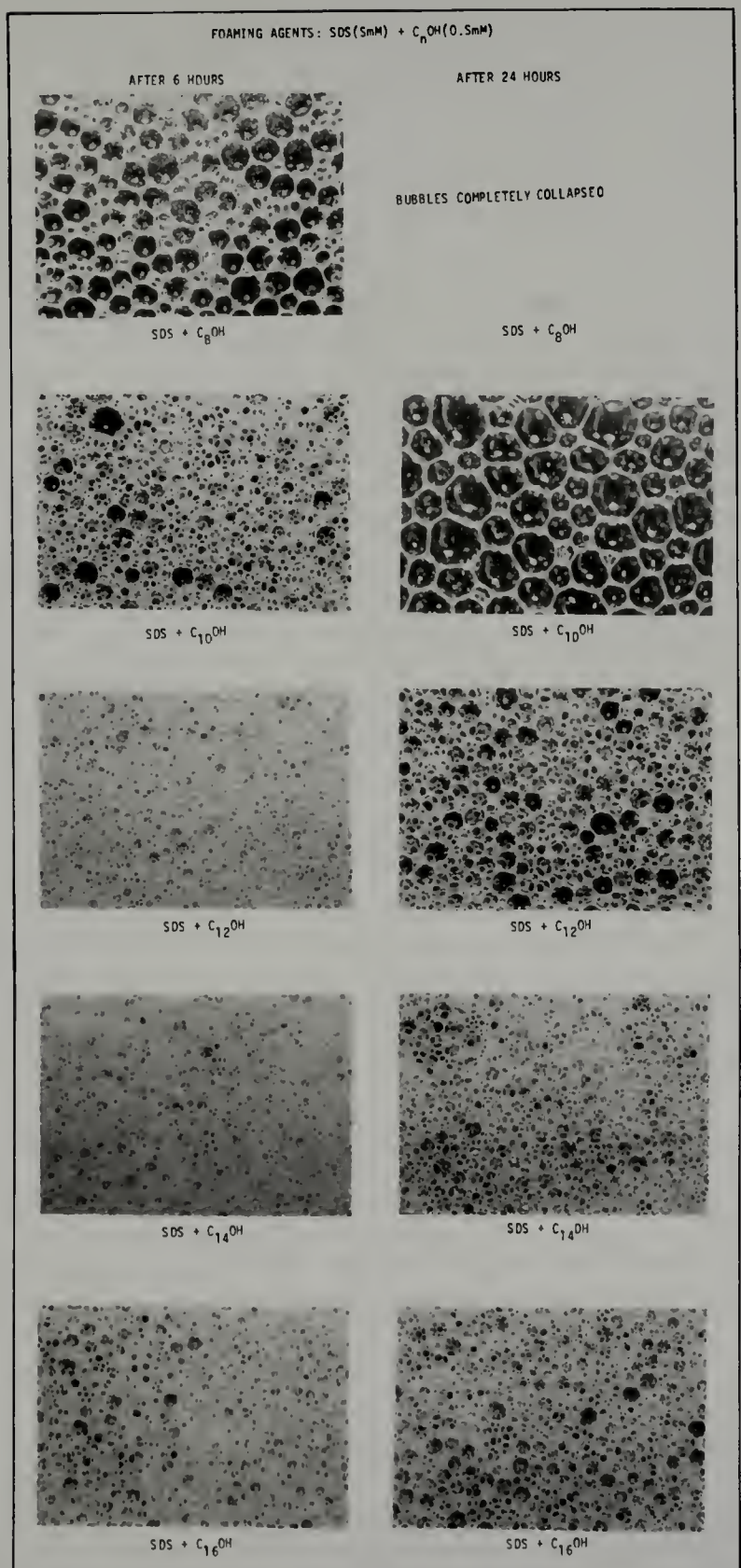

Figure 2.28. Photographs of Foams for Mixture of SDS with Alkyl Alcohols at Various Time Intervals after the Foams Were Produced.

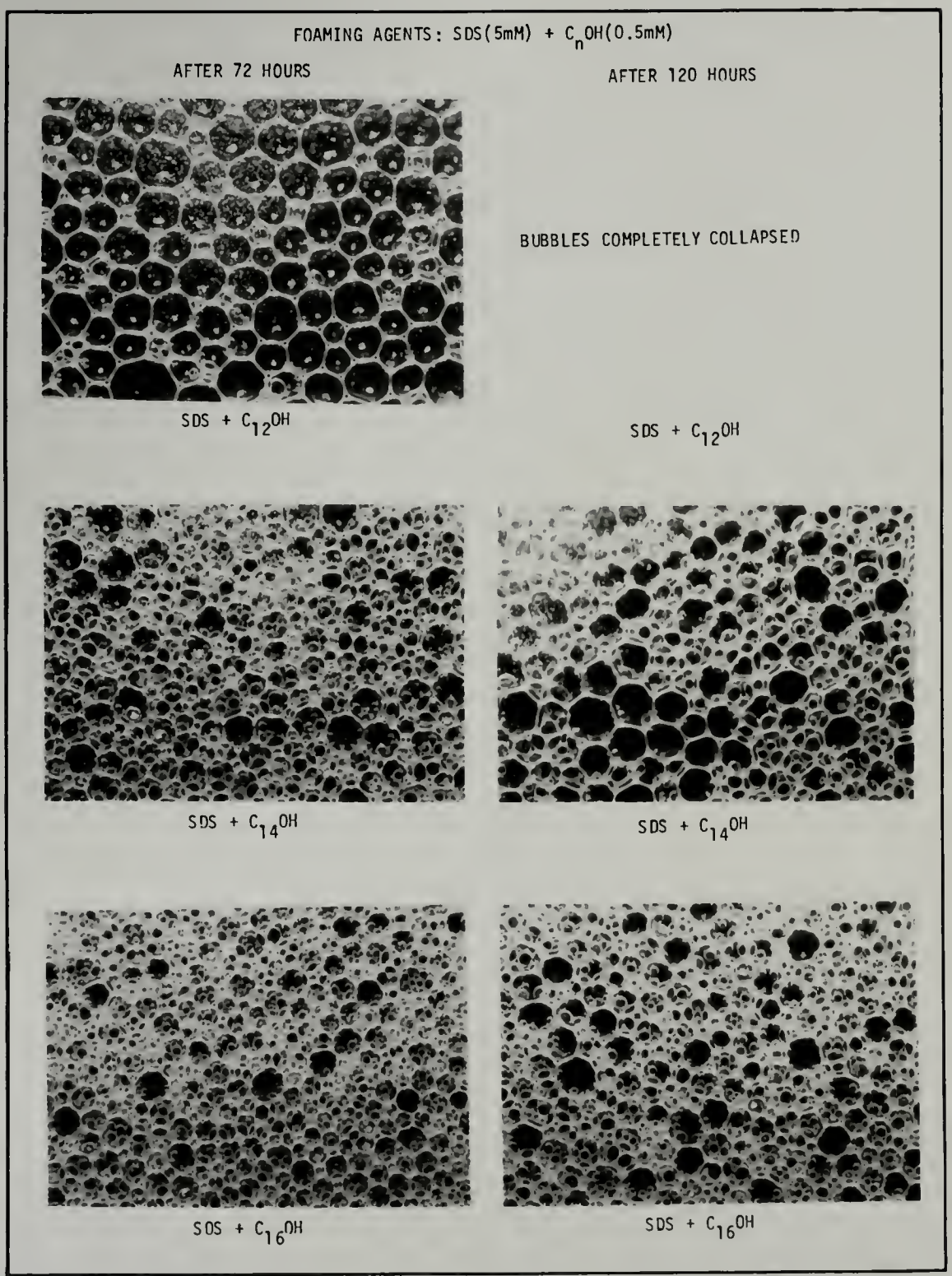

Figure 2.29. Photographs of Foams for Mixture of SDS with Alkyl Alcohols at Various Time Intervals after the Foams Were Produced.

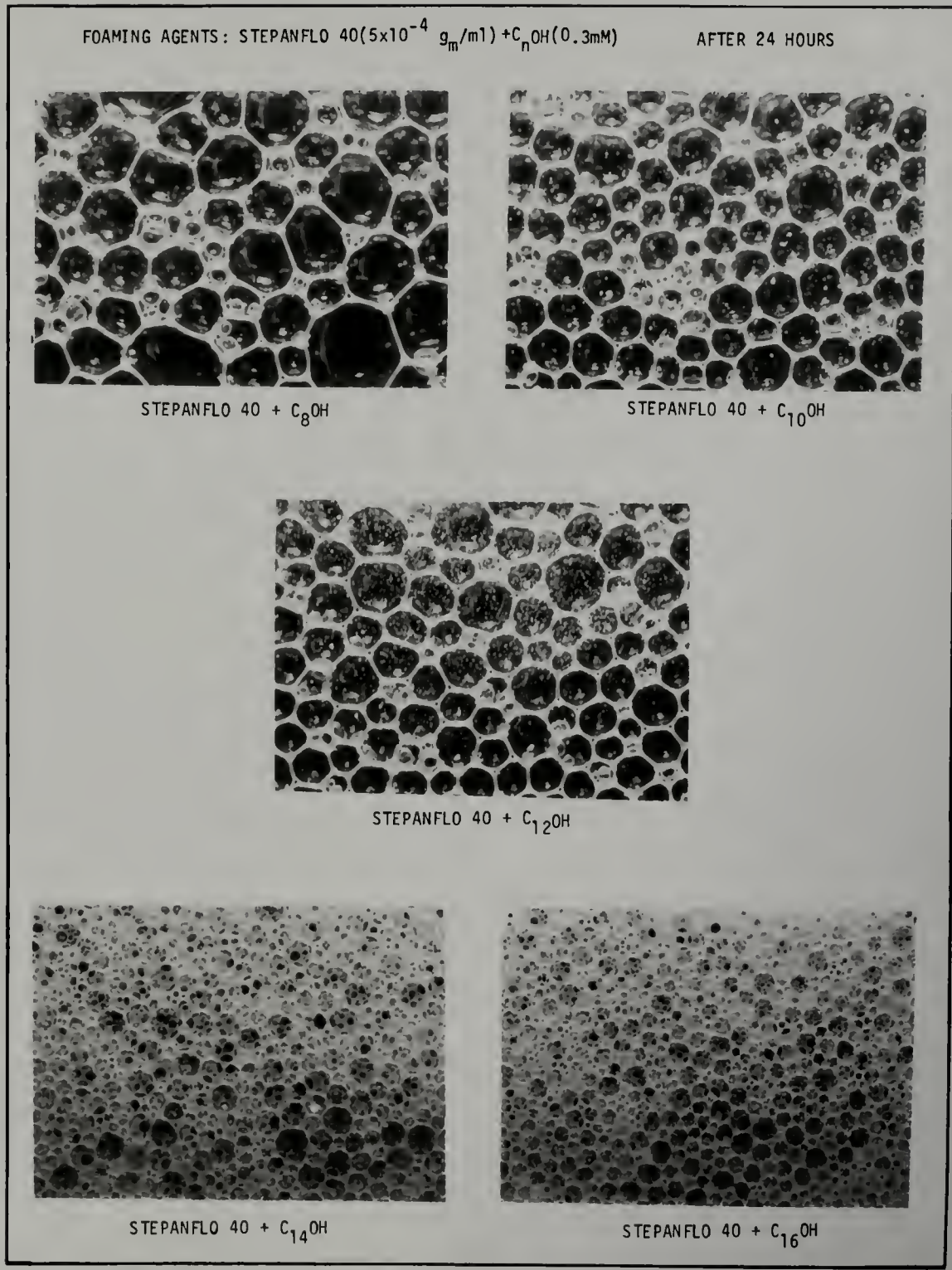

Figure 2.30. Photographs of Foams for Mixture of Stepanflo 40 with Alkyl Alcohols at 24 Hours after the Foams Were Produced.

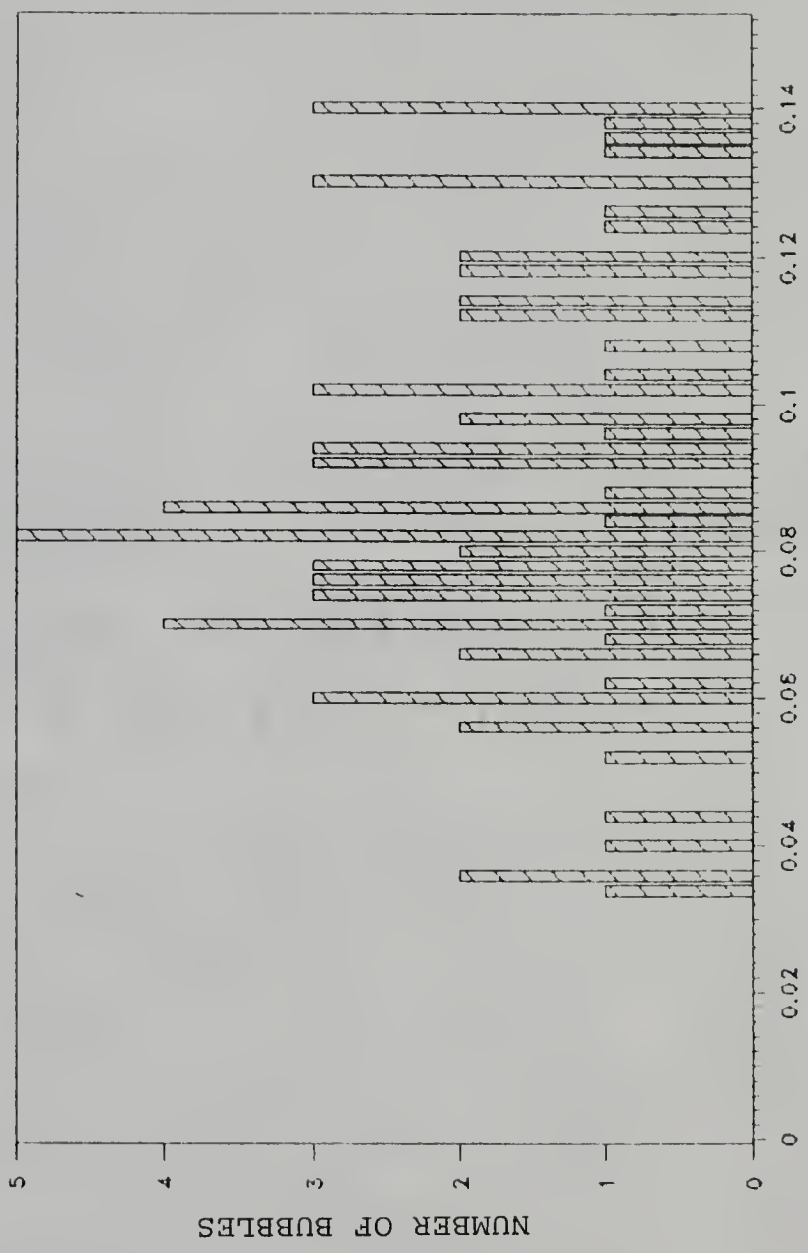

Figure 2.31. Histograms of Bubble Size Distribution for Suntech IVA Foam at 60 Minutes after the Foam Was Produced.

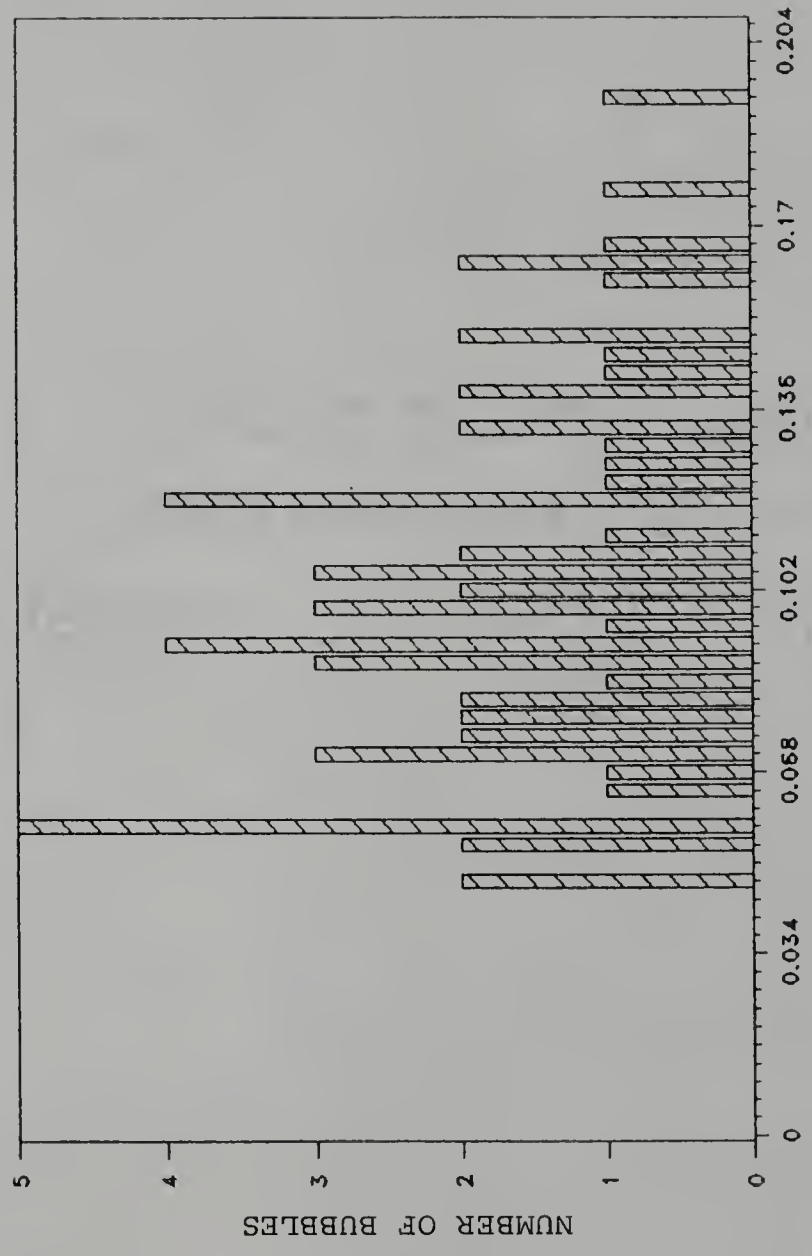

Figure 2.32. Histograms of Bubble Size Distribution for Suntech IVB Foam at 60 Minutes after the Foam Was Produced.

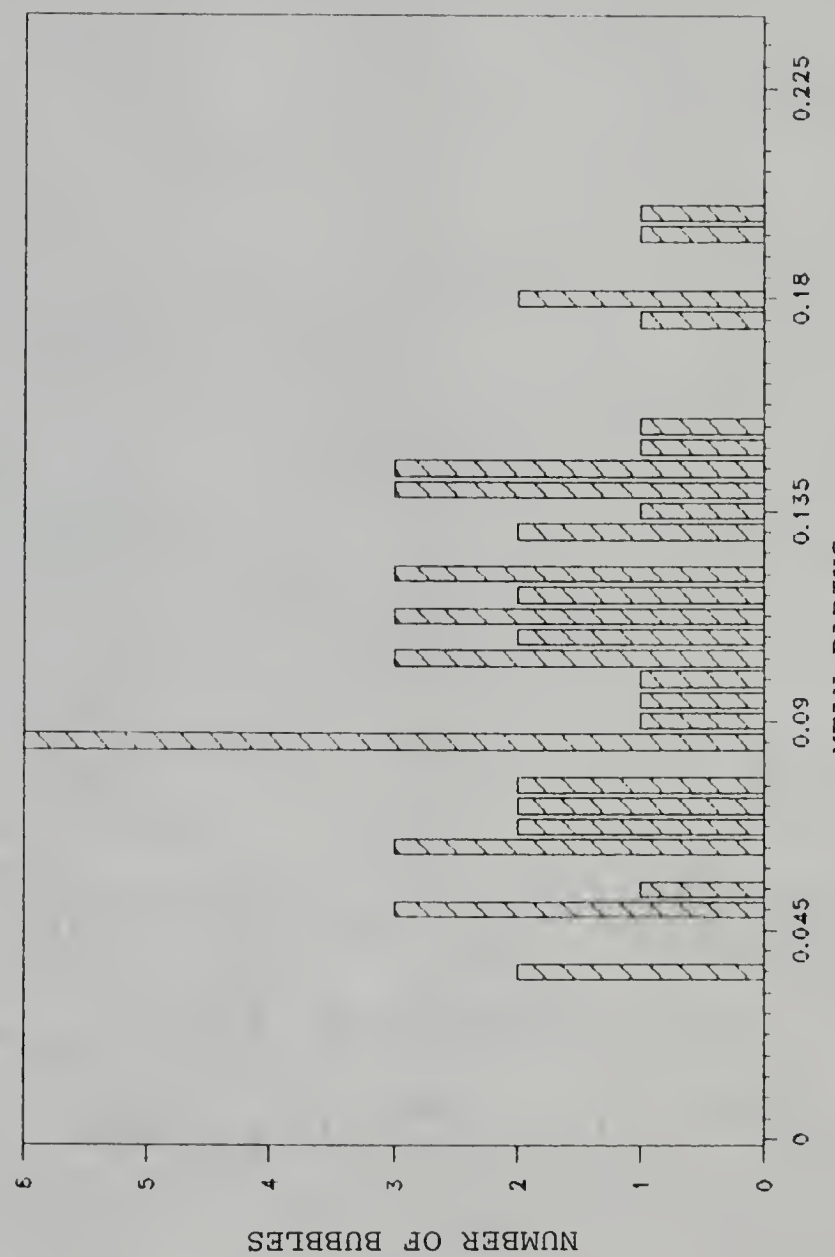

Figure 2.33. Histograms of Bubble Size Distribution for Suntech IVC Foam at 60 Minutes after the Foam Was Produced.

Suntech IVA, B, and C are 8.97×10^{-2} cm, 10.3×10^{-2} cm, and 10.64×10^{-2} cm, respectively.

The average bubble size was a minimum for the mixed foaming systems SDS + $C_{16}OH$ (Figures 2.28 and 2.29). The experiment was repeated at least five times and the trends were very reproducible. As mentioned previously, a large amount of bubbles were easy to produce for the system of SDS + C_8OH, SDS + $C_{10}OH$, and SDS + $C_{12}OH$, but not for the system of SDS + $C_{14}OH$ and SDS + $C_{16}OH$. It seems that the energy required to generate bubbles increases with the increase of hydrocarbon chain length of alcohols. The higher the required energy, the smaller the bubble size and the less foam produced for a given concentration of foaming agent. Once the bubbles (i.e., SDS + $C_{14}OH$ or SDS + $C_{16}OH$) were formed, they could last a long time without breaking. This can be interpreted in terms of the hydrophobicity of hydrocarbon chain and the rate of adsorption/desorption of solute at the interface. The hydrophobic force keeps the surfactant molecules at the interface. It does not mean that SDS + $C_{14}OH$ or SDS + $C_{16}OH$ can always produce stable foams because the work applied to the foam has to be considered. For instance, they may not produce any foam at a low pressure. Although the rate of drainage of SDS + $C_{16}OH$ foam is faster than that of SDS + $C_{14}OH$ foam (Figure 2.23), the former can stay at a very high foam quality without breaking. Therefore, the slowest rate of coalescence of the bubbles was observed for the system of

SDS + $C_{16}OH$ and, consequently the smallest average bubble size was found after a long period of time (Figure 2.29). Similar results (Figure 2.30) were observed for the mixed foaming systems Stepanflo 40 + C_nOH and were consistent with the trend of the rate of drainage. Based on relative comparison, the measurements of bubble size distribution for the mixed foaming systems are still very useful in comparing the foam stability.

2.4.8 Microscopic View of Foam Flow in Micromodel

Figure 2.34 shows the photomicrographs of foams generated inside the micromodel. It is evident that the mixed surfactants of same chain length (SDS + $C_{12}OH$) produced smaller foam bubbles and more lamellae than the surfactant system with dissimilar chain length. These photomicrographs indicate that the injection of a gas in the micromodel filled with surfactant solution can generate foam in-situ.

From these photomicrographs and the results of the previous section it is clear that the bubble size distribution is different for mixed foaming systems, SDS + C_nOH (n = 8, 10, 12, 14, and 16), inside and out of the micromodel. It is evident that for a given concentration, the bubble size of a foaming agent depends on the foaminess, foam stability, pore size, pressure, etc.

The mechanism of foam flow through porous media described by Holm [63] is of a moving continuous liquid

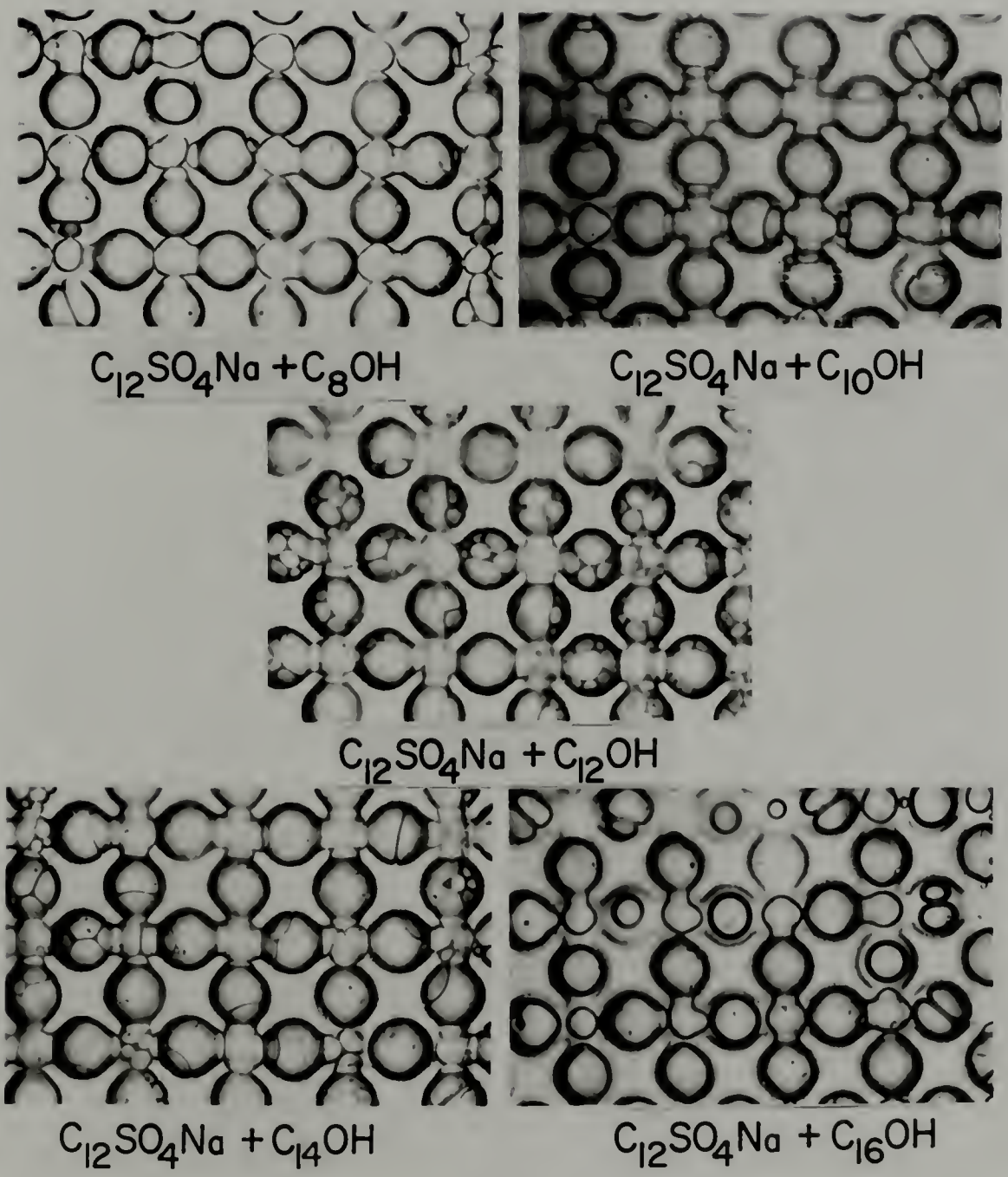

Figure 2.34. Photomicrograph of Foams in Micromodel.

phase and a discontinuous, internal gas phase moving discretely or by rupture of the gas cells. Sharma et al. [79] proposed two mechanisms of gas flow in porous media in the presence of surfactant solution (Figure 2.35). Foams with high stability follow the bubble-train mechanism, whereas foams with low stability follow the pop and burst mechanism in a given porous medium. Of course, this mechanism also depends on the amount of foam generated in-situ and the bubble size relative to the pore size.

2.5 Conclusions

In this chapter the surface properties of the foaming agents and the foam stability were discussed. The effects of adding long chain alcohols on the foaming agents were also investigated. The following conclusions were drawn from the studies in this chapter.

1. The presence of long chain alcohols in the foaming agents, SDS and Stepanflo 40, had considerable influence on their surface properties as well as on the foam stability. There was no such influence on Suntech IV.
2. For mixed foaming systems, SDS + C_nOH (n=8, 10, 12, 14, and 16), minimum surface tension, maximum surface viscosity [33], maximum foaminess, and the slowest rate of drainage at the early stage were observed when both components of the system had the same chain

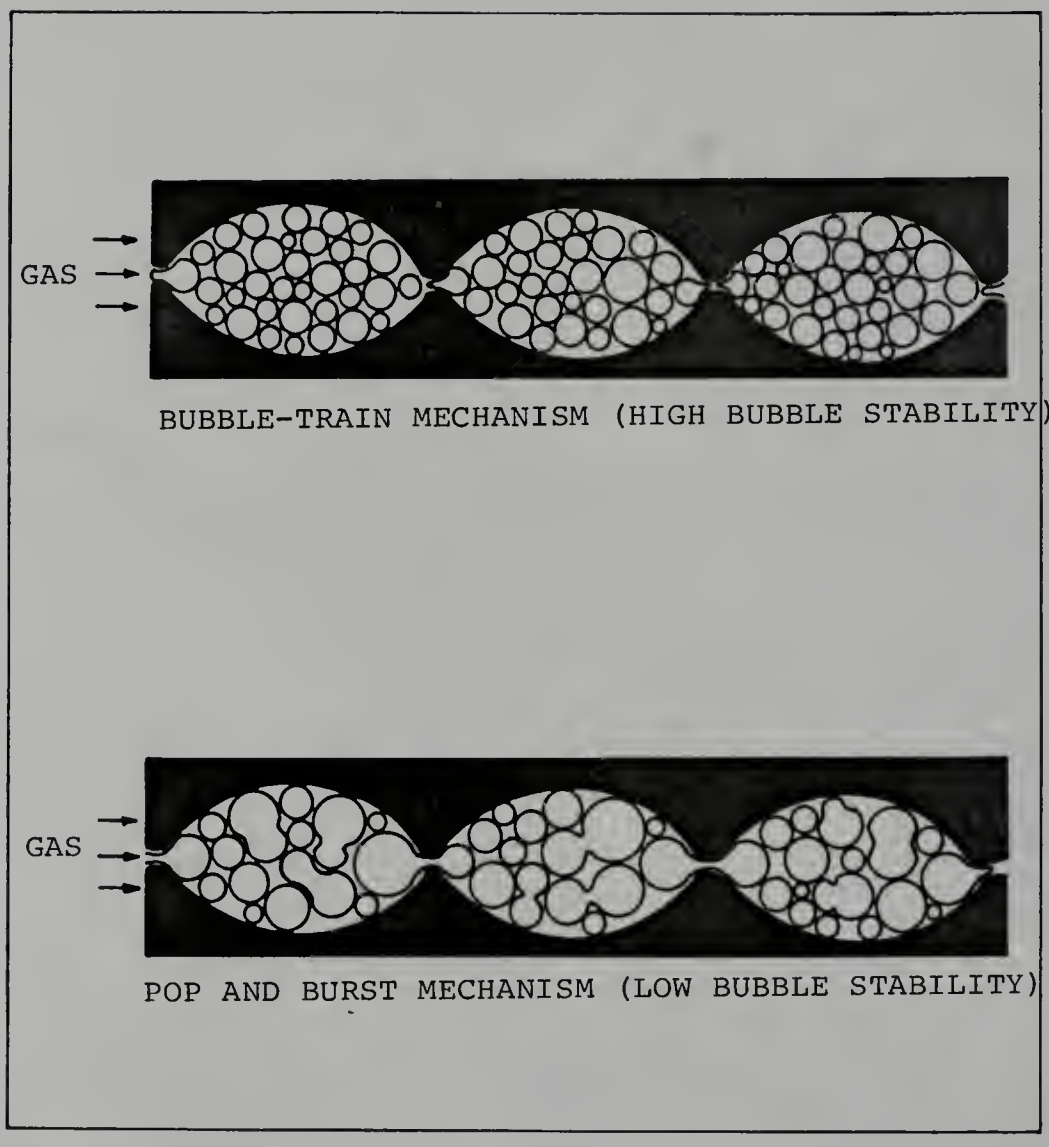

Figure 2.35. Two Mechanism of Gas Flow in Porous Media Filled with Surfactant Solution.

length (SDS + $C_{12}OH$). However, the minimum foam quality and minimum apparent foam viscosity were observed for the system consisting of SDS + $C_{10}OH$; the slowest rate of drainage at the later period was found for the system of SDS + $C_{14}OH$.

3. For mixed foaming systems, Stepanflo 40 + C_nOH (n=8, 10, 12, 14, and 16), minimum surface tension was observed for Stepanflo 40 with the addition of dodecyl alcohol; whereas, maximum foaminess, minimum foam quality, and minimum apparent foam viscosity were observed for the system consisting of either Stepanflo 40 + $C_{10}OH$ or Stepanflo 40 + $C_{12}OH$; the slowest rate of drainage was found for the system of Stepanflo 40 + $C_{16}OH$.
4. The foaming agent, SDS + $C_{12}OH$, produced the smallest bubbles in the micromodel. The number of lamellae decreased as the difference in SDS + C_nOH chain length increased.
5. From the bubble size distribution measurements, the average bubble size decreased as the hydrocarbon chain length of alcohol increased. It seems that the energy required to generate foam bubbles increases with the increase of chain length of alcohols. The higher the required energy, the smaller the bubble size and the less foam produced for a given concentration of mixed foaming system.
6. The overall studies on the surface properties of the

mixed foaming systems show that the effect of chain length compatibility is not observed for the rate of drainage and bubble size distribution. These exceptional cases can be explained by the surfactant molecules' packing pattern at the liquid/air interface, rate of adsorption/desorption of solute at the interface, and the rheology of the thin liquid films. It should be noted that it does not mean that the theory of chain length compatibility is not true. It illustrates that not all surface properties of the mixed foaming agents can be predicted from the chain length compatibility effects. In addition to the factors mentioned above, other factors such as the work done on the system and the method used to generate the foam have to be considered.

CHAPTER III

FLUID DISPLACEMENT IN POROUS MEDIA BY IN-SITU FOAM

3.1 Introduction

It has been shown [64] that the foam generated in-situ can be used to block the flow of gas in both consolidated and unconsolidated porous media. The pressure at which gas flow is blocked increases with the saturation of surfactant solution in porous media as well as the concentration of surfactant in the solution. From gas tracer studies, Nahid [80] also showed that the existence of an immobile gas saturation increased with the concentration of the surfactant. The immobile gas saturation ranged from 4% in the absence of a surfactant up to 30% at a surfactant concentration of 1%. The effect of foam on gas permeability is one of the most important aspects for tertiary oil recovery processes. In the presence of foams, the effective permeability of a porous medium to each phase is considerably reduced as compared to the permeability measured in the absence of foams [63,65]. The presence of oil in a porous medium decreased the effectiveness of foams in reducing permeabilities of gas and water [6,81].

However, it was found that certain surfactants were very effective in reducing gas permeability even in the presence of oil. The continuous injection of several other surfactants also increased their effectiveness in the presence of oil.

The main objective of this study was to correlate the effect of surface properties of foaming agents and foam stability on the foam behavior in porous media. The parameters measured and correlated for foam flooding processes included fluid displacement efficiency, breakthrough time, effective air mobility, and pressure distribution in porous media. The fluid displacement efficiency is defined as the ratio of the fluid recovered to the total fluid in a porous medium until the breakthrough of gas phase. The breakthrough time is the time taken by the gas to breakthrough at the producing site of the porous media. The fluid displacement efficiency of foam in heterogeneous porous media was also studied. The results of these investigations would be relevant in evaluating foam as a blocking agent for controlling underground gas flow as well as an oil recovery agent under specific reservoir conditions.

3.2 Materials and Methods

3.2.1 Materials

All chemicals used in the experiments were the same as

described in Chapter II. The sand used as a porous medium was purchased from AGSCO Corp., Paterson, New Jersey. The sand had absolute permeability of 2-3 darcys and porosity of 38%. The pressure transducers (DP-15) used for the measurements of pressure across a porous medium were obtained from Validyne Engineering Corp., Northridge, California. The chart recorders (Health/Schlumberger Model 225) were purchased from Health Company, Benton, Michigan. The liquid was pumped using Cheminert metering pump (Model EMP-2), Laboratory Data Control, Riviera Beach, Florida. The sand was packed using wrist action shaker (Model 75), Burrell Corp., Pennsylvania. Compressed air and CO_2 were purchased from AIRCO Company, Gainesville, Florida.

3.2.2 Methods

At room temperature, the experiments were conducted under different concentrations of foaming agents and types of the porous medium to analyze foam behavior in porous media. A polyvinyl pipe (2"IDx18"L) was packed with sand using a wrist action shaker at a flow rate of sand about 5 cm^3/min. The sandpack (Figure 3.1) was flushed vertically with CO_2 about an hour to replace interstitial air. Deionized water was pumped through using a Cheminert metering pump, and the pore volume (V_p) of the porous medium was determined. About three pore volumes of water (or brine) were pumped through at various flow rates to wash out CO_2 as well as to determine absolute permeability

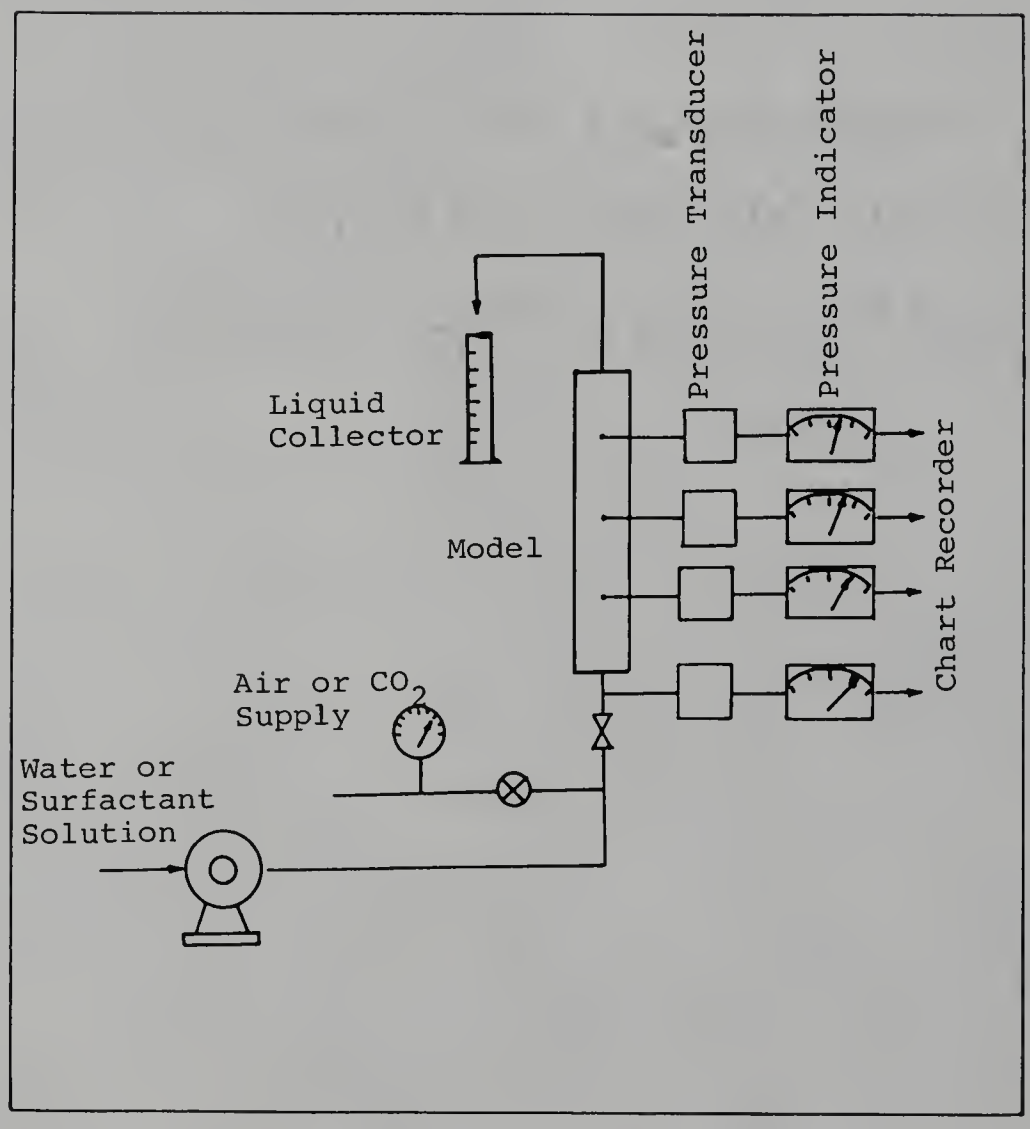

Figure 3.1. Schematic Diagram of the Experimental Set Up for Flow through Porous Media Studies.

of the porous medium using Darcy's law [82]. After the porous medium was saturated with water (or brine), about three pore volumes of foaming solution with known concentration were pumped at constant flow rate (4 ml/min), followed by air injection. The pressure differences across the porous medium were measured using pressure transducers and chart recorders. The liquid at outlet was collected at different time intervals. The breakthrough time and total fluid recovery were recorded.

In order to determine the fluid displacement efficiency in heterogeneous porous media, a series of experiments were conducted. The sand packs containing a non-porous (e.g., stainless steel) core or a porous (e.g., Berea core) core were prepared as shown in Figure 3.2. The Berea core had permeability of about 275 millidarcys and porosity of 20%. The dimensions of the pipe used for sand packs were 12" diameter and 18" length. The stainless steel core and Berea core packed inside the sand had the same shape and the size (1"x1"x12"). From these two types of porous media, one can easily determine the fluid displaced from low permeability porous media (i.e., Berea core) in the absence and presence of foam.

3.3 Effective Mobility of Air in the Presence of Foam

In order to interpret the flow behavior of foam in a porous medium, the effective air mobility was calculated

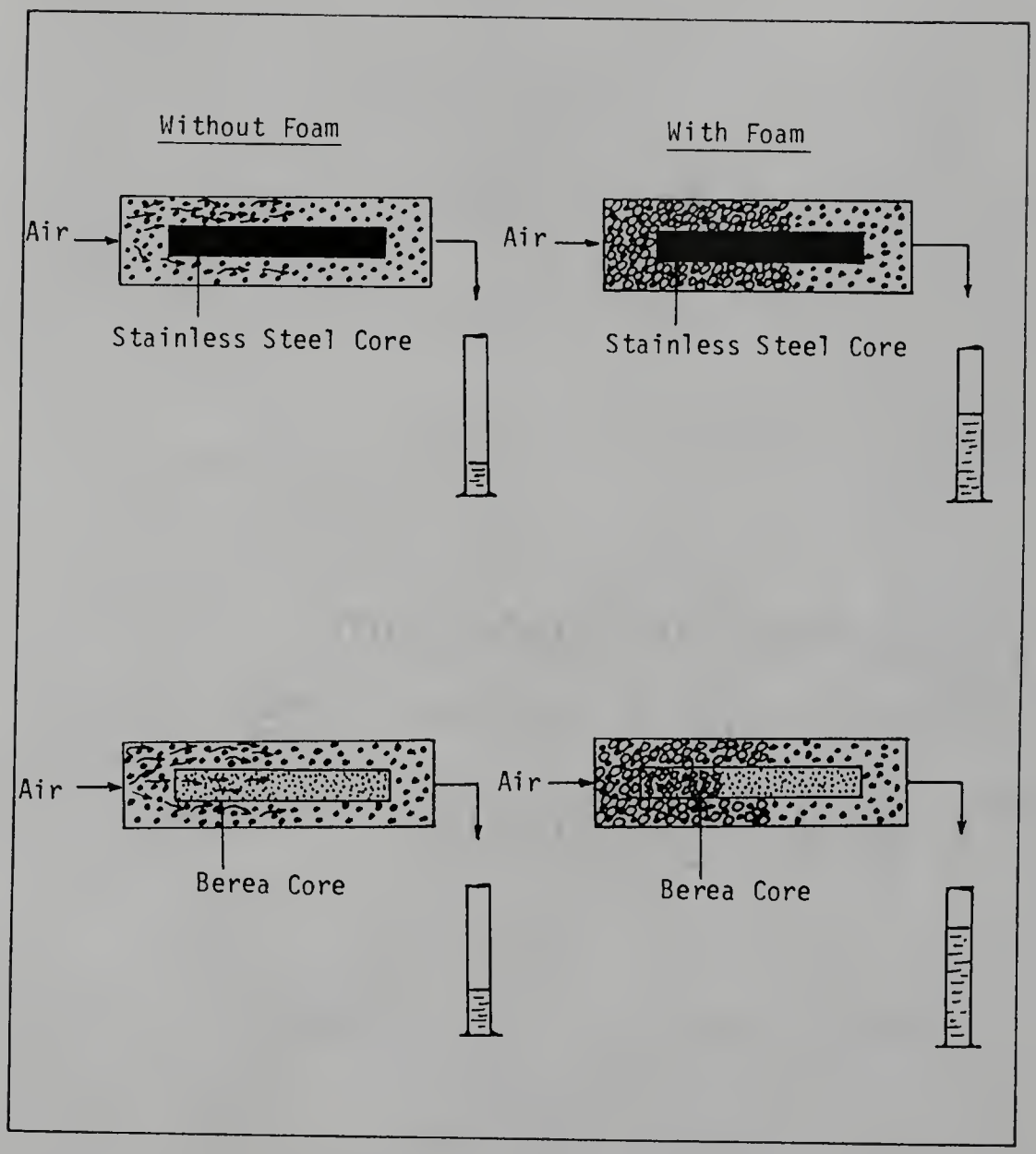

Figure 3.2. Schematic Diagram of the Heterogeneous Porous Media for Fluid Displacement Experiments with and without Foam.

using the breakthrough time and fluid displacement efficiency. It was assumed that the flow of air in the porous medium obeyed Darcy's law. Darcy's law for a gas phase flowing at steady state in a linear system is given as follows [82]

$$q_{sc} = \frac{T_{sc} A k_g (P_1^2 - P_2^2)}{P_{sc} T Z L \mu_g} \qquad (3.1)$$

where q_{sc} is the constant gas flow rate measured at a standard absolute pressure (P_{sc}) and temperature (T_{sc}), A is the flow cross-sectional area, k_g is the effective gas permeability, T is the flow temperature, Z is the gas compressibility factor at flow condition, L is the length of a porous medium, μ_g is the gas viscosity, and P_1 and P_2 are the upstream and downstream absolute pressures. The fluid displacement experiments were conducted at room temperature and the downstream pressure (P_2) was kept atmospheric. The pressure drops across porous media were always less than 30 psi so that the gas compressibility factor (Z) was approximately equal to 1. The gas flow rate (q_{sc}) may be approximately replaced by an average flow rate, Q_v/t_b, where Q_v is the total volume of the fluid collected at the gas breakthrough time (t_b). Equation (3.1) can be rewritten as follows

$$\frac{Q_v}{t_b} = \frac{k_g A \Delta(P^2)}{\mu_g L} \qquad (3.2)$$

where $\Delta(P^2) = \frac{P_1^2 - P_2 2}{P_{sc}}$

The effective mobility of the air, assuming foam behaves as a single fluid, is the ratio of permeability (k_g) to viscosity (μ_g). Hence,

$$\text{effective air mobility} = \frac{Q_v L}{t_b A \Delta(P^2)}$$

3.4 Results and Discussion

3.4.1 Fluid Displacement in Porous Media with Foaming Agents

Sharma and co-workers [33] have shown that the amount of fluid recovered from sand packs or Berea cores in the absence of foaming agents was very low because of the channelling effect and gravity override of air. For sand packs, fluid displacement efficiency slightly decreased as pressure increased. However, for Berea cores, a continuous increase in fluid displacement efficiency was observed up to 25 psi and remained constant with a further increase in pressure. A sharp decrease in breakthrough time was observed for both cases at low pressure and remained constant at high pressure. It is clear that the air mobility has to be controlled to reduce the channeling effect and gravity override in order to improve the fluid displacement efficiency.

The fluid displacement efficiency and breakthrough time increased with the increase of surfactant concentration in the porous medium (Figure 3.3 and 3.4). A

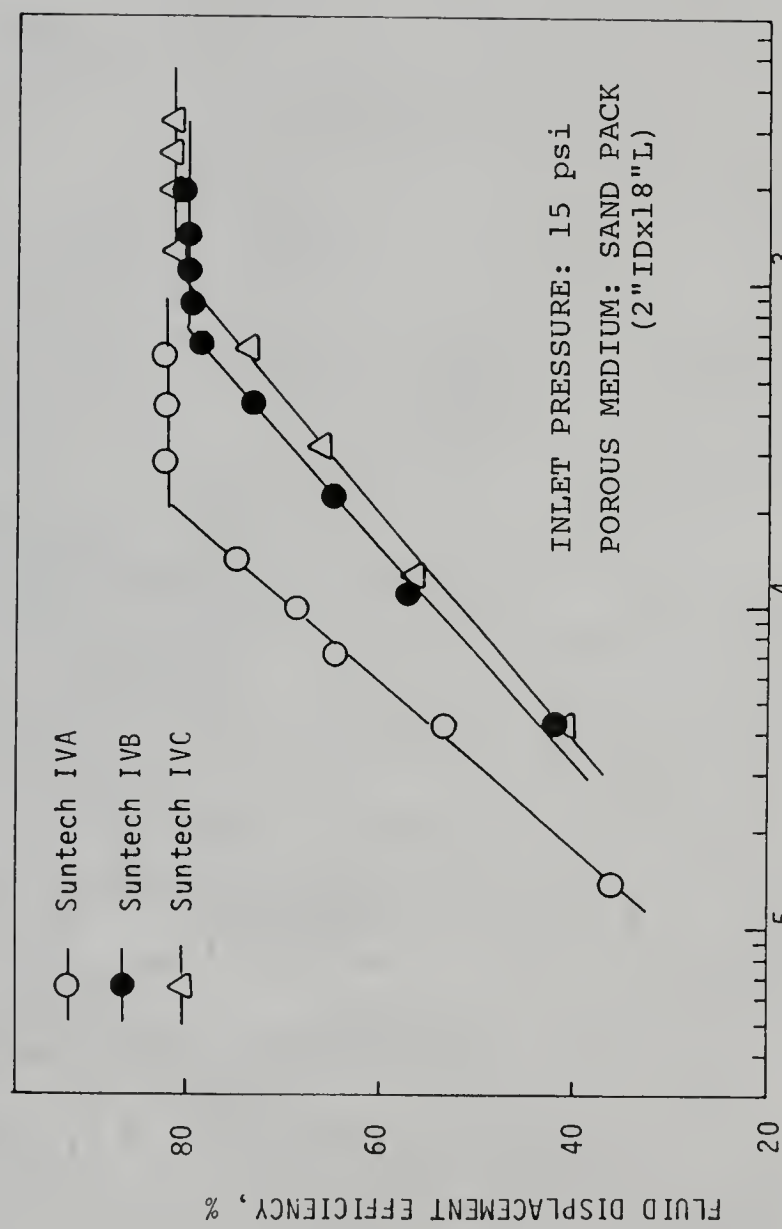

Figure 3.3. Effect of the Concentration of Suntech IV Surfactants on Fluid Displacement Efficiency.

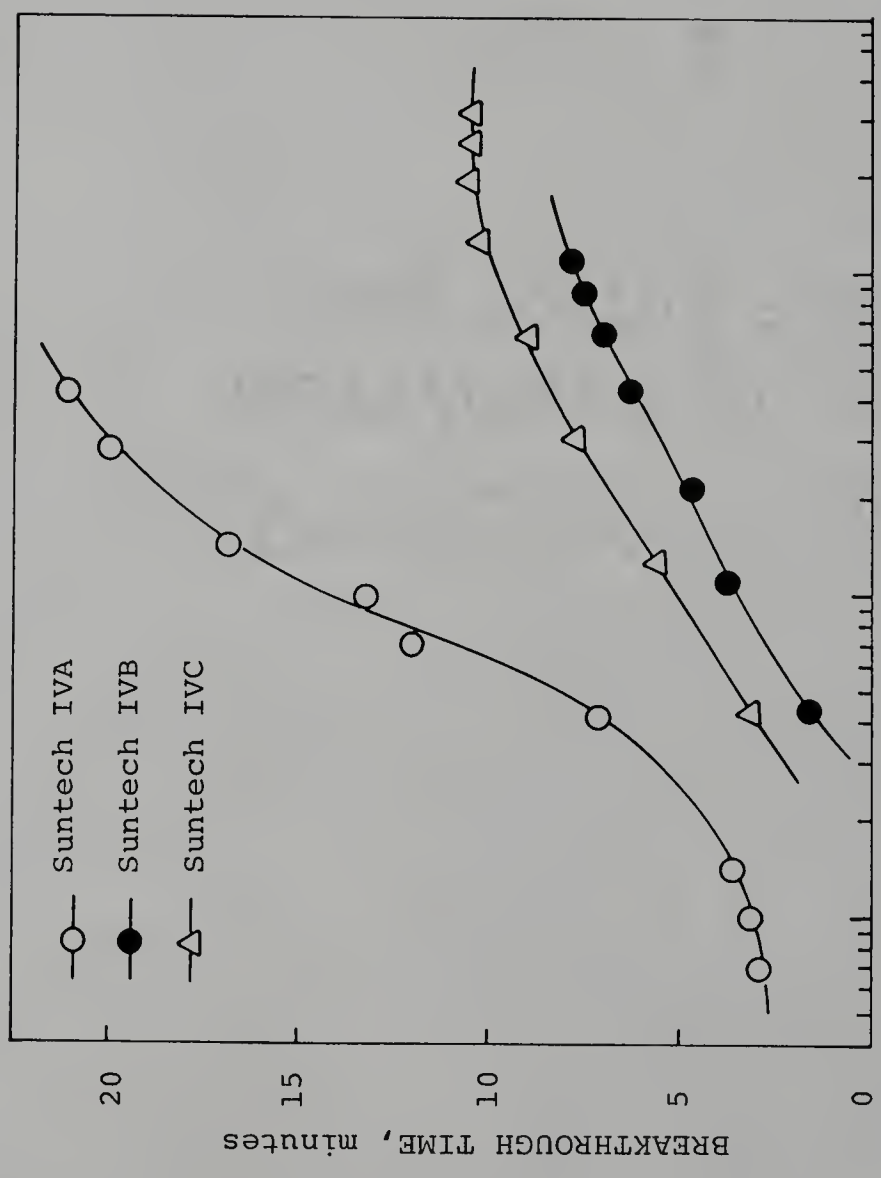

Figure 3.4. Variation in Breakthrough Time as a Function of the Concentration of Suntech IV Surfactants.

sharp increase in fluid displacement efficiency was observed below the CMC, and there was little effect on fluid displacement efficiency beyond the CMC. On the other hand, the breakthrough time continuously increased as the concentration of surfactant increased. The effective air mobility versus the concentration is shown in Figure 3.5. In general, the effective air mobility decreased with the increase of surfactant concentration. Obviously, Suntech IVA reduced air mobility to a greater extent than Suntech IVB or IVC. From previous studies on the surface properties of Suntech IVA, IVB, and IVC, it is likely that the foaming agent with the properties of lower surface tension, higher surface viscosity, and smaller bubble size reduced effective air mobility as well as increased breakthrough time in the porous medium. The structures and physical properties of the porous medium have to be considered in addition to the foam stability and surface properties of the foaming agents because they often interact with each other. Similarly, Stepanflo 40 gave the highest fluid displacement efficiency and breakthrough time of all Stepanflo surfactants (Figure 3.6). Again, these results correspond to the properties of the lowest foam quality, lowest apparent foam viscosity, and highest foaminess of Stepanflo 40. It implies that a foaming agent with the properties mentioned above can easily produce a stable in-situ foam which reduces significantly the channeling

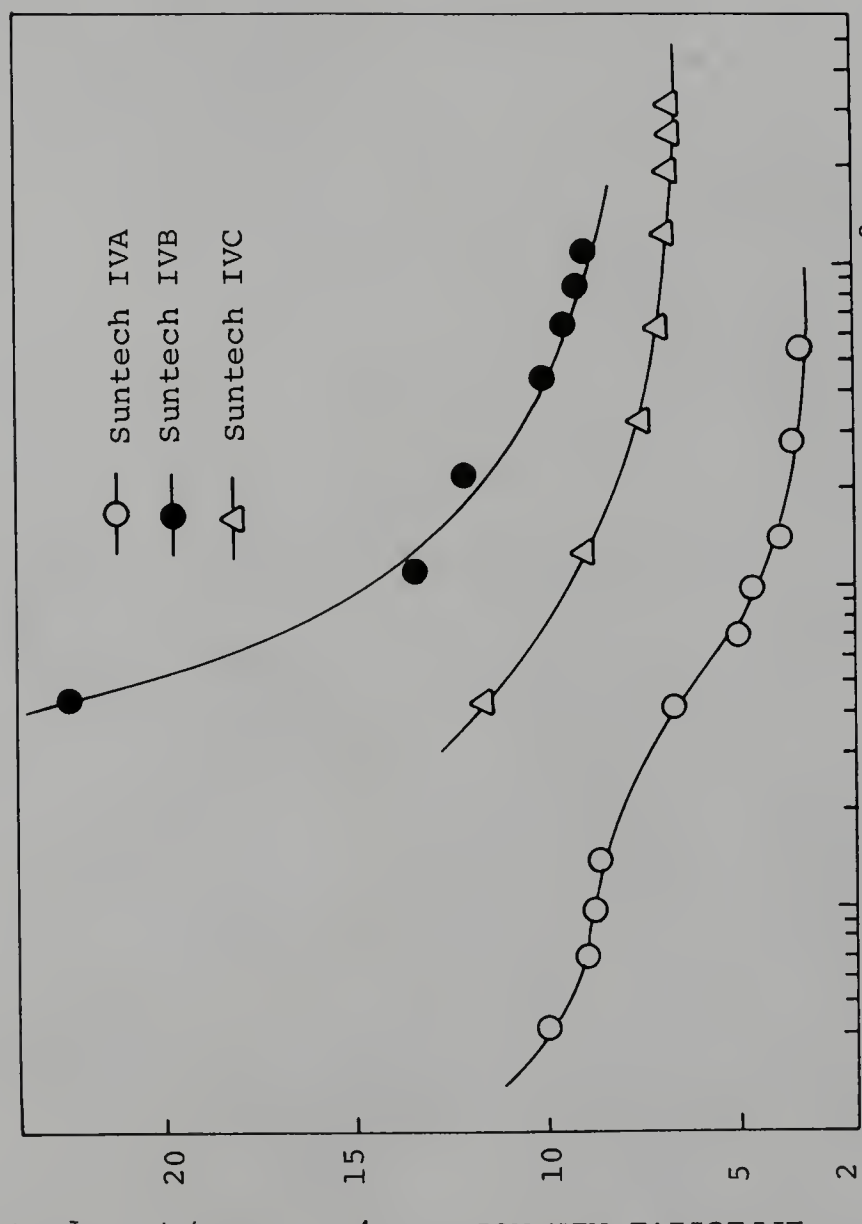

Figure 3.5. Effect of the Concentration of Suntech IV Surfactants on Effective Air Mobility.

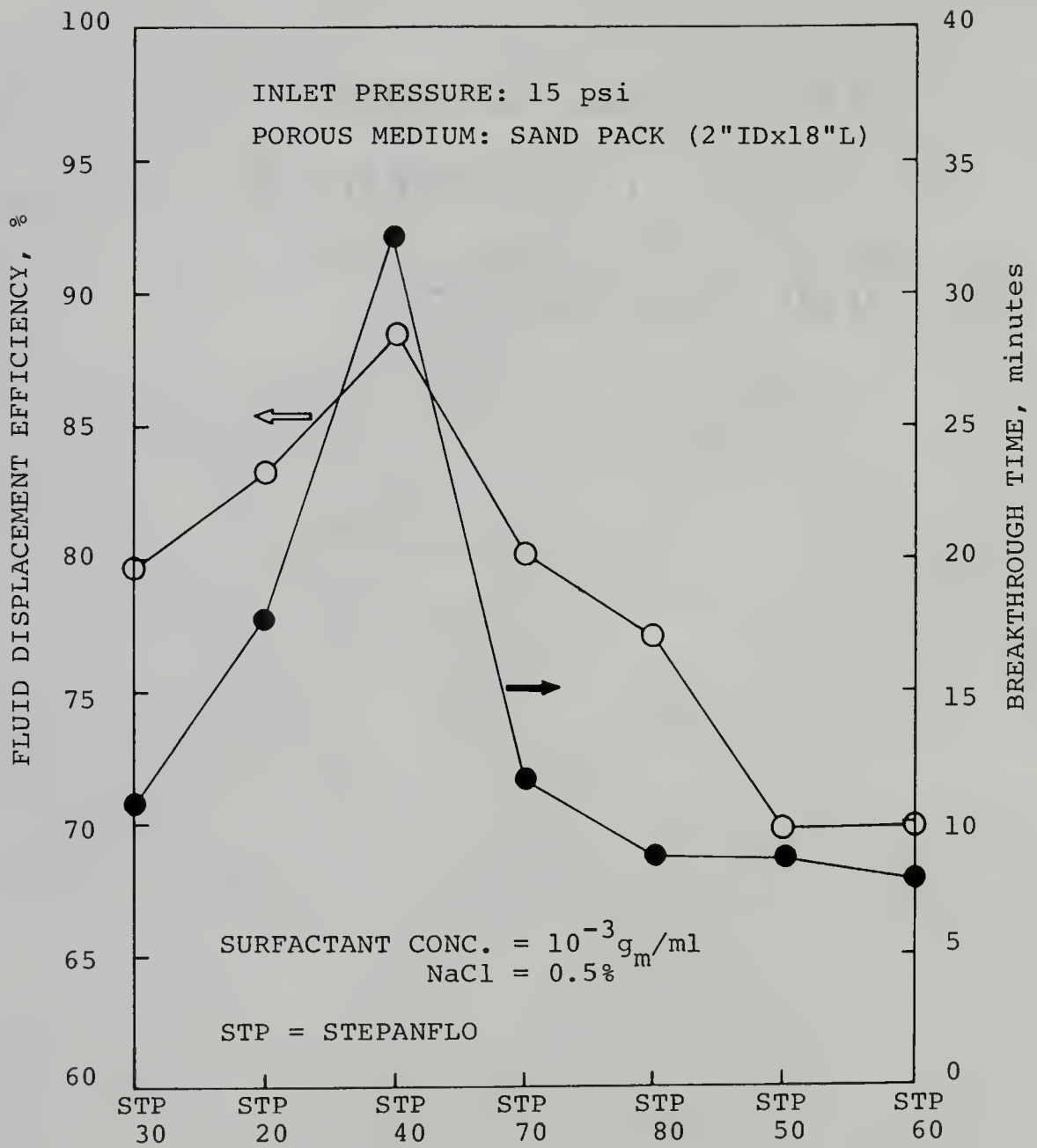

Figure 3.6. Fluid Displacement Efficiency and Breakthrough Time Produced by Stepanflo Surfactants.

effect and the gravity override of air, as well as the permeability of the porous medium to air.

In order to study the effect of chain length compatibility on fluid displacement in porous media, pure surfactant, SDS, and commercial surfactants, Stepanflo 40 and Suntech IVA, with various long chain alcohols were used as mixed foaming agents. Figures 3.7-3.10 show the fluid displacement, breakthrough time, and effective air mobility as a function of chain length of alkyl alcohols. It was observed that the fluid displacement efficiency, breakthrough time, and effective air mobility were significantly influenced by the chain length of alcohols added in SDS or Stepanflo 40 solution. But adding alkyl alcohols had little effect on Suntech IVA. As mentioned in the previous section, the number of carbon atoms in Suntech IVA molecules is between 22 and 24 and the structure of the molecules is not a straight hydrocarbon chain. It was expected that the addition of long chain alcohols would have little effect on the surface properties of mixed surfactants and the fluid displacement in porous media. Experimental results indeed showed that the fluid recovered by Suntech IVA with various alkyl alcohols was the same or even lower than that of Suntech IVA without adding alcohols.

For Stepanflo 40, the fluid displacement efficiency increased from 84% to 90% with the increase of hydrocarbon chain length of alcohols from C_8 to C_{10}, respectively.

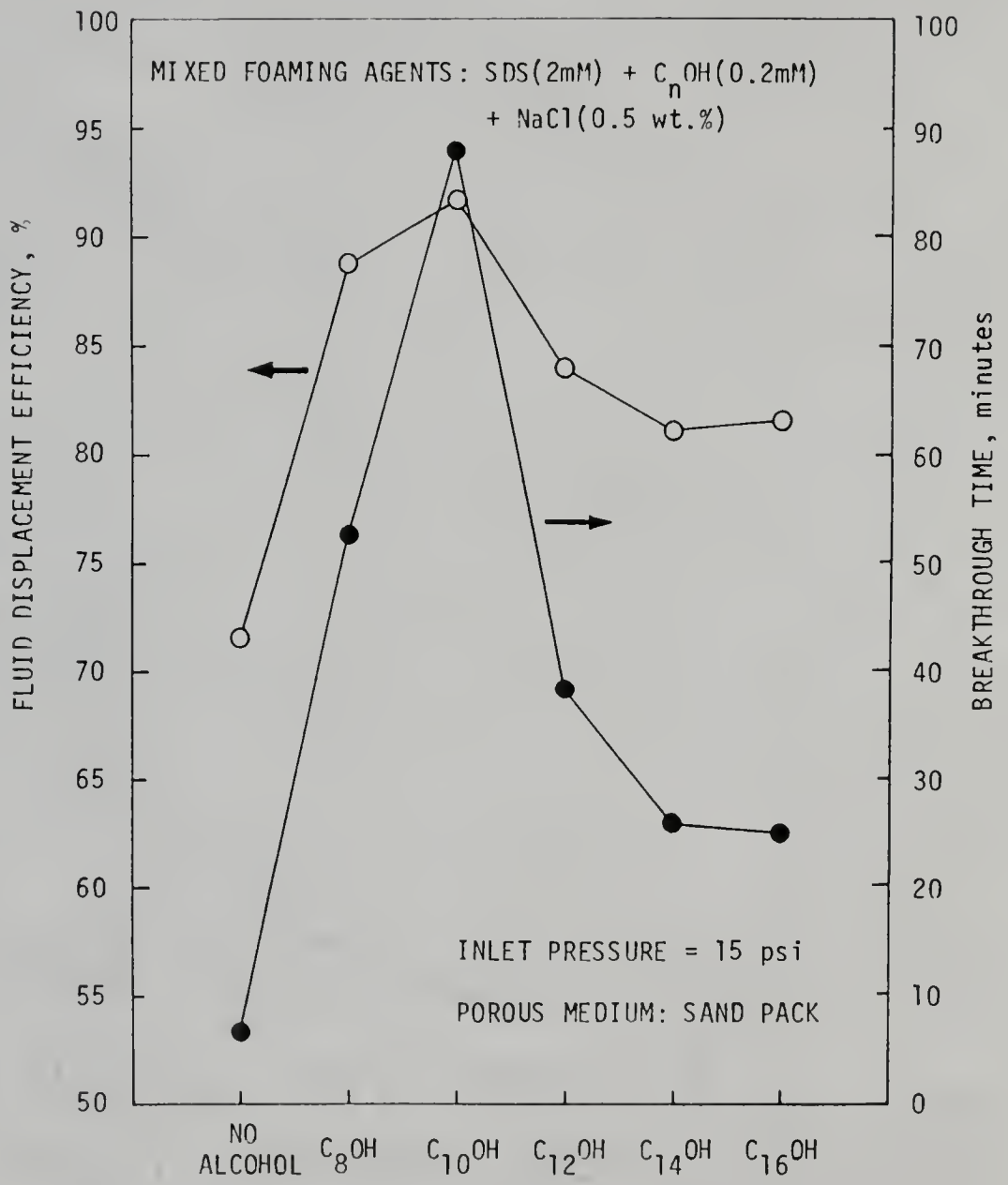

Figure 3.7. Effect of SDS with Different Alkyl Alcohols on Fluid Displacement Efficiency and Breakthrough Time.

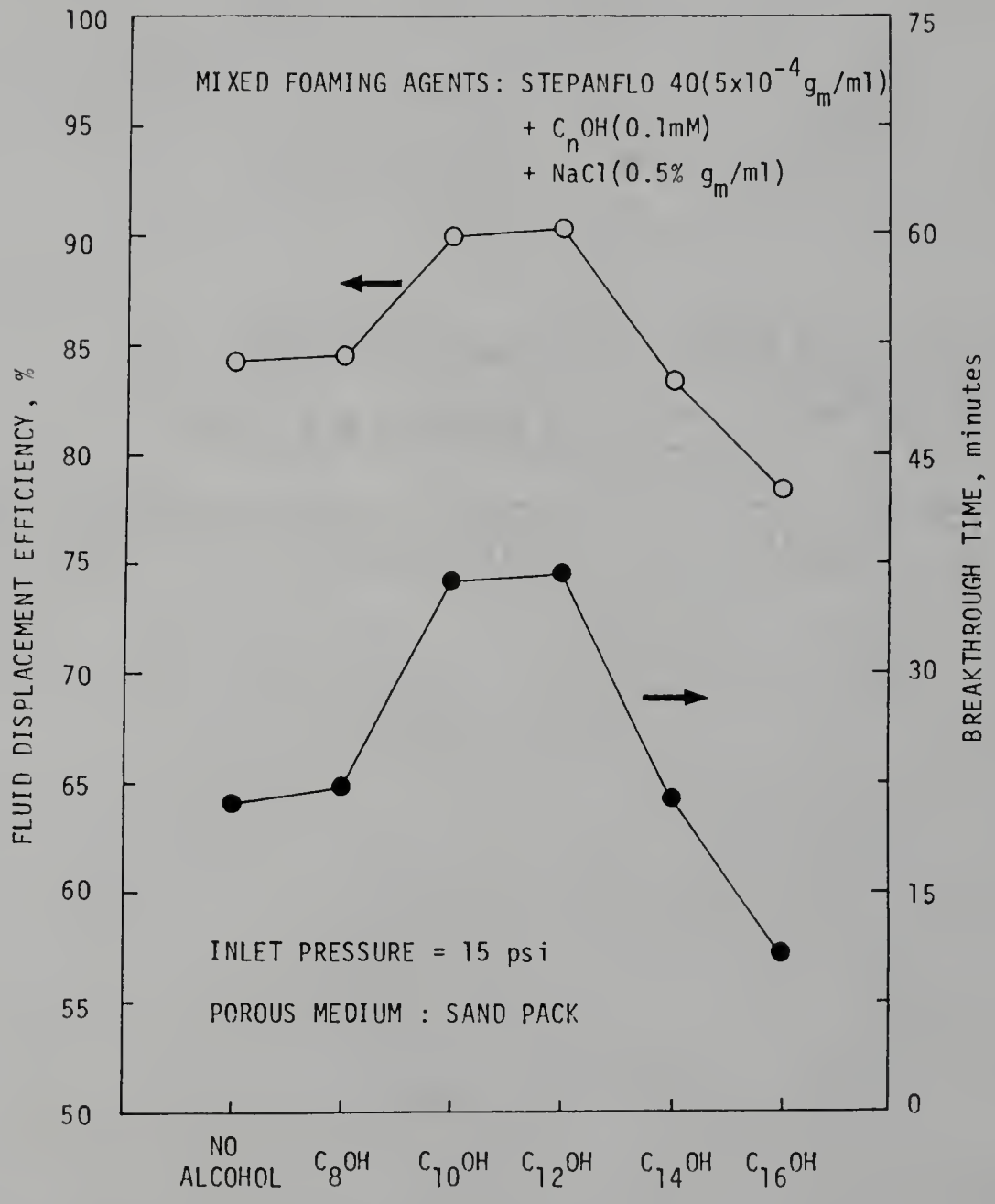

Figure 3.8. Effect of Stepanflo 40 with Different Alkyl Alcohols on Fluid Displacement Efficiency and Breakthrough Time.

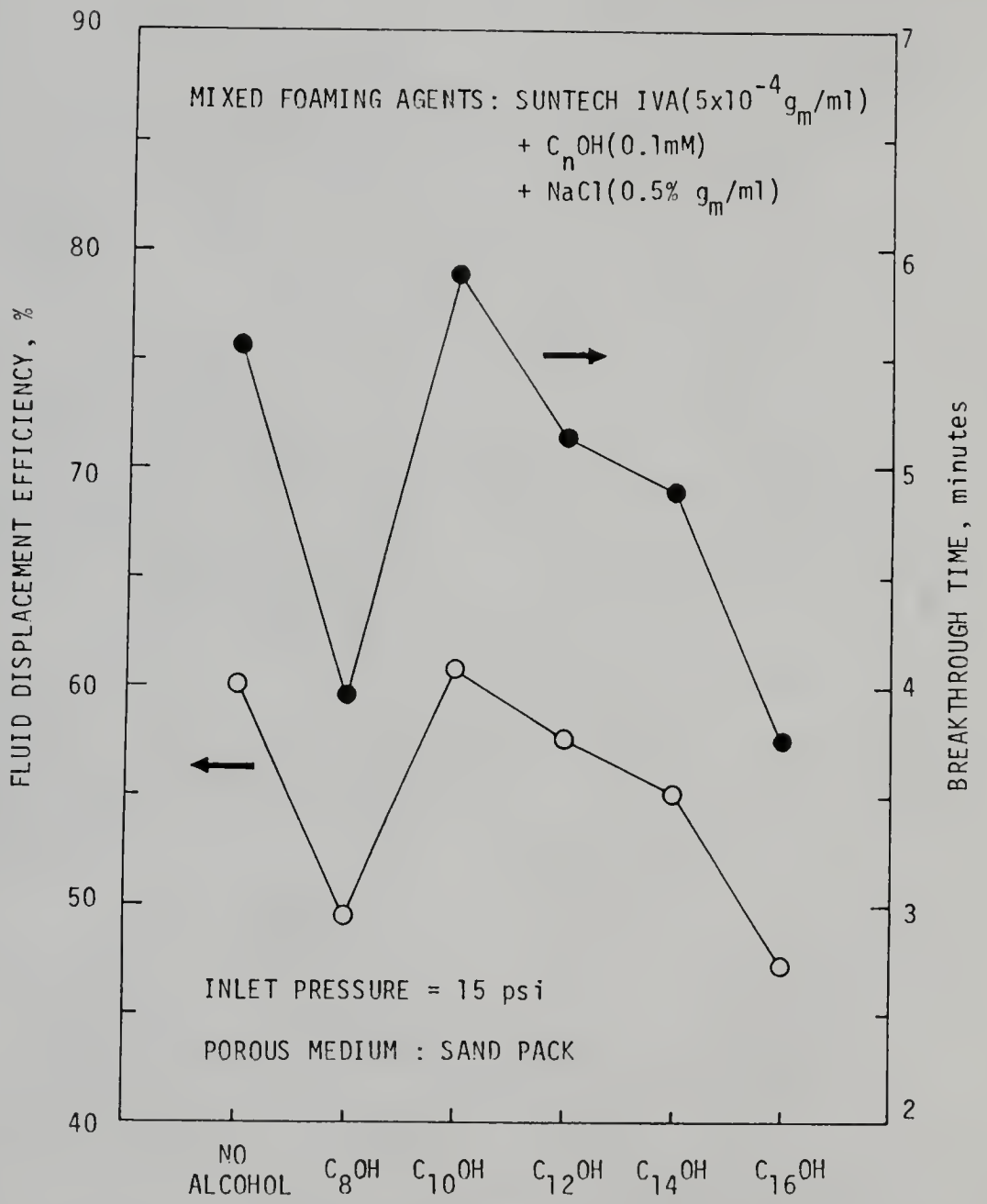

Figure 3.9. Effect of Suntech IVA with Different Alkyl Alcohols on Fluid Displacement Efficiency and Breakthrough Time.

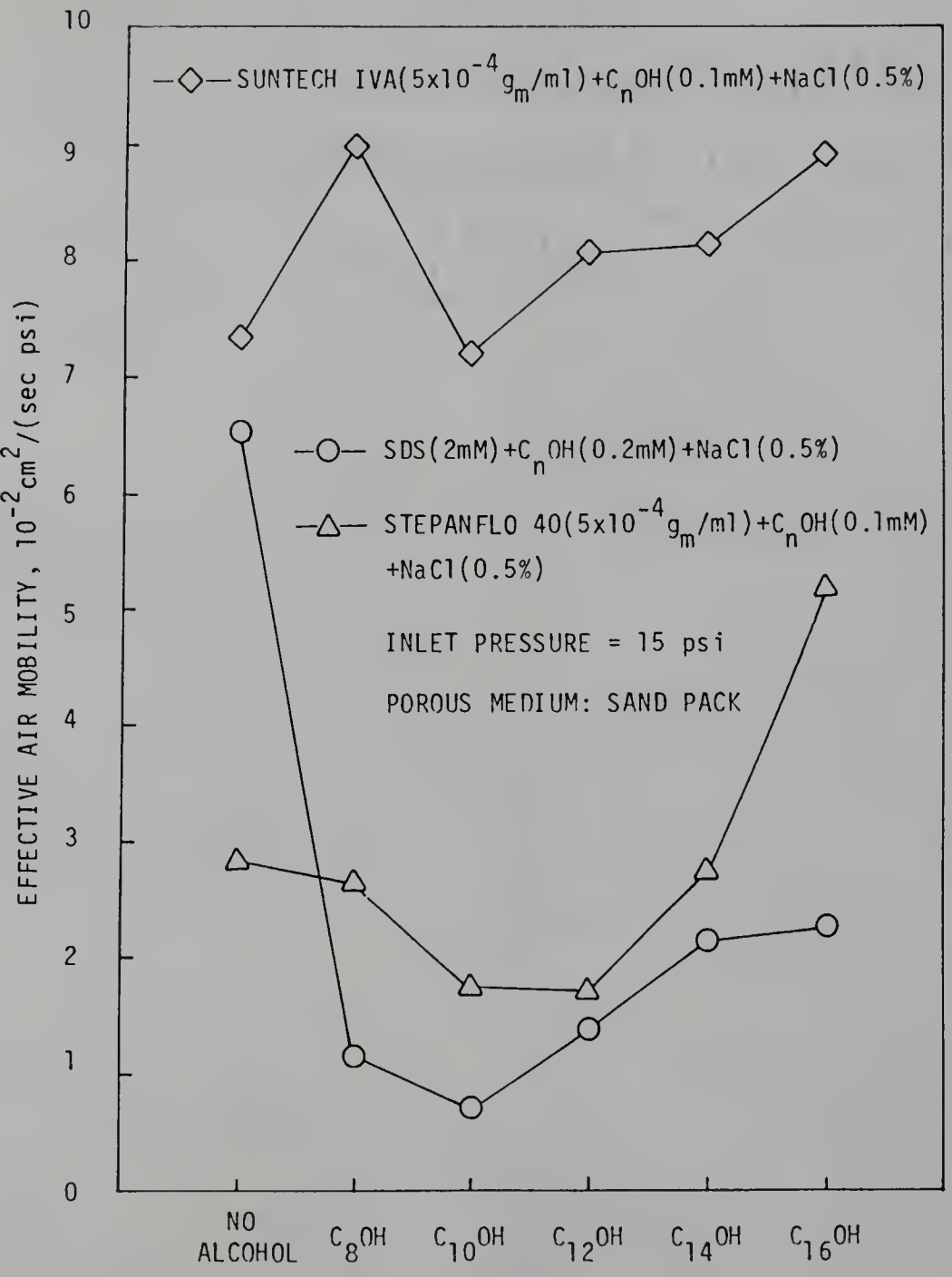

Figure 3.10. Effect of Surfactants with Different Alkyl Alcohols on Effective Air Mobility.

There was almost the same effect on fluid displacement by adding decyl or dodecyl alcohol in Stepanflo 40 solution. The breakthrough time and effective air mobility were also found to be maximum and minimum, respectively when decyl or dodecyl alcohol was added in the Stepanflo 40 solution. Interestingly, the efficiency became lower and the air mobility became higher by adding $C_{16}OH$ as compared to the system without adding any alcohol. According to the bubble size distribution measurements, the smallest average bubble size and the least foam production were observed for the system of Steapnflo 40 + $C_{16}OH$. This implies that the high foam stability observed outside porous media need not correspond to a high fluid displacement in porous media. Under a constant inlet pressure, the amount of foam generated in the porous medium is so small that is not enough to block all the channels, which in turn leads to an early air breakthrough. Meanwhile, from the foam quality study, the foam generated by adding hexadecyl alcohol was even dryer than that without adding any alcohol. It seems that foam quality has a greater effect on the fluid displacement in the porous medium than the other surface properties. Although the major components and molecular structure of Stepanflo 40 are unknown, it appears that the chain length of alkyl alcohols does affect the molecular packing at the liquid/air interface and surface properties of foaming solutions as well as fluid displacement in porous media.

Experimental results (Figure 3.7 and 3.10) for the mixed foaming agents, SDS + C_nOH (n=8, 10, 12, 14, and 16), showed that the fluid displacement efficiency and breakthrough time were at maximum and the effective air mobility was at a minimum when the system consisted of SDS and decyl alcohol. This is contrary to the theory of chain length compatibility which predicts that these extrema should occur when both components of the mixed foaming system have the same chain length (i.e., SDS + $C_{12}OH$). In this respect, the results differ from Sharma's reports [21,32,33]. The same experiments described in Sharma's work were repeated and the results are shown in Figure 3.11. It is clear that the same trend was observed as was seen in this work. That is to say, both the fluid displacement efficiency and the breakthrough time increased with the increase of hydrocarbon chain length of alcohols from C_8 to C_{10}, then suddenly decreased as chain length increased further. The effective air mobility had a reverse profile which showed that the lowest air mobility was found using SDS + $C_{10}OH$. The maximum efficiency obtained by using SDS + $C_{10}OH$ + NaCl mixture was up to 91% (Figure 3.7). The effective air mobility doubled and tripled as the chain length of alcohols increased from C_{10} to C_{12} and C_{10} to C_{14}, respectively (Figure 3.10).

The results of this study on the surface properties of the mixed foaming agents, SDS + C_nOH, are summarized in Table 3.1. Although the system of SDS + $C_{12}OH$ possesses a

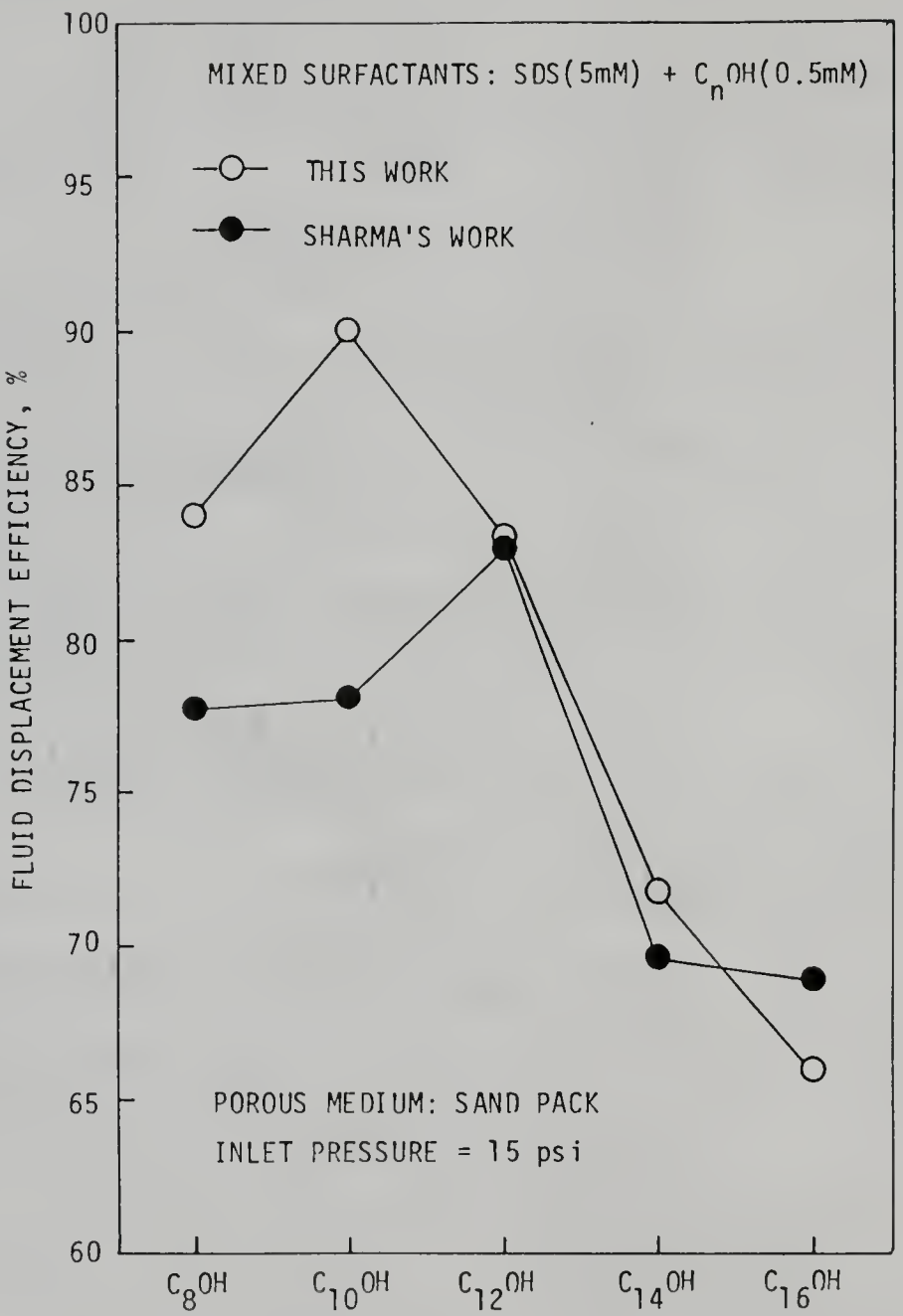

Figure 3.11. Comparison of Fluid Displacement Efficiency Using SDS(5mM)+C_nOH(0.5mM) with Sharma's Results.

Table 3.1 Summary of the Surface Properties of the Mixed Foaming Agents of SDS with Different Alkyl Alcohols.

Measurements	System with extreme
Surface Tension	minimum found for SDS+C_{12}OH
Surface Viscosity	maximum found for SDS+C_{12}OH [33]
Foaminess	maximum found for SDS+C_{12}OH or SDS+C_{10}OH
Foam Quality	minimum found for SDS+C_{10}OH
Apparent Foam Viscosity	minimum found for SDS+C_{10}OH or SDS+C_{12}OH
Rate of Drainage	minimum found for SDS+C_{12}OH or SDS+C_{14}OH
Average Bubble Size	minimum found for SDS+C_{16}OH
Bubble Size of in-situ Foam in a Micromodel	minimum found for SDS+C_{12}OH
Fluid Displacement Efficiency	maximum found for SDS+C_{10}OH
Breakthrough Time	maximum found for SDS+C_{10}OH
Effective Air Mobility	minimum found for SDS+C_{10}OH

minimum in surface tension, a maximum in surface viscosity, a maximum in foaminess, and a minimum in bubble size of in-situ foam, it does not yield a maximum in fluid displacement efficiency and breakthrough time. Possible explanations for these experimental results are given as follows. The energy required to generate a unit volume of foam may increase with the increase of hydrocarbon chain length of alcohols in surfactant solution. The higher the required energy, the lesser the volume of foam produced for a given concentration of foaming agent. Therefore, under constant pressure, the highest fluid displacement efficiency for a specified porous medium depends on the volume of foam generated in-situ, foam stability, and the bubble size relative to the pore size.

3.4.2 Fluid Displacement in Heterogeneous Porous Media with Foaming Agents

In order to determine the effect of in-situ foam on blocking low permeability porous media, the fluid displacement experiments were performed as described in the experimental section. The results of experiments without foam indicate that about 10% of the fluid can be recovered from the low permeability porous medium (i.e., Berea core). This implies that the most of air passes through the high permeability porous medium and only a small portion of air passes through low permeability zone. The fluid displacement efficiency as a function of surfactant

concentration is shown in Figure 3.12. It is clear that the concentrations of Suntech IVA up to 0.0075% (g_m/ml) have little effect on fluid displaced from low permeability zone (i.e., Berea core) in the heterogeneous porous media. As the concentration of surfactant was increased, a sharp increase in fluid displacement efficiency from the low permeability zone was observed up to a concentration of 0.02% (g_m/ml) and beyond this concentration the fluid displacement did not increase significantly.

Assuming that foams lose their macroscopic properties in channels which are smaller than ten bubble diameters, Dietz [83] reported that for the foams with quality higher than 0.8, the foam can be considered as a homogeneous fluid only if the permeabilities of the porous media exceed 800 millidarcy. The permeability of Berea core used in this experiment was about 275 millidarcy. Experimental results showed that foams were generated in-situ and "flowed" through a low permeability zone. This implies that a two-phase flow of "foam" exists in low permeability porous media and this flow can not be described by quasi-single-phase flow of a foam showing the same flow behavior as measured outside the porous media.

It appears from these results that the foam generated in-situ by a Suntech IVA concentration of up to 0.0075% is not able to provide enough resistance to air flow. Therefore, the air passes through the high permeability channels of the porous media up to the concentration of

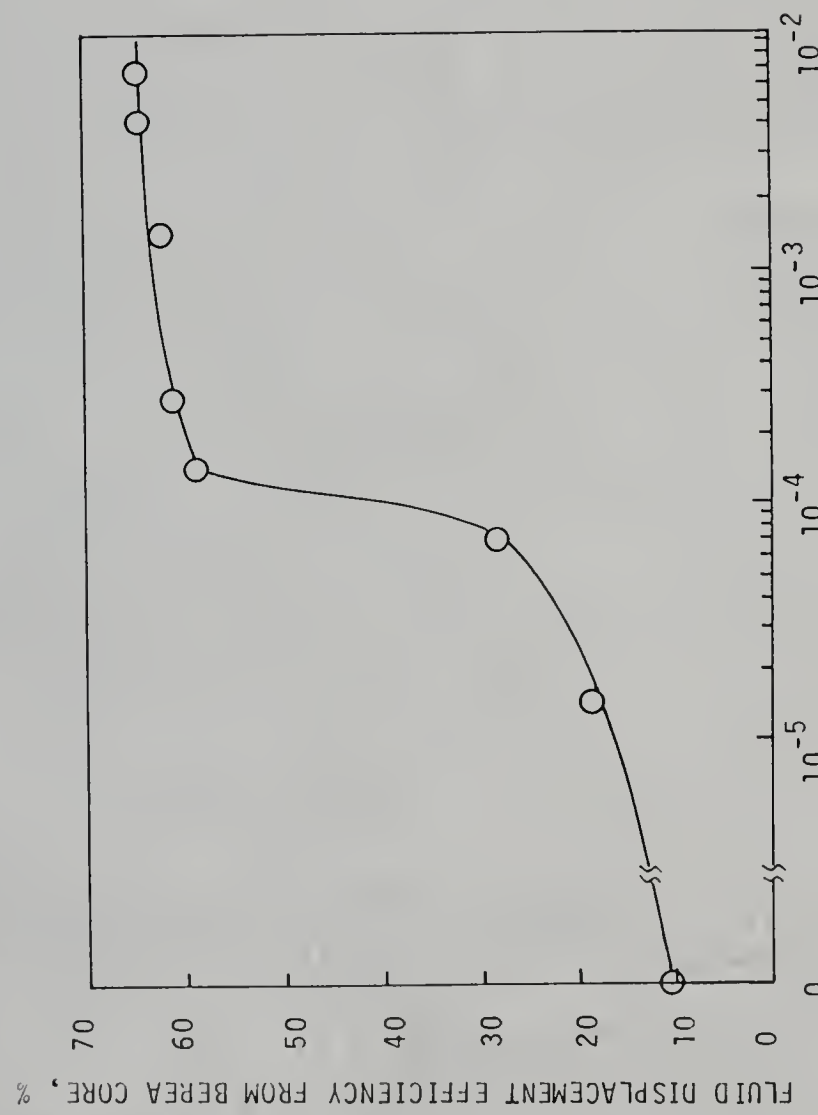

Figure 3.12. Fluid Recovery from Berea Core in Heterogeneous Porous Media versus Concentration of Suntech IVA.

0.0075%. Beyond this concentration, the surfactant films are stable enough to provide resistance to the air flow as well as produce large number of lamellae to displace fluid from additional pores. A Suntech IVA concentration close to the CMC can enhance the efficiency of fluid displacement from low permeability porous media from 10% to 60%. This improvement in fluid displacement efficiency in the presence of foam suggests that the foams can be used to divert gas or steam from high permeability zones to low permeability zones in heterogeneous porous media.

The total fluid recovery from Berea core as a function of SDS concentration mixed with the same concentration of salt (0.5%) and alkyl alcohols (1 mM) is shown in Figure 3.13. In general, the fluid displacement in heterogeneous porous media had the same trend as that in the homogeneous porous medium. For mixed surfactants of SDS and decyl alcohol, the concentration of SDS up to 0.01% (g_m/ml) did not have much effect on fluid displacement from Berea core. For all other mixed surfactant systems, this minimum concentration was 0.02% (g_m/ml). As the concentration increased, a sharp increase in fluid displacement efficiency in the low permeability zone (i.e., the Berea core) was observed at 0.01% and 0.02% (g_m/ml) for SDS+C_{10}OH system and the rest of mixed surfactant systems, respectively. The maximum efficiency (70%) was obtained using the mixed system of SDS+C_{10}OH.

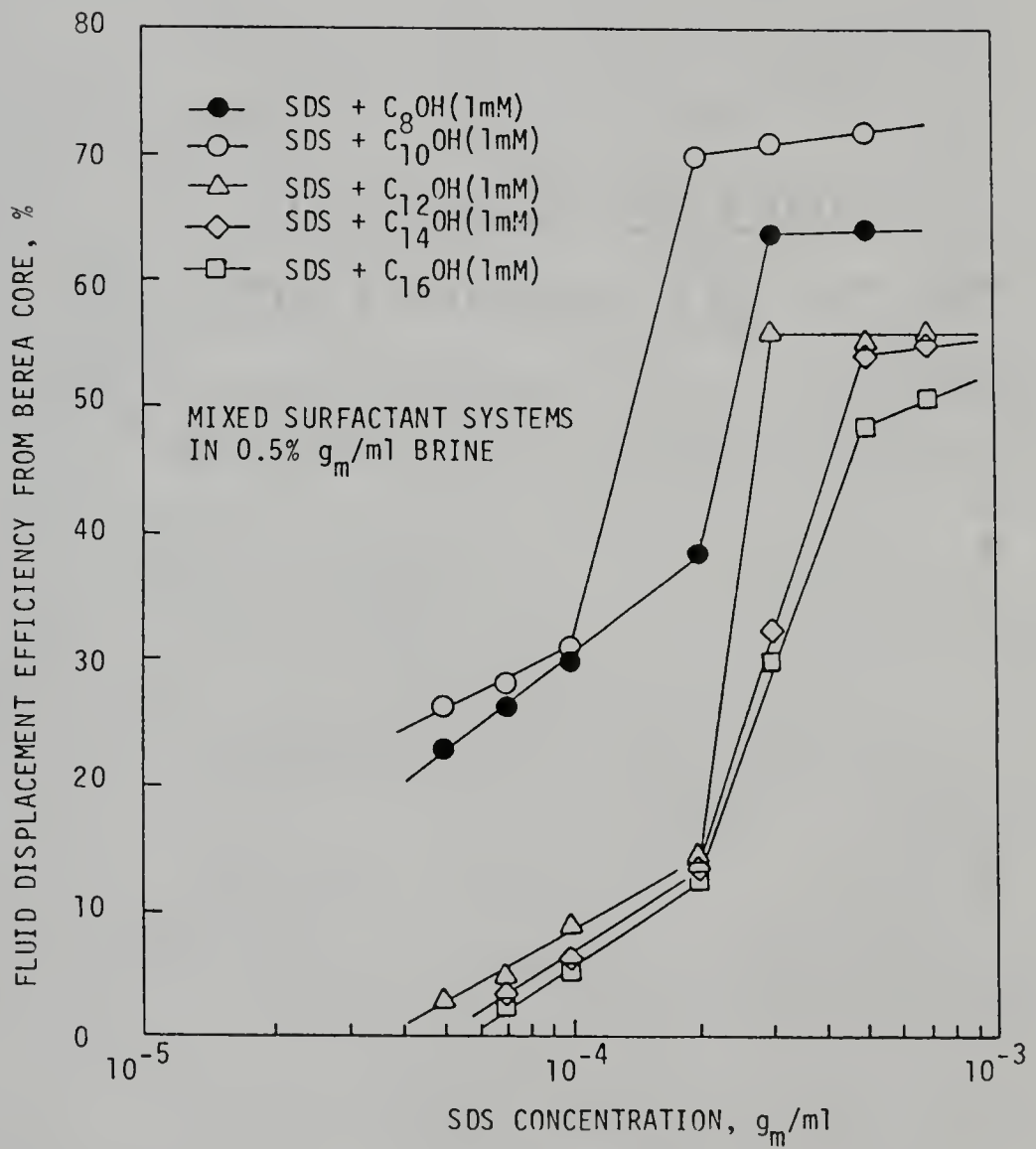

Figure 3.13. Fluid Recovery from Berea Core in Heterogeneous Porous Media as a Function of SDS Concentration Mixed with Alkyl Alcohols and Salt.

One interesting phenomenon observed (Figures 3.14-3.16) was that the highest fluid displacement efficiency and breakthrough time as well as the lowest effective air mobility were found for the sand pack rather than sand pack with the Berea core or with the stainless steel core. It may be concluded that at the constant inlet pressure, foam can displace more liquid from a homogeneous porous medium than it does in a heterogeneous porous media. It should be noted that the fluid displacement in porous media by in-situ foam is very sensitive to the applied pressure. Because the pressure may determine the mechanism of foam flow in porous media. Owete [84] has shown that there was an optimum pressure under which the highest fluid displacement efficiency was obtained from two parallel sand packs with different permeabilities. Only at this optimum pressure foam will invade and block most of the channels of the heterogeneous porous media, producing the highest fluid displacement efficiency.

3.4.3. Effect of Slug Size on Fluid Displacement in Porous Media

Figure 3.17 shows the variation in fluid displacement efficiency in the heterogeneous porous media versus volume of injected surfactant solution. The results indicate that there was no appreciable change in fluid displacement efficiency beyond 0.5 pore volume (PV) slug size. The breakthrough time did not show the same behavior as the

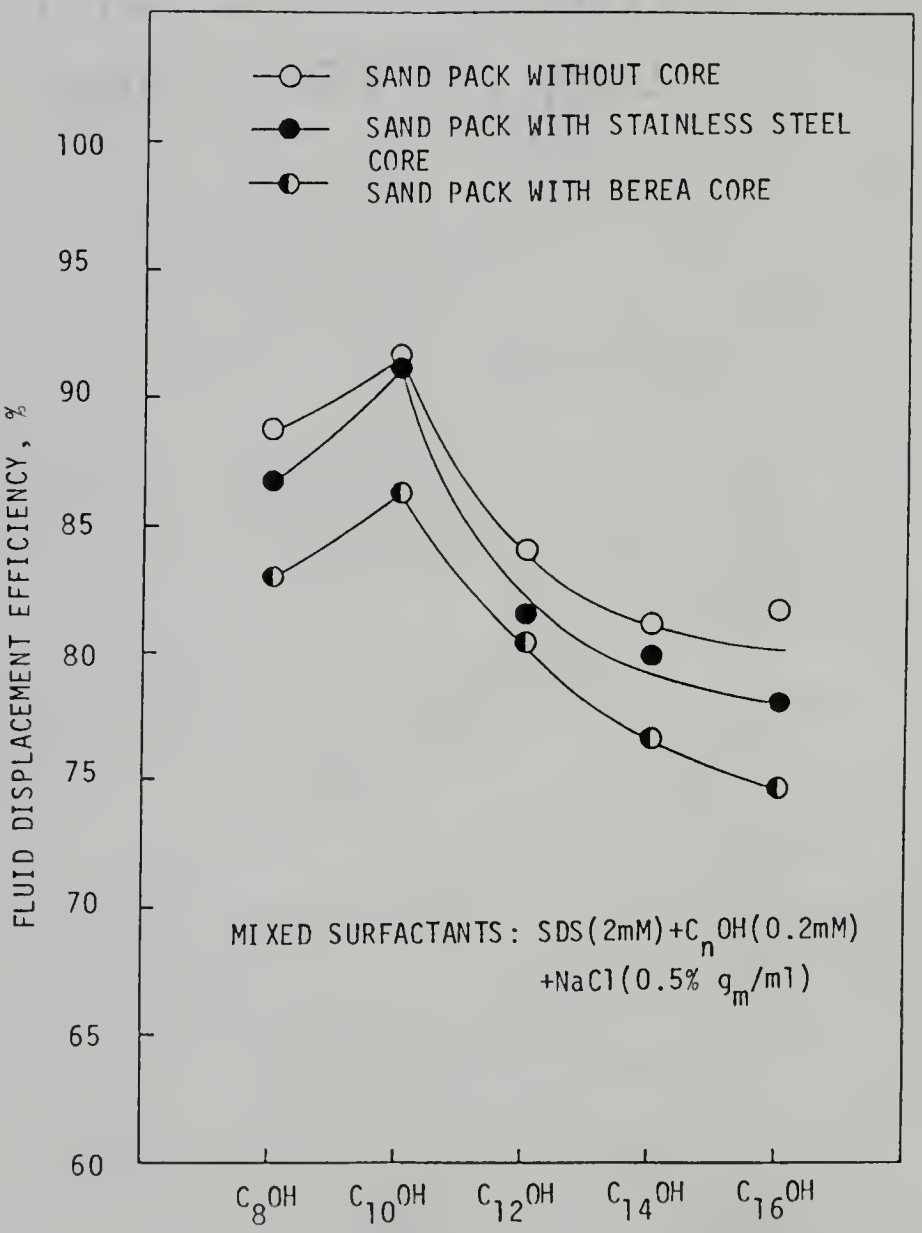

Figure 3.14. Effect of SDS with Different Alkyl Alcohols on Fluid Displacement Efficiency in Various Porous Media.

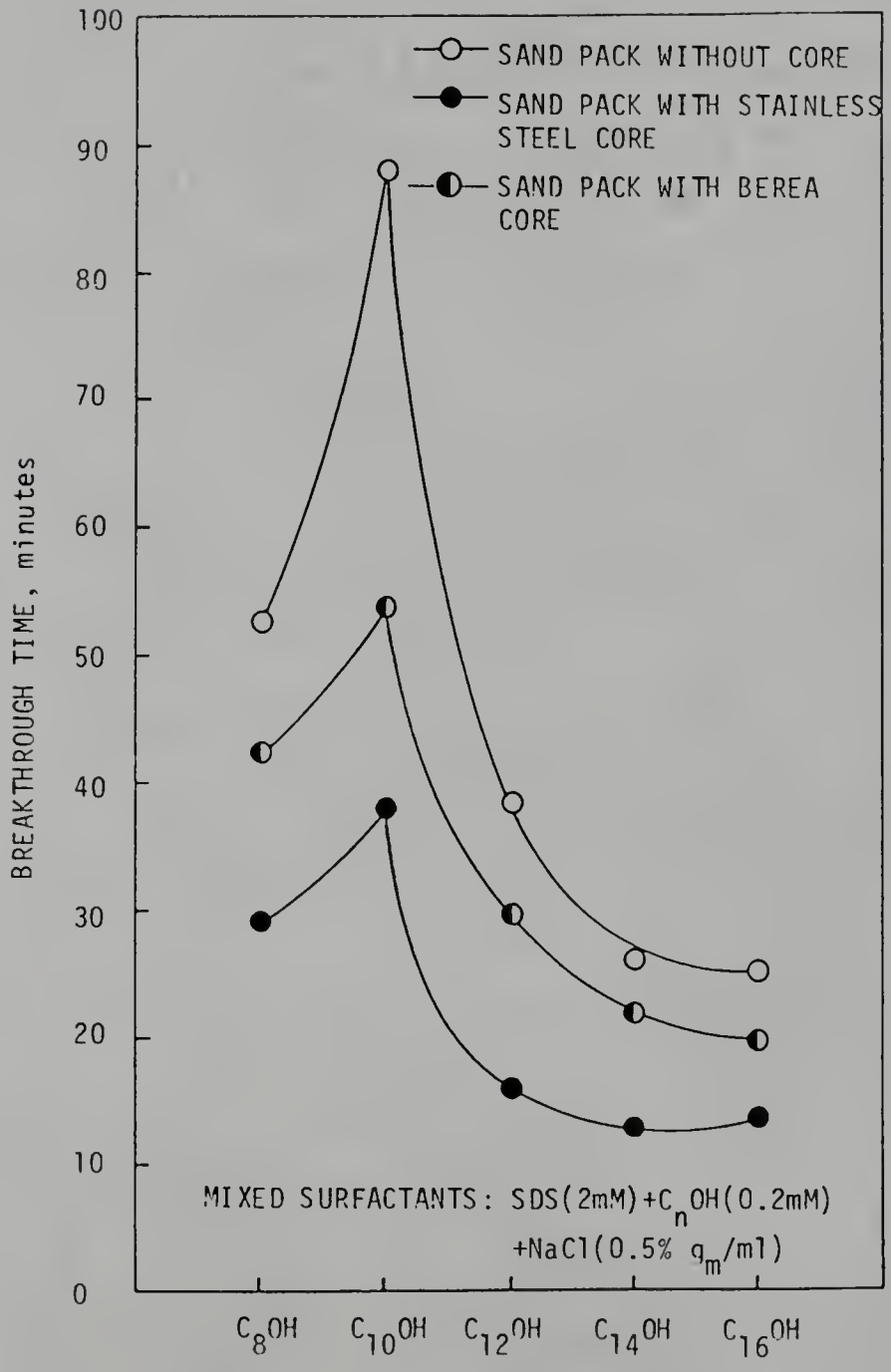

Figure 3.15. Effect of SDS with Different Alkyl Alcohols on Breakthrough Time in Various Porous Media.

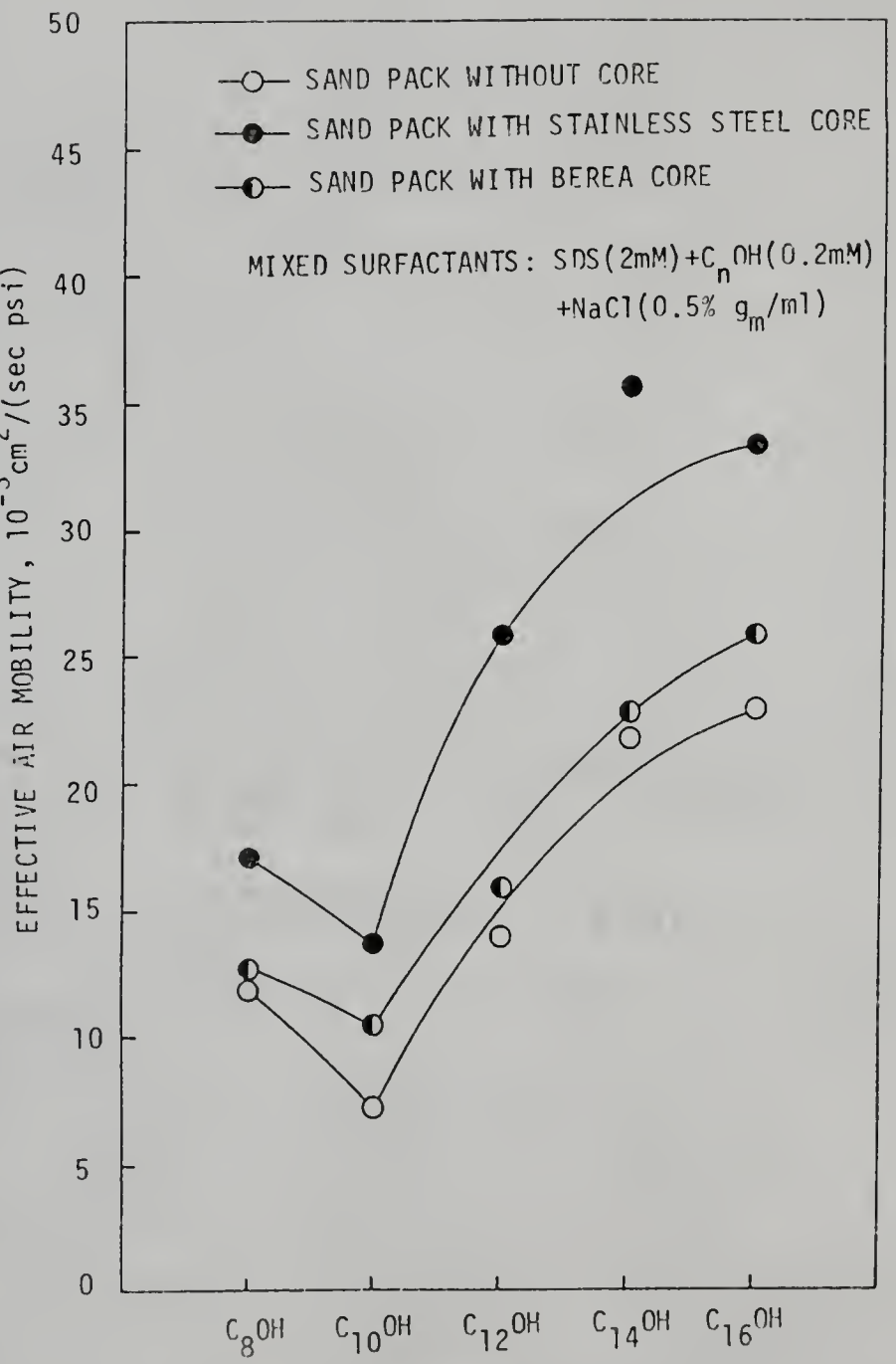

Figure 3.16. Effect of SDS with Different Alkyl Alcohols on Effective Air Mobility in Various Porous Media.

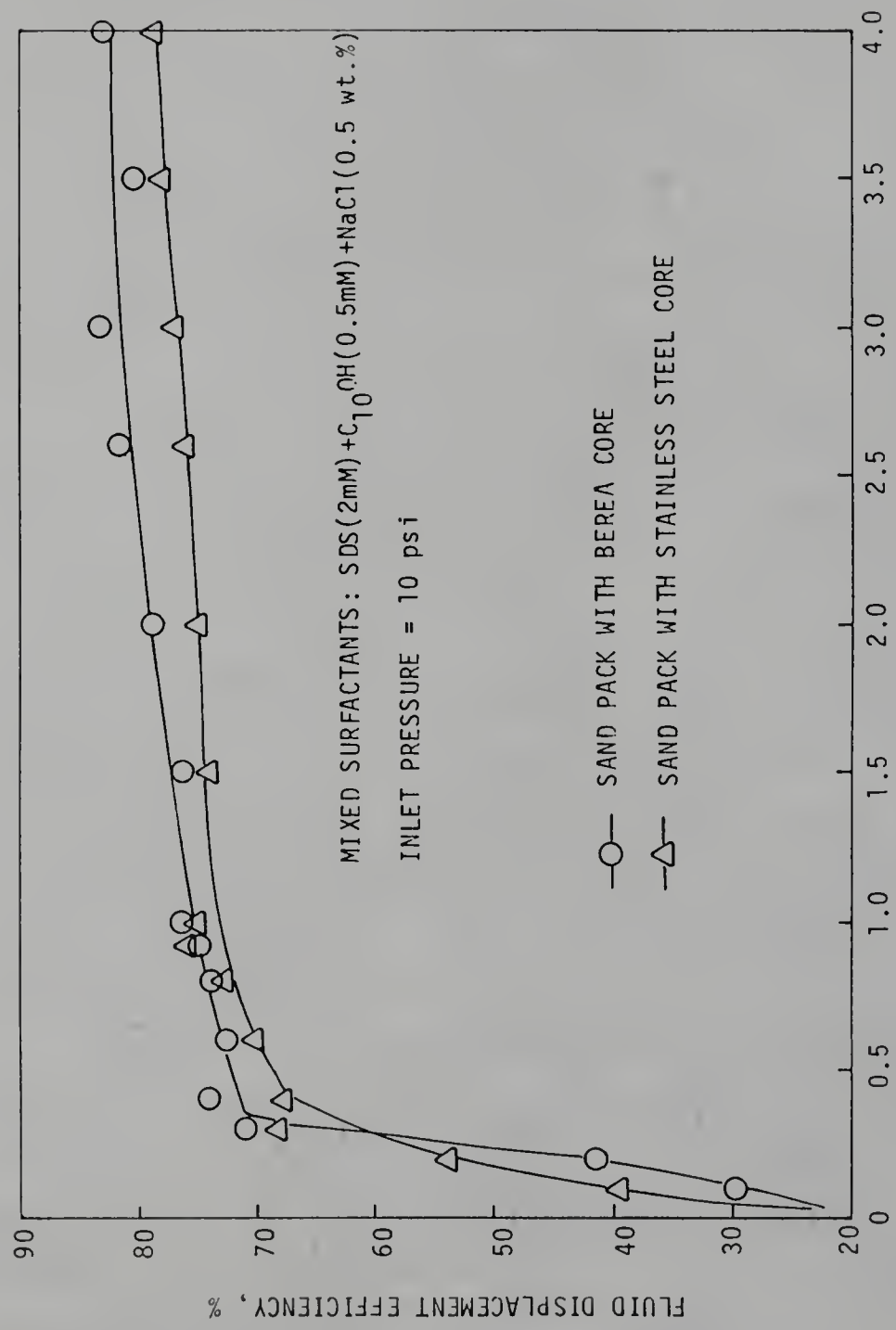

Figure 3.17. Variation in Fluid Displacement Efficiency as a Function of the Volume of Surfactant Solution Injected into Various Porous Media.

fluid displacement efficiency with respect to injected slug size (Figure 3.18). The breakthrough time increased with the increase of the slug size until 3.0 PV. The long breakthrough time is due to the high elasticity and stability of the in-situ foam which may result from adsorption/desorption of decyl alcohol molecules on sand particles. This high elasticity, stability foam can only be produced at a certain surfactant/alcohol concentrations. In practice, any slug size between 0.6 PV and 3.0 PV may give rise to a good fluid displacement as well as a good air mobility control.

The total fluid recovery from Berea core as a function of slug size is shown in Figure 3.19. A slug size of up to 0.3 PV had little effect on the fluid recovery from Berea core. The fluid displacement efficiency did not increase significantly when the slug size were larger than 0.5 PV. These results reveal that the foam generated in-situ does pass through the low permeability zone.

3.4.4 Pressure Distribution in Porous Media during the Foam Flooding Process

During the foam flooding process, it was observed that the pressure at a fixed point decreased as time increased before the front of foam approached this point (Figure 3.20). The pressure at a fixed point was measured as the difference between the point's absolute pressure and atmospheric pressure. The minimum pressure was observed

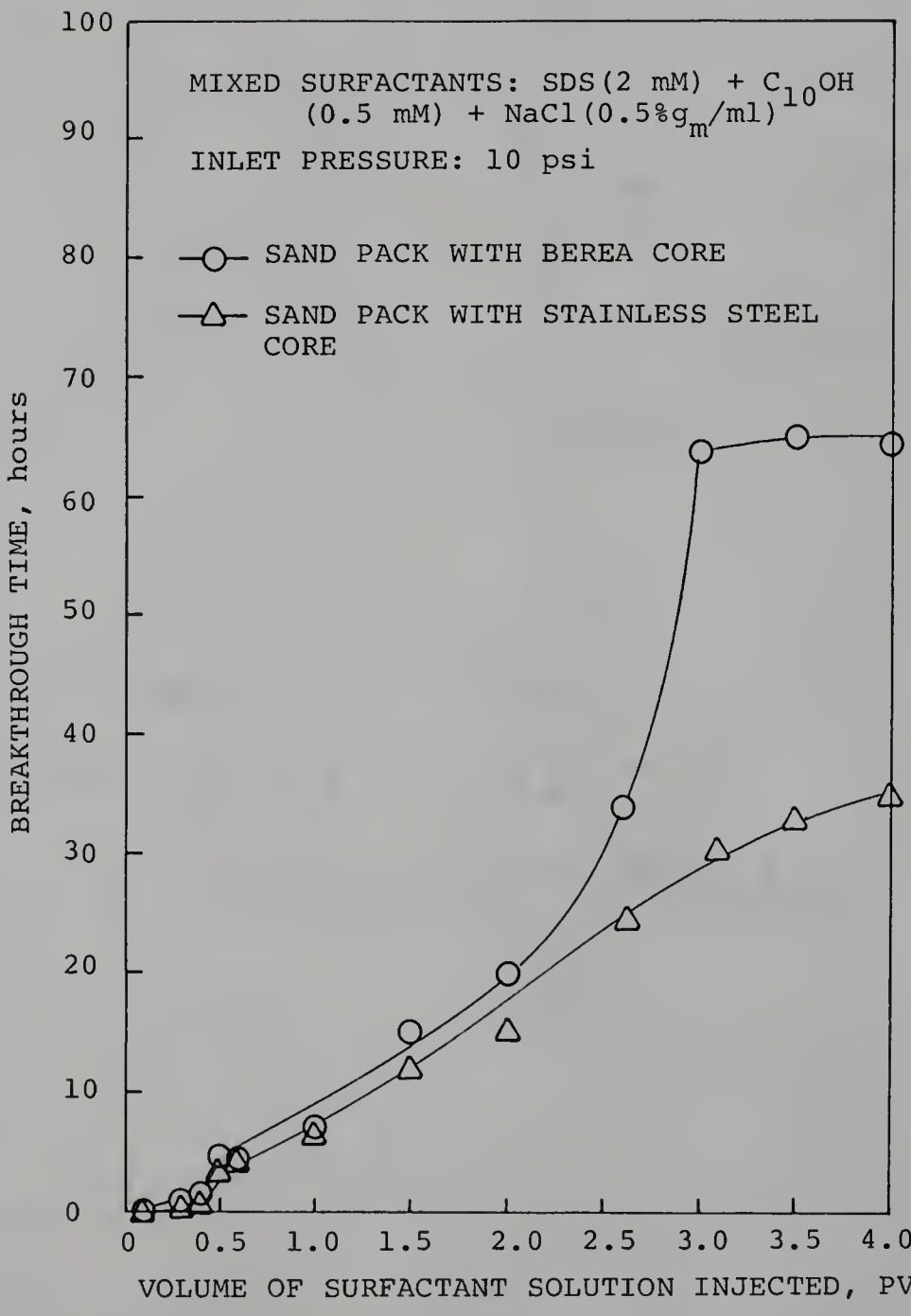

Figure 3.18. Variation in Breakthrough Time as a Function of the Volume of Surfactant Solution Injected into Various Porous Media.

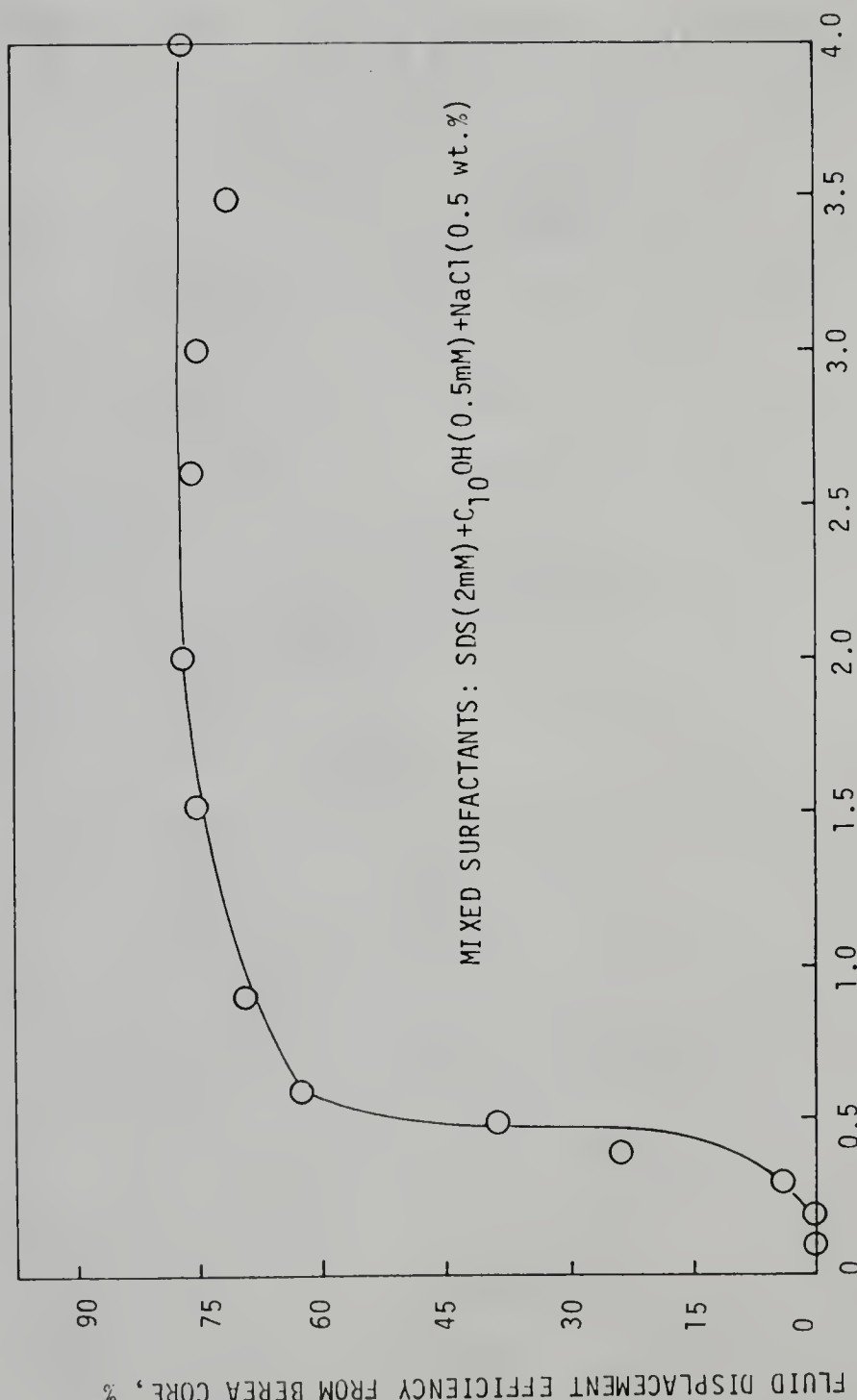

Figure 3.19. Fluid Recovery from Berea Core as a Function of the Volume of Surfactant Solution Injected into Heterogeneous Porous Media.

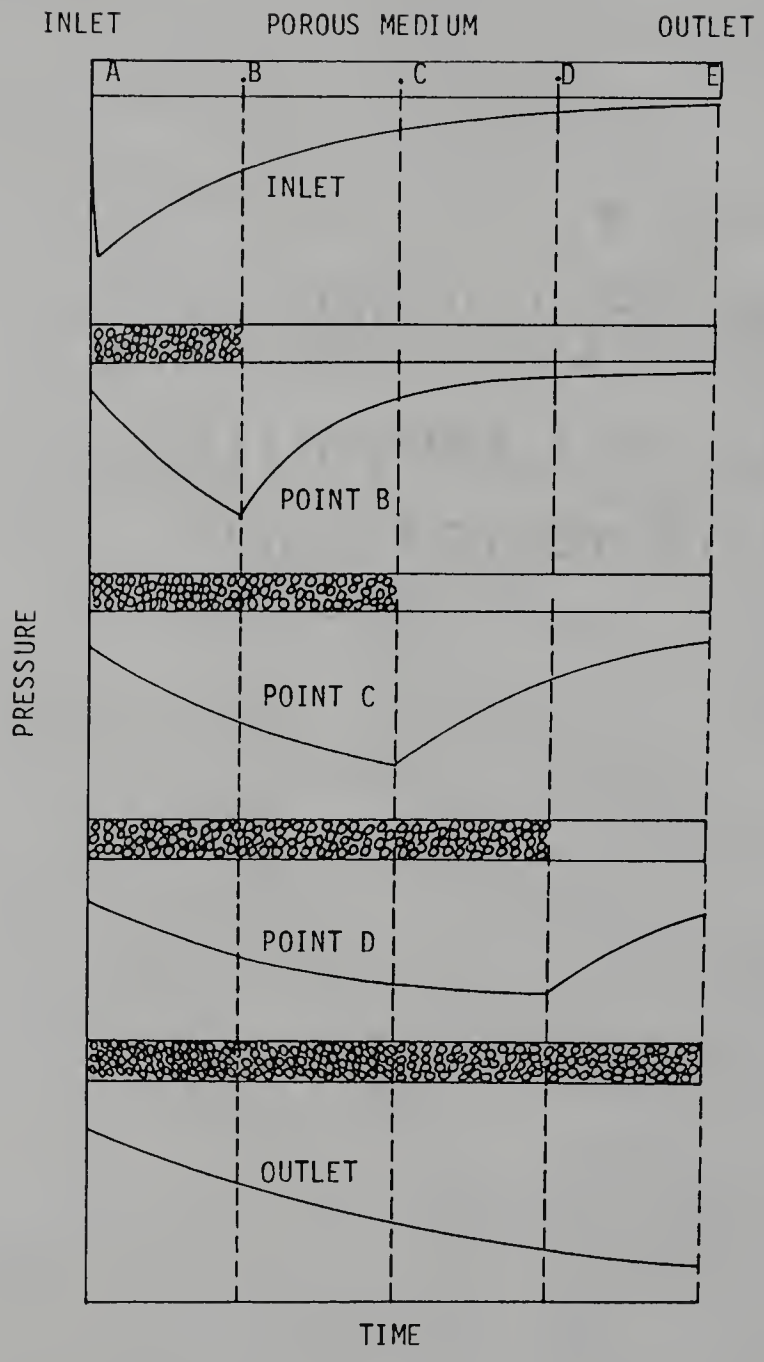

Figure 3.20. Schematic Illustration of the Pressure Distribution in Porous Media during the Foam Flooding Process.

when the front of the foam reached this point. The pressure suddenly increased as the front of the foam went beyond this point and then progressively increased until the foam breakthrough. The pressures at breakthrough time for three fixed points which were located at L/4, 2L/4, and 3L/4 (L = length of the porous medium) were measured for a given concentration of surfactant with different long chain alcohols. Figure 3.21 illustrates a typical pressure distribution measured at these fixed points during the foam flooding process. It demonstrates that foam behaved like a high viscosity plug flow displacing a low viscosity fluid (e.g., water).

Figure 3.22 shows the pressure drops at breakthrough time between two points, L/4 and 3L/4, along three different types of porous media. It is clear that the pressure drops in these porous media increased with the increase of the hydrocarbon chain length of alcohols from C_8 to C_{10}, then it decreased as chain length increased further. The trend is consistent with the fluid displacement efficiency and breakthrough time as a function of hydrocarbon chain length. As mentioned earlier, SDS with $C_{10}OH$ rather than $C_{12}OH$ possesses high foamability and can produce stable foam in sand pack. This implies that a large number of stable bubbles or lamellae which caused a high pressure drop existed in the pores during the foam flooding using the SDS + $C_{10}OH$ mixture. The more stable bubbles or lamellae produced in the porous medium, the

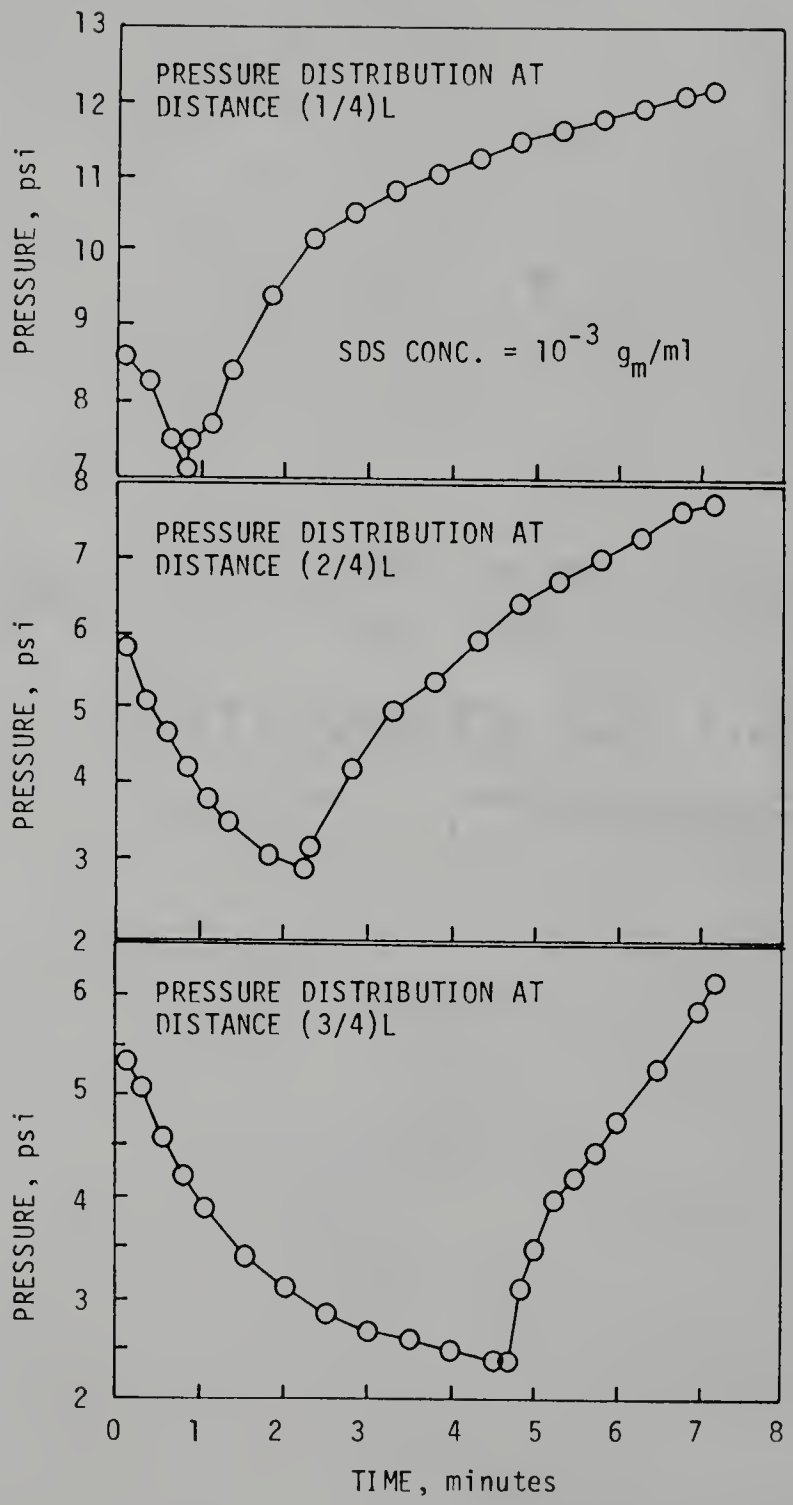

Figure 3.21. A typical Pressure Distribution Measured at Several Fixed Points during the Foam Flooding Process.

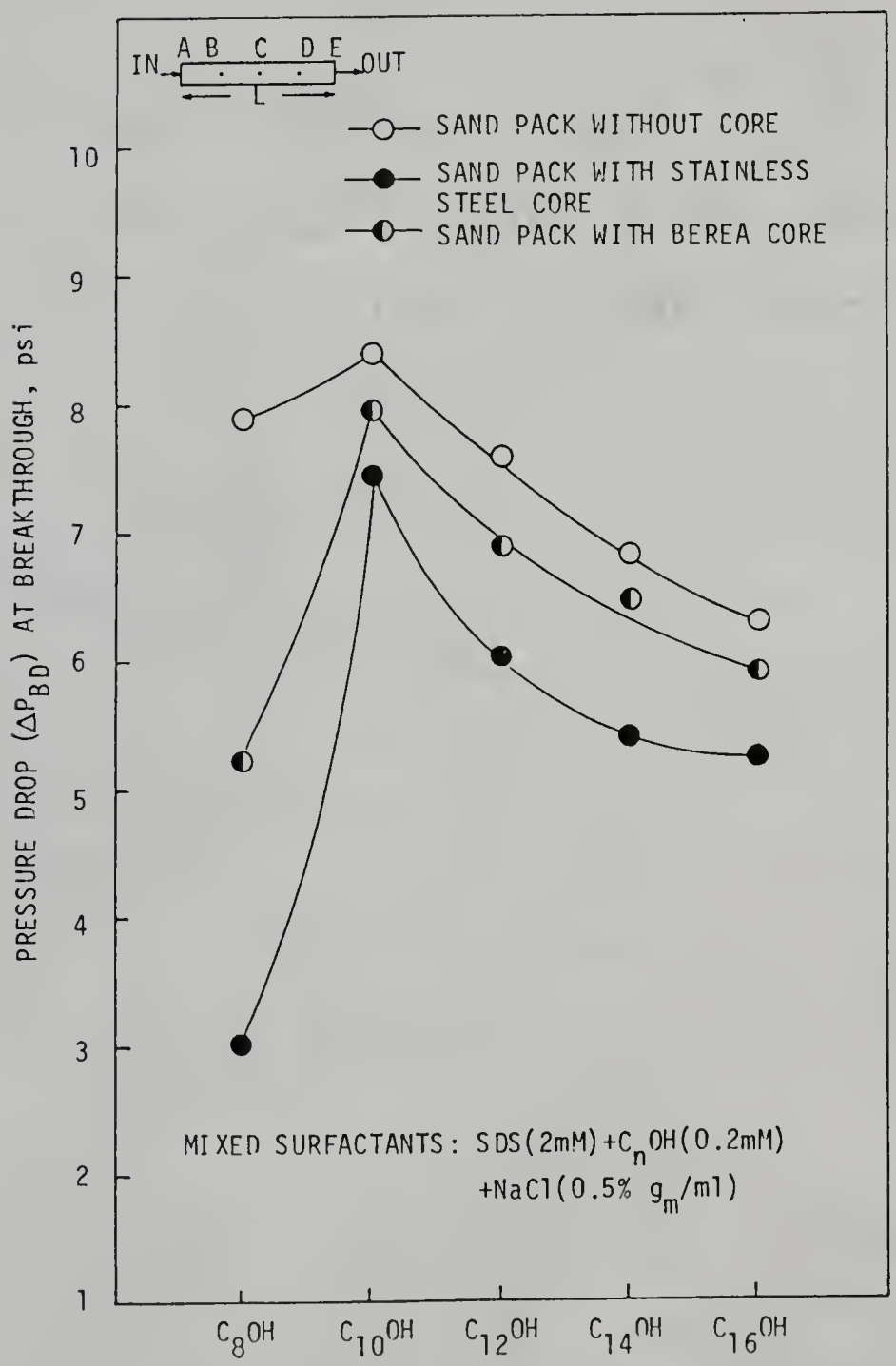

Figure 3.22. Pressure Drops at Breakthrough Time between Two Fixed Points along Various Porous Media.

higher the pressure drop expected. Experimental results (Figure 3.22) indeed showed that the highest pressure drop was measured for the sandpack (i.e., homogeneous porous medium), then for the sand pack with Berea core and the sand pack with stainless steel core, respectively. This implies that the channels in homogeneous porous media are easily invaded and blocked by in-situ foam compared with that in heterogeneous porous media. The more the channels are invaded and blocked, the higher the pressure developed in porous media. From these results, it may be concluded that at a constant inlet pressure, the fluid displacement efficiency is proportional to the pressure drop developed in the porous medium during the foam flooding. Figure 3.23 shows the relationship between the pressure drop at breakthrough and the fluid displacement efficiency of various mixed surfactant systems (e.g., SDS + C_nOH or Stepanflo 40 + C_nOH, etc.). It is evident that higher fluid displacement is associated with higher breakthrough pressures. This is presumably due to larger number of lamellae in porous media. These results were obtained using the homogeneous sand packs.

3.5 Conclusions

In this chapter the foam behavior in porous media was studied by measuring the fluid displacement efficiency, breakthrough time, effective air mobility, and pressure

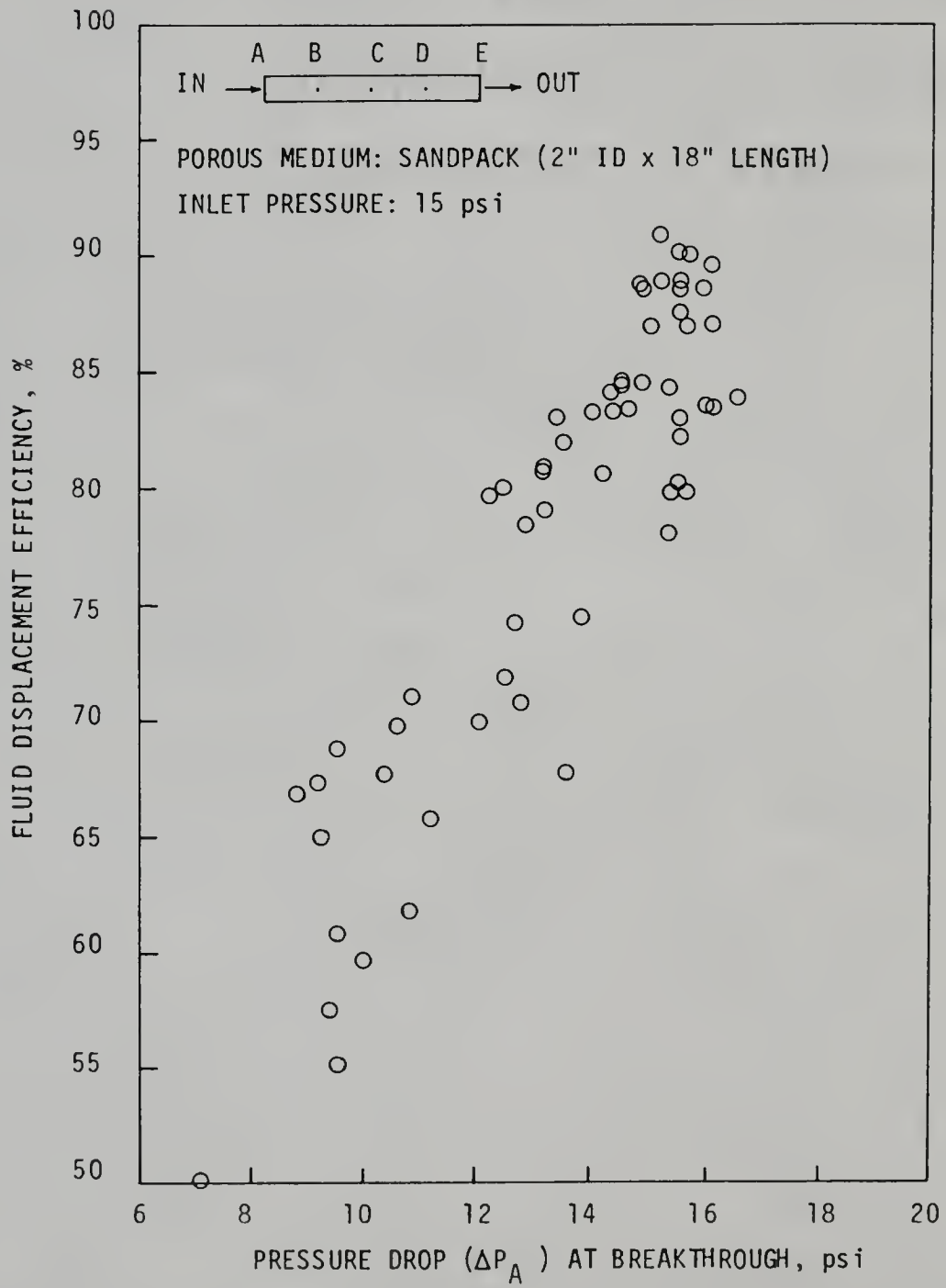

Figure 3.23. Variation in Fluid Displacement Efficiency as a Function of the Pressure Drops at Breakthrough Time.

distribution. The effect of chain length compatibility on the fluid displacement was examined and correlated to the surface properties of the mixed foaming agents. The following conclusions were drawn from the studies in this chapter.

1. The foam behavior in porous media was well correlated to the surface properties of the foaming agents without adding any alcohol.
2. With the exception of Suntech IV, the presence of long chain alcohols in foaming agents, SDS and Stepanflo 40, had considerable effect on the flow of foam through porous media. The use of mixed foaming agents improved fluid displacement efficiency, breakthrough time, and effective air mobility compared to results obtained by the foaming agent alone.
3. Under constant inlet pressure, the higher the pressure developed by foam in porous media, the greater the fluid displacement efficiency. The higher pressure developed in porous media was due to a greater number of channels being invaded and blocked by in-situ foam.
4. From the studies of surface properties of the mixed foaming agents, only the minima of the foam quality and apparent foam viscosity correspond to the maximum of the fluid displacement efficiency. Otherwise, there is no correlation between the surface properties and the fluid displacement.
5. For a given concentration of the mixed foaming agents,

the fluid displacement efficiency depends on the stability of foam, the amount of foam generated in-situ (i.e., foaminess), and the bubble size relative to the pore size.

6. The effect of chain length compatibility was not observed for the fluid displacement experiments. Not only the foam properties, but also the permeability of the porous medium, pore size, and physical properties of matrix have to be considered.
7. On the basis of the surface properties of the foaming agents observed outside the porous medium, it can narrow down the selections of the foaming agents for the application of the foam flooding. Although we cannot precisely predict the foam behavior in porous media by only observing the surface properties of the foam outside the porous medium. However, the latter can elucidate tremendously useful information for interpretation of the foam behavior in porous media.

CHAPTER IV

MODELING OF FOAM FLOW IN POROUS MEDIA

4.1 Introduction

The injection of foam into a porous medium creates a large number of resilient interfaces, which exert a piston-like force on the fluid to be displaced. This phenomenon is called Jamin effect. The process is highly efficient since the foam first finds its way into the largest pores, in which it tends to block further flow. The smaller pores are thus invaded next, and so on until the entire permeable zone has been filled with the foam. Laboratory experiments have shown that vertical sweep efficiency is much improved by the injection of foam, but the mechanism of foam/fluid displacment are still not fully understood.

The flow of foam in circular tubes filled with a porous material is encountered frequently in chemistry, biology, and engineering. It is also of interest in petroleum engineering, especially the displacement of oil with gas, water, and miscible flooding [85].

Usually, two approaches are adopted for the theory of

flows in porous media [86]. In the first, quantities are introduced on a macroscopic scale that describe the state of a porous medium containing fluids. Some of these quantities have an obvious definition (e.g., porosity); other, less easily justified, are rather intuitive (e.g., pressure). The principle of this approach can be justified by experiment in nature. The second way of constructing the theory of flow in porous media would be to start from the elementary laws of viscous flow in a pore and from the laws of capillarity [58,86], then apply statistical methods to porous media. This procedure gives perfect definitions for all of the fundamental quantities and derivations of the laws. Unfortunately, such a approach has been limited to the simplest phenomena, i.e., flow of a single fluid in a capillary. Therefore, in this work, the first approach will be used even though it is a rather rough approximation.

This chapter presents two mathematical models. The first model can predict pressure and velocity profiles in a porous medium during the process of fluid displacement by foam. Since foam stability is affected by many factors, it is very difficult to study the mechanisms of foam/oil displacement in porous media by laboratory tests. Instead of foam/oil displacement, a series of foam/liquid displacement experiments have been conducted and results are compared with model's predictions. Theoretically, this model can be used to predict the mechanisms of foam/oil displacement as long as foam flowing like a plug-type flow.

The second one simulates a steady-state foam flow through porous media. Although some assumptions have to be made in the derivation of the model, it is still useful to predict the velocity profiles, volume flow rate, and approximate breakthrough time. Moreover, the foam viscosity in a porous medium may be estimated by this model if the volume flow rate of the foam is provided.

4.2 Theory

4.2.1 Displacement of Fluid by Foam

As mentioned ealier, almost all theories that describe phenomena in porous media lead to macroscopic laws applicable to blocks whose dimensions are large compared with those of pores. Consequently, these laws lead to equations in which the medium is treated as if it were continuous, homogeneous, and characterized by the local values of a certain number of coefficients defined for all points. For example, the definition of porosity: the average porosity of a block in a porous medium is the ratio of the pore space to the bulk volume of the block. If the block under consideration has properties that differ significantly from one place to another, we may wish to describe the porosity more accurately by introducing a local porosity. This property may be defined for each point in the medium as follows: a partial volume surrounding the point under consideration is theoretically isolated, and

the average porosity of this portion is taken. The element of volume chosen must be sufficiently small to enable a local property of the medium to be defined, but must be large enough in relation to the pore size. It is obvious that the local porosity depends on the volume element taken and on the structure of the porous medium surrounding the point under consideration. Very heterogeneous porous media are conceivable for which the local porosity cannot be defined. The same argument is also true for all other physical properties and parameters with respect to flow through a porous medium. We will assume in the following discussion that the porous media to be studied do not present this difficulty.

For the flow of a fluid through a porous medium the equations of continuity and motion may be replaced by modified equation of continuity [57]

$$\varepsilon \frac{\partial \rho}{\partial t} = -(\nabla \cdot \rho \vec{v}) \tag{4.1}$$

and Darcy's law [82]

$$\vec{v} = -\frac{k}{\mu}(\nabla P - \rho \vec{g}) \tag{4.2}$$

where ε = porosity of the porous medium

k = permeability of the porous medium

μ = viscosity of the fluid

$\vec{v}$ = superficial velocity averaged over a small region of space -- small with respect to

macroscopic dimensions in the flow system but large with respect to the pore size.

P = pressure

$\vec{g}$ = acceleration of gravity

ρ = fluid density at any pressure P.

When foam is considered as a homogeneous fluid, it can be treated as a fluid with both variable density and viscosity. It is well known that the value of foam density is between that of dispersed phase (i.e., gas) and continuous phase (i.e., liquid), and its apparent viscosity is considerably higher than those of either constituent phase. Since foam viscosity changes are small compared with density changes that occur with changes in pressure, it may be assumed as a constant in equation (4.2). For most purposes, the equation of state of the foam may be written as

$$\rho = \rho_o P^m EXP(\beta P) \tag{4.3}$$

where ρ_o = fluid density at unit pressure

m, β = constant parameters

In order to simplify the mathematics, we assume that foam behaves like a "compressible liquid" with the property of

$$\rho = \rho_o EXP(\beta P) \tag{4.4}$$

Now consider a porous medium filled with surfactant solution. Continuously inject air at one end and collect liquid at the other end until foam breakthrough. In this system, liquid is displaced by foam, and both are

considered to be immiscible fluids. We also assume that the front head of foam is never passing the foam/liquid interface. In general, the flow of a fluid through a porous medium is governed by equation (4.1), (4.2), and (4.3). For a surfactant solution, the density is constant, only equation (4.2) is required when it flows through the porous medium. Rewrite these equations in cylindrical coordinates for foam and liquid, respectively:

Foam

$$\varepsilon \frac{\partial \rho_f}{\partial t} = - \frac{\partial}{\partial z} [\rho_f (v_f)_z] \tag{4.5}$$

$$0 = - \frac{\partial P_f}{\partial z} - \frac{\mu_f}{k} (v_f)_z \tag{4.6}$$

$$\rho_f = \rho_o \text{EXP}(\beta P_f) \tag{4.7}$$

Liquid

$$0 = - \frac{dP_L}{dz} - \frac{\mu_L}{k} (v_L)_z \tag{4.8}$$

The subscripts f and L refer to the foam and liquid, respectively. It is usual to neglect the force of gravity, since it is small with respect to the pressure terms. Integration of equation (4.8) gives the general solutions,

$$P_L = P_2 + \frac{\mu_L}{k} (v_L)_z (L - z) \qquad z > Z \tag{4.9}$$

At the foam/liquid interface,

$$P_2^* = P_2 + \frac{\mu_L}{k} (v_L)_z (L - Z) \tag{4.10}$$

where P_L = the pressure at the location of z

P_2 = the pressure at outlet

L = the length of porous media

Z = location of the foam/liquid interface

Note that Z and $(v_L)_z$ are function of time.

By differentiating equation (4.6) and (4.7), respectively we obtain

$$\frac{\partial (v_f)_z}{\partial z} = - \frac{k}{\mu_f} \frac{\partial^2 P_f}{\partial z^2} \tag{4.11}$$

and $$\frac{\partial^2 P_f}{\partial z^2} = (\frac{1}{\beta \rho_f}) \frac{\partial^2 \rho_f}{\partial z^2} - \frac{1}{\beta \rho_f^2} (\frac{\partial \rho_f}{\partial z})^2 \tag{4.12}$$

Substituting (4.11) and (4.12) into equation (4.5) we have

$$(\frac{k}{\varepsilon \mu_f \beta}) \frac{\partial^2 \rho_f}{\partial z^2} = \frac{\partial \rho_f}{\partial t} \tag{4.13}$$

with the following boundary conditions:

(1) $\rho_f(z,0) = 0 \qquad 0 < z < Z$

(2) $\rho_f(0,t) = \rho_1 = \rho_o EXP(\beta P_1) \qquad t > 0$

(3) $\rho_f(Z,t) = \rho_1^* = \rho_o EXP(\beta P_1^*) \qquad t > 0$

The general solutions of equation (4.13) is

$$\rho_f(z,t) = \rho_o EXP(\beta P_1) + [\rho_o EXP(\beta P_1^* - \rho_o EXP(\beta P_1)](z/Z) +$$

$$\sum_{n=1}^{\infty} \frac{2}{n\pi} [\rho_o EXP(\beta P_1^*) \cos(n\pi) - \rho_o EXP(\beta P_1)] \sin(\frac{n\pi z}{Z}) EXP(\frac{-n^2 \pi^2 Kt}{Z^2}) \tag{4.14}$$

where $K = \dfrac{k}{\varepsilon \mu_f \beta}$

Since the foam/liquid interface is gradually moving downstream, there must exist a pressure drop at the interface. The difference between forces exerted by the fluids on the each side of the interface is balanced by

capillary forces [85]. It can be mathematically described by the following equation

$$P_1^* - P_2^* = (2\sigma/R)\cos\alpha \qquad (4.15)$$

where P_1^*, P_2^* = pressure at the interface for foam and liquid, respectively

σ = surface tension

α = wetting angle, it is zero for complete wetting

R = average curvature radii of the interface

Combining (4.10) and (4.15) gives

$$P_1^* = (2\sigma/R) + P_2 + (\mu_L/k)(v_L)_z(L-Z) \quad \text{with } \alpha = 0 \qquad (4.16)$$

From equation (4.7) we have $$P_f = \left(\frac{1}{\beta}\right)\ln\left(\frac{\rho_f}{\rho_o}\right) \qquad (4.17)$$

From (4.6) it follows that

$$(v_f)_z = -\left(\frac{k}{\mu_f}\right)\left(\frac{1}{\beta\rho_f}\right)\frac{\partial\rho_f}{\partial z} \qquad (4.18)$$

where

$$\frac{\partial\rho_f}{\partial z} = \frac{\rho_o EXP(\beta P_1^*) - \rho_o EXP(\beta P_1)}{Z} + \sum_{n=1}^{\infty}\frac{2}{Z}[\rho_o EXP(\beta P_1^*)\cos(n\pi) - \rho_o EXP(\rho P_1)]\cos\left(\frac{n\pi z}{Z}\right)EXP\left(\frac{-n^2\pi^2 Kt}{Z^2}\right)$$

P_f and $(v_f)_z$ can be calculated immediately by substitution of (4.14) and (4.16).

4.2.2 Modeling of Foam Flow through Porous Media

The flow of a fluid through a porous medium may be described by an empirical modification of Darcy's law which was suggested by Brinkman [87]:

$$0 = -\nabla P - \frac{\mu}{k}\vec{v} + \mu\nabla^2\vec{v} + \rho\vec{g} \qquad (4.19)$$

where P = pressure of the system

μ = viscosity of the fluid

k = permeability of the porous medium

ρ = fluid density at pressure

$\vec{g}$ = acceleration of gravity

$\vec{v}$ = superficial velocity averaged over a small region of space -- small with respect to macroscopic dimensions in the flow system but large with respect to the pore size.

The term $\mu\nabla^2 v$ is intended to account for distortion of the velocity profiles near containing walls. Again, the gravity term will be neglected. Analytic solutions of Equation (4.19) which require the use of the equation of continuity, the equation of state, and characteristic properties of the porous medium are difficult to obtain. It is often advantageous, therefore, to be satisfied with approximate solutions obtained from simplified conditions.

Now consider a steady-state flow through a tube of radius R_o which is filled with a porous material of uniform permeability k. Assume the system is axisymmetric and the pressure profile is a function of z-direction only. In cylindrical coordinates (Figure 4.1), equation (4.19) reduces to

$$\mu\frac{\partial^2 v_z}{\partial r^2} + \frac{\mu}{r}\frac{\partial v_z}{\partial r} + \mu\frac{\partial^2 v_z}{\partial z^2} - \frac{\mu}{k} v_z - \frac{dP}{dz} = 0 \qquad (4.20)$$

with the following boundary conditions:

(1) $v_z(0,z)$ = finite

(2) $v_z(R_o,z) = 0$

(3) $v_z(r,0) = v_1$

(4) $v_z(r,L) = v_2$

where v_1 = average superficial velocity at inlet

v_2 = average superficial velocity at outlet

In equation (4.20), the pressure gradient may be any type of function of z which depends on the characteristics of the foam and the porous medium. In order to obtain an analytic solution of equation (4.20), two special cases are discussed as follows.

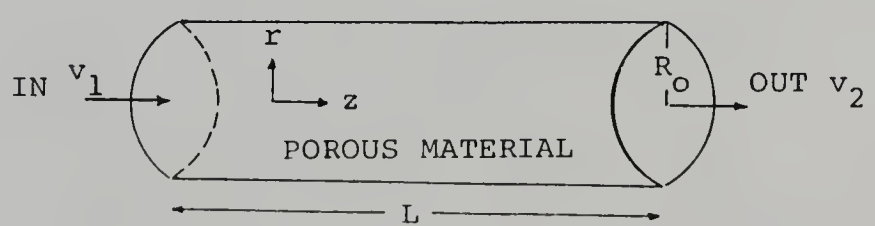

Figure 4.1. Cylindrical Coordinates System.

Case I

If foam is treated as a homogeneous fluid with constant density and viscosity, from modified equation of continuity it is easy to show that $\nabla \cdot v = 0$

Equation (4.20) reduces to

$$\frac{d^2 v_z}{dr^2} + \frac{1}{r}\frac{dv_z}{dr} - \frac{1}{k}\left[v_z - \left(\frac{k}{\mu}\right)\frac{\Delta P}{L}\right] = 0 \qquad (4.21)$$

with the following boundary conditions:

$v_z(0)$ = finite and $v_z(R) = 0$

where $\Delta P = P_1 - P_2$

$$\text{Define} \quad r = k^{1/2}x, \quad \phi = v_z - \frac{k}{\mu}\frac{\Delta P}{L} \qquad (4.22)$$

By differentiating (4.22) and inserting it into (4.21) we have

$$x^2 \frac{d^2\phi}{dx^2} + x\frac{d\phi}{dx} - x^2\phi = 0 \qquad (4.23)$$

Equation (4.22) is a modified Bessel's differential equation and its general solution is

$$\phi(x) = C_1 I_o(x) + C_2 K_o(x)$$

$$\text{or} \quad v_z(r) = \frac{k}{\mu}\frac{\Delta P}{L} + C_1 I_o\left(\frac{r}{k^{1/2}}\right) + C_2 K_o\left(\frac{r}{k^{1/2}}\right) \qquad (4.24)$$

where I_o = modified Bessel function of the first kind of order zero

K_o = modified Bessel function of the second kind of order zero.

By applying the boundary conditions to equation (4.24), we

obtain a velocity distribution in the r-direction:

$$v_z(r) = \frac{k}{\mu}\frac{\Delta P}{L}\{1 - [I_o(\frac{r}{k^{1/2}})/I_o(\frac{R}{k^{1/2}})]\} \qquad (4.25)$$

The average velocity $\langle v_z \rangle$ is calculated by summing up all the velocities over a cross section and then dividing by the cross-sectional area:

$$\langle v_z \rangle = \frac{\int_0^{2\pi}\int_0^R v_z\, r dr d\theta}{\int_0^{2\pi}\int_0^R r dr d\theta}$$

$$\langle v_z \rangle = (\frac{k\Delta P}{\mu L})\{1 - 2\frac{k^{1/2}}{R}[I_1(\frac{R}{k^{1/2}})/I_o(\frac{R}{k^{1/2}})]\} \qquad (4.26)$$

where I_1 = modified Bessel function of the first kind of order first.

The volume rate of flow Q is the product of area and average velocity:

$$Q = \pi R^2(\frac{k\Delta P}{\mu L})\{1 - 2\frac{k^{1/2}}{R}[I_1(\frac{R}{k^{1/2}})/I_o(\frac{R}{k^{1/2}})]\} \qquad (4.27)$$

Interestingly, equation (4.27) reduces to the Hagen-Poiseuille law when $k \to \infty$ (i.e., fluid flows through a circular tube without porous material).

Case II

If the pressure profile can be expressed by the relationship:

$$dP/dz = \alpha EXP(\theta z)$$

where α and θ are parameters and determined by

experimental data, then equation (4.20) is an elliptic partial differential equation with non-homogeneous boundary conditions and can be divided into two problems.

Problem 1 $$\mu \frac{d^2U}{dz^2} - \frac{\mu}{k} U - \frac{dP}{dz} = 0 \qquad (4.28)$$

boundary conditions : $U(0) = v_1$, $U(L) = v_2$

Problem 2 $$\mu \frac{\partial^2 W}{\partial r^2} + \frac{\mu}{r} \frac{\partial W}{\partial r} + \mu \frac{\partial^2 W}{\partial z^2} - \frac{\mu}{k} W = 0 \qquad (4.29)$$

boundary conditions: $W(0,z) + U(z)$ is finite

$$W(R_o, z) = -U(z)$$

$$W(r,0) = 0$$

$$W(r,L) = 0$$

The general solution of equation (4.28) is:

$$U(z) = A_1 \cosh\left(\frac{z}{k^{1/2}}\right) + A_2 \sinh\left(\frac{z}{k^{1/2}}\right) + (\alpha k e^{\theta z})/[\mu(\theta^2 k - 1)] \qquad (4.30)$$

where $A_1 = v_1 - (\alpha k)/[\mu(\theta^2 k - 1)]$

$$A_2 = v_2 \operatorname{csch}\left(\frac{L}{k^{1/2}}\right) - v_1 \coth\left(\frac{L}{k^{1/2}}\right) + \frac{\alpha k}{\mu(\theta^2 k - 1)}\Big[$$

$$\left(\coth\left(\frac{L}{k^{1/2}}\right) - e^{\theta L} \operatorname{csch}\left(\frac{L}{k^{1/2}}\right)\right)\Big]$$

The superposition of all solutions of equation (4.29) is given by:

$$W(r,z) = \sum_{n=1}^{\infty} D_n I_o(M_n r) \sin\left(\frac{n\pi z}{L}\right), \quad n = 1, 2, 3, \ldots \qquad (4.31)$$

where $M_n = [(n\pi/L)^2 + (1/k)]^{1/2}$

$$D_n = -(4/L^2)\left[\left(\int_0^L zU(z) \sin\left(\frac{n\pi z}{L}\right) dz\right)/I_o(M_n R_o)\right]$$

$$v_z(r,z) = U(z) + W(r,z)$$

$$\text{i.e., } v_z(r,z) = A_1 \cosh\left(\frac{z}{k^{1/2}}\right) + A_2 \sinh\left(\frac{z}{k^{1/2}}\right) + (\alpha k e^{\theta z})/[\mu(\theta^2 k - 1)]$$

$$+ \sum_{n=1}^{\infty} D_n I_o(M_n r) \sin\left(\frac{n\pi z}{L}\right), \quad n = 1, 2, 3, \ldots \qquad (4.32)$$

Equation (4.32) describes the superficial velocity distribution in the porous medium. The average volume rate (Q) of the fluid can be obtained by:

$$Q = \frac{(\pi R_o^2) \int_0^L \int_0^{2\pi} \int_0^{R_o} v_z(r,z)\, r\, dr\, d\theta\, dz}{\int_0^L \int_0^{2\pi} \int_0^{R_o} r\, dr\, d\theta\, dz}$$

$$\text{or } Q = \frac{2\pi}{L}\left\{\frac{R_o^2}{2}\left[A_1 k^{1/2} \sinh\left(\frac{L}{k^{1/2}}\right) + A_2 k^{1/2}\left(\cosh\left(\frac{L}{k^{1/2}}\right) - 1\right)\right.\right.$$

$$\left.\left. + (\alpha k)/[\mu\theta(\theta^2 k - 1)](e^{\theta L} - 1)\right] + \sum_{i=1}^{\infty} \frac{2LD_i R_o}{i\pi M_i} I_1(M_i R_o)\right\}$$

$$i = 1, 2, 3, \ldots \qquad (4.33)$$

The approximate breakthrough time (t_b) is given by

t_b = (pore volume)/(average volume rate)

Hence, the breakthrough time can be predicted if the average superficial velocity at inlet and outlet, the pressure distribution of the system, the viscosity of the fluid, and the permeability of the porous medium are known.

4.3 Results and Discussion

In order to make certain the models accurately describe the foam flow in porous media, two major phenomena observed during experiments, the pressure distribution and the velocity profile, will be discussed and compared with the results obtained from the models.

4.3.1 Displacement of Fluid by Foam

In the derivation of the model, foam density was described as if the foam behaved like a "compressible liquid". However, the compressibility (β) in the equation of state of the foam is lacking because of its difficulity to measurement. In the absence of any better data, compressibilities of pure liquids listed in Chemical Engineers' Handbook (1973) may be used for the model. The magnitude of compressibilities of pure liquids is in the range of 5×10^{-6} to 100×10^{-6}. Since foam is a gas-like "compressible liquid", its compressibility is expected to be at least 100×10^{-6}. Hence, an arbitrary value, 100×10^{-6}, is chosen as the foam compressibility. Another factor, foam viscosity, was assumed constant over the system even though it was dependent on the pressure as well as the pore size. The actual data for foam viscosity are not available in the literature. A rough value was assigned during the calculation based on the measurements of apparent foam viscosity conducted outside porous media. It should be

noted that all of the in-situ foam properties are functions of the pore structures and surface properties of the porous media in addition to the properties of foaming agent itself.

From Equation (4.14) and (4.16), the foam density at any time and position can be easily calculated if the movement (i.e., Z function) of the foam/liquid interface is provided. This is the limitation of the model because the movement of the interface not only depends on the time, but also on the properties of foaming agent as well as the pore structures. It implies that there exists a time-dependent Z function for each given foaming agent and porous medium. Moreover, the foam/liquid interface is an ideal surface which probably does not exist in the real system. It is hard to measure even if this interface exists. Fortunately, an approximate method might be employed to obtain the time-dependent Z function. The liquid recovery (V, ml) was recorded as a function of time (t, sec) and a polynomial relationship (V_t), V/(pore volume) vs. time, was found by non-linear curve fitting. An average time-dependent Z function is equal to (V_t x pore volume)/(cross-section area). As mentioned previously, each given system corresponds to a special Z function. Tables 4.1-4.3 summarize the average time-dependent Z function for several different foaming agents. It can be seen that the coefficient A plays an important role in the Z function. The smaller the coefficient A, the slower the movement of

Table 4.1 Average Time-dependent Z Function for Mixed Foaming Agents of Stepanflo Surfactants

SURFACTANT	A	B	C
Stepanflo 20	9.443	-4.476×10^{-1}	1.033×10^{-2}
Stepanflo 30	15.190	-1.185×10^{0}	4.313×10^{-2}
Stepanflo 40	6.560	-2.117×10^{-1}	2.943×10^{-3}
Stepanflo 50	11.311	-1.781×10^{-1}	1.848×10^{-2}
Stepanflo 60	5.849	-1.776×10^{-1}	1.802×10^{-3}
Stepanflo 70	13.300	-9.209×10^{-1}	3.207×10^{-2}
Stepanflo 80	10.737	-6.020×10^{-3}	6.377×10^{-3}

FOAMING AGENTS: STEPANFLO (10^{-3} g_m/ml) + NaCl(0.5 wt.%)

INLET PRESSURE: 15 psi

POROUS MEDIUM: SAND PACK (18"L x 2"D)

Z FUNCTION: (pore vol./cross-section area)$(At + Bt^2 + Ct^3)$

t: Time, minutes

Table 4.2 Average Time-dependent Z Function for Mixed Foaming Agents of SDS + C_nOH + NaCl

SURFACTANT	A	B	C
SDS + C_8OH	4.762	-1.100×10^{-1}	9.965×10^{-4}
SDS + C_{10}OH	3.356	-5.223×10^{-2}	2.985×10^{-4}
SDS + C_{12}OH	5.204	-1.560×10^{-1}	2.058×10^{-3}
SDS + C_{14}OH	10.172	-4.676×10^{-1}	1.042×10^{-2}
SDS + C_{16}OH	4.962	-9.554×10^{-2}	1.244×10^{-3}

FOAMING AGENTS: SDS (2 mM) + C_nOH (0.2 mM) + NaCl(0.5 wt.%)

INLET PRESSURE: 15 psi

POROUS MEDIUM: SAND PACK (18"L x 2"D)

Z FUNCTION: (pore vol./cross-section area)$(At + Bt^2 + Ct^3)$

t: Time, minutes

Table 4.3 Average Time-dependent Z Function for Mixed Foaming Agents of Stepanflo 40 + C_nOH + NaCl

SURFACTANT	A	B	C
Stepanflo 40 + C_8OH	10.131	-5.455×10^{-1}	1.187×10^{-2}
Stepanflo 40 + $C_{10}OH$	7.424	-2.719×10^{-1}	3.867×10^{-3}
Stepanflo 40 + $C_{12}OH$	6.754	-2.430×10^{-1}	3.341×10^{-3}
Stepanflo 40 + $C_{14}OH$	8.173	-3.659×10^{-1}	7.893×10^{-3}
Stepanflo 40 + $C_{16}OH$	11.256	-5.812×10^{-1}	2.009×10^{-2}

FOAMING AGENTS: STEPANFLO 40 (5×10^{-4} g_m/ml) + C_nOH (0.1 mM) + NaCl(0.5 wt.%)

INLET PRESSURE: 15 psi

POROUS MEDIUM: SAND PACK (18"L x 2"D)

Z FUNCTION: (pore vol./cross-section area)$(At + Bt^2 + Ct^3)$

t: Time, minutes

the interface. In the meantime, the average velocity of the liquid $(v_L)_z$ can be obtained by taking the first derivative of the Z function. Once the Z function is determined, the foam density is calculated by Equation (4.14) and (4.16). The pressure distribution and velocity profile can be computed immediately by substitution of Equation (4.14) and (4.16) into (4.17) and (4.18).

The first step in the verification process is a check of the pressure distribution at some specified locations in the system. Experimental data at three specified points, (i.e., L/4, 2L/4, and 3L/4, L is the length of the porous medium), and the data predicted by the model are shown in Figures 4.2 and 4.3, respectively. It can be seen that the model results are in agreement with the experimental data. Referring to Figures 4.2 and 4.3, the pressure drop at a specified point gradually decreases as time increases before the front of foam reaches this point. The minimum pressure drop is found when the foam front arrives at this point. Then an increase in pressure is observed as the foam front passes this point until the foam breakthrough. These facts illustrate that the model can simulate the foam displacing a fluid as described by the pressure distribution very well.

The second verification step consists of a comparison of the measured velocity profile with the data predicted by the model. Since experimental data of the velocity profile at any specified point (except inlet and outlet) in the

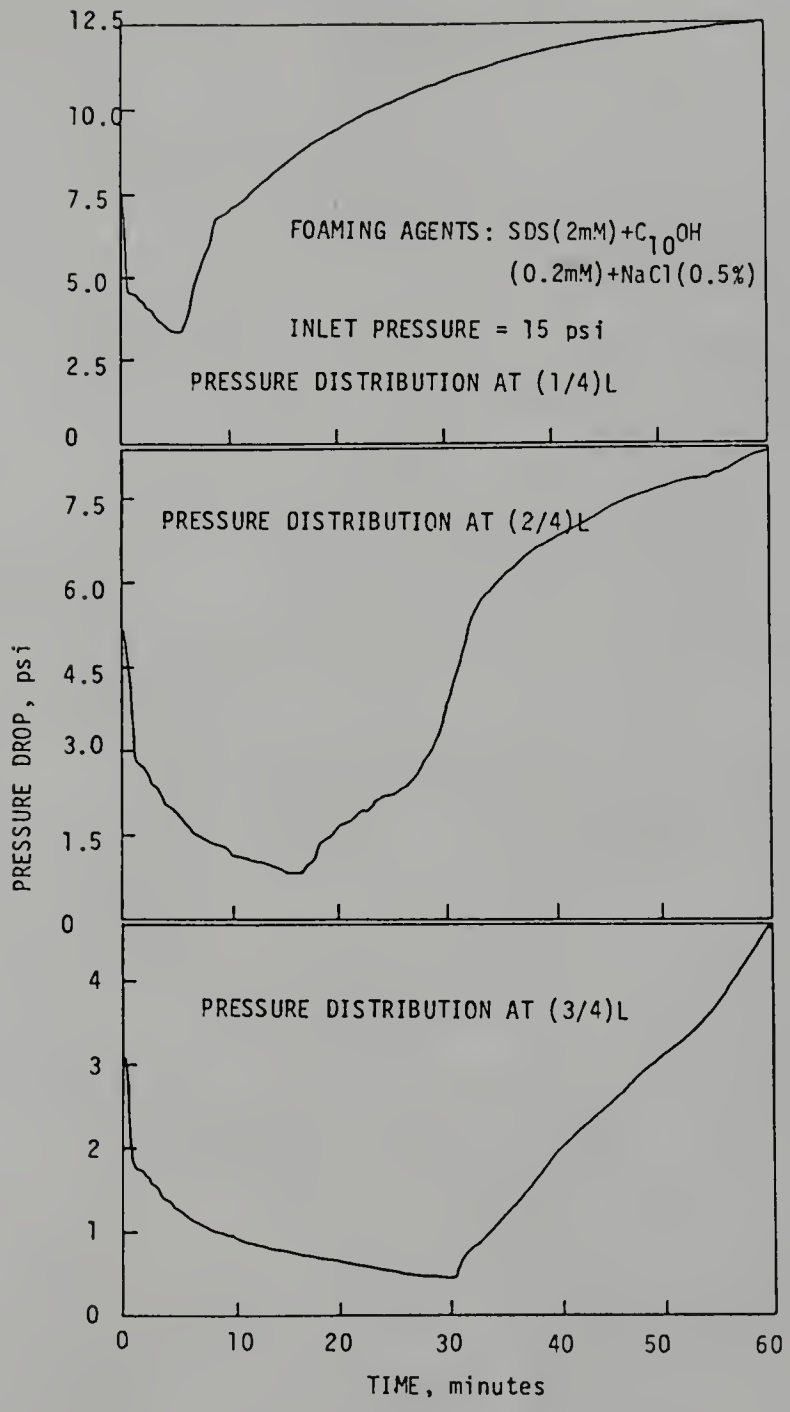

Figure 4.2. Pressure Distribution Measured at Several Fixed Points during the Foam Flooding Process.

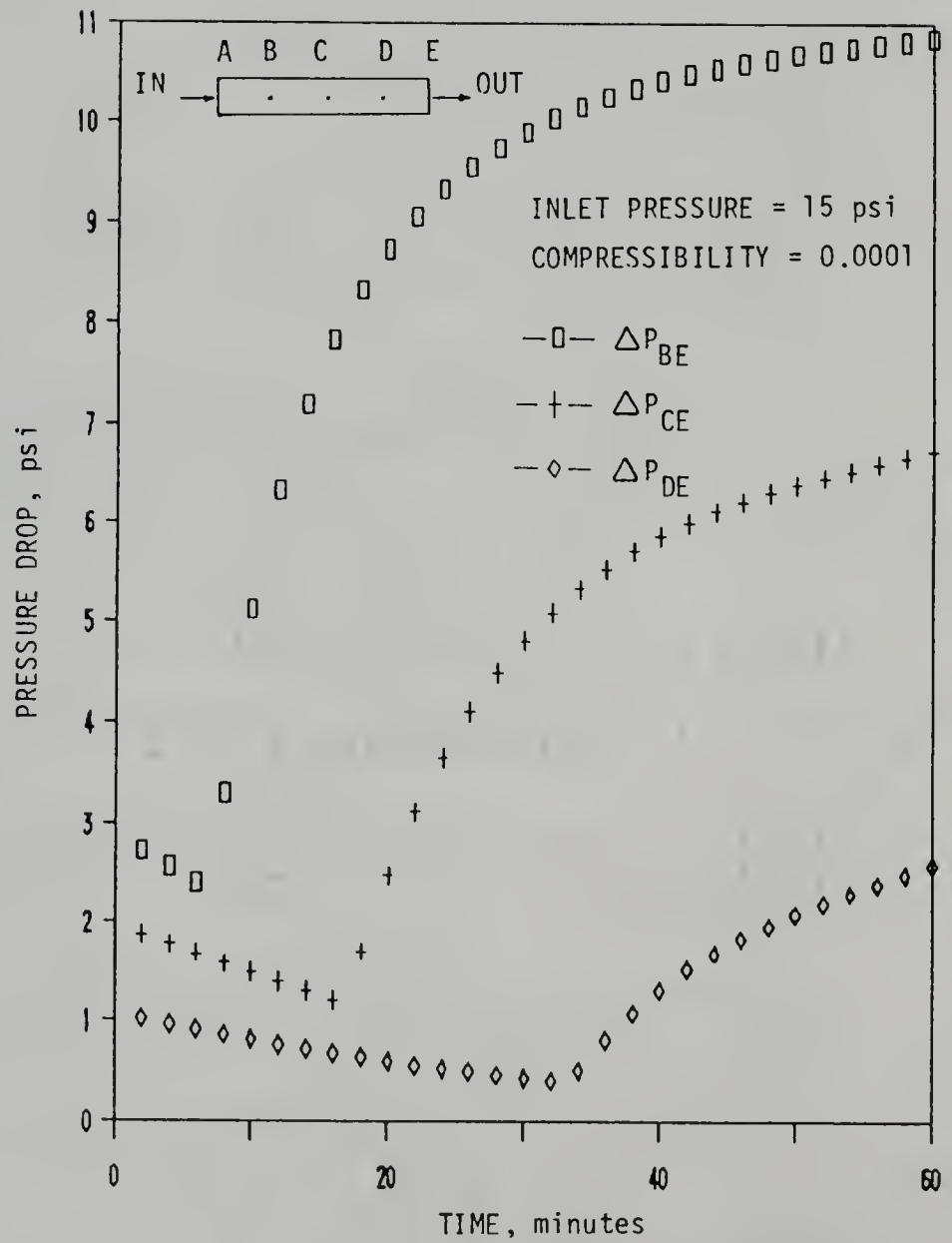

Figure 4.3. Pressure Distribution Predicted by the Model at Several Fixed Points along a Porous Medium.

system are not available, the average velocity profile at the producing site is used for comparison. Figure 4.4 shows the comparison of the velocity profiles at three specified locations predicted by the model with the experimental results measured at the outlet. It is of interest that a sudden drop in velocity profile is observed at a specified point when the foam front goes beyond this point. Afterward, the velocity profile is slightly decreasing until the foam breakthrough. Although the average velocity profile at the outlet does not show the characteristic of the sudden velocity drop, a sharp decrease in velocity profile at early foam flooding process is observed. This is a strong evidence that foam reduces the air mobility to a great extent. Therefore, one would not be surprised to observe the sudden velocity drop at a specified point when the foam front passes this point. Based on the discussion mentioned above, the model of foam displacing fluid can be used to describe the velocity profile at any time and position over the entire system.

The effect of foam compressibility (β) on the pressure distribution and velocity profile was studied with the model. Model results predict that the value of compressibility has little effect on the pressure and velocity if all of the parameters, except β, in Equation (4.14) and (4.16) are fixed. Tables 4.4-4.6 show the pressure and velocity at the L/4 location as a function of time for three different values of foam compressibility.

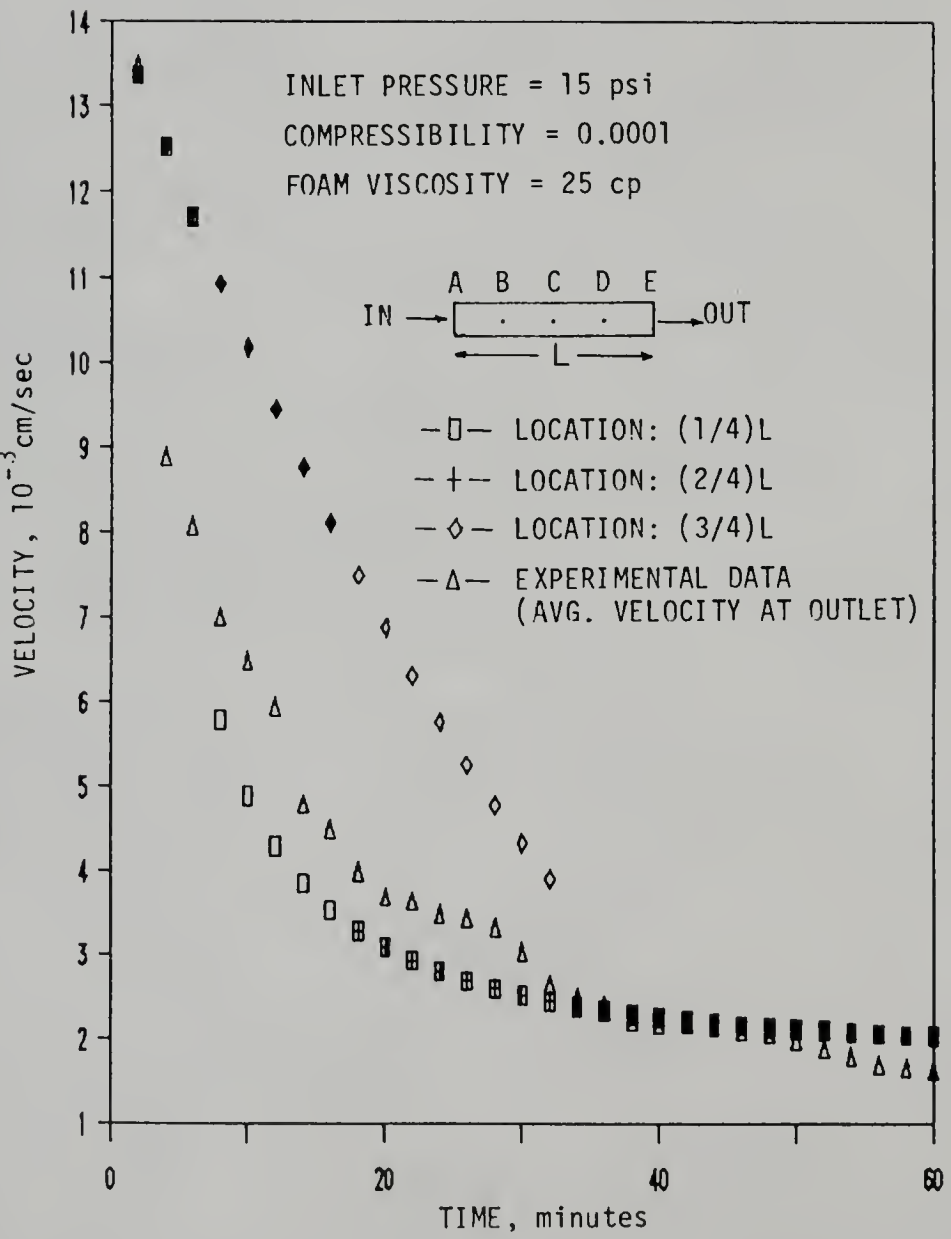

Figure 4.4. Comparison of Velocity Profiles at Several Fixed Points Predicted by the Model with Experimental Data Measured at the Outlet.

Table 4.4 Predictions of Pressure and Velocity at L/4 for a Foam Compressibility of 0.01.

TIME (min)	PRESSURE (psi)	VELOCITY (cm/sec)
2.0	2.740	1.337×10^{-2}
6.0	2.419	1.172×10^{-2}
10.0	5.133	4.895×10^{-3}
14.0	7.208	3.862×10^{-3}
18.0	8.357	3.291×10^{-3}
22.0	9.081	2.931×10^{-3}
26.0	9.573	2.687×10^{-3}
30.0	9.922	2.514×10^{-3}
34.0	10.177	2.387×10^{-3}
38.0	10.368	2.292×10^{-3}
42.0	10.511	2.221×10^{-3}
46.0	10.622	2.166×10^{-3}
50.0	10.710	2.123×10^{-3}
54.0	10.782	2.087×10^{-3}
58.0	10.847	2.055×10^{-3}
60.0	10.878	2.039×10^{-3}

SIZE OF POROUS MEDIUM: 18"L x 2"D

PERMEABILITY OF POROUS MEDIUM: 2.5 darcys

FOAM VISCOSITY: 25 cp

INLET PRESSURE: 15 psi

Table 4.5 Predictions of Pressure and Velocity at L/4 for a Foam Compressibility of 0.001.

TIME (min)	PRESSURE (psi)	VELOCITY (cm/sec)
2.0	2.740	1.337×10^{-2}
6.0	2.419	1.172×10^{-2}
10.0	5.124	4.885×10^{-3}
14.0	7.194	3.860×10^{-3}
18.0	8.343	3.291×10^{-3}
22.0	9.066	2.933×10^{-3}
26.0	9.557	2.690×10^{-3}
30.0	9.907	2.517×10^{-3}
34.0	10.163	2.390×10^{-3}
38.0	10.353	2.296×10^{-3}
42.0	10.497	2.225×10^{-3}
46.0	10.609	2.170×10^{-3}
50.0	10.696	2.127×10^{-3}
54.0	10.768	2.091×10^{-3}
58.0	10.833	2.059×10^{-3}
60.0	10.864	2.043×10^{-3}

SIZE OF POROUS MEDIUM: 18"L x 2"D

PERMEABILITY OF POROUS MEDIUM: 2.5 darcys

FOAM VISCOSITY: 25 cp

INLET PRESSURE: 15 psi

Table 4.6 Predictions of Pressure and Velocity at L/4 for a Foam Compressibility of 0.0001.

TIME (min)	PRESSURE (psi)	VELOCITY (cm/sec)
2.0	2.740	1.337×10^{-2}
6.0	2.419	1.172×10^{-2}
10.0	5.118	4.886×10^{-3}
14.0	7.186	3.864×10^{-3}
18.0	8.342	3.294×10^{-3}
22.0	9.078	2.934×10^{-3}
26.0	9.568	2.691×10^{-3}
30.0	9.919	2.518×10^{-3}
34.0	10.164	2.391×10^{-3}
38.0	10.357	2.298×10^{-3}
42.0	10.497	2.228×10^{-3}
46.0	10.620	2.170×10^{-3}
50.0	10.690	2.130×10^{-3}
54.0	10.777	2.092×10^{-3}
58.0	10.847	2.061×10^{-3}
60.0	10.865	2.045×10^{-3}

SIZE OF POROUS MEDIUM: 18"L x 2"D

PERMEABILITY OF POROUS MEDIUM: 2.5 darcys

FOAM VISCOSITY: 25 cp

INLET PRESSURE: 15 psi

Generally speaking, the pressure insignificantly increases as β increases, whereas the velocity almost negligibly decreases. It is concluded that the selected value of the foam compressibility has no significant effect on the prediction of foam flooding process if the time-dependent Z function is provided.

Another important factor which may influence the pressure and velocity is the foam viscosity. Figure 4.5 shows the effect of foam viscosity on the velocity profile. It is clear that the velocity is significantly affected by the foam viscosity. The larger the foam viscosity, the slower the velocity. The foam viscosity has little effect on the pressure. It can be seen from Equation (4.17).

By checking the pressure distributions and velocity profiles in the system, the results show that this model gives accurate descriptions of the fluid displacement by foam. The usefulness of the model is to predict the pressure distribution and velocity profile for any foam flooding process as long as the average volume flow rate at the producing site is available.

4.3.2 Modeling of Foam Flow through Porous Media

In order to simplify the mathematical simulation, foam is treated as a homogeneous fluid with constant density and viscosity. The actual values for the in-situ foam viscosity and density are not measurable and are not available in the literature. Therefore, approximate values were used

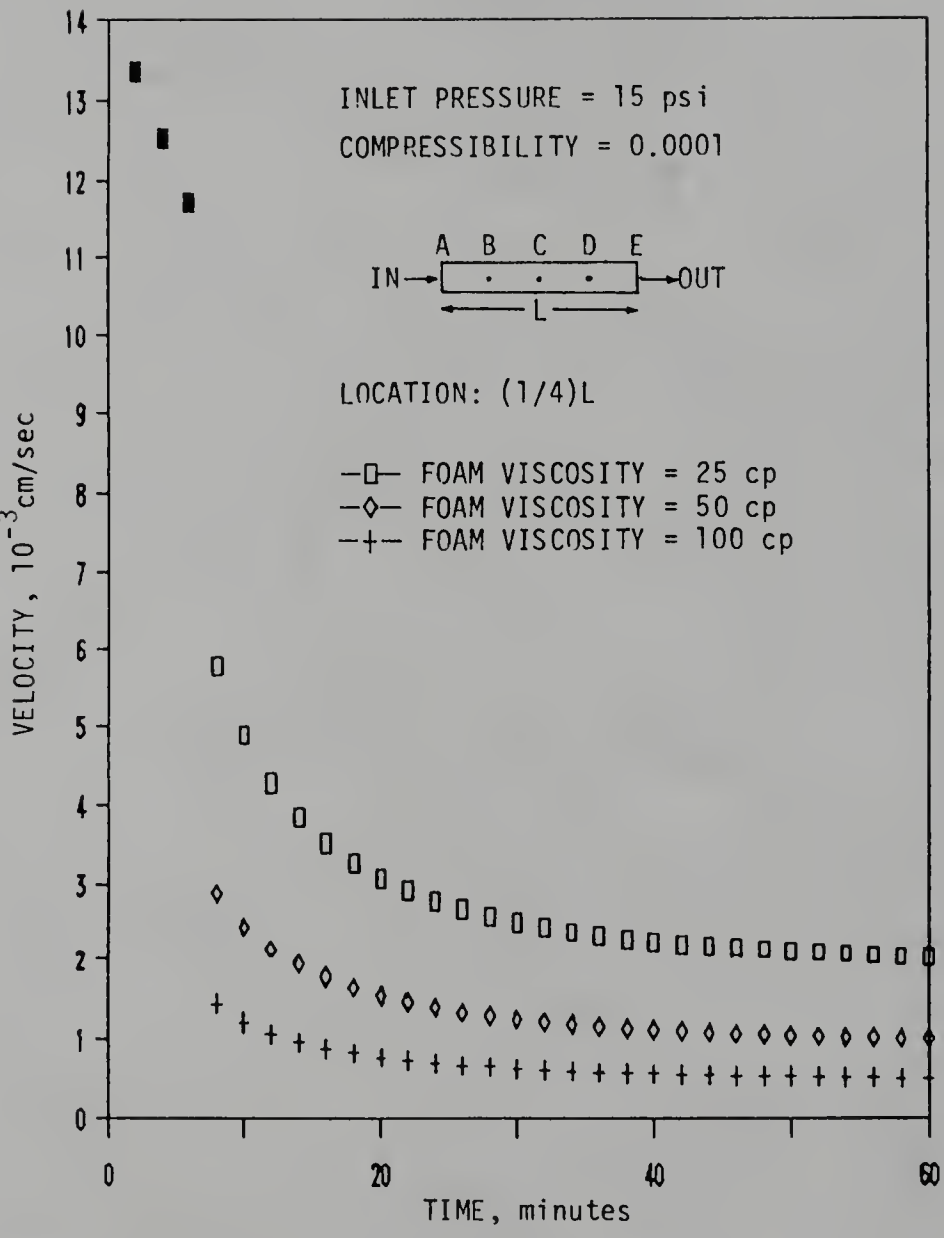

Figure 4.5. Prediction of Velocity Profile as a Function of Foam Viscosity.

according to the experimental results of the apparent viscosity and foam quality measured outside porous media. Assuming that the pressure drop across the porous medium is a linear function, then the velocity profile in r-direction and the volume flow rate can be easily calculated by Equation (4.25) and (4.27). Figure 4.6 shows the velocity profiles as a function of radius for various permeabilities (k) of the porous media. It is evident that the velocity in r-direction increases with the increase of permeability. All the velocity profiles shown in Figure 4.6 are parabolic and the maximum velocity occurs at the center of the circular conduit where r = 0. The velocity is a maximum when the permeability is infinite (i.e., there is no porous material in the conduit). The velocity profiles are significantly affected by foam viscosity (Figure 4.7). The higher the foam viscosity, the lower the velocity. The volume flow rates as a function of foam viscosity for various permeabilities of the porous media are shown in Figure 4.8. The volume flow rate increases with increasing the permeability of porous media. On the other hand, the volume flow rate sharply decreases, then gradually decreases as the foam viscosity increases. Equation (4.27) is known as the Hagen-Poiseulle equation when the permeability of the porous media approaches infinity. No resistance from the porous material results in the maximum volume flow rate. Figure 4.7 indeed shows that the maximum volume flow rate is always obtained when k is infinite.

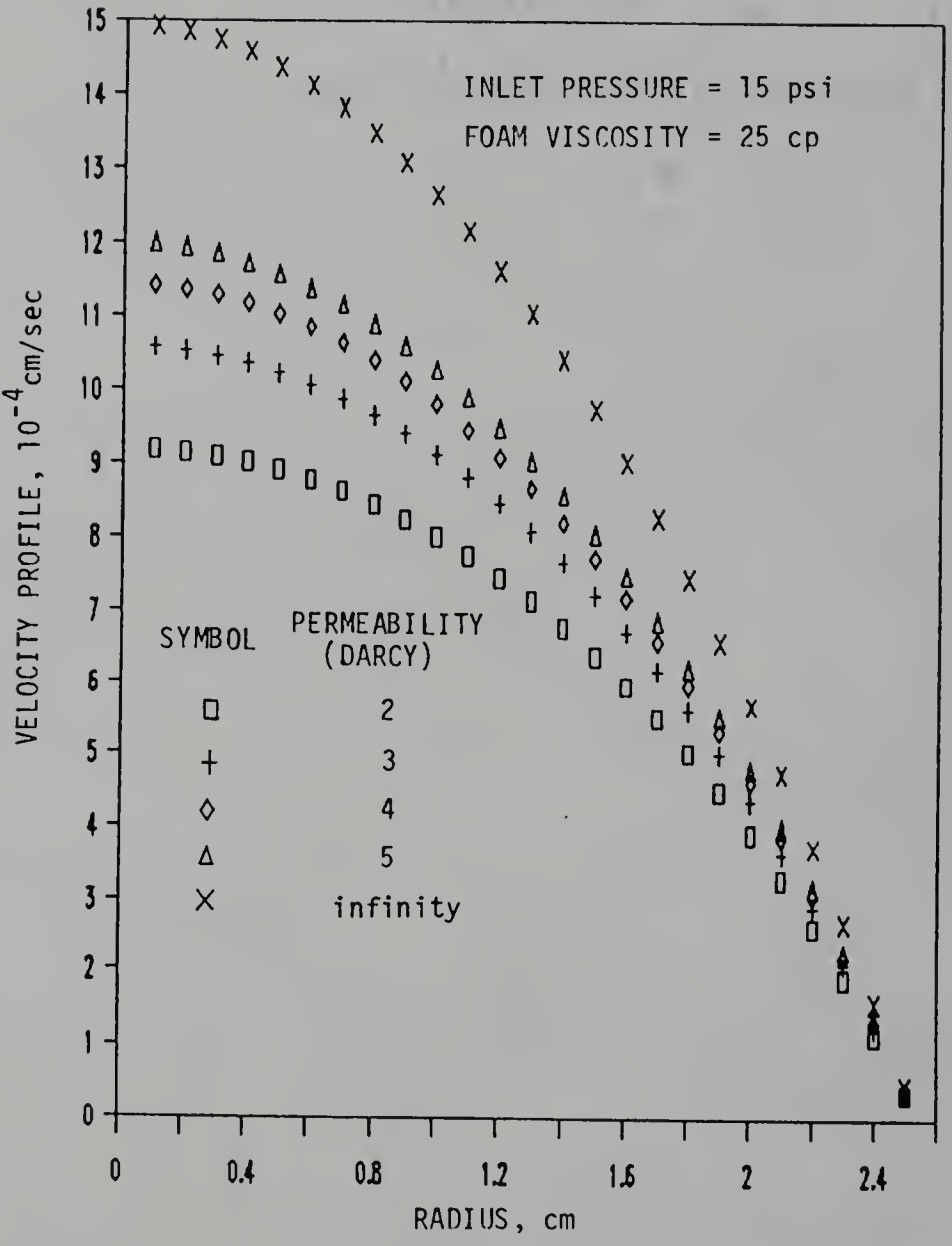

Figure 4.6. Prediction of Velocity Profile as a Function of Radius for Various Porous Media.

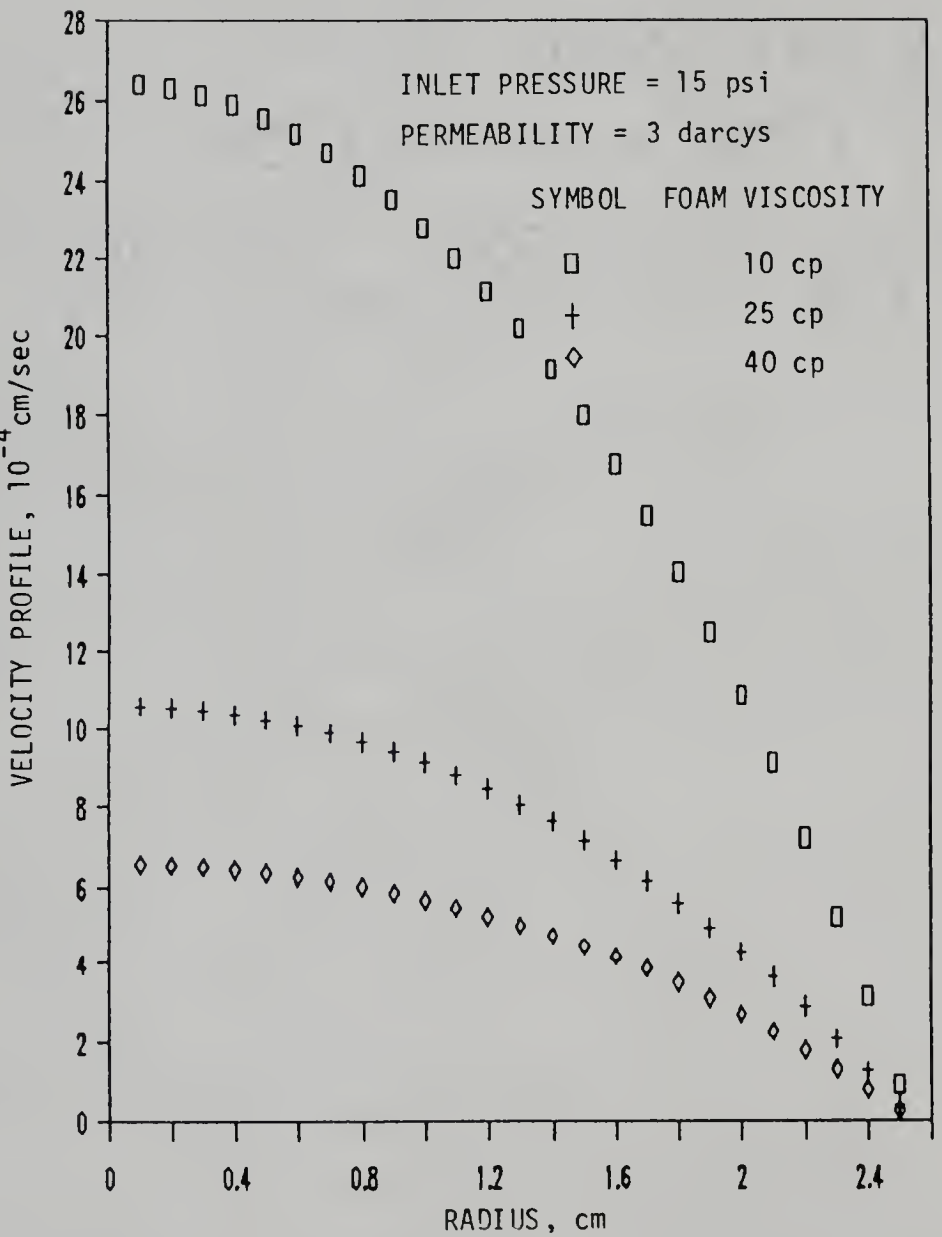

Figure 4.7. Effect of Foam Viscosity on Velocity Profile Predicted by the Model.

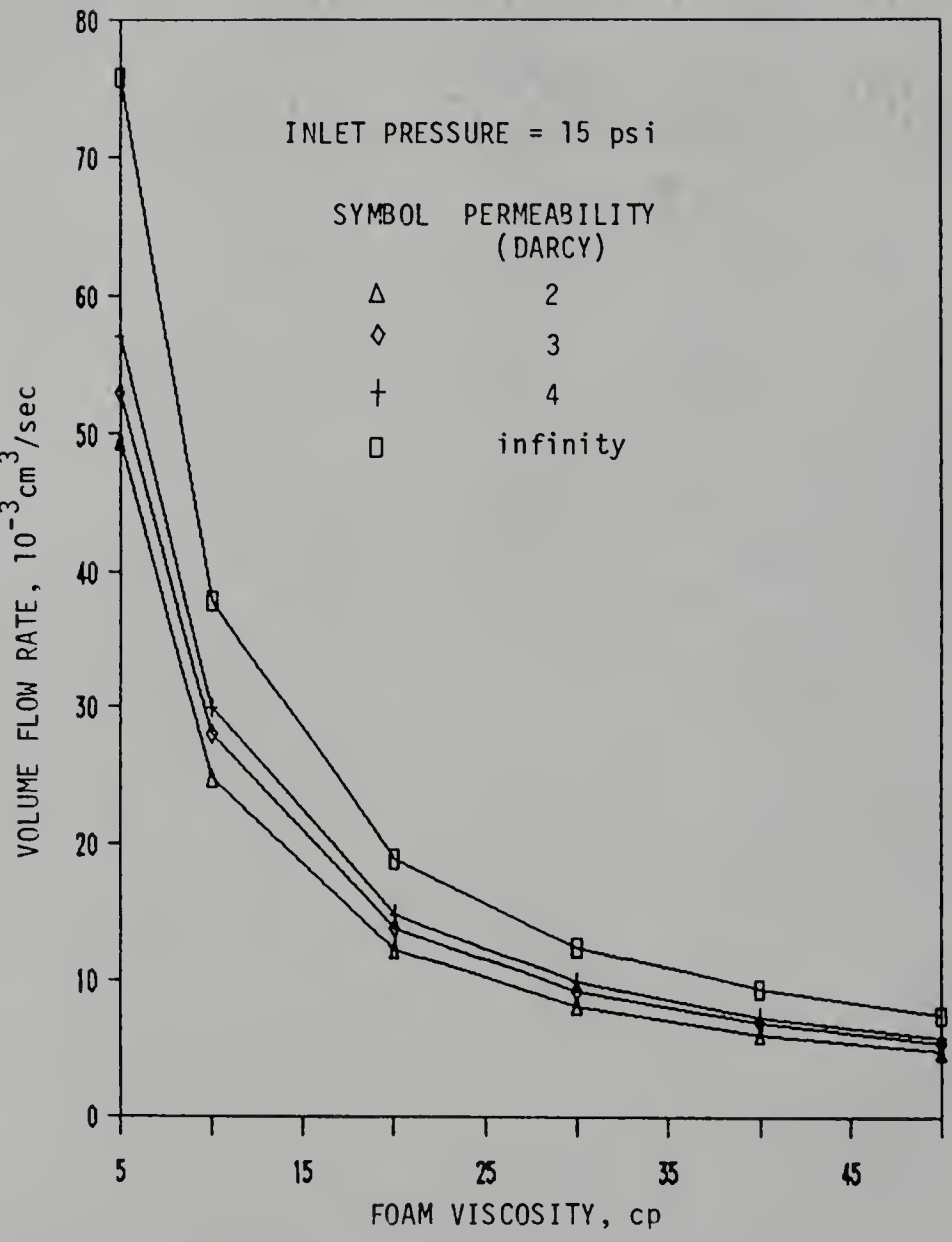

Figure 4.8. Prediction of Volume Flow Rate as a Function of Foam Viscosity for Various Porous Media.

From experimental data the average volume flow rate at the foam breakthrough was about 20×10^{-3} cm^3/sec. If the permeability of the porous media is 4 darcys then the foam viscosity is around 17 centipoises based on Figure 4.8. Results obtained from the model illustrate that it can simulate the foam flow through porous media very well. If the foam viscosity, density, and the pressure drop per unit length are constant in the real system, the foam viscosity in the porous media may be determined by the model with the given average volume flow rate.

4.4 Conclusions

Based on the investigations conducted in this chapter, the following conclusions can be drawn:

1. Model values of the pressure distributions and velocity profiles are consistent with the experimental data. That is to say, the model of foam displacing fluid can accurately predict the system behavior of fluid displacement by foam.
2. The model of foam displacing fluid can be used to predict the pressure distribution and velocity profile for any foam flooding process if the average volume flow rate at the producing site is provided.
3. Model predicted velocity profiles indicate that the fluid velocity decreases with the increase of the foam

viscosity. Experimentally, the foam viscosity had little effect on the pressure distributions.

4. The model of foam flow through porous media can be verified by checking the velocity profiles in r-direction and the volume flow rate. The velocity profiles are parabolic and the maximum velocity occurs at the center of the circular conduit where r = 0. Both the velocity in r-direction and the volume flow rate increase with the increase of the permeability of the porous media.
5. The foam viscosity in a porous medium may be estimated by the model of foam flow through porous media if the foam is treated as a homogeneous fluid with constant denisty and viscosity as well as the average volume flow rate is given.

CHAPTER V

STABILITY OF THIN FILMS

5.1 Introduction

The understanding of foam stability and foam breaking required understanding the mechanism of interactions between two films. The equilibrium thickness between two foam bubbles depends on forces acting on the thin films. These forces [45] include electrostatic repulsive force, London-van der Waals attractive force, steric repulsion force, capillary force (i.e., border suction) and gravity. The electrostatic force is due to the similarly charged electrical double layers surrounding the bubbles. The London-van der Waals force results from the electromagnetic dispersion forces between the constituent molecules of the films. The steric repulsion force is identified with the properties of adsorbent-solvent layer. The repulsion forces will resist further thinning of the films, whereas the London-van der Waals force enhances the thinning of the films. If bubble films are rigid and are not touching each other, then the thickness of the film is reduced to about

1000Å, the steric effect, gravity, and border suction are usually negligible as compared to the electrostatic and London-van der Waals forces. The theory which deals with a balance between simultaneous repulsive and attractive forces is called DLVO theory. The equilibrium thickness is of the order of magnitude predicted by DLVO theory and decreases with increasing ionic strength as expected.

5.2 DLVO Theory

An expression for the potential energy of interaction between two bubbles is the basis for prediction of foam stability. DLVO theory, developed by Derjaguin and Landau [88] and Verwey and Overbeek [89], assumes a balance between simultaneous repulsive and attractive forces of the interacting bubbles. The total potential energy between two bubbles is given by the superposition of repulsive energies and attractive energies (Figure 5.1). To stabilize the bubbles, the repulsive interactions must be increased to the point where they can overcome the attractive interactions. Hamaker [90] has shown that the potential energy of interaction due to London-van der Waals force is given by the following equation:

$$V_A = -(1/6)A_h\{2A_1A_2/[H_o^2-(A_1+A_2)^2] + 2A_1A_2/[H_o^2-(A_1-A_2)^2 + \ln[(H_o^2-(A_1+A_2)^2)/(H_o^2-(A_1-A_2)^2)]\} \quad (5.1)$$

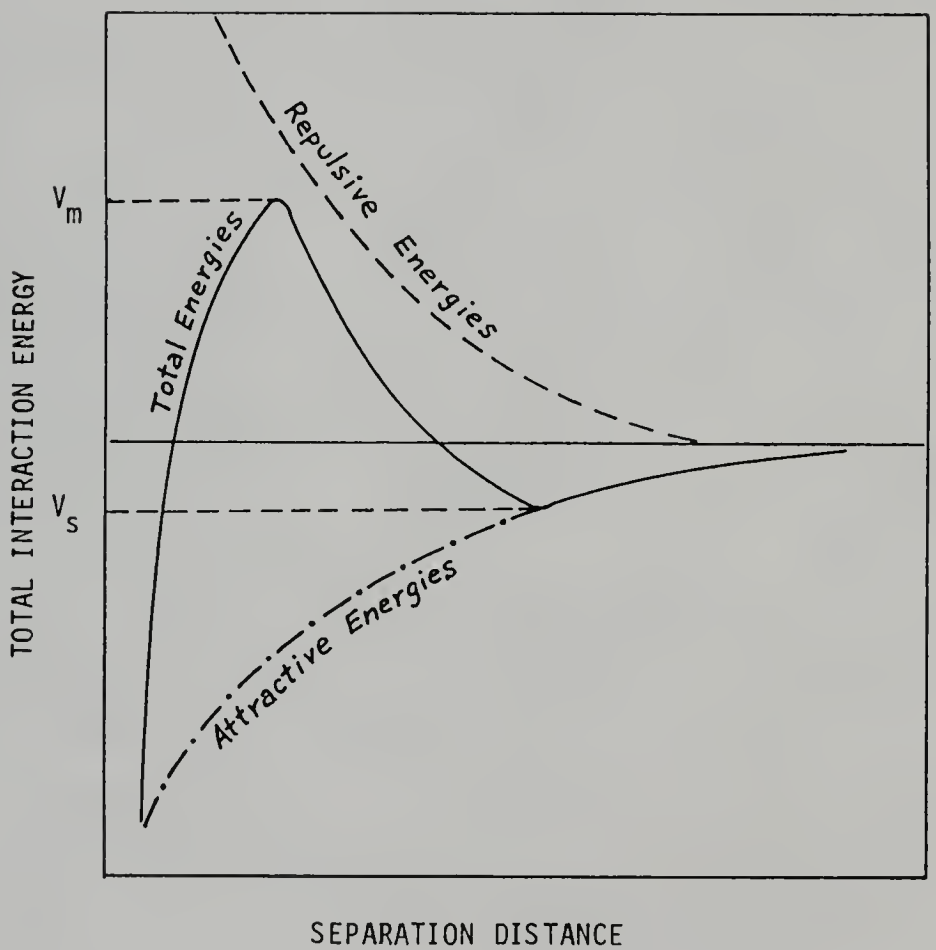

Figure 5.1. Potential Energy as a Function of Separation Distance.

where A_h = Hamaker constant

H_o = the shortest distance between the surfaces of two bubbles

A_1, A_2 = the radius of bubbles 1 and 2, respectively.

For the repulsive interaction energy, so far, there is no general solution available in the literature.

Several approximate methods of determining the repulsive interactions such as Derjaguin's method [91], Langmuir's method [92], linear superposition approximation [93], integral equation method [94], and Hogg's method [95] etc., have been reviewed. The assumptions in these methods allow DLVO theory to be reduced to an ordinary differential equation which describes electrical potential as a function of perpendicular distance from the solid surface.

Recently, Ring's work [96] has calculated the interaction potential for spherical particles under more general conditions by numerical methods. However, Ring restricted his work to univalent salts even though the technique mentioned in his work is not necessarily limited to this condition. The main object of this work was to obtain a general numerical solution of the Poisson-Boltzmann equation in two-dimensional bispherical coordinates. The solution then used to calculate the potential energy of interaction between two spherical bubbles.

5.3 Derivation

The statistically preferred positions of ions are described as an average charge density which depends on the distance from an ion, i, of charge $Z_i e$, and the electrostatic potential at this position is governed by Poisson's equation

$$\nabla^2 \phi = -(1/D) \sum_i Z_i e (n_i^+ - n_i^-) \qquad (5.2)$$

where ϕ = electrostatic potential

D = permittivity of the medium

Z_i = valence of the ionic species, i, in the solution

e = electronic charge

n_i^+ = local concentration of ionic species, i, of valence $+Z_i$

n_i^- = local concentration of ionic species, i, of valence $-Z_i$

The Boltzmann distribution describes thermal disorder motion of ions and the tendency of ions to surround an ion with opposite charge. If the bulk concentrations (numbers) per unit volume of ionic species, i, of valence $+Z_i$ and $-Z_i$ are n_{oi}^+ and n_{oi}^- respectively, then their local concentration is

$$n_i^+ = n_{oi}^+ \mathrm{EXP}(-Z_i e\phi/kT) \qquad (5.3)$$

and

$$n_i^- = n_{oi}^- \mathrm{EXP}(Z_i e\phi/kT) \qquad (5.4)$$

Poisson's equation (5.2) with the assumption of indistinguishable ions of the same valence is then the Poisson-Boltzmann equation

$$\nabla^2\phi = -(e/D)\sum_i Z_i[n_{oi}^{+}EXP(-Z_i e\phi/kT) - n_{oi}^{-}EXP(Z_i e\phi/kT)] \quad (5.5)$$

In terms of the dimensionless potential $\Phi = e\phi/kT$, equation (5.5) becomes

$$\nabla^2\Phi = -(e^2/DkT)\sum_i Z_i[n_{oi}^{+}EXP(-Z_i\Phi) - n_{oi}^{-}EXP(Z_i\Phi)] \quad (5.6)$$

In bispherical coordinates [97] (Figure 5.2), the Poisson-Boltzmann equation (5.6) (Appendix A) becomes

$$[(\cosh\eta-\cos\theta)/a]^2\left[\frac{\partial^2\Phi}{\partial\eta^2} - \left(\frac{\sinh\eta}{\cosh\eta-\cos\theta}\right)\frac{\partial\Phi}{\partial\eta} + \frac{\partial^2\Phi}{\partial\theta^2} + [\cot\theta-[\sin\theta/(\cosh\eta-\cos\theta)]](\partial\Phi/\partial\theta) + (1/\sin^2\theta)(\partial^2\Phi/\partial\varepsilon^2\right]$$
$$= -(e^2/DkT)\sum_i Z_i[n_{oi}^{+}EXP(-Z_i\Phi) - n_{oi}^{-}EXP(Z_i\Phi)] \quad (5.7)$$

Note that the term, $[(\cosh\eta-\cos\theta)/a]^2$, appeared on the wrong side of the equation in Ring's paper [96]. Since the potential distribution is symmetric in ε direction, equation (5.7) becomes

$$[(\cosh\eta-\cos\theta)/a]^2\left[\frac{\partial^2\Phi}{\partial\eta^2} - \left(\frac{\sinh\eta}{\cosh\eta-\cos\theta}\right)\frac{\partial\Phi}{\partial\eta} + \frac{\partial^2\Phi}{\partial\theta^2} + [\cot\theta-[\sin\theta/(\cosh\eta-\cos\theta)]](\partial\Phi/\partial\theta)\right]$$
$$= -(e^2/DkT)\sum_i Z_i[n_{oi}^{+}EXP(-Z_i\Phi) - n_{oi}^{-}EXP(Z_i\Phi)] \quad (5.8)$$

Equation (5.8) is an elliptic partial differential equation over the domain $\{ \eta_2 < \eta < \eta_1,\ 0 < \theta < \pi \}$ with the

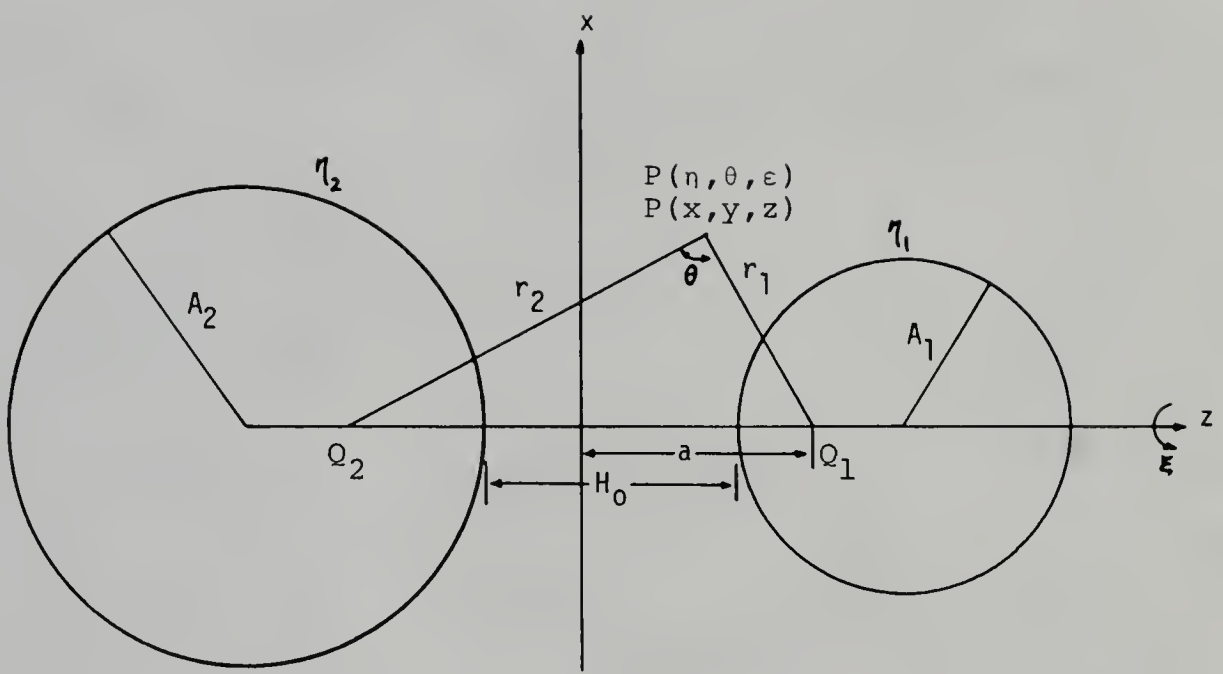

Figure 5.2. Bispherical Coordinates System. $\eta = \ln(r_2/r_1)$, Where Q_1 and Q_2 Are Limit Points at $\eta \to \infty$, $-\infty$, Respectively.

following boundray conditions

$$\Phi = \Phi_1 \quad \text{at} \quad \eta = \eta_1 \quad \text{for all} \quad 0 < \theta < \pi \qquad (5.9)$$

$$\Phi = \Phi_2 \quad \text{at} \quad \eta = \eta_2 \quad \text{for all} \quad 0 < \theta < \pi \qquad (5.10)$$

$$(\partial\Phi/\partial\theta) = 0 \quad \text{at} \quad \theta = 0 \quad \text{for all} \quad \eta_2 < \eta < \eta_1 \qquad (5.11)$$

$$(\partial\Phi/\partial\theta) = 0 \quad \text{at} \quad \theta = \pi \quad \text{for all} \quad \eta_2 < \eta < \eta_1 \qquad (5.12)$$

The alternating direction implicit method is adopted in this work because of its high efficiency. Although the range of θ is theoretically from π to zero, the practical range of θ should be from π to a specified value, say δ, (a small number but greater than zero). One reason is that the term, $\sinh\eta/(\cosh\eta-\cos\theta)$, is undefined at $\theta = 0$ and $\eta = 0$ and will produce a mathematical overflow during the computation. This defect was not discussed in Ring's work. An angle, α, is determined such that the interaction area will cover all points on one particle surface which interacts with all points on the other particle surface. This approach not only meets practical application but also gives higher accuracy and less computer memory space required. If δ was chosen very close to zero, $(\partial\Phi/\partial\theta)$ should approach zero. So, the boundary condition along curve $\theta = \delta$ (e.g., 0.03491 rad.) may be determined by solving equation (5.8) with the substitution of θ by δ. Meantime, boundary condition along line $\theta = \pi$ can also be obtained by applying boundary condition (5.12) to the governing equation (5.8). Figure 5.3 shows the bispherical coordinate system and symbols used to determine the bispherical coordinates and the angle α for a given set of

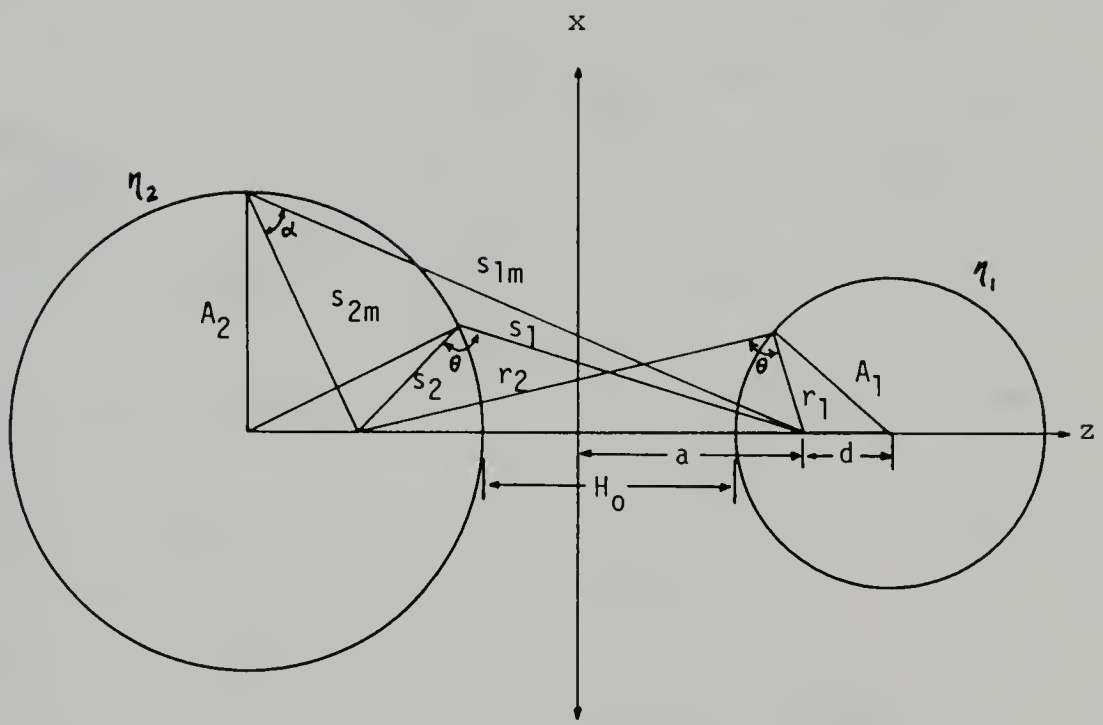

Figure 5.3. Bispherical Coordinates System and Symbols Used to Determine the Bispherical Coordinates.

particles. The following relationships (Appendix B) are required:

$$\operatorname{acsch}\eta_1 = A_1 \tag{5.13}$$

$$\operatorname{acsch}|\eta_2| = A_2, \quad \eta_2 < 0 \tag{5.14}$$

$$A_1 + A_2 + H_o = \operatorname{acoth}\eta_1 + \operatorname{acoth}|\eta_2| \tag{5.15}$$

$$\ln(r_2/r_1) = \eta_1 \tag{5.16}$$

$$r_1^2 + r_2^2 - 2r_1 r_2 \cos\theta = 4a^2 \tag{5.17}$$

$$\ln(s_2/s_1) = \eta_2, \quad \eta_2 < 0 \tag{5.18}$$

$$s_1^2 + s_2^2 - 2s_1 s_2 \cos\theta = 4a^2 \tag{5.19}$$

$$\alpha = \cos^{-1}[(s_{1m}^2 + s_{2m}^2 - 4a^2)/(2s_{1m}s_{2m})] \tag{5.20}$$

where

$$s_{1m} = [A_2^2 + (A_1 + A_2 + H_o - d)^2]^{1/2} \tag{5.21}$$

$$s_{2m} = s_{1m}\,\mathrm{EXP}(\eta_2) \tag{5.22}$$

$$d = A_1 - [4a^2/[\mathrm{EXP}(2\eta_1) + 1 + 2\mathrm{EXP}(\eta_1)]^{1/2}] \tag{5.23}$$

Once the potential distribution between two bubbles was found by solving equation (5.8) with the boundary conditions (5.9)-(5.12), the repulsive interaction energy for this system could be calculated:

$$V_R(H_o) = [V_1(H_o)+V_2(H_o)] - [V_1(\infty)+V_2(\infty)] \tag{5.24}$$

where

$$V_1(H_o) + V_2(H_o) = [(\pi a D k^2 T^2)/e^2]* \{ - \Phi_1 \int_\alpha^\pi [\sin\theta/(\cosh\eta_1 - \cos\theta)][(\partial\Phi/\partial\eta)|_{\eta_1}]d\theta + \Phi_2 \int_\alpha^\pi [\sin\theta/(\cosh\eta_2 - \cos\theta)][(\partial\Phi/\partial\eta)|_{\eta_2}]d\theta \} \tag{5.25}$$

It is clear that there are no interactions between bubbles

separated by an infinite distance. Therefore, $V_1(\infty)$ and $V_2(\infty)$ can be obtained individually by solving general Poisson-Boltzmann equation in spherical coordinates, then from potential distribution and surface charge density; the free energy of each particle is calculated by surface integral. In Ring's work, the infinite separation distance was taken to be five Debye lengths. This assumption may be inappropriate for large size bubbles with high surface potential or in a low ionic strength solution. Equation (5.24) gives the sign convention that positive values of energy correspond to repulsion and negative values to attraction.

The total potential energy between two bubbles is given by the superposition of repulsive energy and attractive energy, $V_T = V_R + V_A$. Since the attractive force cannot be manipulated as much as the electrical repulsive force, the repulsive interactions must play the critical role in determining the stability of foams.

5.4 Numerical Method

The above considerations reduce DLVO theory to the problem of solving an elliptic partial differential equation in bispherical coordinates. Figure 5.4 shows a mapping of bispherical coordinates onto x-y space. If each side of the system is divided into m increments, the problem involves the solution of a set of m-1 simultaneous

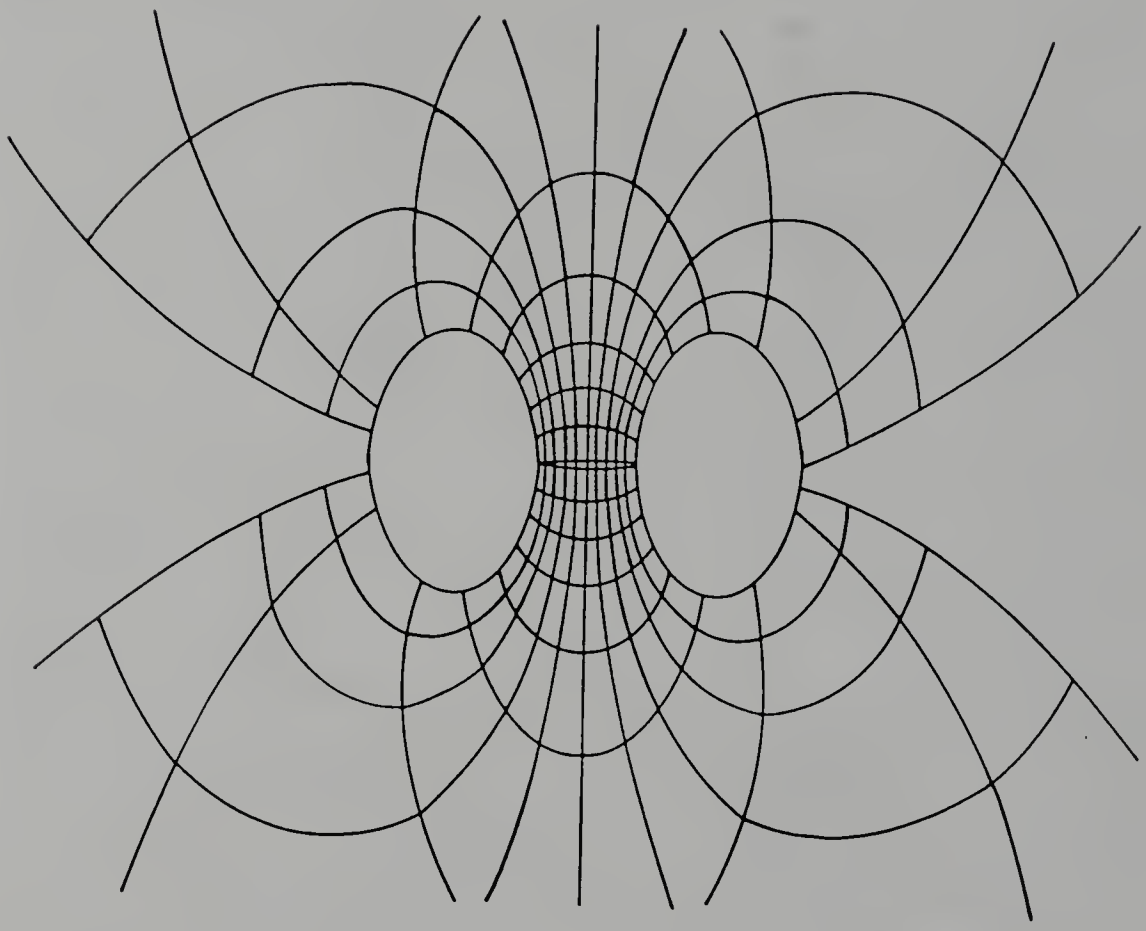

Figure 5.4. A Mapping of Bispherical Coordinates onto x-y Space.

equations [98,99]. Note the large change in mesh size in the system. Specially, the area close to the lower boundary (i.e., $\theta = \delta$) possesses tremendously big grid size which may influence numerical accuracy and stability. This is because there are not enough grid points in these regions containing sharp potential gradients. In order to resolve the problem, a simple stretching function [100] has been made to generate more grid points in the system near the boundary $\theta = \delta$:

$$\bar{\theta} = \ln\left(\frac{\beta + \theta/\pi}{\beta - \theta/\pi}\right) \Big/ \ln\left(\frac{\beta + 1}{\beta + 1}\right)$$

where β is the stretching parameter and $1 < \beta < \infty$. There is no stretching in η direction.

Denoting the current iteration by the superscript (p+1), and the preceding iteration by (p), equation (5.8) can be rewritten in the finite difference form

$$\frac{\Phi_{j,k+1}^{(p+1)} - 2\Phi_{j,k}^{(p+1)} + \Phi_{j,k-1}^{(p+1)}}{(\Delta\eta)^2} - A(k\Delta\eta, j\Delta\theta)\left(\frac{\Phi_{j,k+1}^{(p+1)} - \Phi_{j,k-1}^{(p+1)}}{2\Delta\eta}\right)$$

$$+ \frac{\Phi_{j+1,k}^{(p)} - 2\Phi_{j,k}^{(p)} + \Phi_{j-1,k}^{(p)}}{(\Delta\theta)^2} + B(k\Delta\eta, j\Delta\theta)\left(\frac{\Phi_{j+1,k}^{(p)} - \Phi_{j-1,k}^{(p)}}{2\Delta\theta}\right)$$

$$= C(k\Delta\eta, j\Delta\theta)\{\Sigma_i Z_i [n_{oi}^{+} \mathrm{EXP}(-Z_i\Phi) - n_{oi}^{-} \mathrm{EXP}(Z_i\Phi)]\} \qquad (5.26)$$

where $A(k\Delta\eta, j\Delta\theta) = \sinh(k\Delta\eta)/[\cosh(k\Delta\eta) - \cos(j\Delta\theta)]$

$B(k\Delta\eta, j\Delta\theta) = \cot(j\Delta\theta) - \{\sin(j\Delta\theta)/[\cosh(k\Delta\eta) - \cos(j\Delta\theta)]\}$

$C(k\Delta\eta, j\Delta\theta) = [a/(\cosh(k\Delta\eta) - \cos(j\Delta\theta))]^2 * (-e^2/DkT)$

In equation (5.26), unknown values of $\Phi_{j,k}^{(p+1)}$ (i.e., current iteration) appear only in the η direction; all other terms appear in known values from the preceding iteration. If every value of Φ of grid k along a constant θ line in Figure 5.4 is written, then a set of m-1 simultaneous equations are obtained:

$$\begin{bmatrix} -2 & 1-(\Delta\eta/2)A(\Delta\eta,j\Delta\theta) & 0 & \cdots & 0 & 0 \\ 1+(\Delta\eta/2)A(2\Delta\eta,j\Delta\theta) & -2 & 1-(\Delta\eta/2)A(2\Delta\eta,j\Delta\theta) & \cdots & 0 & 0 \\ . & . & . & \cdots & 0 & 0 \\ . & . & . & \cdots & 0 & 0 \\ 0 & 0 & \cdots & 1+(\Delta\eta/2)A[(m-1)\Delta\eta,j\Delta\theta] & -2 & \end{bmatrix}$$

$$\begin{bmatrix} \Phi_{j,1}^{(p+1)} \\ \Phi_{j,2}^{(p+1)} \\ \Phi_{j,3}^{(p+1)} \\ . \\ . \\ \Phi_{j,m-1}^{(p+1)} \end{bmatrix} = \begin{bmatrix} f(\Delta\eta,j\Delta\theta e,\Phi_{j,1}^{(p)})-h(\Delta\eta,j\Delta\theta,\Phi_{j+1,1}^{(p)},\Phi_{j,1}^{(p)},\Phi_{j-1,1}^{(p)})- \\ \Phi_{j,0}^{(p)}[1+(\Delta\eta/2)A(\Delta\eta,j\Delta\theta)] \\ f(2\Delta\eta,j\Delta\theta,\Phi_{j,2}^{(p)})-h(2\Delta\eta,j\Delta\theta,\Phi_{j+1,2}^{(p)},\Phi_{j,2}^{(p)},\Phi_{j-1,2}^{(p)}) \\ f(3\Delta\eta,j\Delta\theta,\Phi_{j,3}^{(p)})-h(3\Delta\eta,j\Delta\theta,\Phi_{j+1,3}^{(p)},\Phi_{j,3}^{(p)},\Phi_{j-1,3}^{(p)}) \\ . \\ . \\ f[(m-1)\Delta\eta,j\Delta\theta,\Phi_{j,m-1}^{(p)}]-h[(m-1)\Delta\eta,j\Delta\theta,\Phi_{j+1,m-1}^{(p)},\Phi_{j,m-1}^{(p)} \\ ,\Phi_{j-1,m-1}^{(p)}]-\Phi_{j,m}^{(p)}\{1-(\Delta\eta/2)A[(m-1)\Delta\eta,j\Delta\theta]\} \end{bmatrix}$$

$$j = 1, 2, 3, \ldots, m-1 \qquad (5.27)$$

where $f(k\Delta\eta,j\Delta\theta,\Phi_{j,k}^{(p)}) = (\Delta\eta)^2 C(k\Delta\eta,j\Delta\theta)\{\sum_i Z_i[n_{oi}^{+}EXP(-Z_i\Phi)-n_{oi}^{-}EXP(Z_i\Phi)]\}$

$$h(k\Delta\eta,j\Delta\theta,\Phi_{j+1,k}^{(p)},\Phi_{j,k}^{(p)},\Phi_{j-1,k}^{(p)})$$

$$= (\Delta\eta/\Delta\theta)^2\{\Phi_{j+1,k}^{(p)}[1+(\Delta\theta/2)B(k\Delta\eta,j\Delta\theta)]-2\Phi_{j,k}^{(p)}+$$

$$\Phi^{(p)}_{j-1,k}[(\Delta\theta/2)B(k\Delta\eta, j\Delta\theta)]\}$$

The Thomas Algorithm [101] is employed to obtain the formal solutions of equation (5.27). Once initial values have been established at the grid points, calculation proceeds as follows: first, the θ direction at each grid point is fixed while solutions are calculated in the η direction; then new values in the η direction are fixed and the process is reversed and new values along θ are calculated. The procedure can be repeated as many times as necessary until convergence is obtained or the number of iterations exceeds a preset limit. This calculation is generally nonconvergent but an underrelaxation method is used to make it convergent. This is particularly important in solving very large sets of simultaneously equations iteratively. The choice of optimum value of the underrelaxation factor is a very complex task. For the system described above, this factor is less than 0.0001.

The total repulsive interaction energy is obtained from equation (5.24) by using the 4th order integration method of Simpson's rule. Figure 5.5 shows the flow diagram of the whole process.

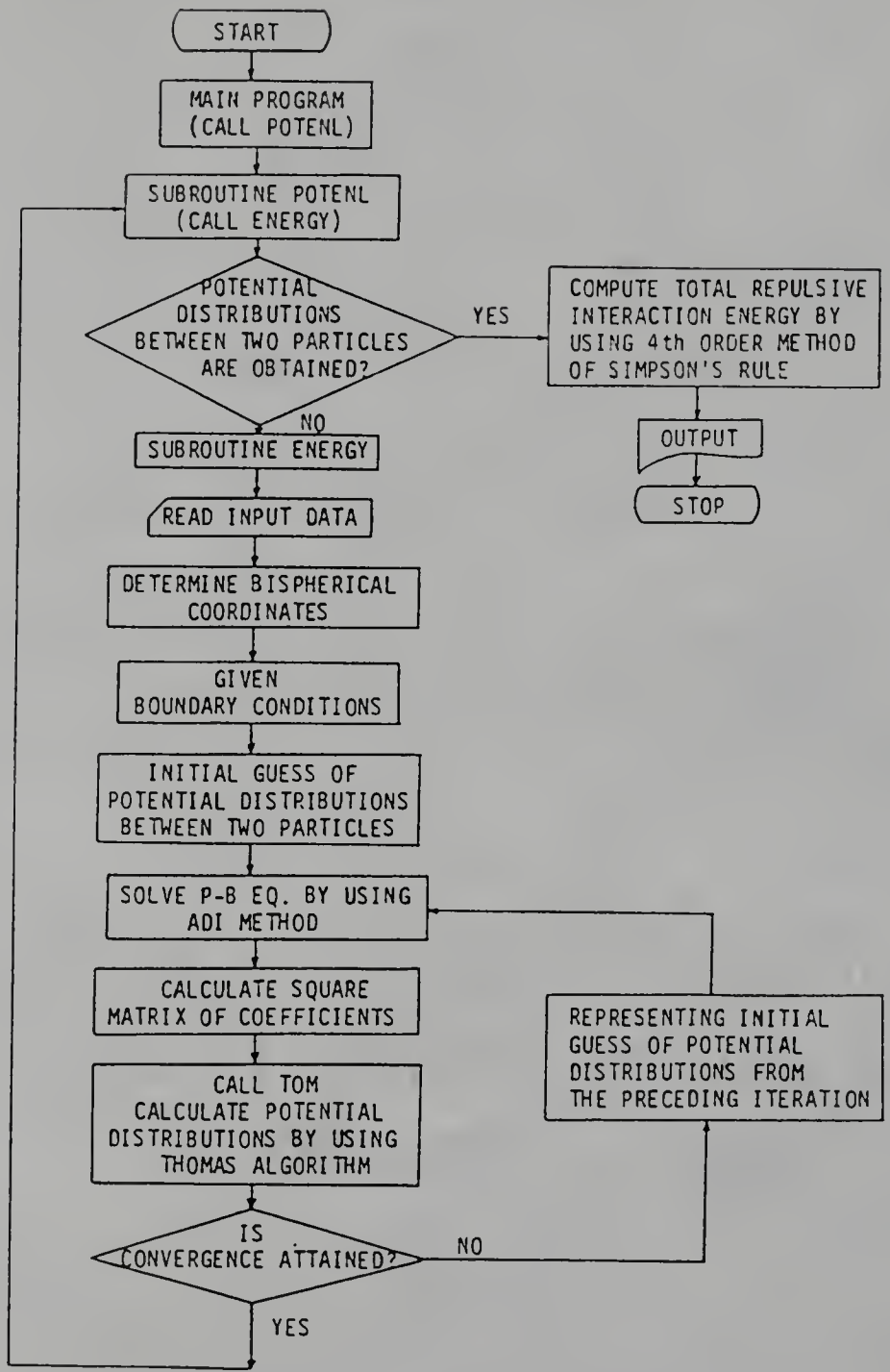

Figure 5.5. Flow Chart of a Numerical Method for Solving the Generalized Poisson-Boltzmann Equation in Bispherical Coordinates.

5.5 Results and Discussion

The repulsive interaction energy predicted from this work is compared with those of Ring and Hogg et al. in Figure 5.6. The curve predicted by this work reveals the same profile as Ring's work. Ring's results show a much steeper asymptote at small separation distance compared with those from this work. This may result from different number of grids in the two systems, different criterion of convergence in the program, different infinite separation distance, and different numerical method used in solving the Poisson-Boltzmann equation. No further comparison between this work and Ring's work can be made since Ring's program is not available. As mentioned in Ring's paper, the results of Hogg et al. show a flattening of the slope (actually the interaction energy is decreasing and even becomes negative) at very small separation distance (e.g., H_o < 1 nm). The difference of repulsive interaction energy between this work and Hogg's work in the range of 1 nm < H_o < 3 nm may be due to the linearization of the Poisson-Boltzmann equation in the latter work. This work gives a greater interaction energy versus separation dependence because the generality of the Poisson-Boltzmann equation is preserved in the derivation. This feature does not included in any other model or approach.

Theoretical repulsive interaction energy curves calculated using the generalized Poisson-Boltzmann equation

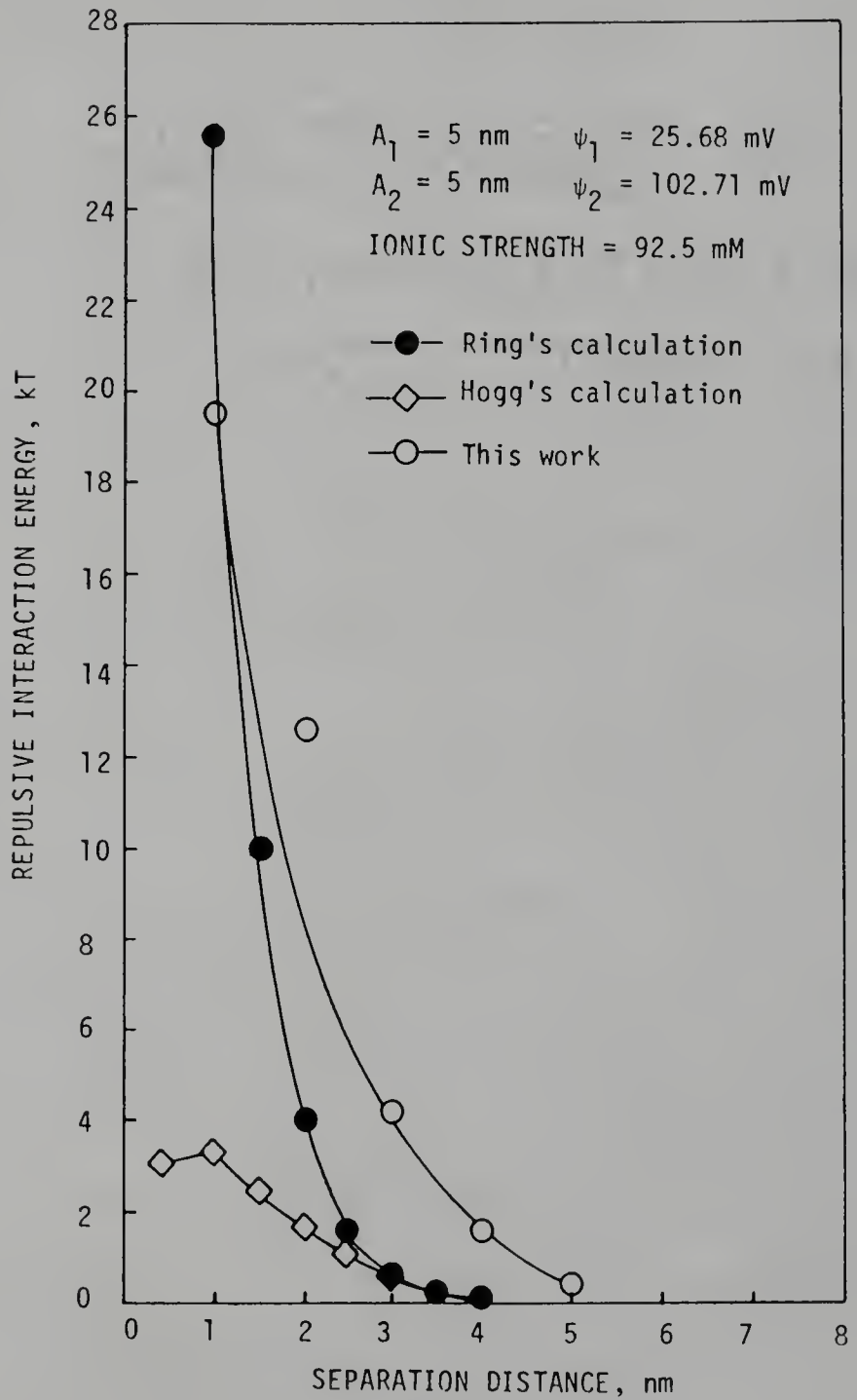

Figure 5.6. Repulsive Interaction Energy as a Function of Separation Distance.

as a function of ionic strength are given in Figure 5.7. Other parameters related to the calculation are indicated in the Figure. It gives a general idea of the effect of ionic strength on total interaction energy. The work required to overcome the energy barrier for coagulation dramatically decreases with increasing electrolyte concentration. This is because of significant compression of electrical double layers by adding more electrolytes in solution.

The effect of number of grids on the repulsive interaction energy is shown in Figure 5.8. It is clear that there is no significant influence on the repulsive interaction energy when the number of grids in θ direction is above 30 while the number of grids in η direction is fixed at 20. The computer time required increases exponentially with the number of grids. Therefore, an optimal number of grids may be determined from Figure 5.8, which gives reasonable accuracy and requires less computing time. Since time consuming computations and large computer memory were required for obtaining the solution of the Poisson-Boltzmann equation, only the demonstration of this work mentioned above has been accomplished so far. Further studies on the application of this program in predicting the foam stability should be continued in future.

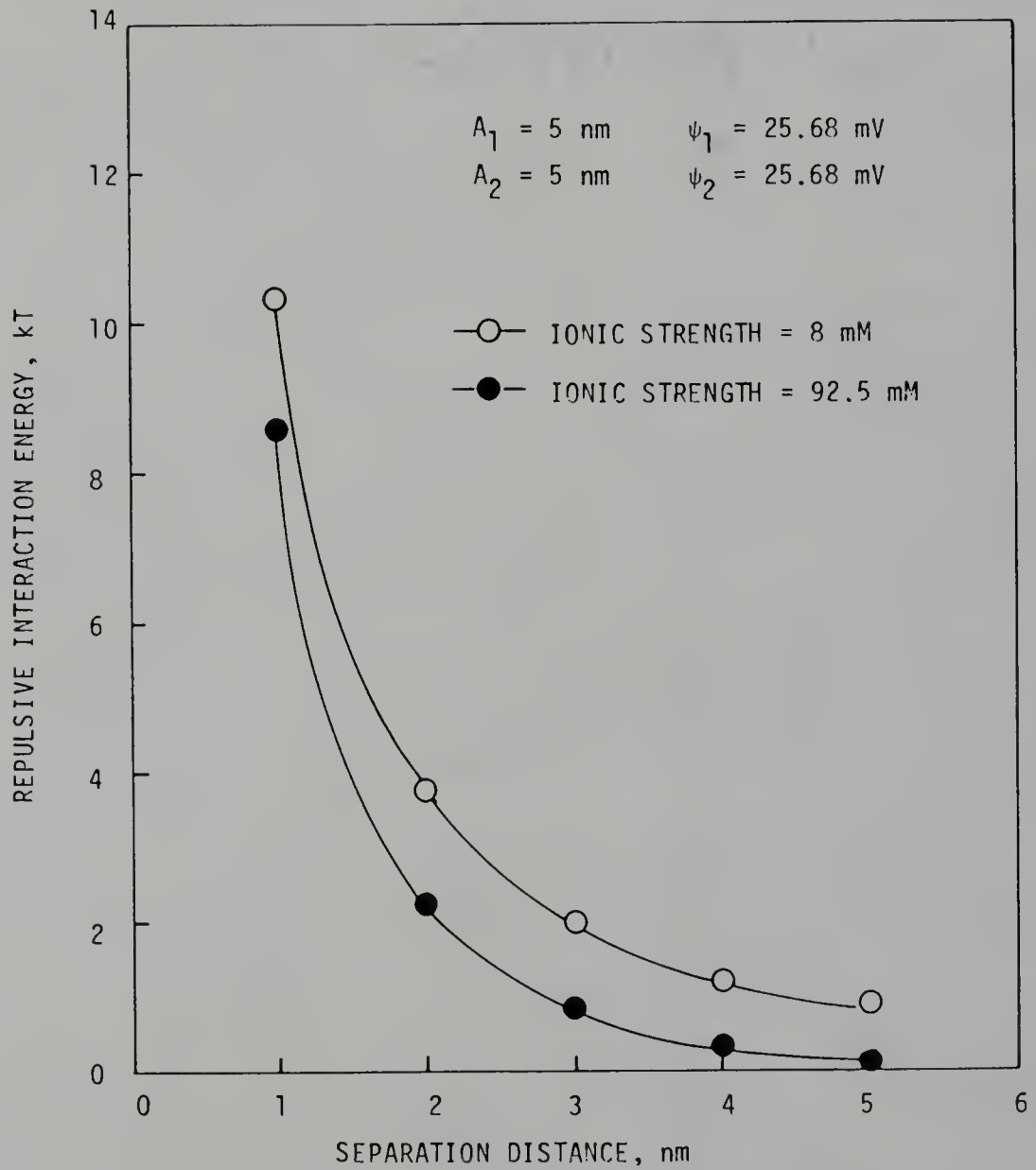

Figure 5.7. Repulsive Interaction Energy as a Function of Ionic Strength.

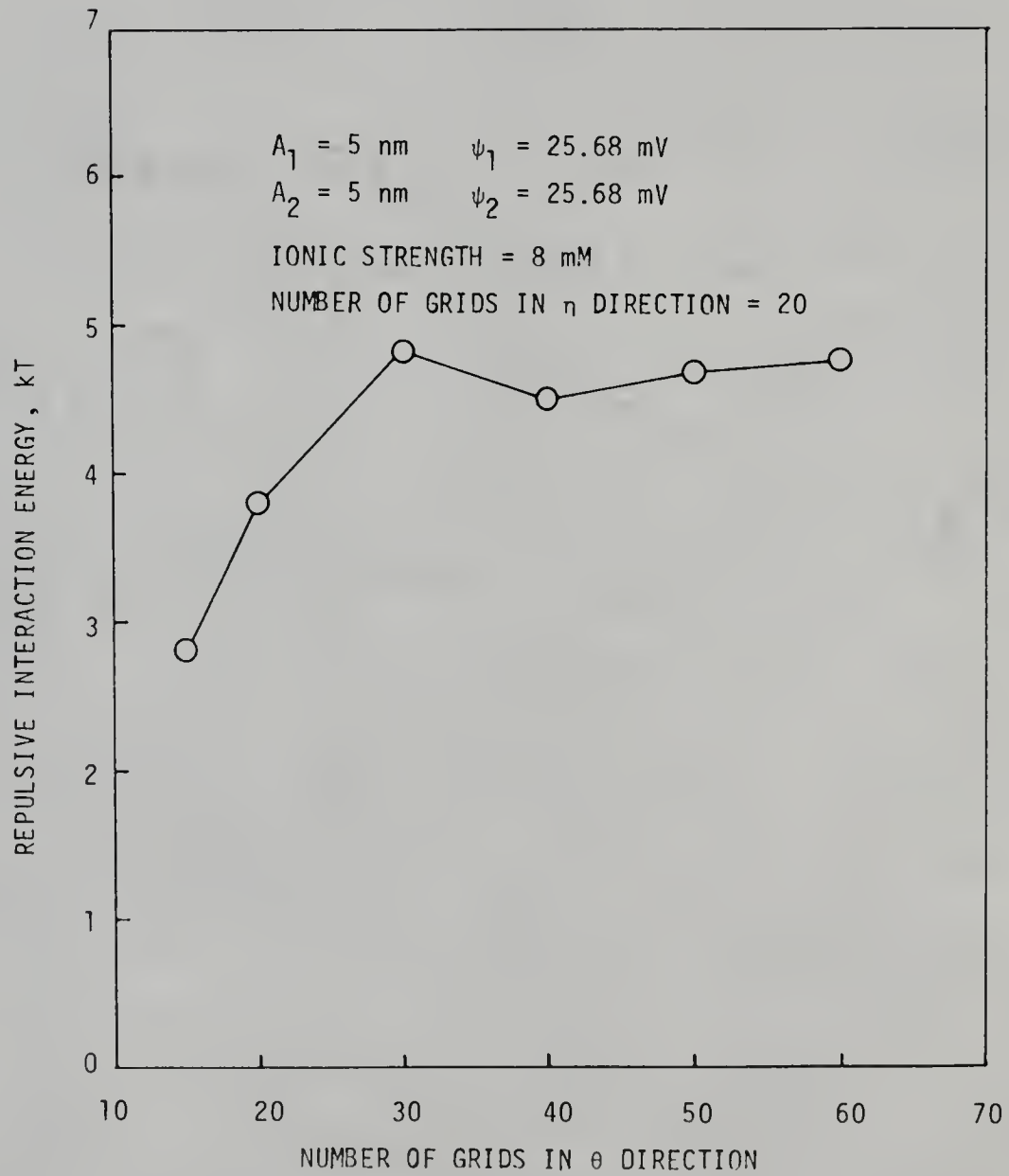

Figure 5.8. Effect of Number of Grids on Repulsive Interaction Energy.

5.6 Conclusions

A numerical solution of the Poisson-Boltzmann equation for two unequal spheres with any surface potential was obtained in bispherical coordinates system using constant potential boundary conditions. The repulsive interaction energy of the two-sphere system was calculated from this numerical solution. The method is completely general because neither simplified equation (e.g., infinite flat plate model) nor other restrictive conditions (e.g., small surface potential, univalent-salt condition, etc.) are required. A comparison is made between this work and other methods. Results show that this work is close to the Ring's results.

CHAPTER VI

EFFECTS OF ADDING POLYMER ON THE FOAM

6.1 Introduction

From the previous studies, it is clear that the foam stability is related to a number of the surface properties of the foam such as surface tension, surface viscosity, foaminess, foam quality, rate of drainage, bubble size distribution, etc. Basically, these properties are mainly determined by interactions between the surfactant molecules at the liquid/gas interface, adsorption/desorption of the surfactant molecules at the interface, and rheology of the adsorbed layer. The tight packing and high viscosity adsorbed layer can be achieved by selecting proper surfactants and foam-promoting additive. It is well known that the elasticity and viscosity of the foam can be improved by the addition of a proper polymer. Goddard and Hannan [34] reported that the increase in foam stability can be obtained by adding a cationic polymer to an SDS solution.

For enhanced oil recovery applications, a stable, viscous foam is desired for the mobility control. Also, the

concentrations of foaming agents are required to keep as low as possible from the economic point of view. It brings the idea up for preparing a stable, viscous foam as follows:

step 1. Find a proper surfactant and co-surfactant if necessary, which can produce fairly high stable foam as well as high fluid displacement efficiency.

step 2. Find an optimum concentration for these selected surfactants.

step 3. Add a small amount of polymer which is compatible with the selected surfactants to improve the stability of the foam.

step 4. Find an optimum polymer concentration under which foam possesses the highest stability, viscosity, and foaminess.

Biopolymer xanthan (FLOCON^{TM} 4800) and hydrolyzed polyacrylamides are anionic polymers and both have been used in tertiary oil recovery for mobility control. The choice between xanthan and polyacrylamide for tertiary oil recovery depends on the rheological properties, the injectivity characteristics, and the cost of the polymer. Although xanthan is more expensive than polyacrylamides, it offers outstanding resistance to shear degradation which is troublesome for polyacrylamides in low permeability porous media. In contrast to polyacrylamides, xanthan has a superior tolerance to high salinity and hardness of water

[102]. In addition to the excellent injectivity of diluted xanthan solution, xanthan is compatible with most surfactants and alcohols at the levels typically used in chemical flooding processes [103]. Due to the various excellent physical properties, xanthan was chosen to study the effect of polymer on the foam.

6.2 Theory

The effect of polymer on surfactant in aqueous solutions was investigated over the last decade. It has been shown that [35-39] water soluble polymers can form "association polyelectrolytes" as a complex in the presence of large, ionizable molecules such as ionic surfactants, dyes, etc. Fishman and Eirich [104] reported that at constant polymer concentration and varying SDS concentration, three regions of behavior was observed. At very low ratios of SDS to polymer (S/P) minimal interaction occurred. At intermediate S/P ratios, clusters or submicelles were formed. At high S/P ratio, these submicelles were converted to mixed regular micelles at a CMC lower than that of pure SDS. Meanwhile, Schwuger [105] proposed a mechanism of interaction between ionic surfactants and nonionic polymers (e.g.,polyglycol ethers): in water, only weak reversible hydrophobic bonding between cationic surfactants and nonionic polymers is formed. In contrast to cationic surfactants, complexing of anionic

surfactants with nonionic polymers is very marked. Besides the hydrophobic bonding, electrical forces seem to be very important. The interactions may have resulted from a partially positive charge transfer to the ether oxygen group and, consequently, the effect of the hydrophilic group of the anionic surfactant is increased.

Goddard and Hannan [34] studied the interactions between the cationic polymer and anionic surfactant. They showed that addition of SDS to the polymer (e.g., cellulose ether) in aqueous solution resulted in progressive reduction of both its solubility and electrophoretic mobility, with maximum precipitation being close to the point of zero mobility. On the other hand, addition of the polymer, itself weakly surface active at the liquid/air interface, to the SDS solution can dramatically reduce the surface tension. They interpreted these results in terms of a highly surface-active polymer/surfactant complex resulting from "head to head" adsorption of the surfactant onto the polymer.

Interactions between similarly charged surfactants and polymers were reported by Desai [40]. In his work, the effect of polyacrylamides on the interfacial tension of anionic surfactants (e.g., TRS 10-80, Petrostep-420, and Texas #2) were studied. He proposed a mechanism, namely, exclusion of the surfactant and polymer from the immediate vicinity of the other, as follows: The polymer molecules do not bind the surfactants due to the electrostatic repulsive

forces, the volume taken up by the polymer molecules is excluded to the surfactant molecules. With charged polymers, a diffuse electrical region surrounding the polymer molecule would also be excluded to the similarly charged surfactant due to the effect of electrical double layers. Effectively, surfactant molecules would be excluded from a volume of the bulk, which in term reduces the interfacial tension. The excluded volume depends on the size of the polymer coil, the number of the polymer molecules, and the charge density of the polymer molecules. Recently, Lee [106] further proved this mechanism using a quasi-elastic light scattering.

Almost all of the reported literatures dealt with surfactant-polymer interactions in relation to the physical properties of the aqueous solutions. Little attention has been devoted to the effect of surfactant-polymer interactions on the foam properties. In this chapter, the effects of adding anionic polymer on the surface properties of the foam containing the anionic surfactant were studied.

6.3 Results and Discussion

6.3.1 Determination of Optimum Concentrations of Foaming Agents

Arbitrary concentrations, 2mM and $3x10^{-4}$ g_m/ml, were chosen for the foaming agents SDS (CMC = 8.2 mM) and Stepanflo 40 (CMC = $3x10^{-4}$ g_m/ml), respectively. Both

foaming agents possessed a fair ability to produce foams which were not quite stable at these concentrations. From the previous studies, we know that foam can be stabilized by adding a small amount of alkyl alcohols. Among these alcohols, the highest fluid displacement efficiency was obtained using decyl alcohol as a co-surfactant. Figure 6.1 and 6.2 show the surface tension of mixed surfactant systems, SDS + $C_{10}OH$ and Stepanflo 40 + $C_{10}OH$, as a function of the concentration of decyl alcohol. It is clear that the surface tension of mixed surfactant systems without salt decreased with the increase of decyl alcohol concentration, and it remained constant or decreased slightly beyond a certain critical concentration of decyl alcohol. The critical concentrations for SDS and Stepanflo 40 are about 1.0 mM and 0.8 mM, respectively. Also, the effect of salt on the surface tension was significantly reduced when the concentrations of decyl alcohol were beyond these critical concentrations. This implies that at the critical concentration the number of surfactant molecules at the liquid/air interface reached a maximum with a tight packing pattern.

A series of fluid displacement experiments were carried out using the same mixed surfactant systems described above. The results (Figure 6.3-6.6) showed that the highest fluid displacement efficiency and breakthrough time as well as the lowest effective air mobility were observed with the system of Stepanflo 40 ($3x10^{-4}$ g_m/ml) +

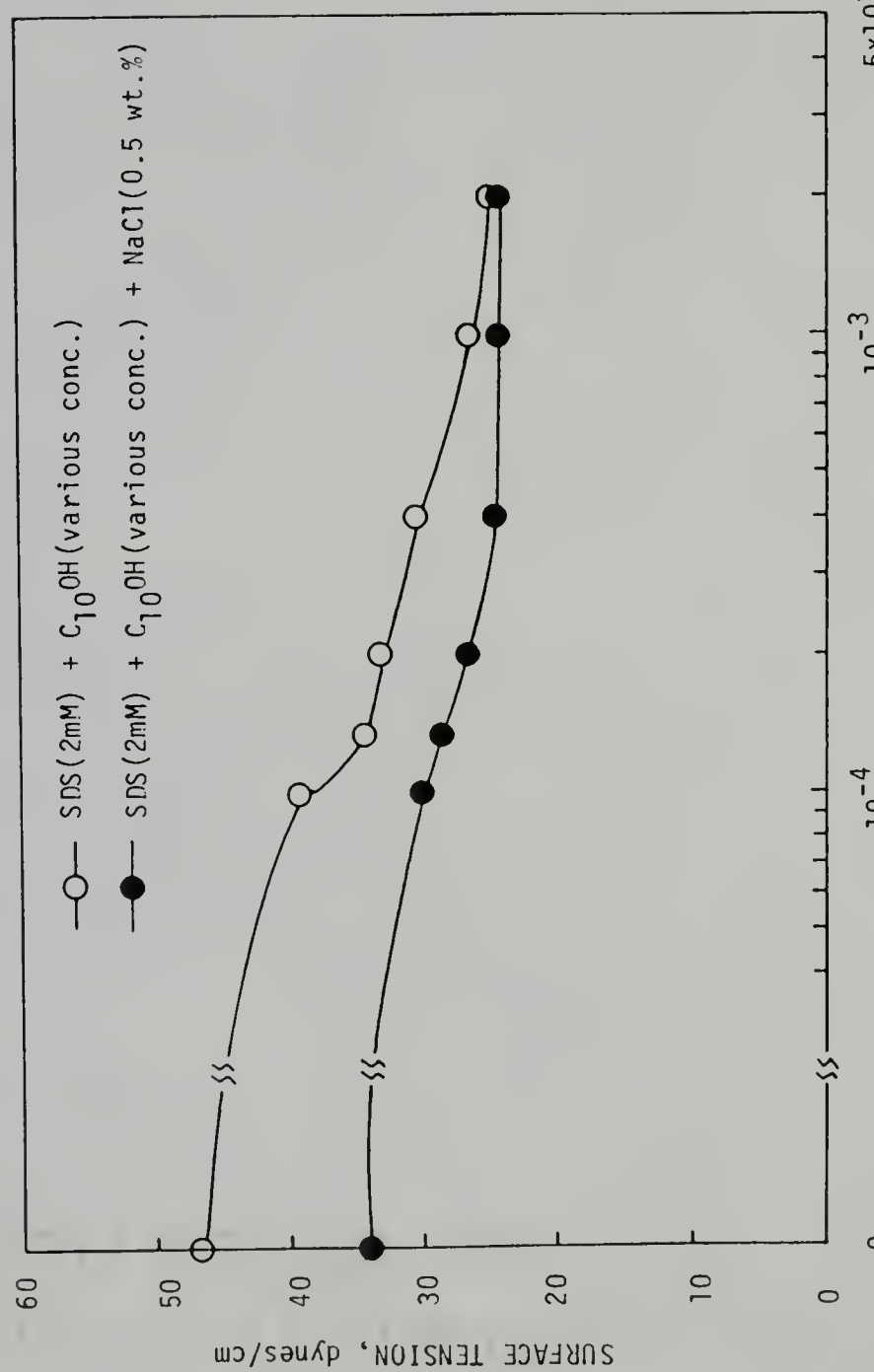

Figure 6.1. Surface Tension of Mixture of SDS + $C_{10}OH$ + NaCl as a Function of the Concentration of Decyl Alcohol.

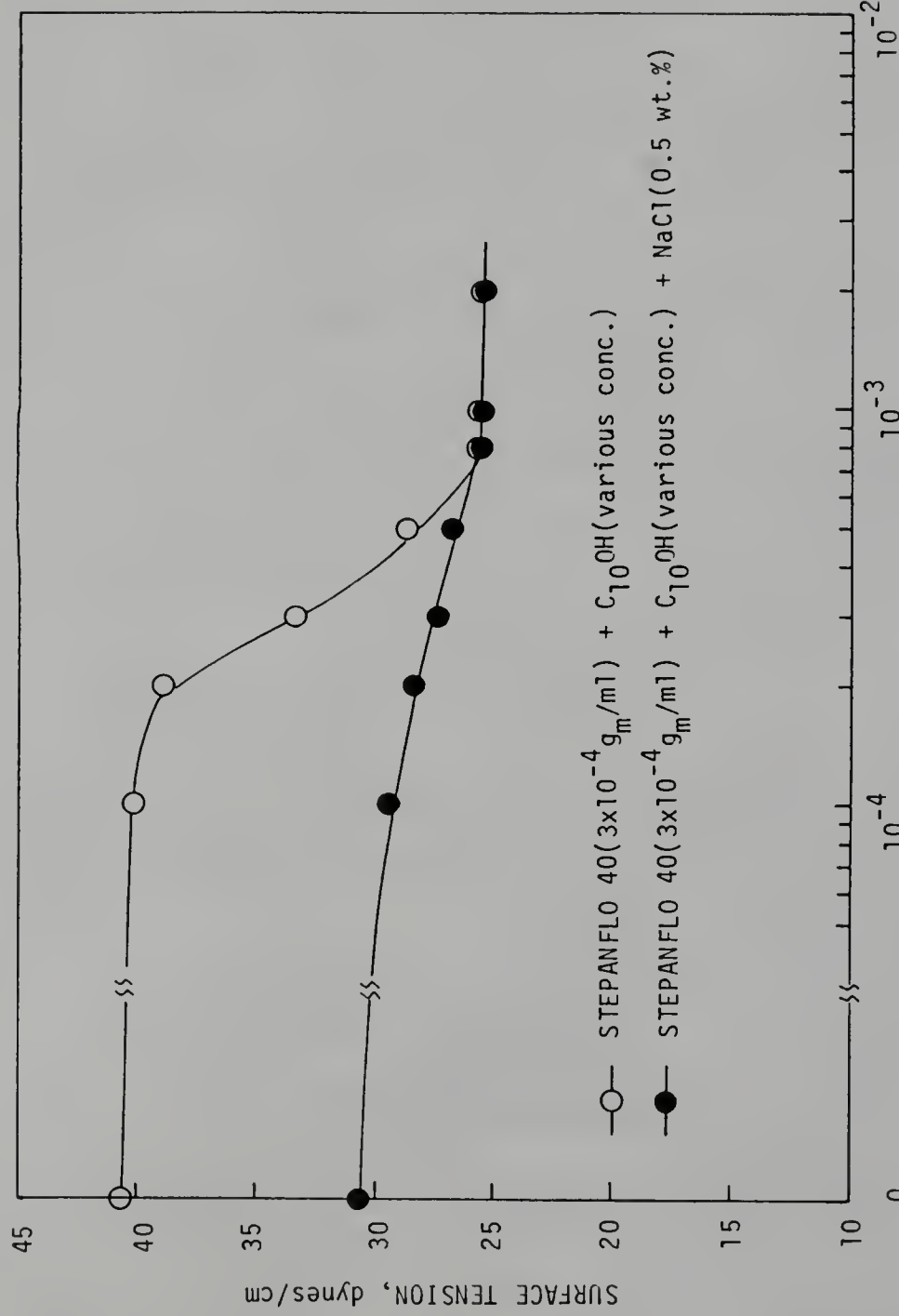

Figure 6.2. Surface Tension of Mixture of Stepanflo 40 + $C_{10}OH$ + NaCl as a Function of the Concentration of Decyl Alcohol.

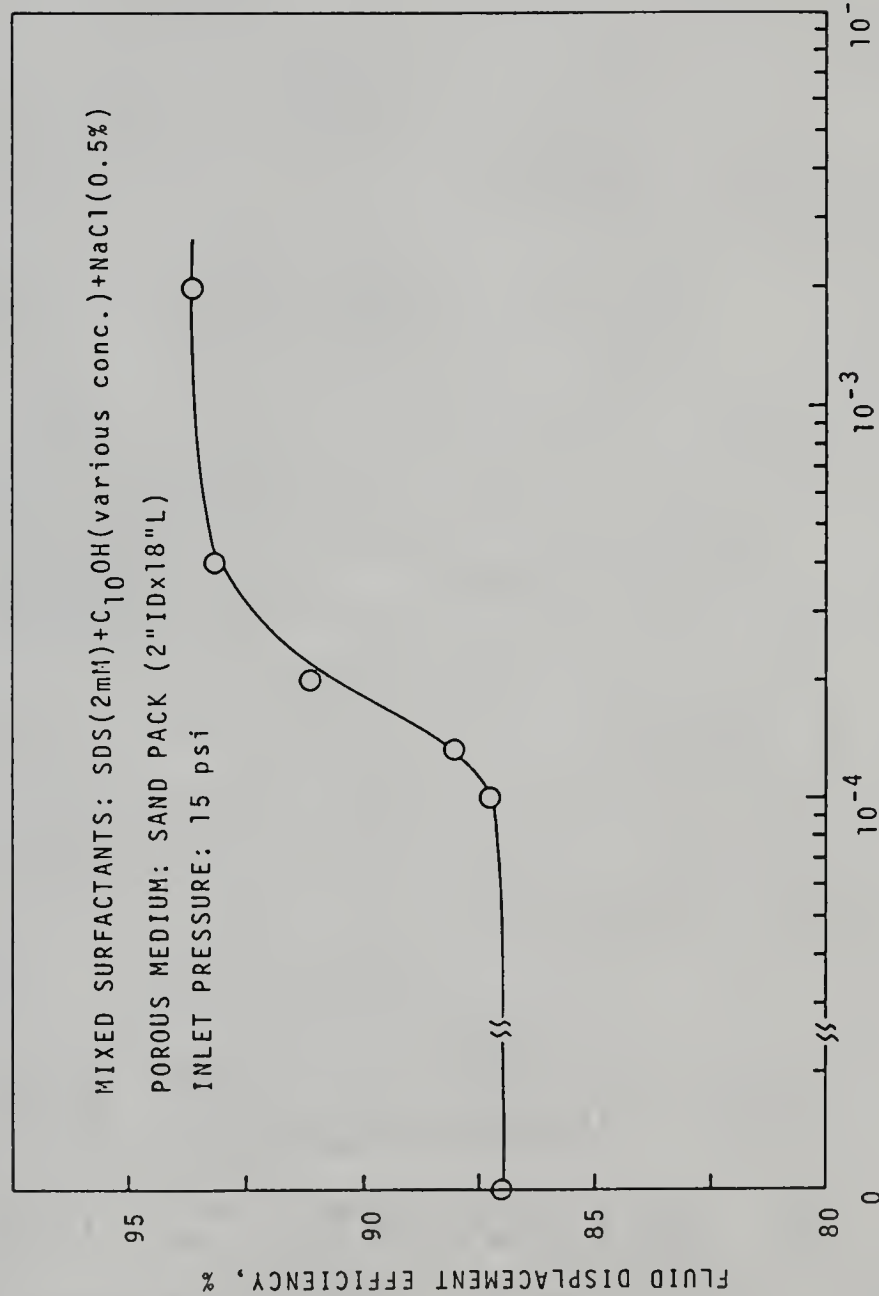

Figure 6.3. Effect of SDS with Different Concentrations of Decyl Alcohol on Fluid Displacement Efficiency.

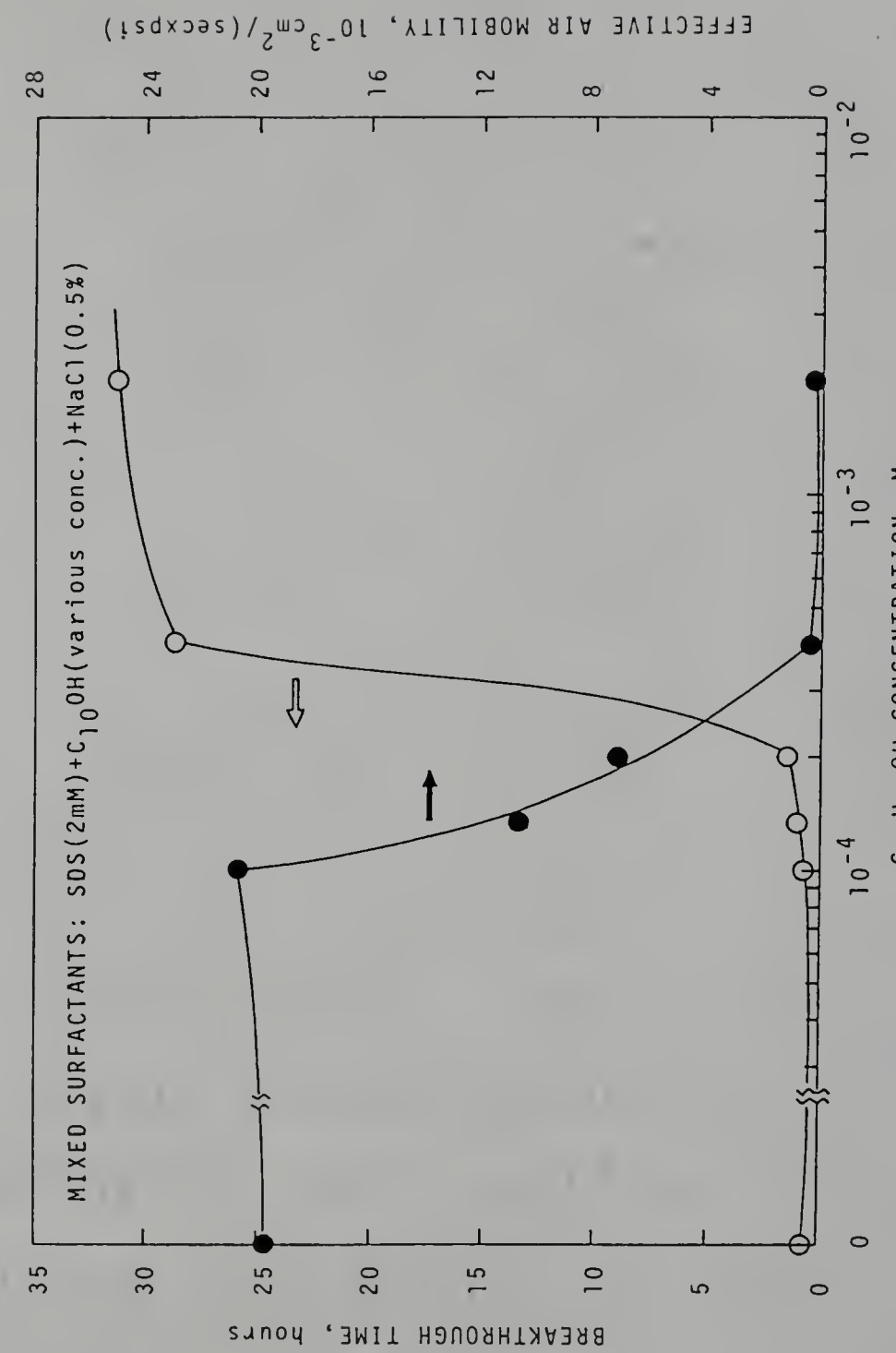

Figure 6.4. Effect of SDS with Different Concentrations of Decyl Alcohol on Breakthrough Time and Effective Air Mobility.

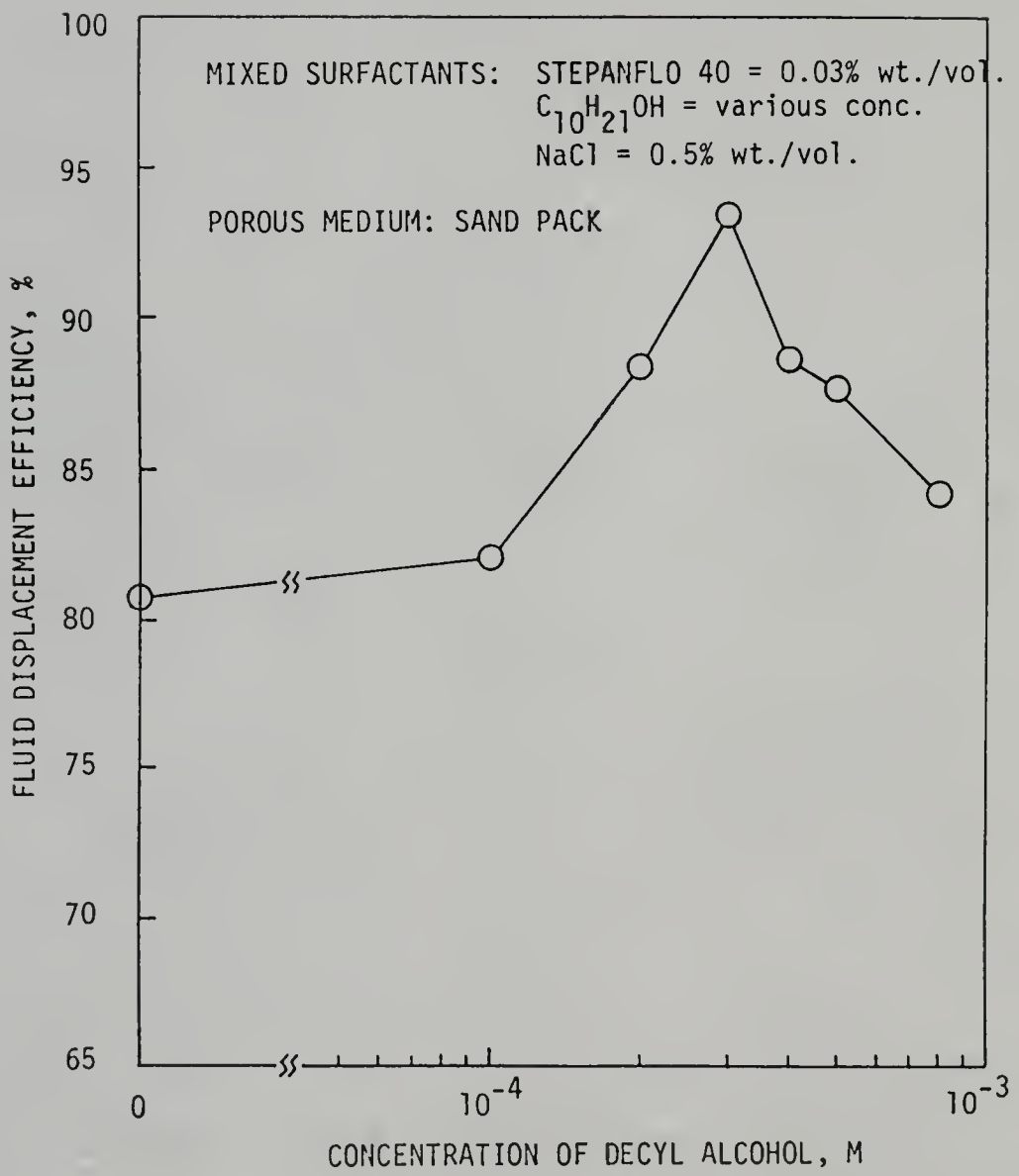

Figure 6.5. Effect of Stepanflo 40 with Different Concentrations of Decyl Alcohol on Fluid Displacement Efficiency.

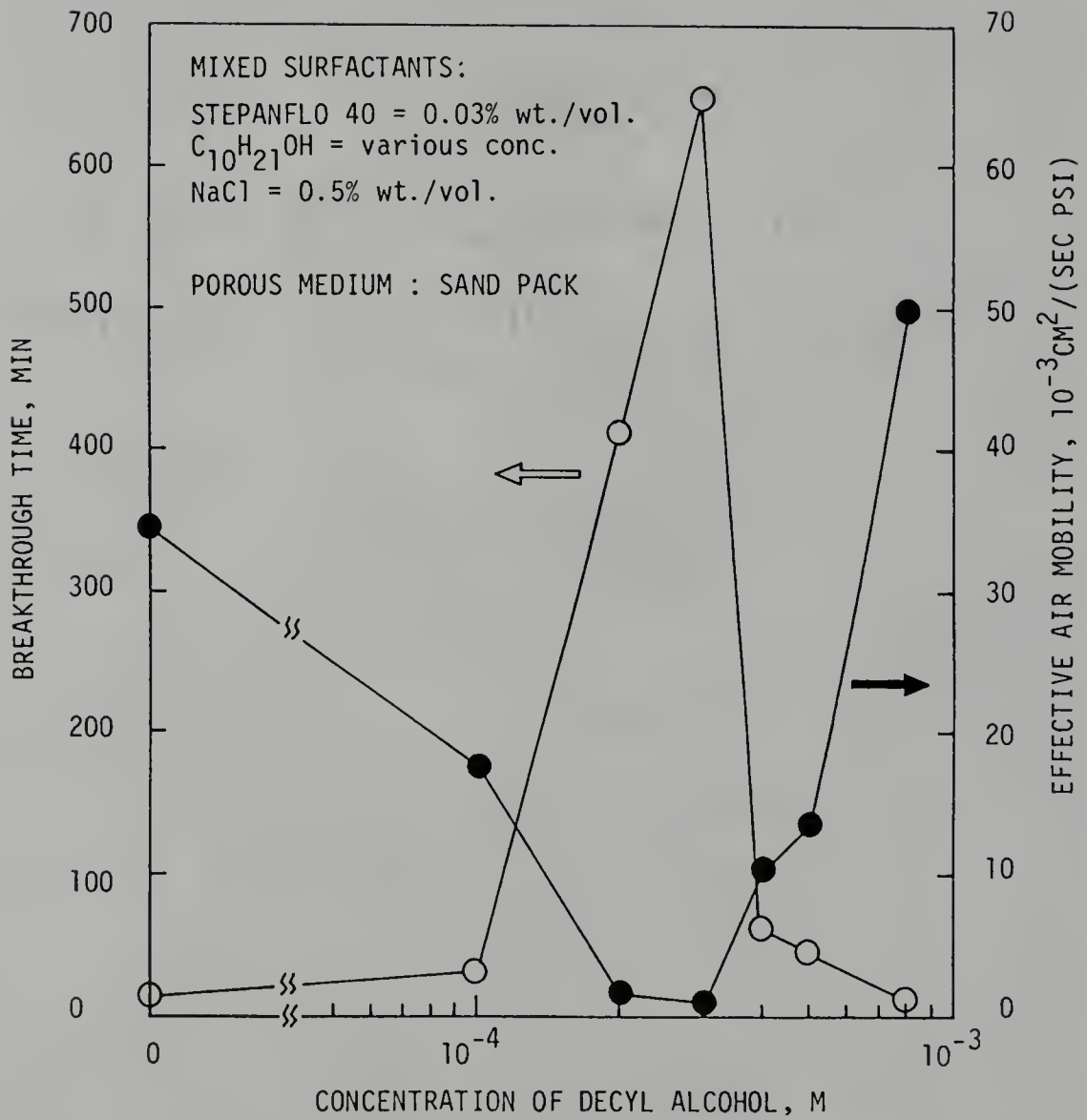

Figure 6.6. Effect of Stepanflo 40 with Different Concentrations of Decyl Alcohol on Breakthrough Time and Effective Air Mobility.

$C_{10}OH$ (0.3 mM) + NaCl (0.5%). On the other hand, there was little change for the system of SDS + $C_{10}OH$ + NaCl when the concentration of decyl alcohol was above 0.5 mM. Therefore, the concentrations, 0.5 mM and 0.3 mM, of decyl alcohol were selected to mix with SDS and Stepanflo 40, respectively for the further study of effects of adding polymer on the foam.

6.3.2 Surface Tension

Surface tension studies show that addition of the xanthan can result in reductions in the surface tension of SDS and Stepanflo 40 solutions in the absence of NaCl (Figures 6.7-6.8). A pronounced reduction in surface tension at low polymer concentrations (e.g., conc. < 200 ppm) was observed and there was little effect on the surface tension at high polymer concentrations. No significant change in surface tension was found by adding polymer to the surfactant solution containing NaCl (0.5%) because the liquid/air interface has been already saturated with surfactant molecules at this moment. No more surfactant molecules can be driven out from the bulk solution due to the addition of the polymer. The surfactant molecules driven out by the polymer can be explained by the effect of excluded polymer volume and the effect of electrical double layer. It should be noted that, in the diagram of surface tension vs. polymer concentration, there were two regions (gradually decreasing then leveling off)

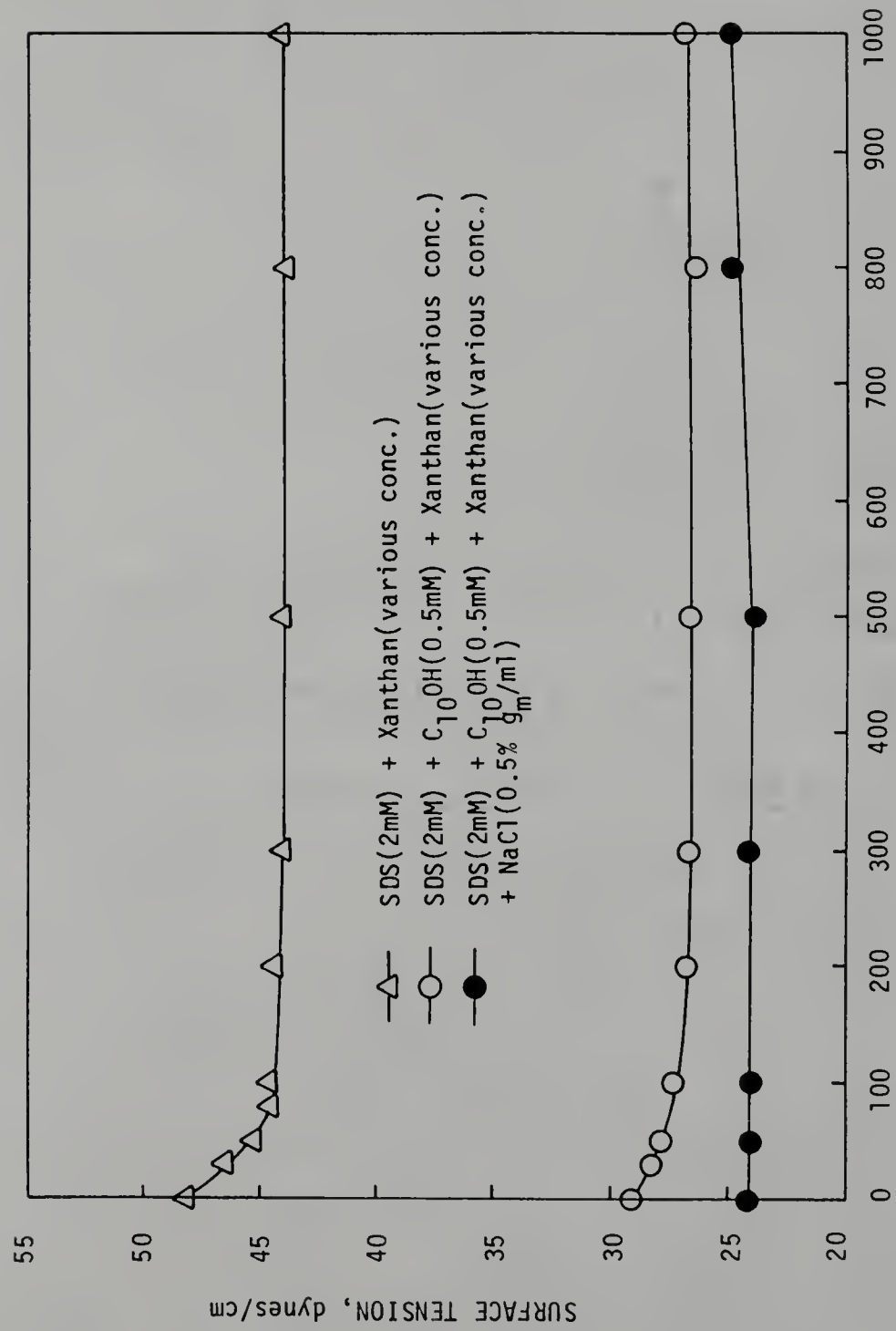

Figure 6.7. Effect on Surface Tension of Adding Xanthan to SDS Solution, with and without Decyl Alcohol.

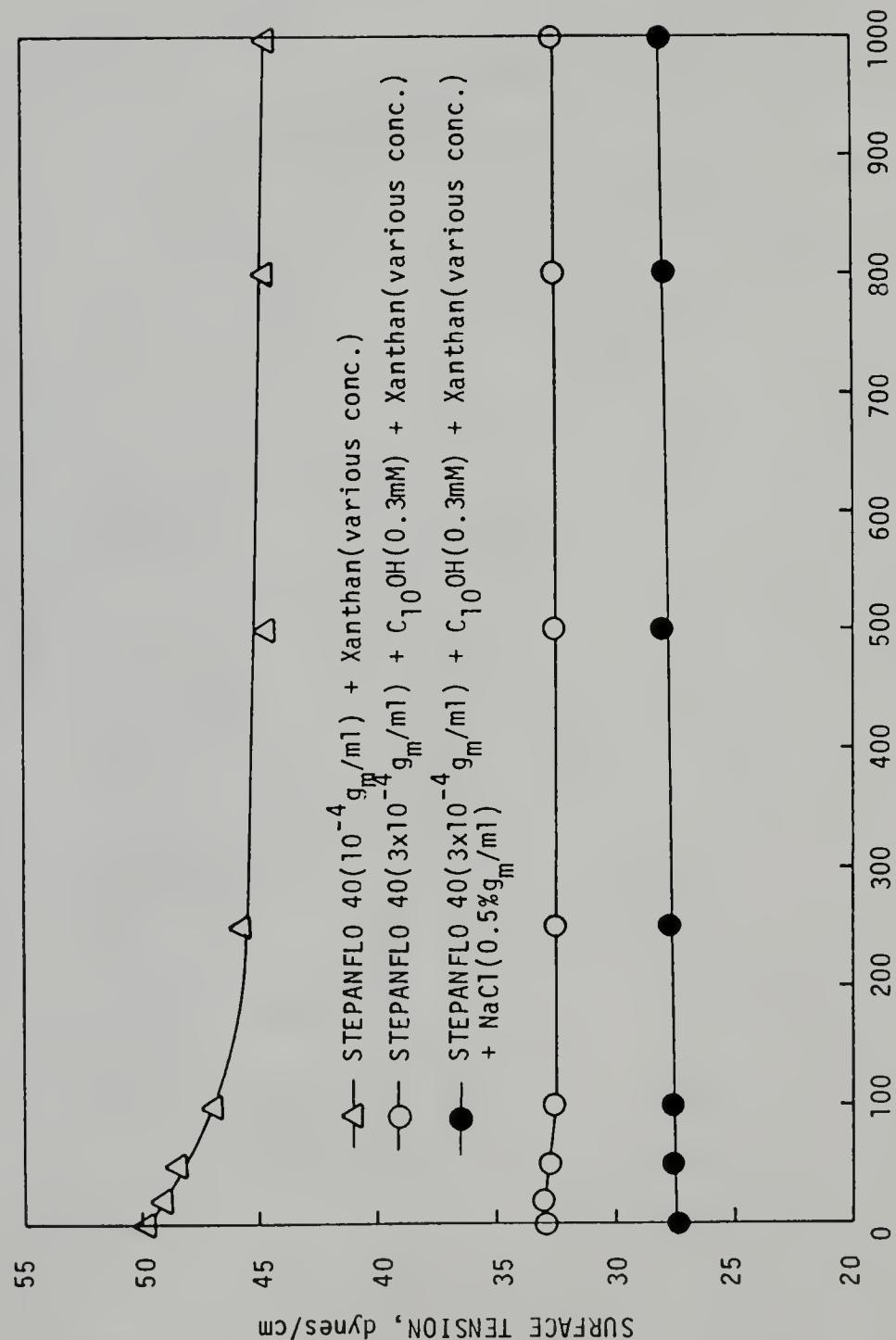

Figure 6.8. Effect on Surface Tension of Adding Xanthan to Stepanflo 40 Solution, with and without Decyl Alcohol.

rather than four regions which were separated by more or less sharp breaks in the curve. The latter usually were observed for the systems of nonionic polymer-anionic surfactant or cationic polymer-anionic surfactant interactions and the surfactant-polymer complex was formed in these systems. For the systems of SDS + xanthan and Stepanflo 40 + xanthan, there were no complexes formed. Also, the interactions of decyl alcohol and xanthan must be very weak compared to the decyl alcohol-SDS interactions. Otherwise, the gradual decrease in surface tension of either SDS + $C_{10}OH$ or Stepanflo 40 + $C_{10}OH$ solution should not be found by adding xanthan.

6.3.3 Foam Quality

The foam quality of mixed foaming agents containing polymer as a function of polymer concentration is shown in Figures 6.9 and 6.10. It is evident that the foam quality decreased with the increase of polymer concentration. These results revealed that a large amount of water was brought into the bubble films due to the polymer. The effect was especially significant at high polymer concentrations. For instance, the foam quality at the polymer concentration of 1000 ppm was lowered to 60% and 73% respectively for the system of SDS + $C_{10}OH$ + xanthan and Stepanflo 40 + $C_{10}OH$ + xanthan. Even after 30 minutes, the foam quality was still quite low compared to the foaming system without adding polymer.

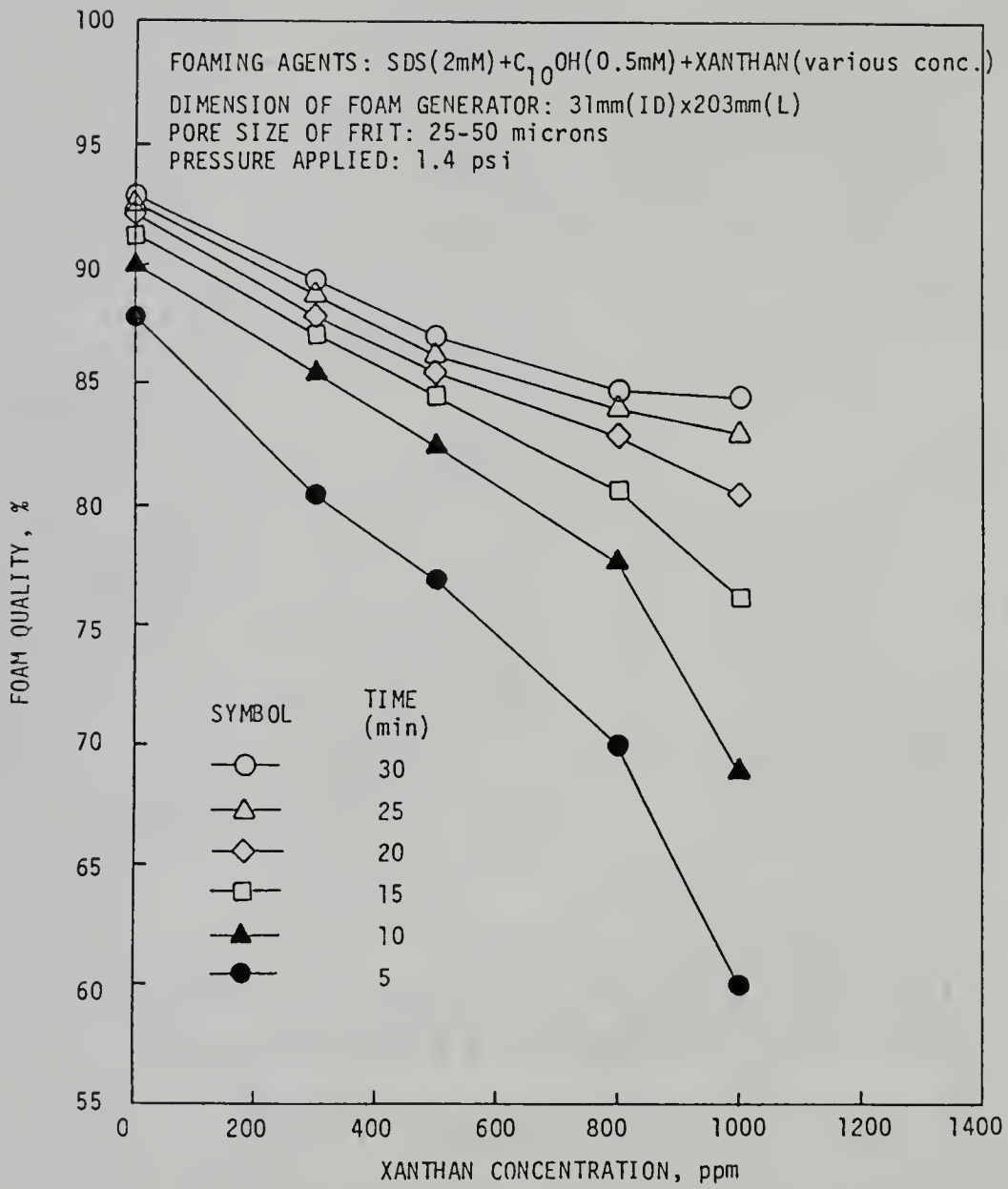

Figure 6.9. Variation in Foam Quality for Mixed Foaming Agents of SDS + $C_{10}OH$ with Different Xanthan Concentrations.

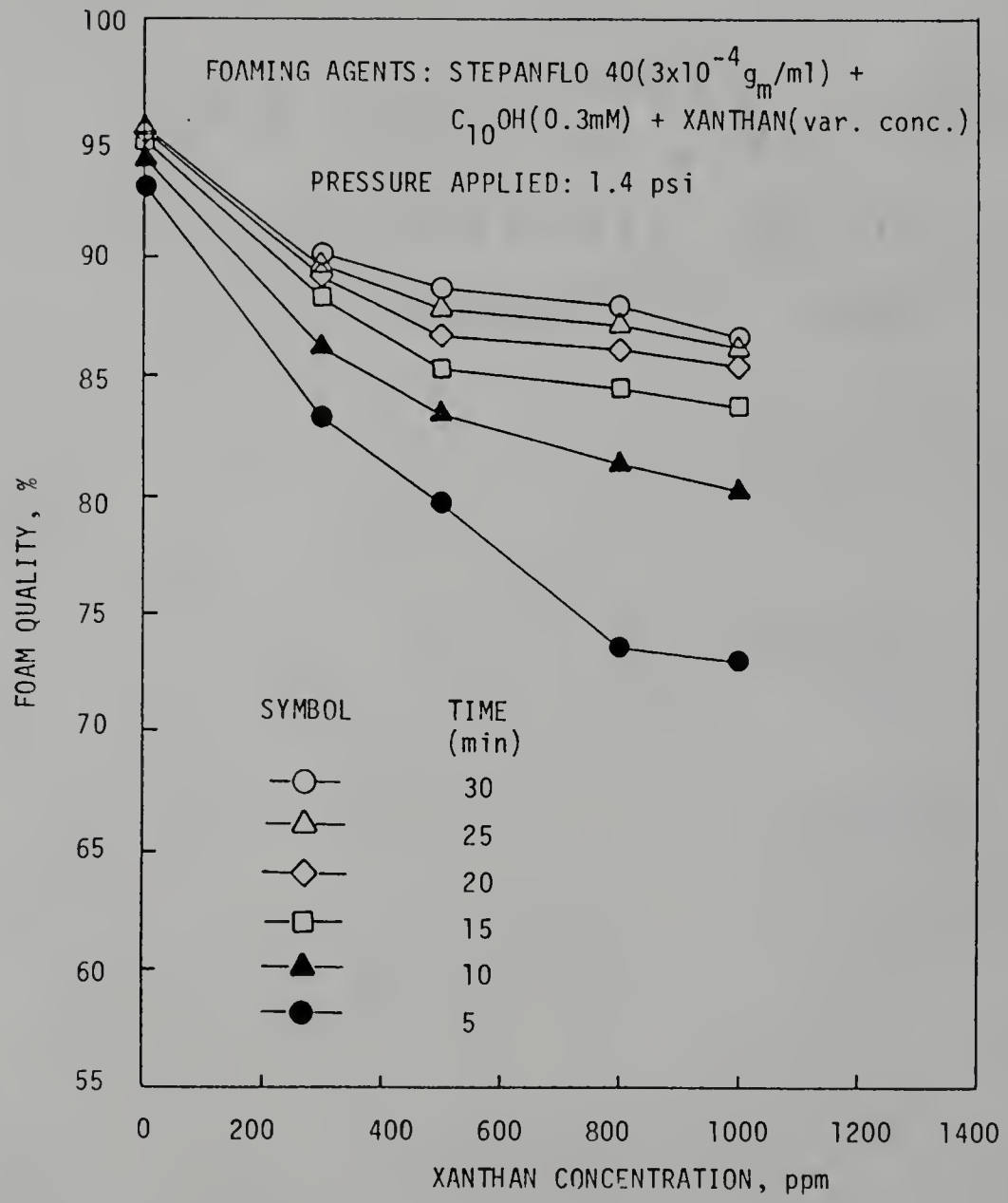

Figure 6.10. Variation in Foam Quality for Mixed Foaming Agents of Stepanflo 40 + $C_{10}OH$ with Different Xanthan Concentrations.

The existence of polymer in the liquid films improved the rheology of the adsorbed layer which in turn reduced the liquid drainage from the foam. Furthermore, the thin films were stabilized due to the stronger similarly charged electrical double layers. Effectively, the foam quality was decreased by the addition of polymer. Figures 6.11 and 6.12 are the same data as Figures 6.9 and 6.10 except the method to plotting. At the initial stage, the liquid drained out very fast for the foam containing high polymer concentration because of gravity. After a certain time (e.g., 20 minutes) the rate of drainage was dramatically decreased due to the viscosity of the liquid films. At this moment, the high water content in the foam was still observed as compared with the foam with low polymer concentration or without polymer.

6.3.4 Rate of Drainage

As mentioned earlier, the rheology of the adsorbed layers was improved and the thin films were stabilized due to the existence of polymer in the foam. Therefore, a direct consequence of the reduction in the rate of drainage was expected. Figures 6.13 and 6.14 indeed show that the rate of drainage was decreased with increase in the polymer concentration. It should be noted that the rate of drainage shown in Figures 6.13 and 6.14 reflects the data recorded after the total liquid volume in the cylinder had reached 50% of the original injected solution. Hence, the fast

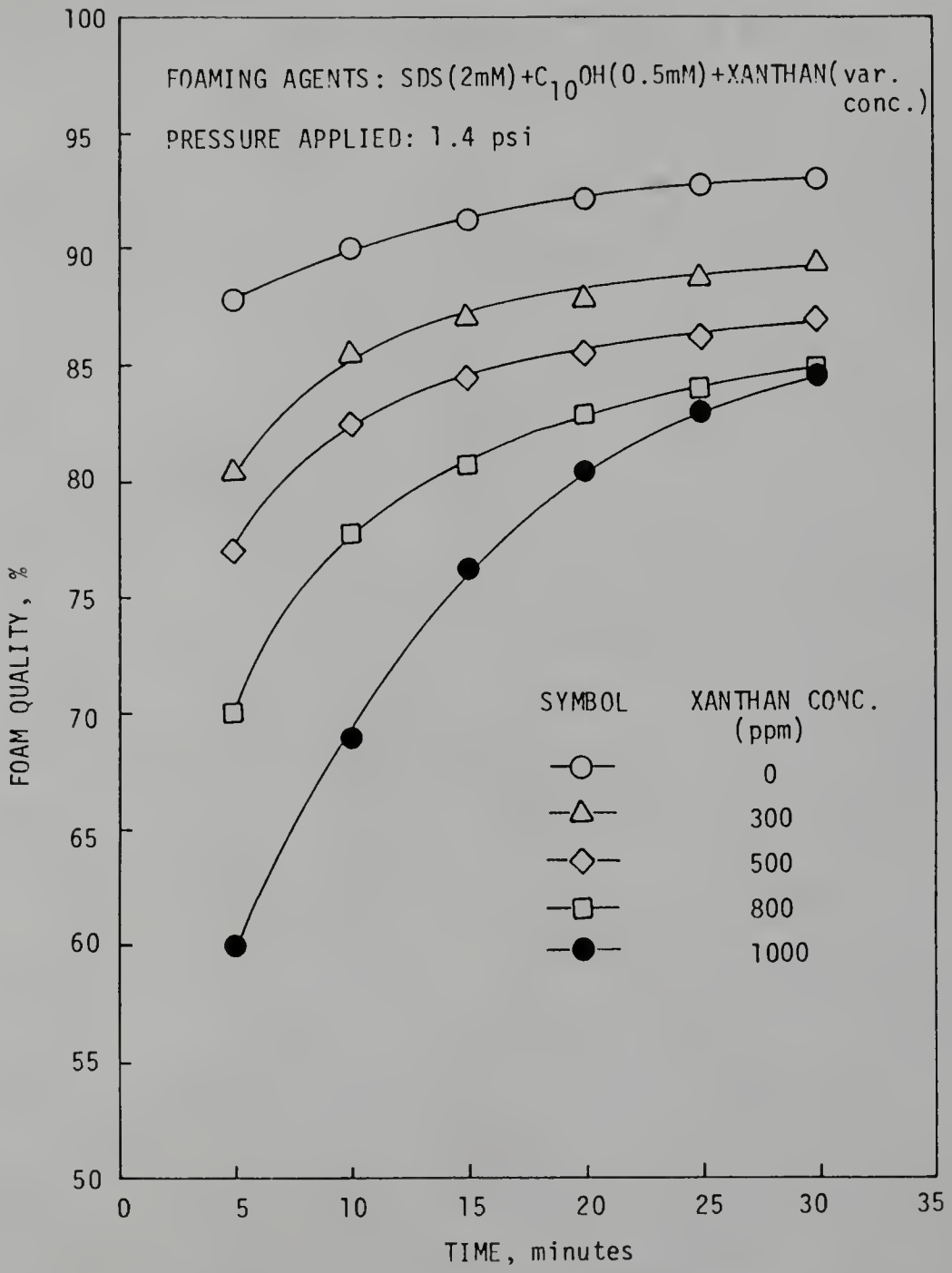

Figure 6.11. Foam Quality of Various Mixed Foaming Agents as a Function of Time.

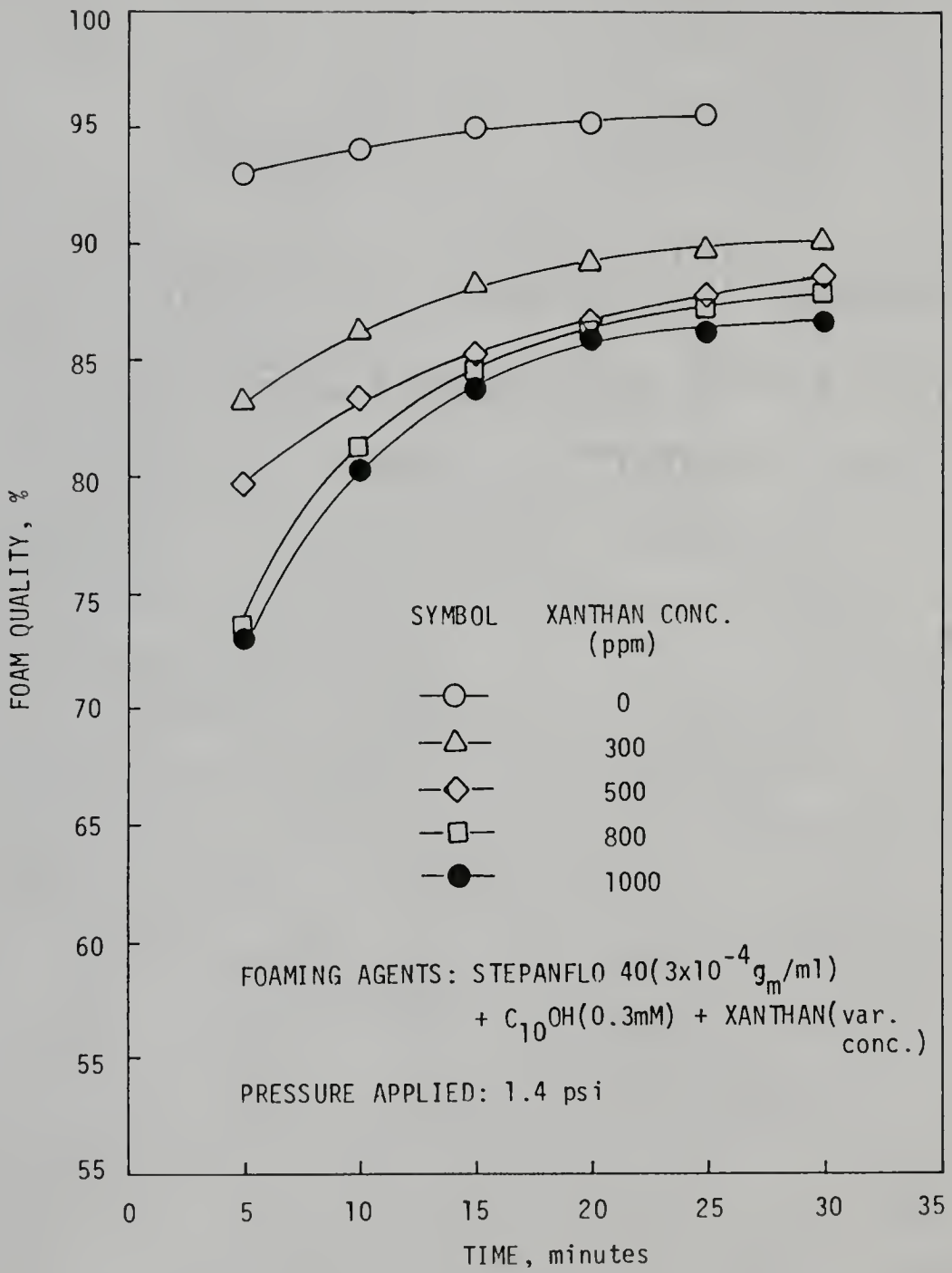

Figure 6.12. Foam Quality of Various Mixed Foaming Agents as a Function of Time.

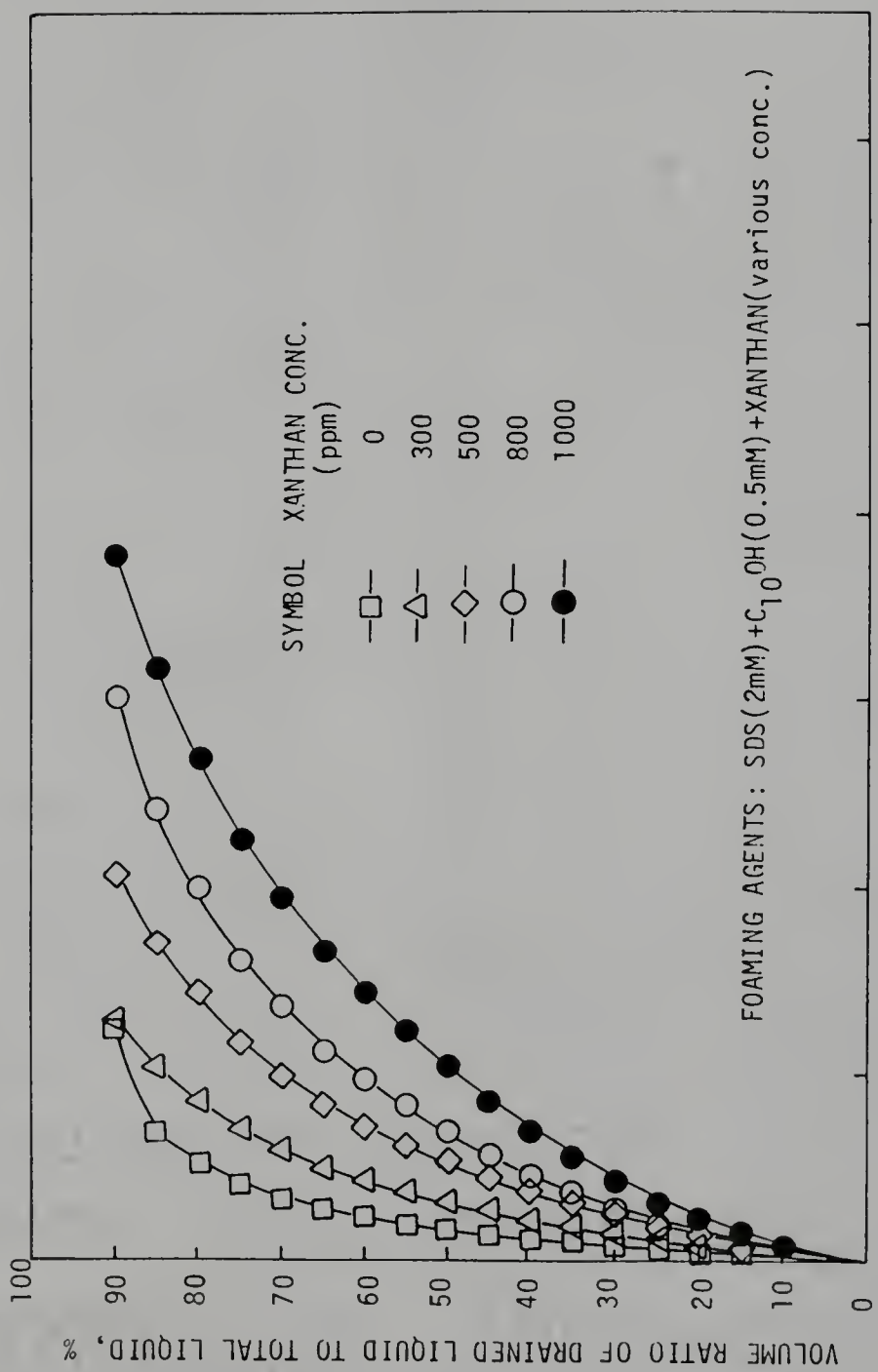

Figure 6.13. Rate of Drainage for Mixed Foaming Agents of SDS + $C_{10}OH$ with Different Concentrations of Xanthan.

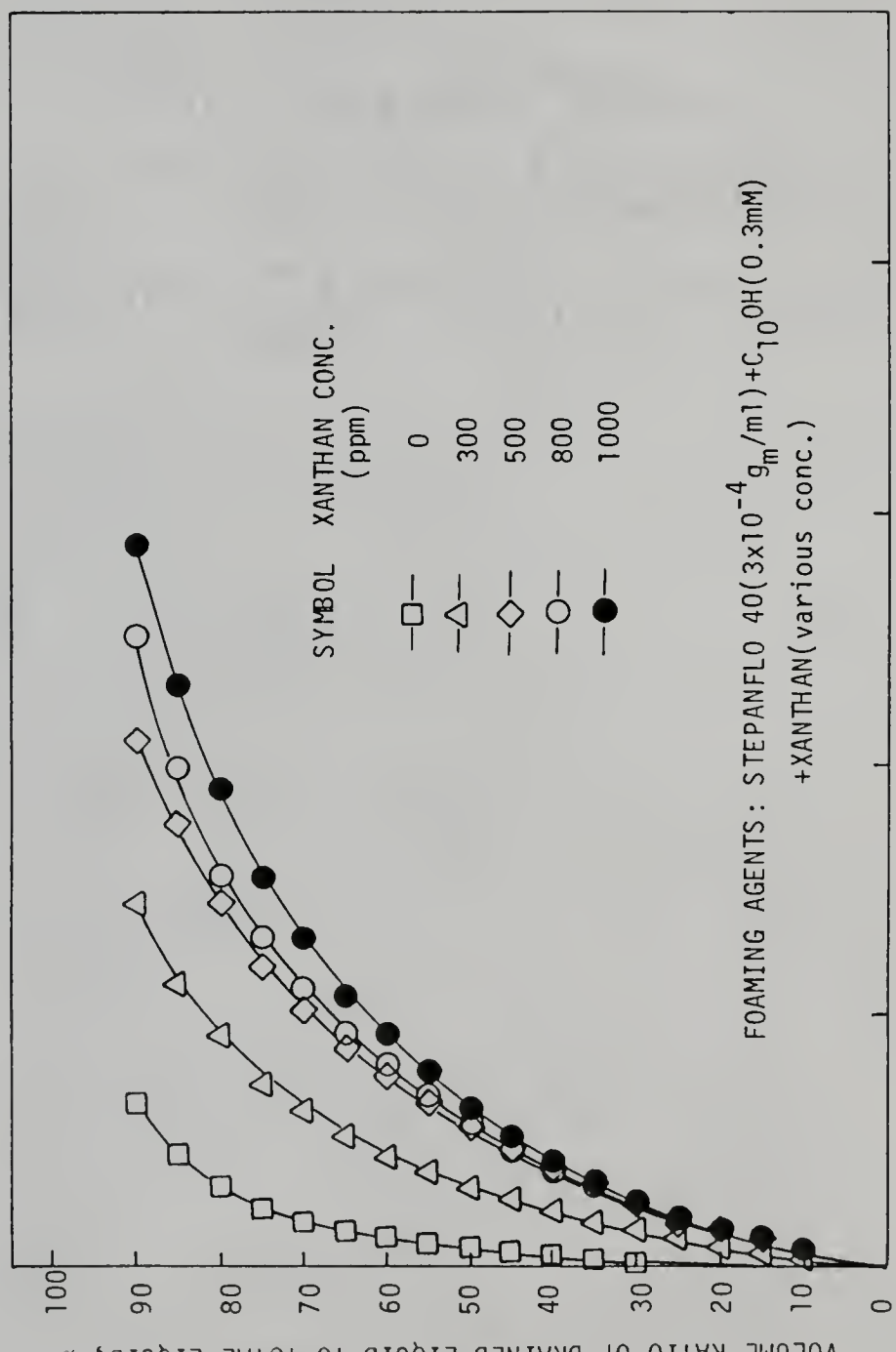

Figure 6.14. Rate of Drainage for Mixed Foaming Agents of Stepanflo 40 + $C_{10}OH$ with Different Concentrations of Xanthan.

liquid drainage for the high polymer concentration at the initial stage was not shown in Figure 6.13 and 6.14.

6.3.5 Apparent Foam Viscosity

It was observed that the polymer imparted to the foam a definite resistance to deformation, a direct consequence of the increased rheology of the liquid films. This effect will increase the apparent foam viscosity. However, the more water brought into the liquid films, the lower the apparent foam viscosity is. There must be an optimum polymer concentration so that the highest apparent foam viscosity is obtained by counterbalancing these two factors. Experimental results (Figure 6.15) showed that the apparent foam viscosity increased with the increase of polymer concentration up to 50 ppm, then it decreased as the concentration increased further. It should be noted that the optimum polymer concentration (50 ppm) existed only under the specified conditions described in Figure 6.15. This value may vary at different conditions. But, it does show that there exists an optimum polymer concentration for the highest apparent foam viscosity of a foaming agent at the given conditions.

6.3.6 Bubble Size Distribution

Photographs of the foams generated by mixed foaming agents with polymer are presented in Figures 6.16 and 6.17. The average bubble size gradually decreased as the polymer

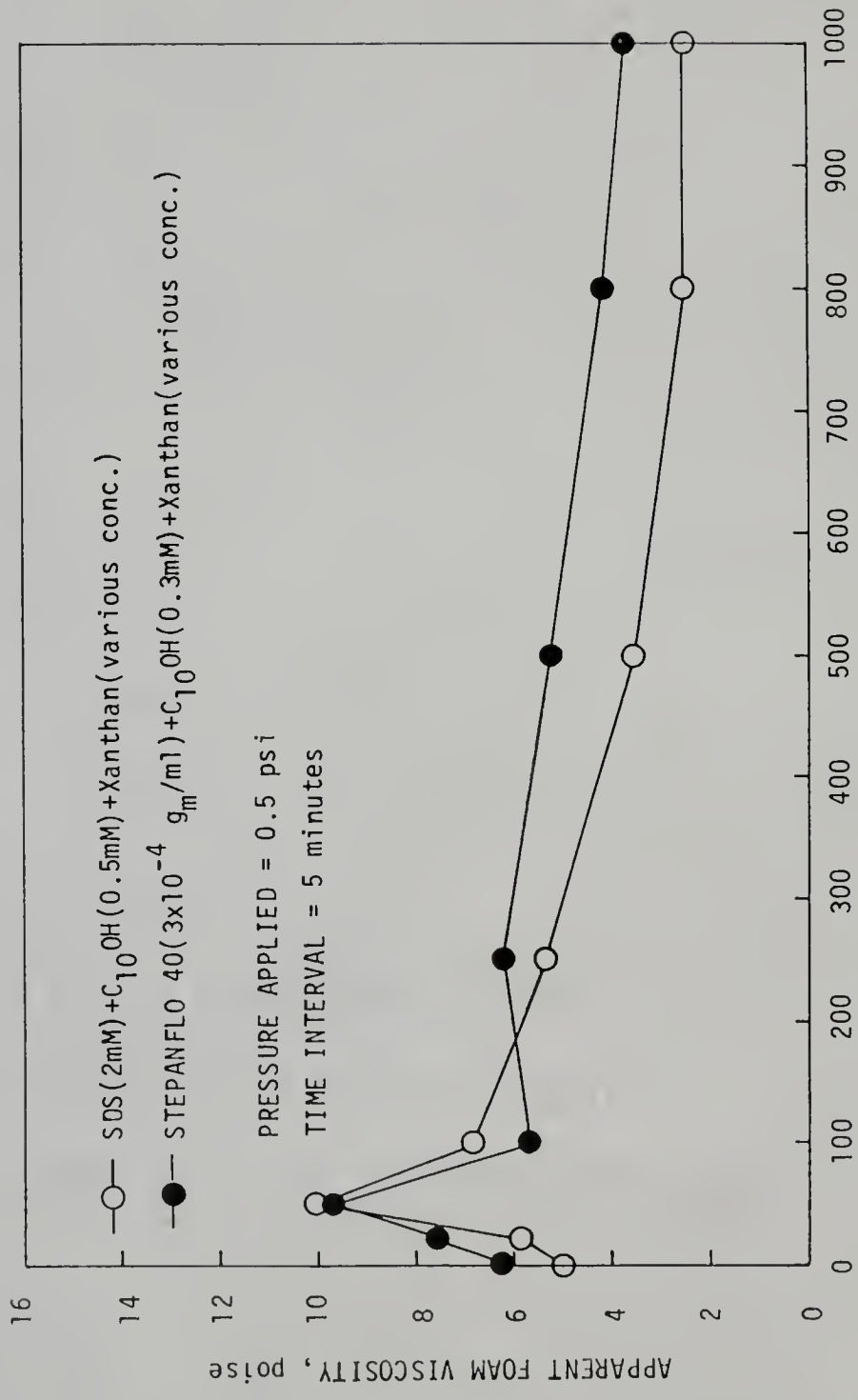

Figure 6.15. Effect of Adding Xanthan on Apparent Foam Viscosity.

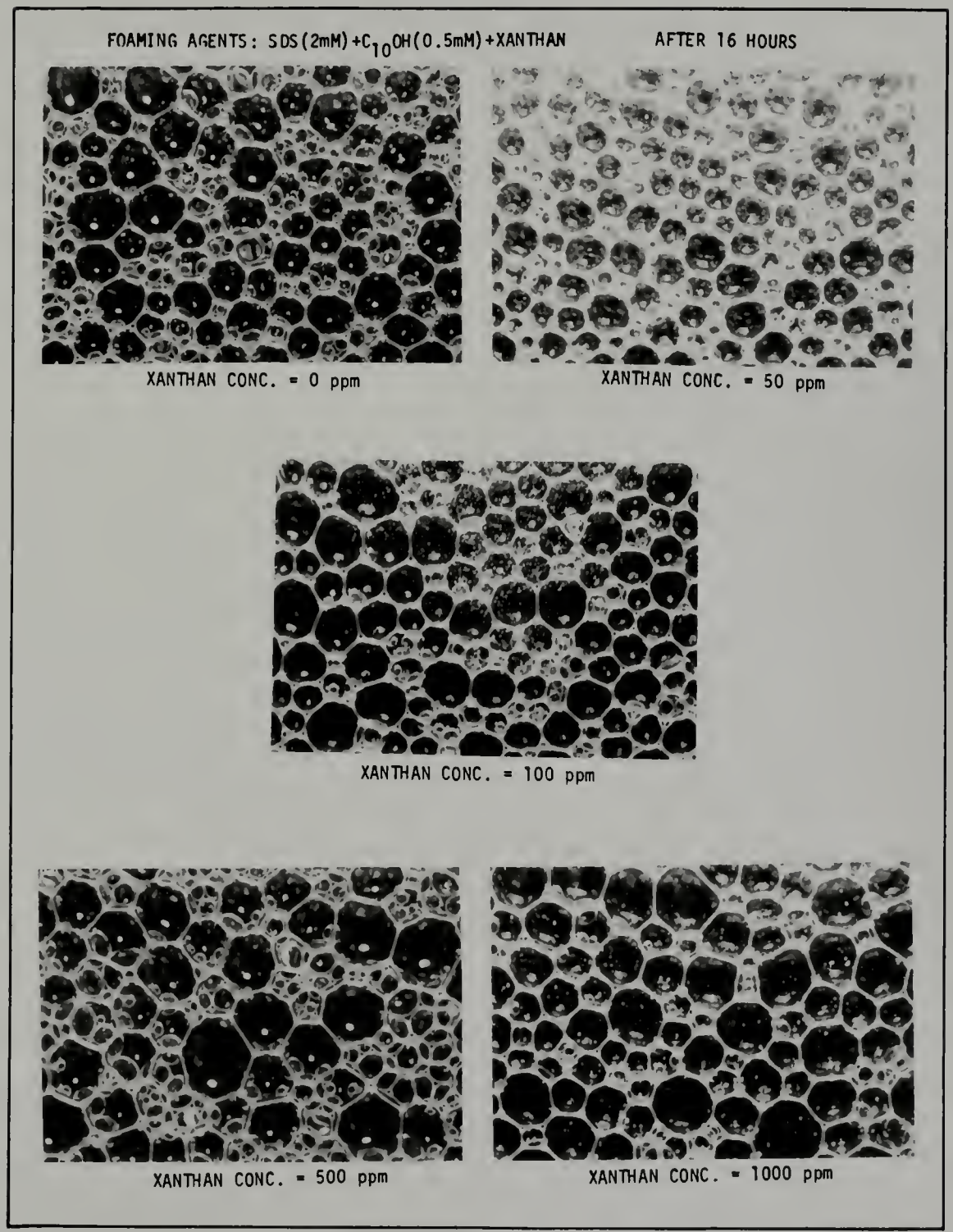

Figure 6.16. Bubble Size for Foams of Mixture of SDS + C_{10}OH with Different Xanthan Concentrations at 16 Hours after the Foams Were Produced.

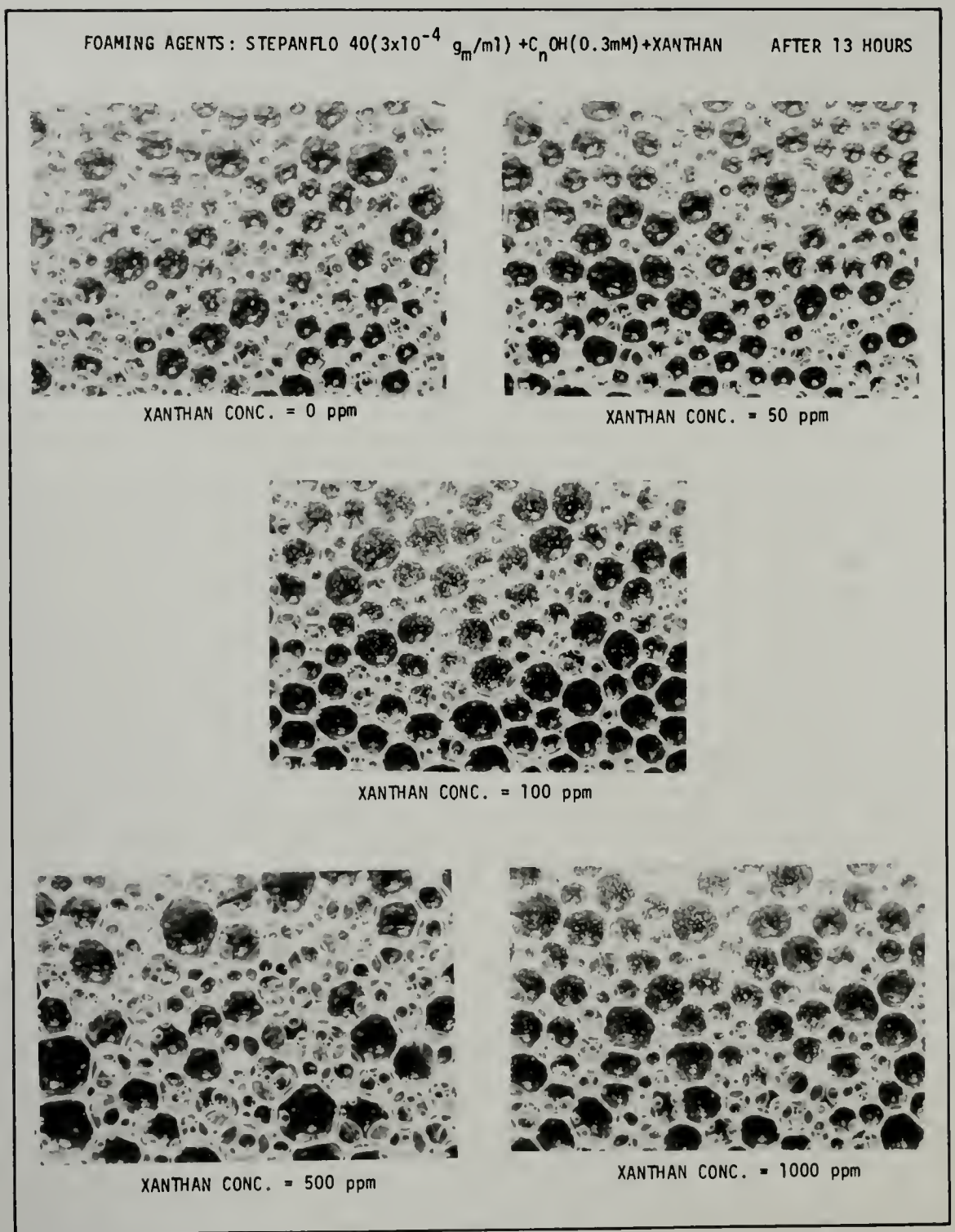

Figure 6.17. Bubble Size for Foams of Mixture of Stepanflo 40 + C_{10}OH with Different Xanthan Concentrations at 13 Hours after the Foams Were Produced.

concentration slightly increased, then it increased with further increase in concentration. The mean radii of the foam bubbles for SDS + $C_{10}OH$ + xanthan and Stepanflo 40 + $C_{10}OH$ + xanthan as a function of polymer concentration are shown in Figure 6.18. It implies that the foam was stabilized in the presence of a small amount of polymer. At a high polymer concentration, the foam was composed of thicker liquid films and consequently, the number of bubbles generated in a definite volume was less compared to the foam with a low polymer concentration. Therefore, the average bubble size was bigger even though the bubbles might last for a long time. The results are consistent with the trend of apparent foam viscosity: there exists an optimum polymer concentration such that the foam possesses the highest stability.

6.4 Conclusions

In this chapter the effects of adding polymer on the foam properties were studied. The interactions between anionic polymer and anionic surfactant were also investigated. Results support the mechanism proposed by Desai [40]. The improvement of surface activity of the surfactants was mainly due to the effect of excluded polymer volume and electrical double layers. The following phenomena about the change of the surface properties of the polymer containing foam were drawn from the studies:

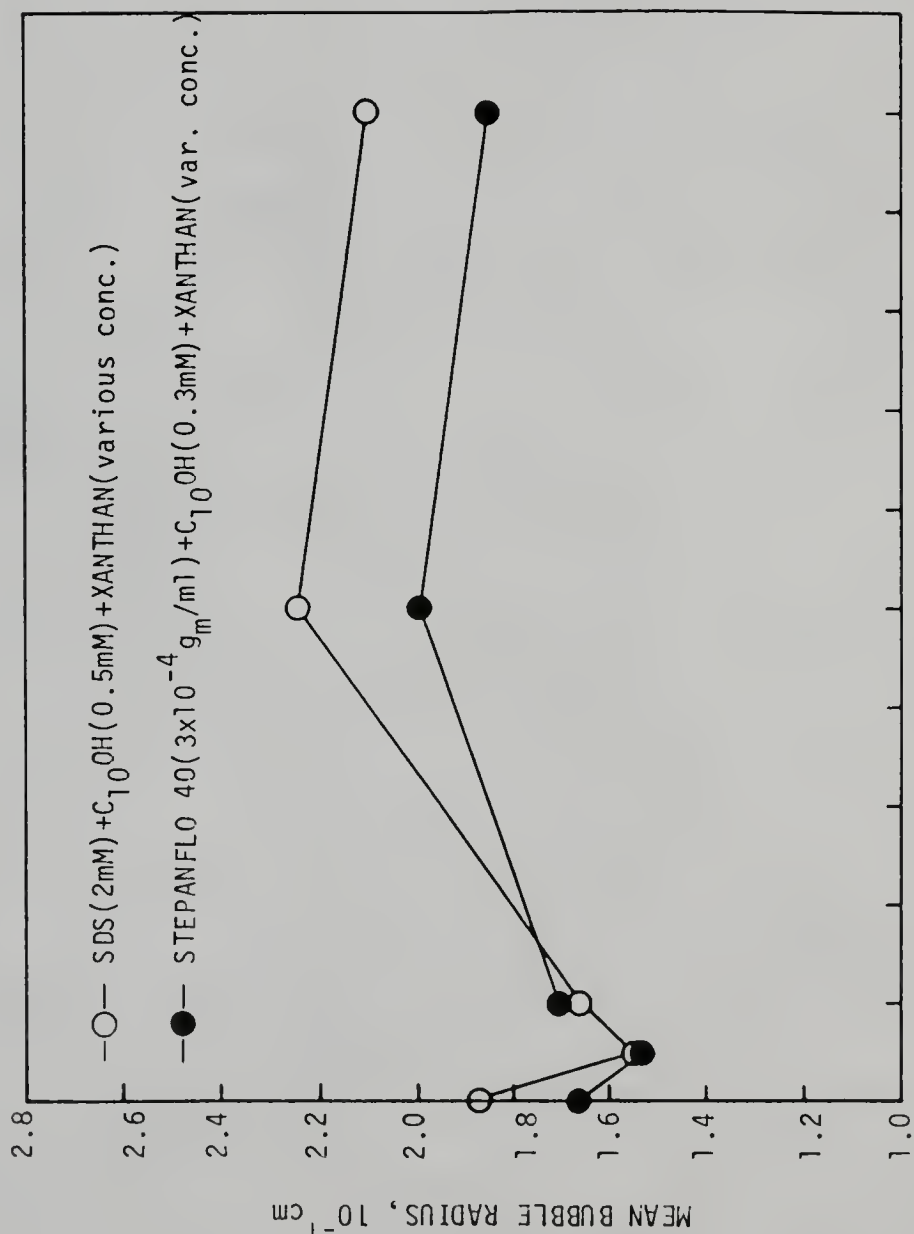

Figure 6.18. Mean Radii of Mixed Foaming Agents as a Function of Xanthan Concentrations.

1. The surface tension of the anionic surfactant solution was reduced by the addition of the anionic polymer. The surfactant molecules driven out by the polymer were caused by the effect of excluded polymer volume and electrical double layers. If the liquid/air interface was saturated with surfactant molecules, no significant change in surface tension was observed by adding polymer.
2. The foam quality decreased with the increase of polymer concentration due to a large amount of water brought into the liquid films by the polymer.
3. The apparent foam viscosity increased with the increase of polymer concentration, then it decreased as the concentration increased further. The optimum polymer concentration for the highest apparent foam viscosity was dependent on the counterbalance of the rheology of the liquid films and the water content in the liquid films.
4. With the exception of the initial stage, the rate of drainage decreased with increase in the polymer concentration. This is due to the improvement of the rheology of the adsorbed layer.
5. The average bubble size gradually decreased as the polymer concentration slightly increased, then it increased as the concentration increased further. It implies that the foam was stabilized in the presence

of a small amount of polymer. The results are consistent with the trend of apparent foam viscosity.

CHAPTER VII

APPLICATIONS OF FLUID FLOW THROUGH POROUS MEDIA

7.1 Heavy Oil Recovery by Foam Flooding

7.1.1 Introduction

When a new oil reservoir is discovered, the reservoir usually possesses the natural pressure to move the oil to the production wells by expansion of volatile components. This stage is called the primary oil recovery. When the natural pressure decreases, it is necessary to increase the pressure by injection of water. The injection of water, so called the secondary oil recovery or water flooding, is stopped when the production cost becomes significant compared to the value of the produced oil. The total oil recovery by the primary and secondary oil recovery is usually less than 40% of the original oil in place. Therefore, the remaining oil, 60%, is the target of the enhanced oil recovery called the tertiary oil recovery.

Residual oil remains in the reservoir after the primary and secondary recovery because (1) a partial sweep of the reservoir and (2) oil trapped by capillary forces in

the invaded zones. The objective of the tertiary oil recovery therefore is either to improve the sweep efficiency or to reduce the capillary forces or to act on both phenomena simultaneously. The sweep efficiency is increased by reducing the mobility ratio between displacing fluid and in-place fluids. This efficiency is significantly decreased as the mobility ratio is much greater than one. A favourable mobility ratio is around one. The elimination of the capillary forces improves the displacement efficiency.

There are several proven techniques for the tertiary oil recovery: surfactant flooding, polymer flooding, foam flooding, surfactant-polymer flooding, CO_2 flooding, caustic solution flooding, steam injection, thermal combustion, microbial method, etc. Among the techniques mentioned above, this work focuses on the foam flooding and compares it with the surfactant flooding, polymer flooding, and surfactant-polymer flooding. The method, namely, surfactant-polymer-foam flooding, was proposed using the foam as a mobility control buffer instead of using a large amount of polymer.

7.1.2 Forces Acting on the Oil Drop Entrapped in Porous Media and the Role of Surfactant

At the end of the secondary oil recovery, the residual oil is in the form of oil ganglia trapped in the pores due to the capillary, viscous, and gravity forces.
The viscous forces are known to be driving forces to

mobilize the residual oil drop while capillary forces are known to be resistant forces which entrap the residual oil drop. The trapped oil drop does not flow until the viscous forces of the displacing fluid exceed the capillary forces. Gravitational forces are expressed in terms of densities. Volumetric sweep efficiency will be decreased due to the density difference between oil, water, and injected fluids. The capillary number, which correlates capillary and viscous forces, is correlated with the level of the residual oil. In general, the level of the residual oil decreases as the capillary number increases [107,108]. When the capillary number is expressed by $N_{ca} = \mu v/\sigma\phi$ (where μ and v are the viscosity and velocity of the displacing fluid, σ is the interfacial tension, and ϕ is the porosity), the value of the capillary number is around 10^{-6} after water flooding and should be increased by 3 to 4 orders of magnitude for tertiary oil recovery processes [109]. It can be easily shown from the definition of the capillary number that there are two possible approaches to increase the capillary number. One is to increase viscous forces, for example, by increasing viscosity and velocity of the displacing fluid. The injection of foam into a porous medium creates a large number of resilient interfaces, which possess high viscosity and exert a piston-like force on the oil to be displaced. Consequently, the foam flooding is employed in the tertiary oil recovery. The second approach is to decrease the interfacial tension.

The use of an appropriate surfactant can decrease interfacial tension from 20 or 30 dynes/cm to 10^{-3} or 10^{-4} dynes/cm. Therefore, the surfactant flooding employs the use of surfactant to mobilize the oil entrapped in porous media by producing ultralow interfacial tension at the oil ganglia/surfactant solution interface. In the surfactant-polymer flooding, surfactant is injected as the form of slug; the slug usually consists of surfactant, alcohol, brine (or water), and sometimes oil and polymer are used as a mobility control buffer.

7.1.3 Results and Discussion

7.1.3.1 Heavy oil recovery by foam flooding

The heavy oil recovery in porous media was measured by air foam flooding, steam foam flooding [110], and the direct foam injection method [111], where foam was generated outside porous media then injected after the surfactant solution flooding. Experimental results showed that only 2% and 12% additional oil was recovered by air foam flooding and steam foam flooding, respectively. The low oil recovery by air foam flooding was mainly due to channeling and gravity override effects resulting from low stable in-situ foam. The steam foam injection presumably decreased the viscosity of heavy oil and generated more foam in porous media than air foam injection, which favors the tertiary oil recovery. At room temperature, if foams

were directly injected into the porous media after surfactant solution flooding, then about 20% additional oil could be obtained [112]. The higher oil recovery, compared to the air foam and steam foam floodings, was obtained because of the high viscosity and stability of the foam in porous media. The oil bank was partially formed due to this high viscosity displacing fluid, which in turn caused higher oil recovery. It should be noted that the early air breakthrough was still observed for the direct foam injection method and the oil recovery was measured until the foam breakthrough. The early air breakthrough implies that the foam inside porous media did not last for a long enough time to block the channels and the air to pass through the easy-go channels then leave the oil ganglia behind. This drawback may be improved by forming a very stable foam in the porous media.

One important factor that is considered to be a detriment of oil recovery by the direct foam injection method is the adjustment of inlet pressure. The inlet pressure has to be just high enough to inject foam slowly into porous media without causing a channeling effect. It is difficult to control the inlet pressure, especially when the foam is not very stable in porous media or when it has been accumulating in part of the porous media. However, this problem can be solved by the modeling of fluid displacement by foam (Chapter IV). The inlet pressure may

be monitored on the basis of the pressure distribution in porous media predicted by the model.

7.1.3.2 Effect of adding polymer on heavy oil recovery by foam flooding

As mentioned earlier, foam stability and viscosity can be improved by adding a small amount of polymer. Several oil recovery experiments were conducted by the injection of foam consisting of various polymer concentrations. Results (Figure 7.1) showed that the additional oil could be recovered from 20% to 45%. Figure 7.1 also shows the tertiary oil recovery by polymer flooding when the same foaming solution was used as a polymer solution. It is evident that the oil recovery by polymer flooding increased with the increase of polymer concentration, whereas the oil recovery by direct foam injection increased first then decreased as the polymer concentration increased. The reason is clear for the polymer flooding: the viscous force is increased by increasing the viscosity of the displacing fluid. The higher the viscous force, the greater the oil recovery. For the direct foam injection method, it is likely that the viscosity of in-situ foam increased with the increase of polymer concentration up to 500 ppm, then decreased as the concentration increased further. A similar trend was observed for the apparent foam viscosity (Chapter VI) even though the maximum apparent viscosity occurred at a different polymer concentration. Meanwhile, the stability

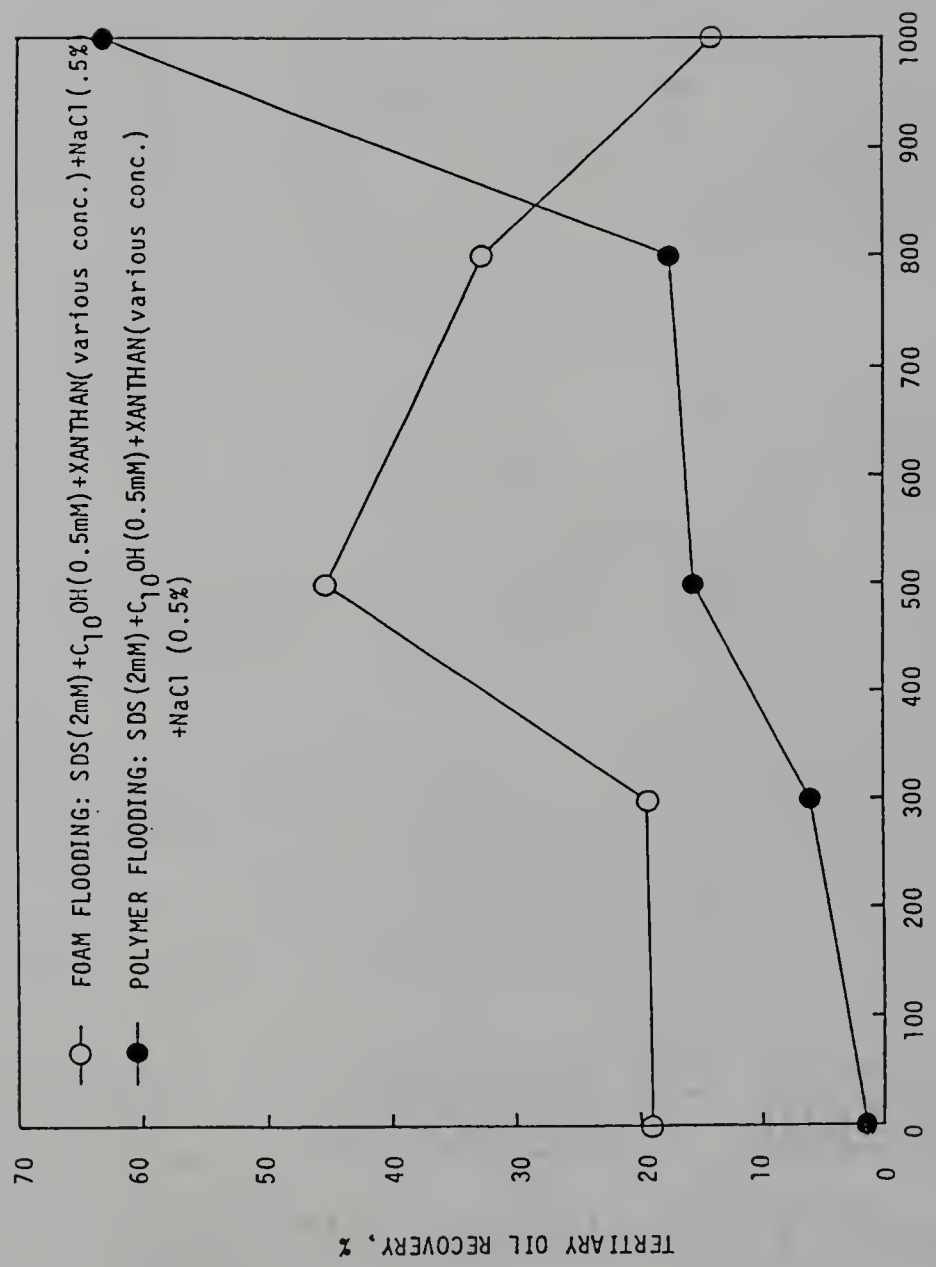

Figure 7.1. Tertiary Oil Recovery by Foam and Polymer Flooding Methods with the Same Foaming Solutions Containing Xanthan.

of in-situ foam might also reach a maximum at the polymer concentration of 500 ppm. From the results of bubble size distribution measured outside porous media, the mean bubble size decreased as the polymer concentration increased, then increased with the further increase of the polymer concentration. It implies that the foam stability increases first then decreases by increasing the polymer concentration. Although the surface properties of the foam inside porous media are hard to measure, the foam behavior in the porous media still can be predicted by observing the foam properties outside porous media. The oil recovery is expected to change with the variations of the viscosity and stability of in-situ foam in the presence of polymer. The trend of oil recovery agreed well with the results of the apparent foam viscosity and bubble size distribution measured outside porous media. One interesting phenomenon was found: the tertiary oil recovery by direct foam injection with the foaming solution containing 500 ppm xanthan was equivalent to the oil recovery by polymer flooding with the polymer solution containing 900 ppm xanthan. Also, better oil recovery was always obtained by the direct foam injection method when the polymer concentration was less than 850 ppm.

The oil production histogram (Figure 7.2) shows that oil cut sharply decreased for the polymer flooding (xanthan conc. = 1000 ppm) at 0.81 pore volume (PV). For the direct foam injection method at the polymer concentration of 500

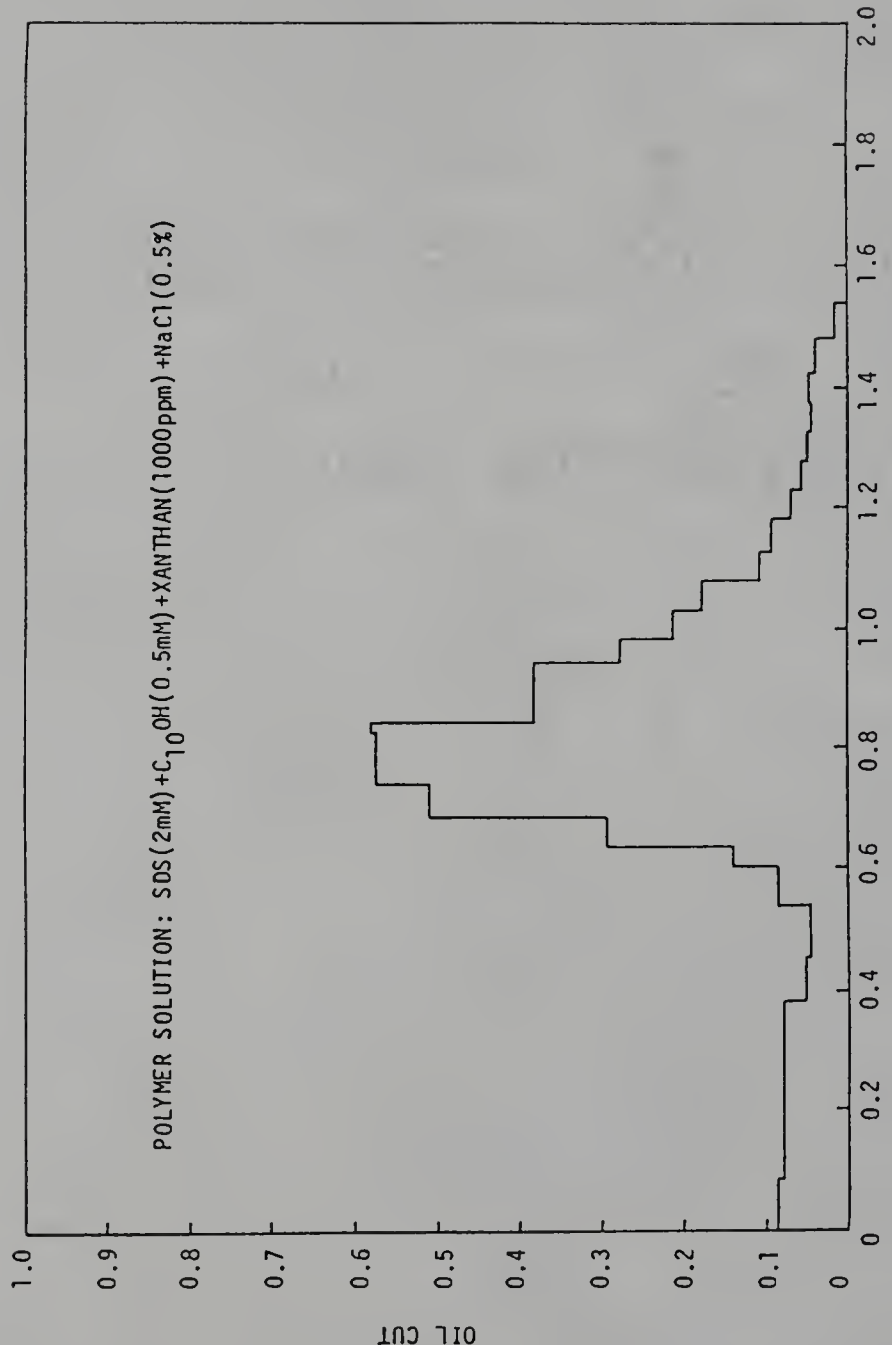

Figure 7.2. Histogram of Oil Production by Polymer Flooding.

ppm, the oil cut sharply decreased at 0.75 PV (Figure 7.3). In both cases, the oil bank was not fully formed due to early invasion of the displacing fluid into the partial oil bank.

7.1.3.3 Heavy oil recovery by surfactant-polymer-foam flooding

Lee and Shah [113] reported that an alcohol-free middle phase microemulsion was successfully formulated for the heavy oil recovery. The results showed that the alcohol-free middle phase microemulsion exhibited larger solubilizing power and lower interfacial tension as well as induced higher heavy oil recovery as compared to the middle phase microemulsion containing a short chain alcohol. Since the purpose of Lee's work was to compare two different systems, namely, alcohol-free and alcohol-containing middle phase microemulsions, a large volume of the surfactant slug was injected without using any mobility control buffer. Later, the method of surfactant-polymer flooding was successfully employed for the tertiary oil recovery. However, a large amount of polymer solution (0.5 - 1.0 PV) has to be injected for the mobility control. In order to maximize the economics of the surfactant-polymer flooding, a concept was proposed so that a small slug of the expensive polymer was required. The method, surfactant-polymer-foam flooding, is schematically shown in Figure 7.4 [111]. The results were compared with the method of

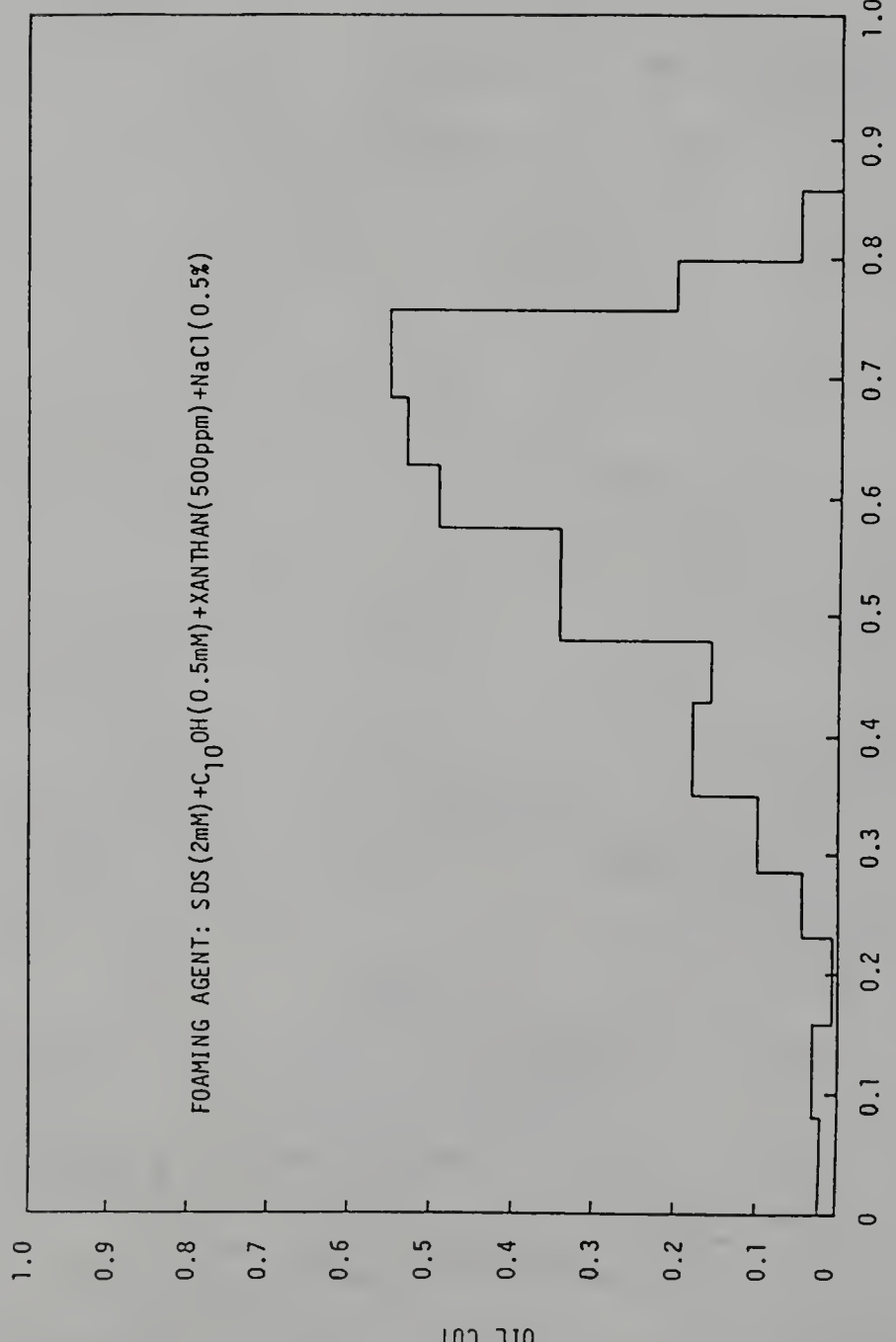

Figure 7.3. Histogram of Oil Production by Foam Flooding.

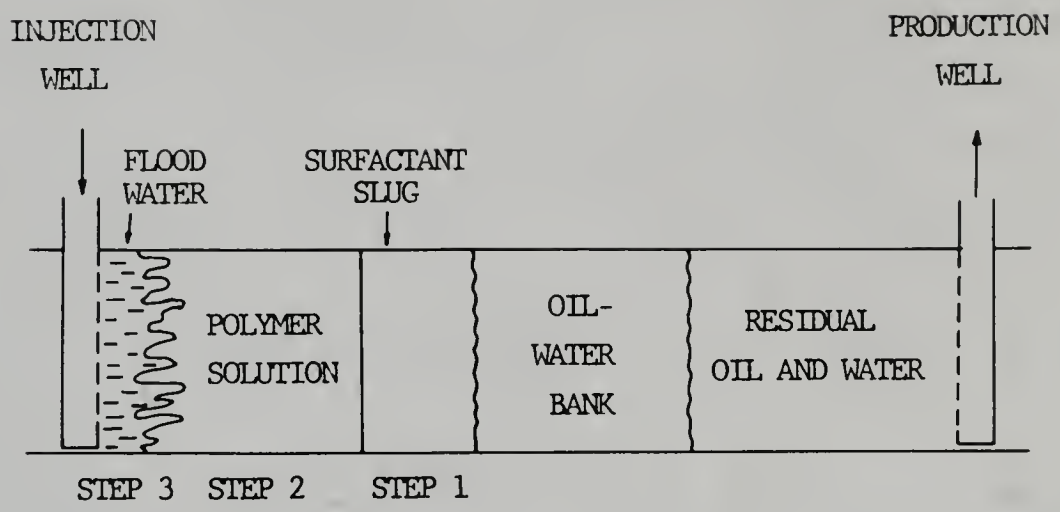

Step 1: inject surfactant-fluid bank (approx. 5-20% pore volume)
Step 2: inject polymer-brine bank (approx. 50-100% pore volume)
Step 3: inject chase-water bank

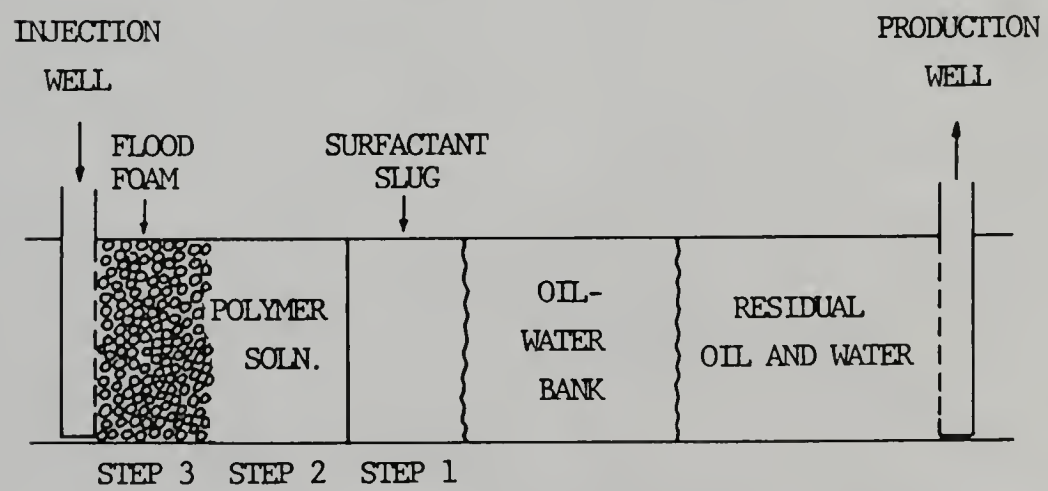

Step 1: inject surfactant-fluid bank (approx. 10% pore volume)
Step 2: inject polymer-brine bank (approx. 10% pore volume)
Step 3: inject foam bank

Figure 7.4. Schematic Diagram of the Surfactant-Polymer-Foam Flooding in Comparison with the Surfactant-Polymer Flooding.

surfactant-polymer flooding and summarized in Figure 7.5. Almost the same oil recovery was obtained by both methods. This demonstrated that the foam can be used as a mobility control buffer for the surfactant-polymer flooding in heavy oil recovery. Figures 7.6 and 7.7 show the oil production histograms. It is clear that the oil bank was well formed and displaced by a piston-like displacing fluid. The low interfacial tension and high viscous force due to the alcohol-free middle phase microemulsion and high viscosity displacing fluid respectively, raised a very great capillary number. The high oil recovery corresponds to this great capillary number.

7.2 Transport Mechanism of Viscoelastic Gels in Porous Media

7.2.1 Introduction

Viscoat™, a new biological polymer containing both sodium chondroitin sulfate and sodium hyaluronate, is used like other viscoelastic gels (e.g., Healon™, hyaluronic acid, etc.) in intraocular surgery. Several of its physical properties have been reported [114-117].

1. Viscoat is a non-Newtonian fluid with a viscosity greater than that of either sodium chondroitin sulfate or hyaluronic acid individually, but less than that of Healon.
2. Viscoat appears to be less affected by shear rate than hyaluronic acid.

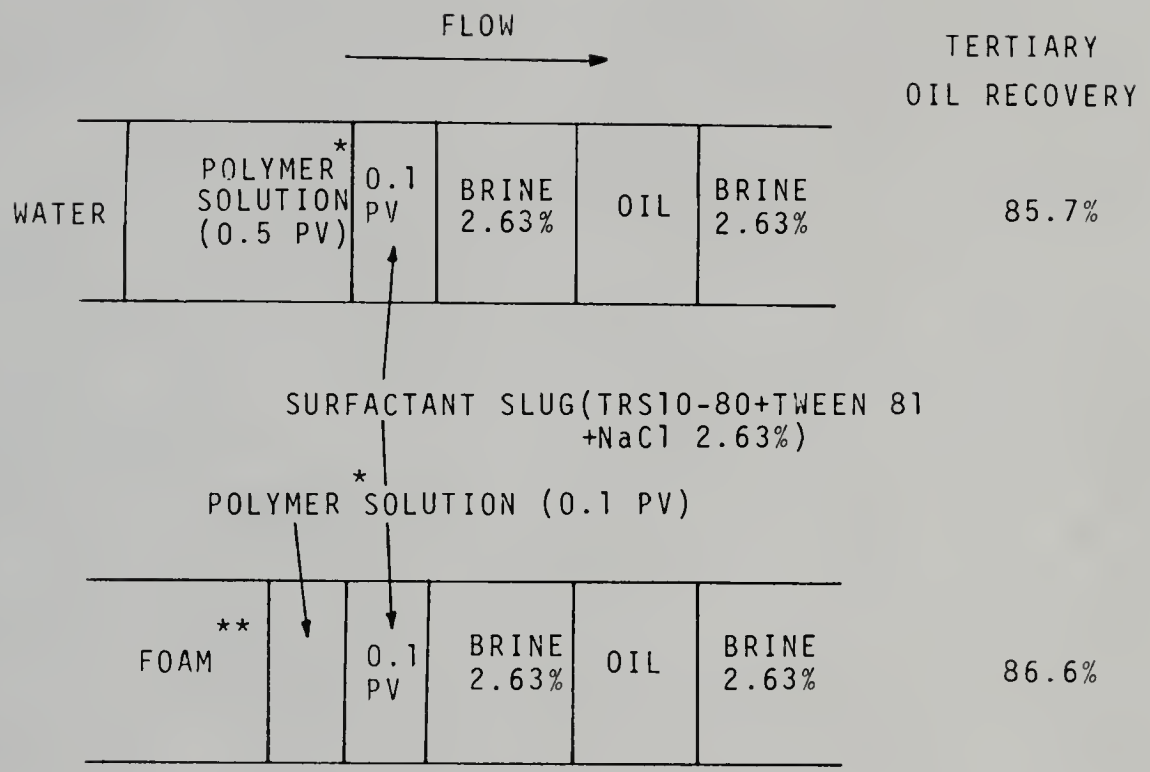

* POLYMER SOLUTION: SDS(2mM)+C_{10}OH(0.5mM)+XANTHAN(2000ppm) +NaCl(2.63%)

** FOAMING AGENT: SDS(2mM)+C_{10}OH(0.5mM)+XANTHAN(500ppm) +NaCl(0.5%)

Figure 7.5. Comparison of Tertiary Oil Recovery by Surfactant-Polymer Flooding and Surfactant-Polymer-Foam Flooding.

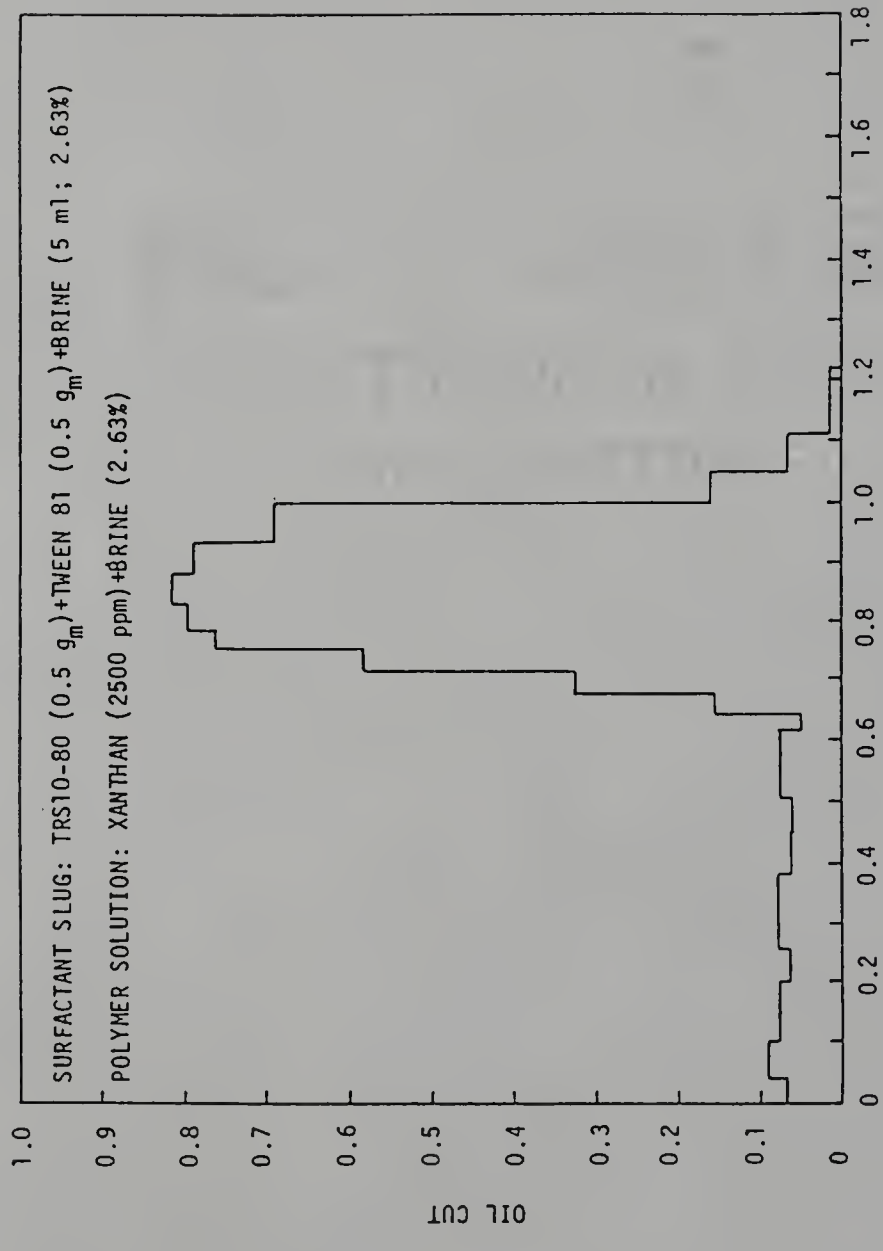

Figure 7.6. Histogram of Oil Production by Surfactant-Polymer Flooding.

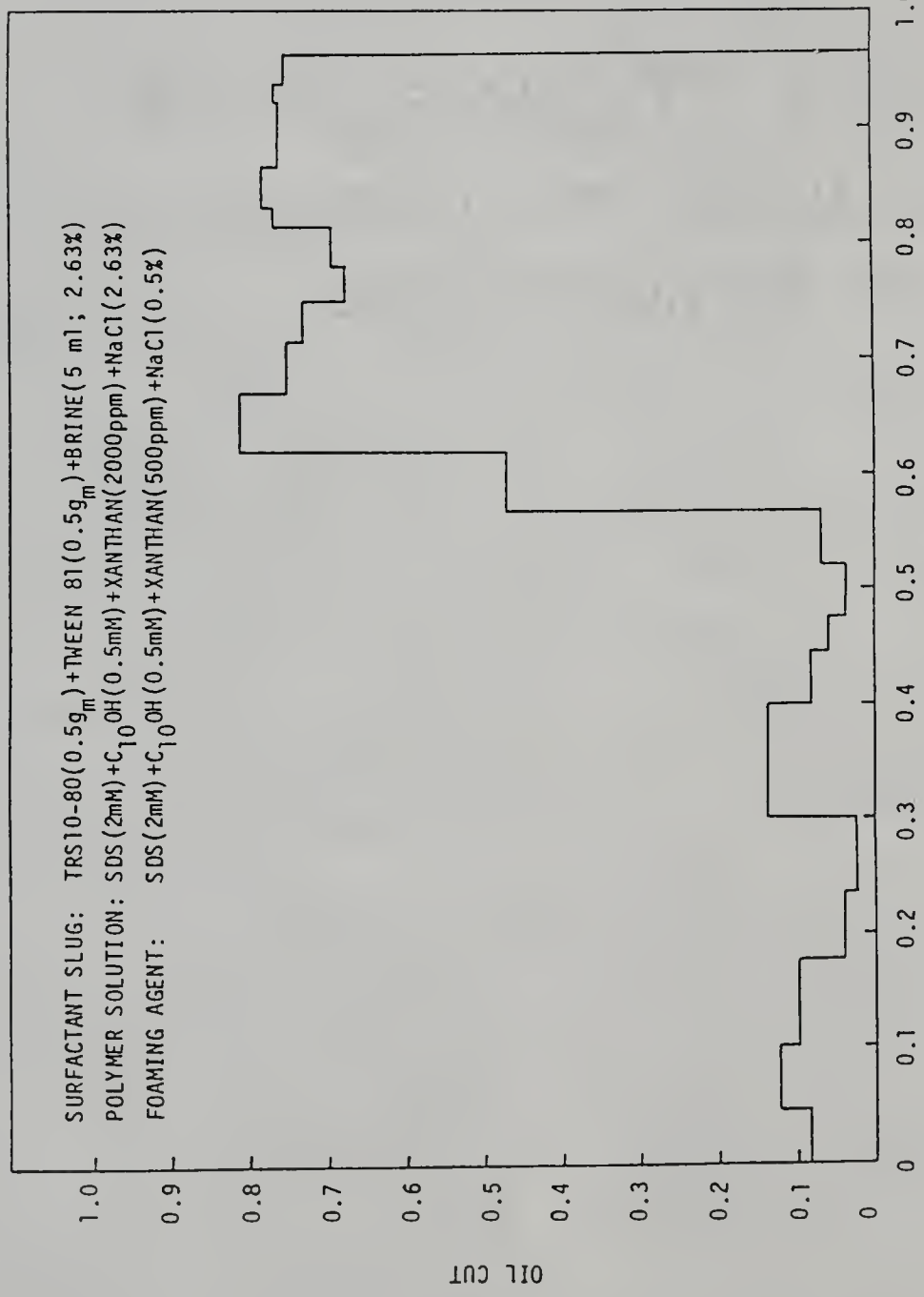

Figure 7.7. Histogram of Oil Production by Surfactant-Polymer-Foam Flooding.

3. The removal of Viscoat from the anterion chamber would be easier than that of hyaluronic acid because of the low yield point of Viscoat.
4. There is no significant difference in the postoperative intraocular pressure of the Viscoat group and the Healon group. However, Viscoat shows a moderate transient rise in intraocular pressure as compared with hyaluronic acid.

7.2.2 Materials and Methods

In order to prove the difference in the postoperative intraocular pressure caused by the viscoelastic gels, a wash-out kinetics was developed as follows:

(1) pack column with microbeads,
(2) flush column first with CO_2, then a balanced salt solution,
(3) load column with polymer solution to be studied at a low flow rate until maximum pressure rise is reached,
(4) measure peak pressure at the given flow rate,
(5) stop polymer flow until pressure drop levels off,
(6) start injecting balanced salt solution through porous media at the same flow rate as step (3),
(7) measure peak pressure and rate of pressure drop until pressure drop levels off.

The experiments were conducted at room temperature under different concentrations of polymer with a porous micromodel to analyze flow behavior of polymer in porous

media. The model made up of a rectangular tubing (2 mm x 4 mm x 25 mm) packed with microbeads (diameter 105-205 microns) having a permeability of 5.4 darcys. The pore volume of the porous media is 0.076 ml. The pressure drop across the porous media was measured using a differential pressure transducer (Validyne DP-15) and a strip chart recorder (Schlumberger SR-204). The biological polymers used in the experiments are: Viscoat, Healon, Amvisc^{TM}, sodium hyaluronate, and chondroitin sulfate.

7.2.3 Results and Discussion

The reproducibility of the wash-out kinetics method was tested by measuring the pressure drop as a function of the volume of balanced salt solution (BSS) injected. The concentration of Viscoat was arbitrarily chosen at 50% (vol./vol.). Figure 7.8 shows that the difference between the maximum peak pressure and the minimum peak pressure is 1.95 mmHg/mm and the experimental error is about 16%. The pressure profiles are quite similar before BSS breakthrough, however there are significant deviations in each experiment after BSS breakthrough. The actual reason is still unknown, but it may be due to the packing which in turn affects the adsorption/retention of polymer and the viscous fingering. Generally speaking, the experiments were quite reproducible in a certain tolerable range. Further study on the dynamic stability of the viscoelastic gels may be helpful to explain the reproducibility of wash-out

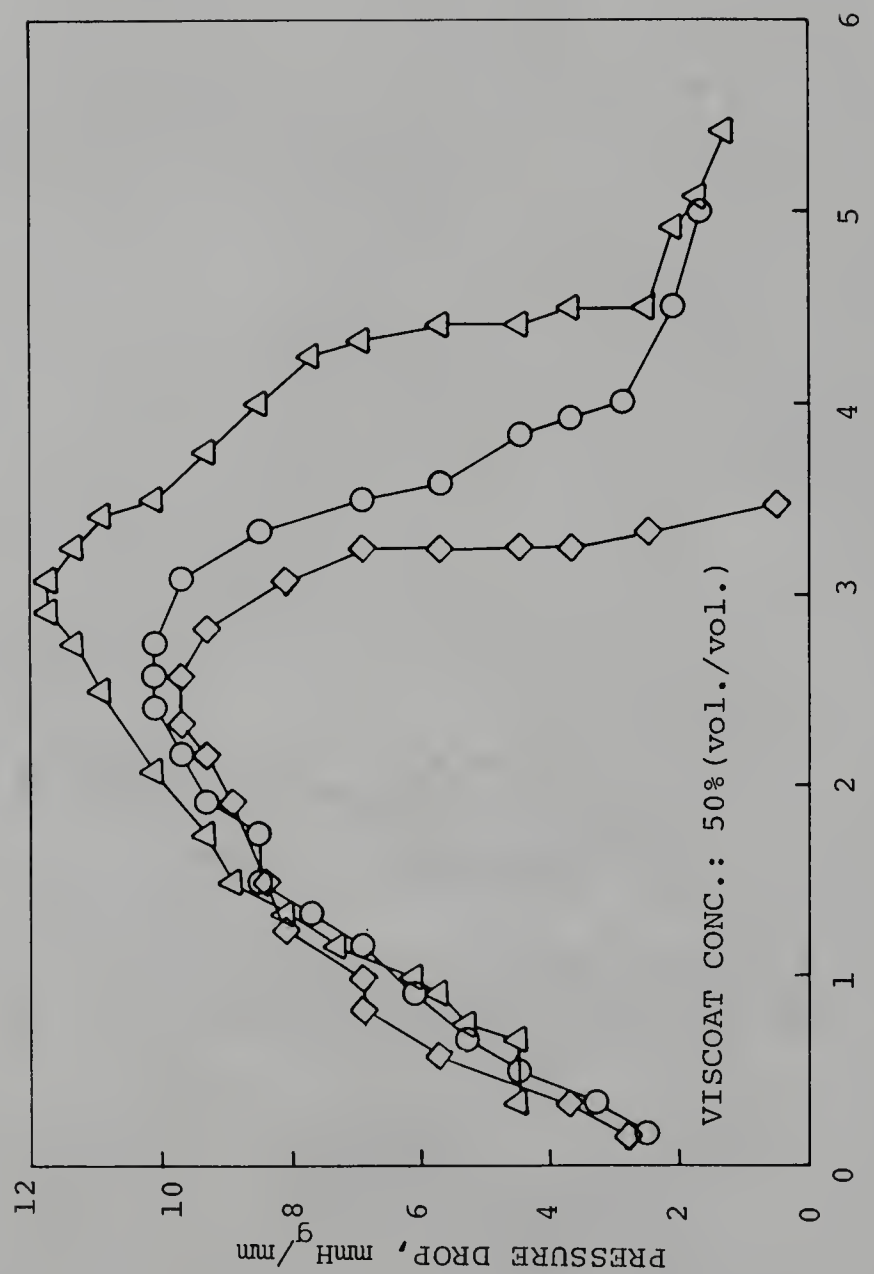

Figure 7.8. Reproducibility of the Wash-out Kinetics Method.

kinetics.

Figures 7.9-7.11 represent the pressure drop as a function of BSS volume injected at the different concentrations of polymers. In general, Healon generates a higher peak pressure than Viscoat and Amvisc, because Healon possesses a higher viscosity and a larger molecular weight and structure which impedes passage through the porous medium. Therefore, one would expect that Healon induces a greater rise in intraocular pressure compared to Viscoat and Amvisc. The experimental data [114] tested in cynomolgus monkey eyes indeed show Healon induces higher intraocular pressure than that of Viscoat. The maximum peak pressure at breakthrough for different concentrations of polymers are shown in Figure 7.12. It is clear that the peak pressure increases with increasing polymer concentration. A sharp increase in peak pressure is approximated at the concentrations of 60-70% (vol./vol.).

In order to study the effect of interaction between two biological polymers (i.e., chondroitin sulfate and sodium hyaluronate) on the flow behavior of polymers in porous media, various concentrations of mixed polymers were prepared and pumped through the model. The pressure profiles as a function of BSS volume injected are shown in Figures 7.13 and 7.14. Figure 7.15 represents the maximum peak pressure at breakthrough for different concentrations of these two polymers. It is apparent that the peak pressure increases with increasing sodium hyaluronate

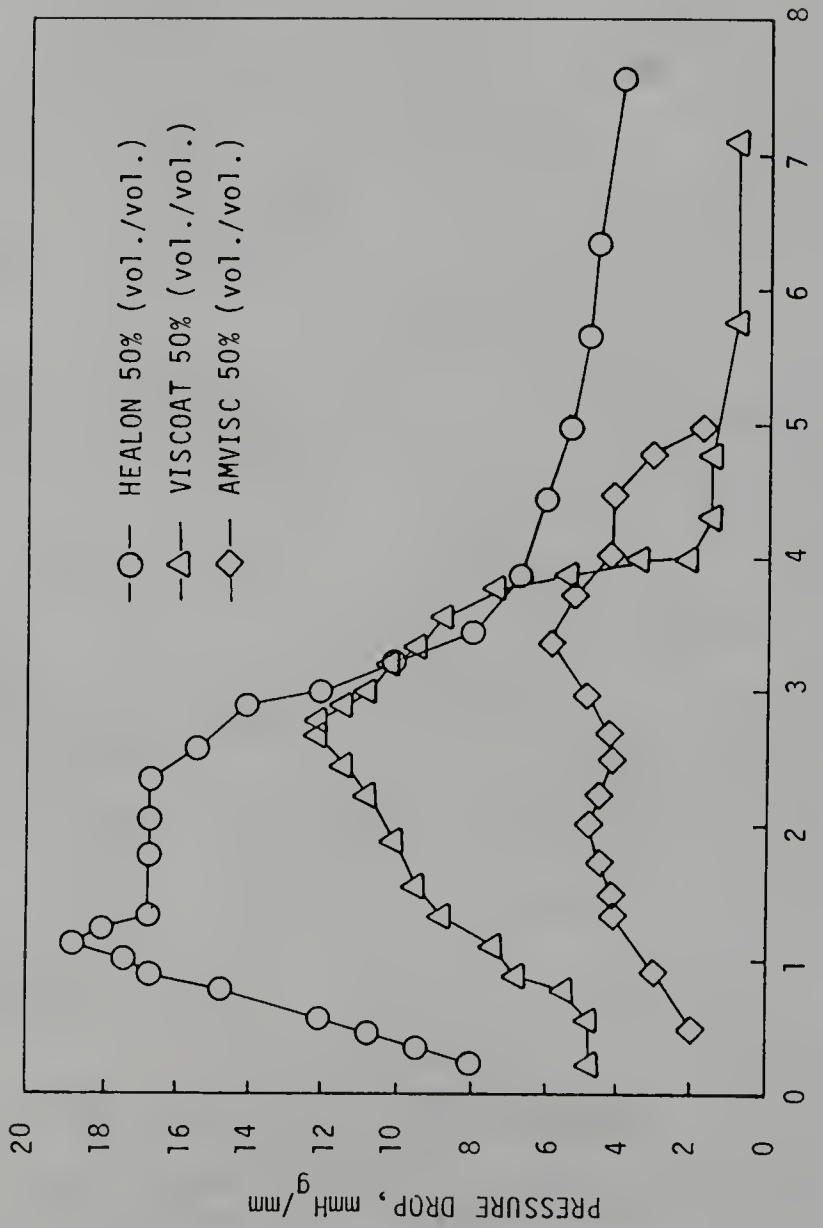

Figure 7.9. Pressure Drops of Various Biopolymers (50% vol./vol.) as a Function of the Volume of Balanced Salt Solution Injected into Porous Media.

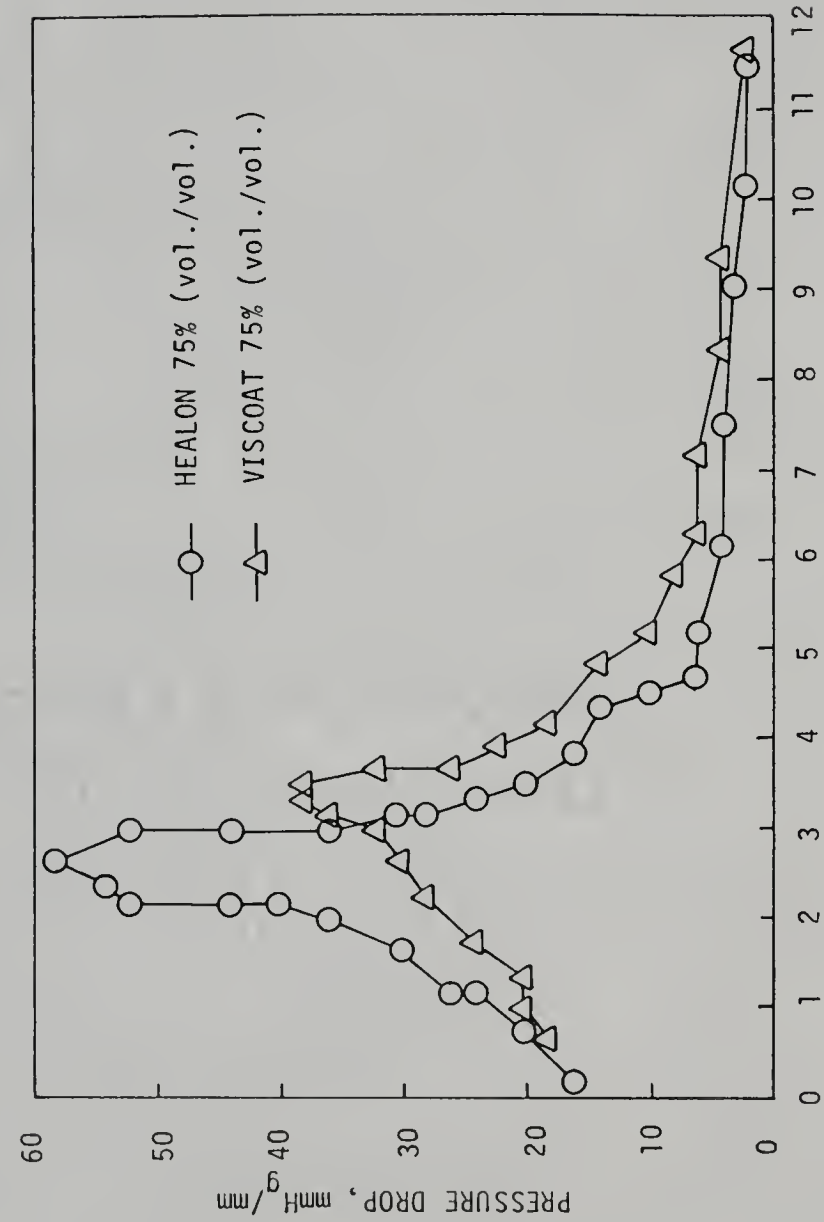

Figure 7.10. Pressure Drops of Various Biopolymers (75% vol./vol.) as a Function of the Volume of Balanced Salt Solution Injected into Porous Media.

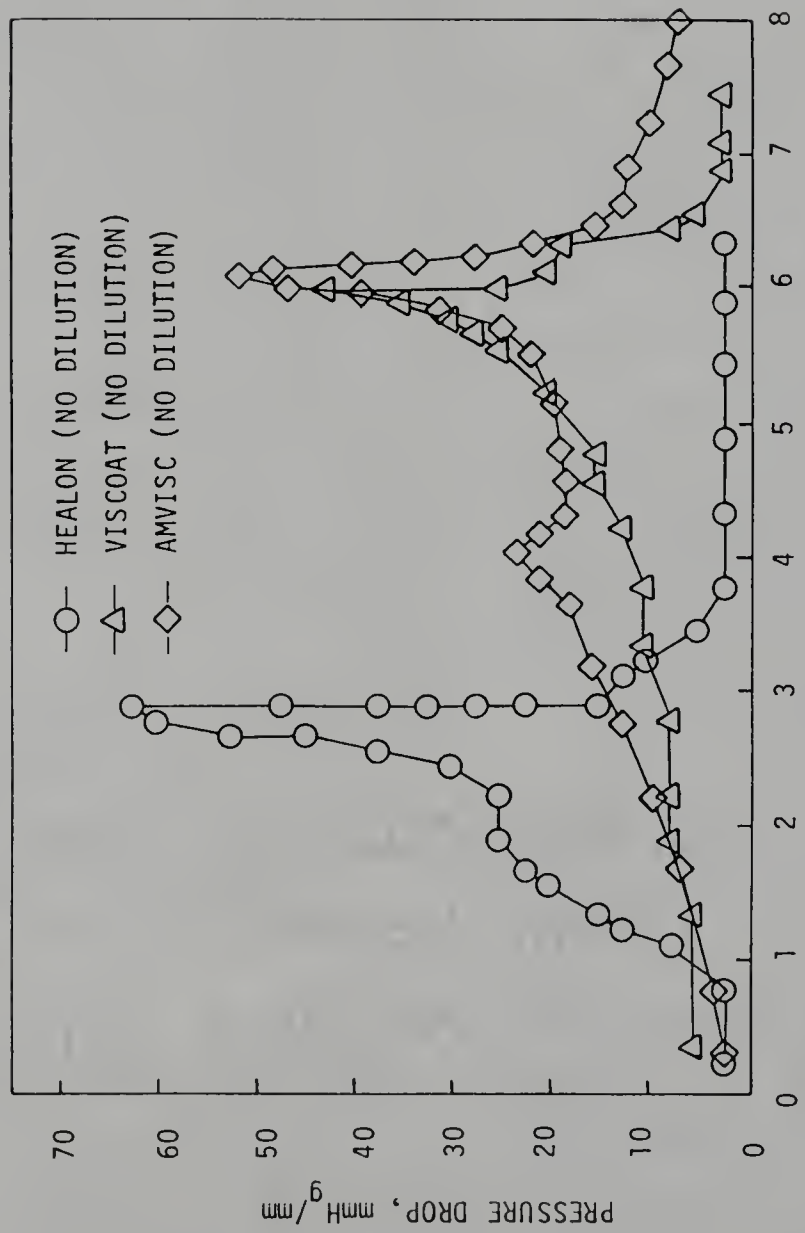

Figure 7.11. Pressure Drops of Various Biopolymers (No Dilution) as a Function of the Volume of Balanced Salt Solution Injected into Porous Media.

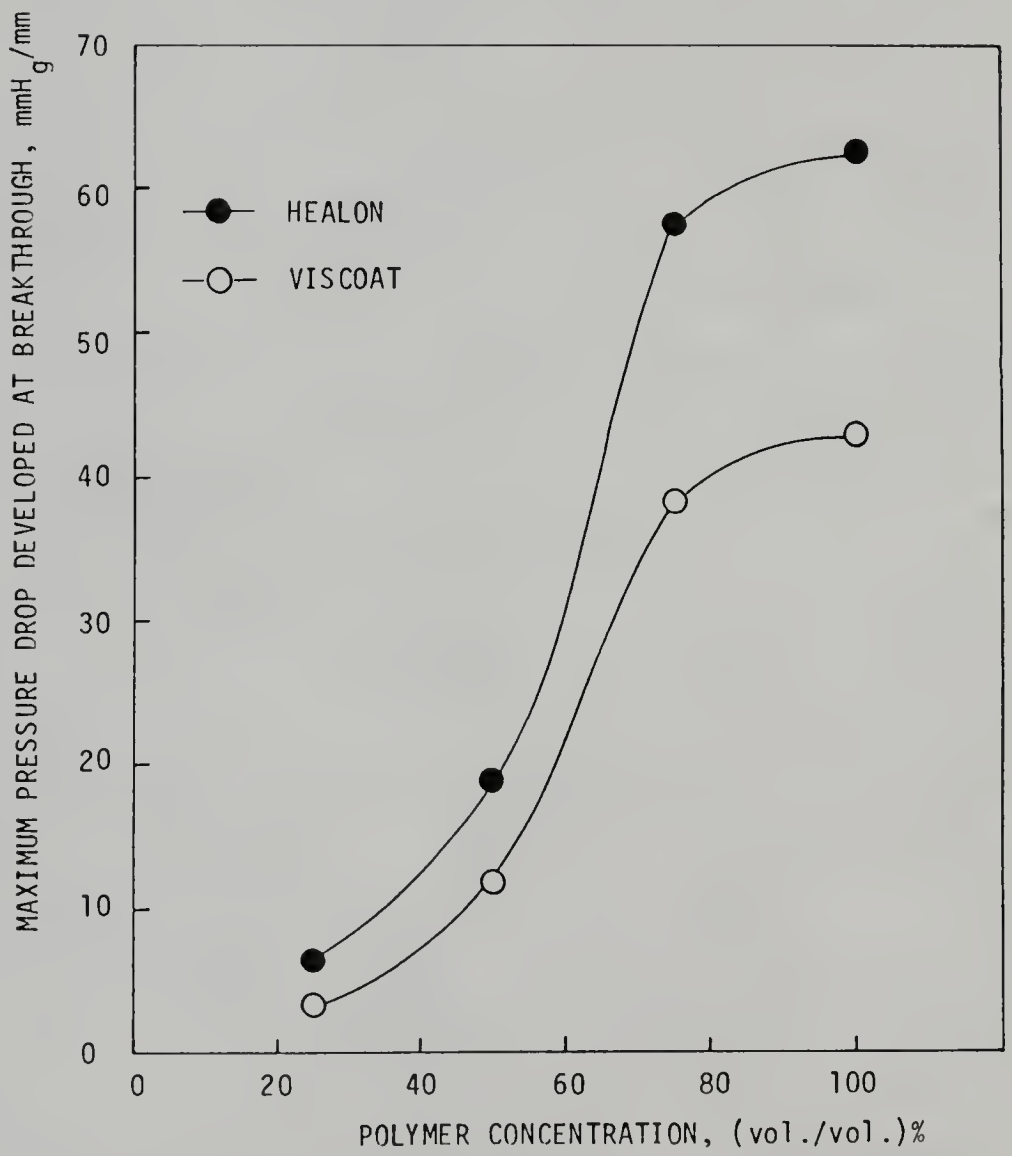

Figure 7.12. Effect of Polymer Concentration on the Maximum Pressure Drop Developed at Breakthrough.

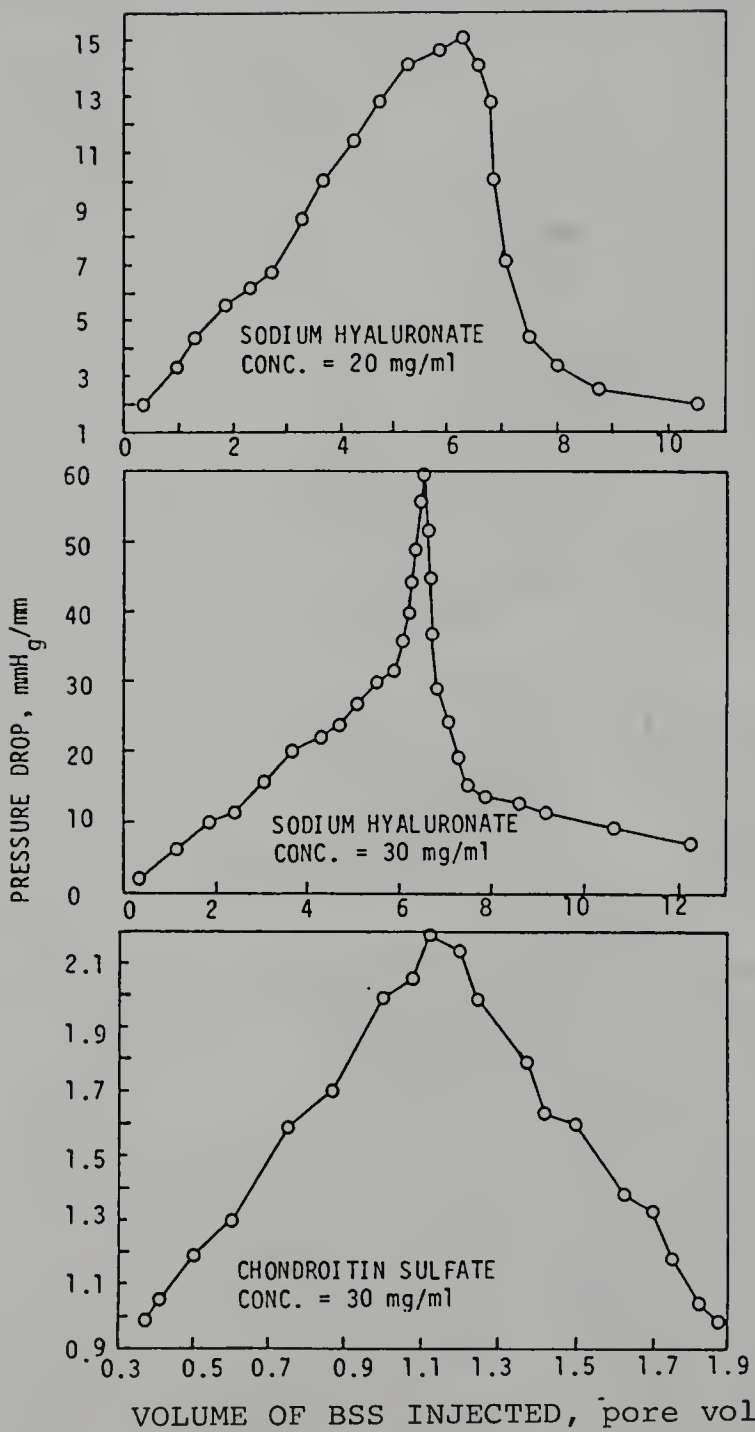

Figure 7.13. Pressure Drops of Sodium Hyaluronate and Chondroitin Sulfate as a Function of Balanced Salt Solution Injected into Porous Media.

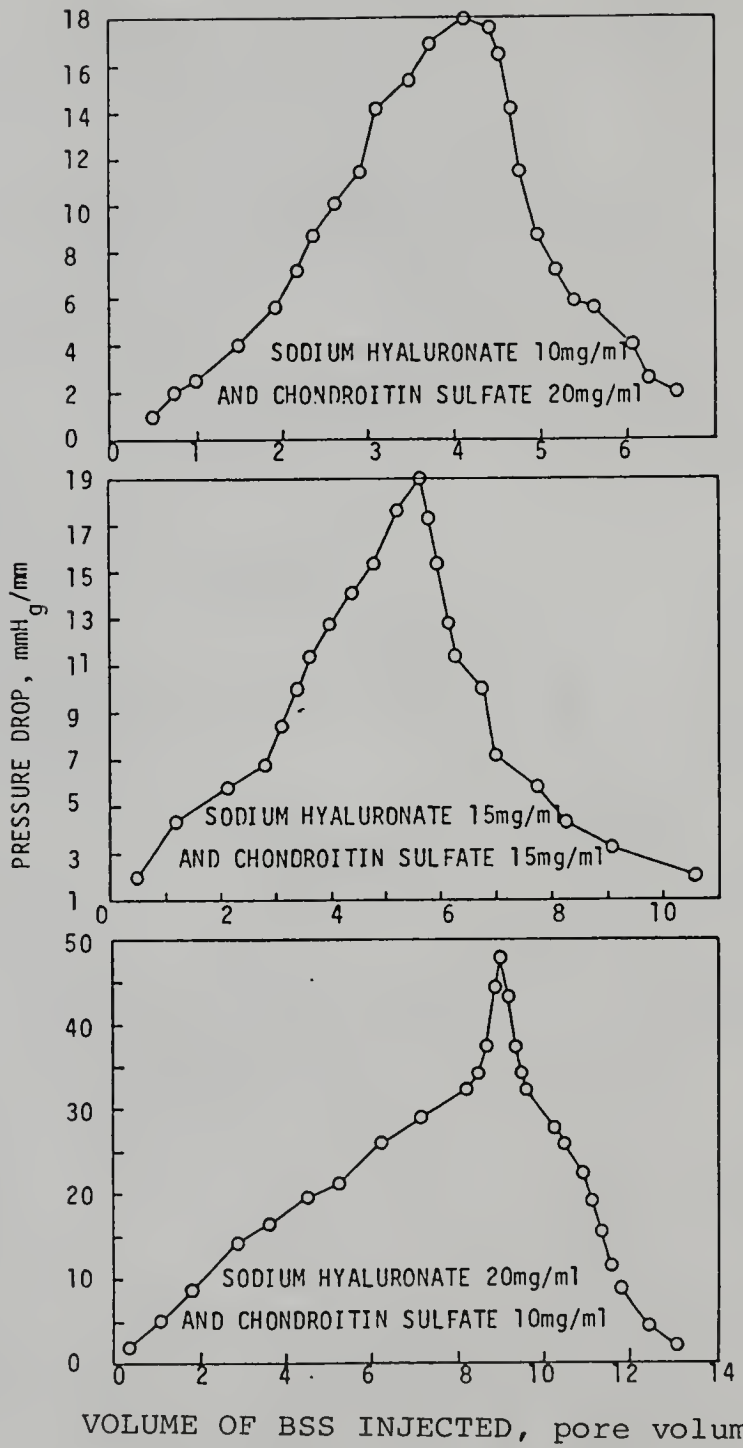

Figure 7.14. Effect of Interaction between Sodium Hyaluronate and Chondroitin Sulfate on Pressure Developed in Porous Media.

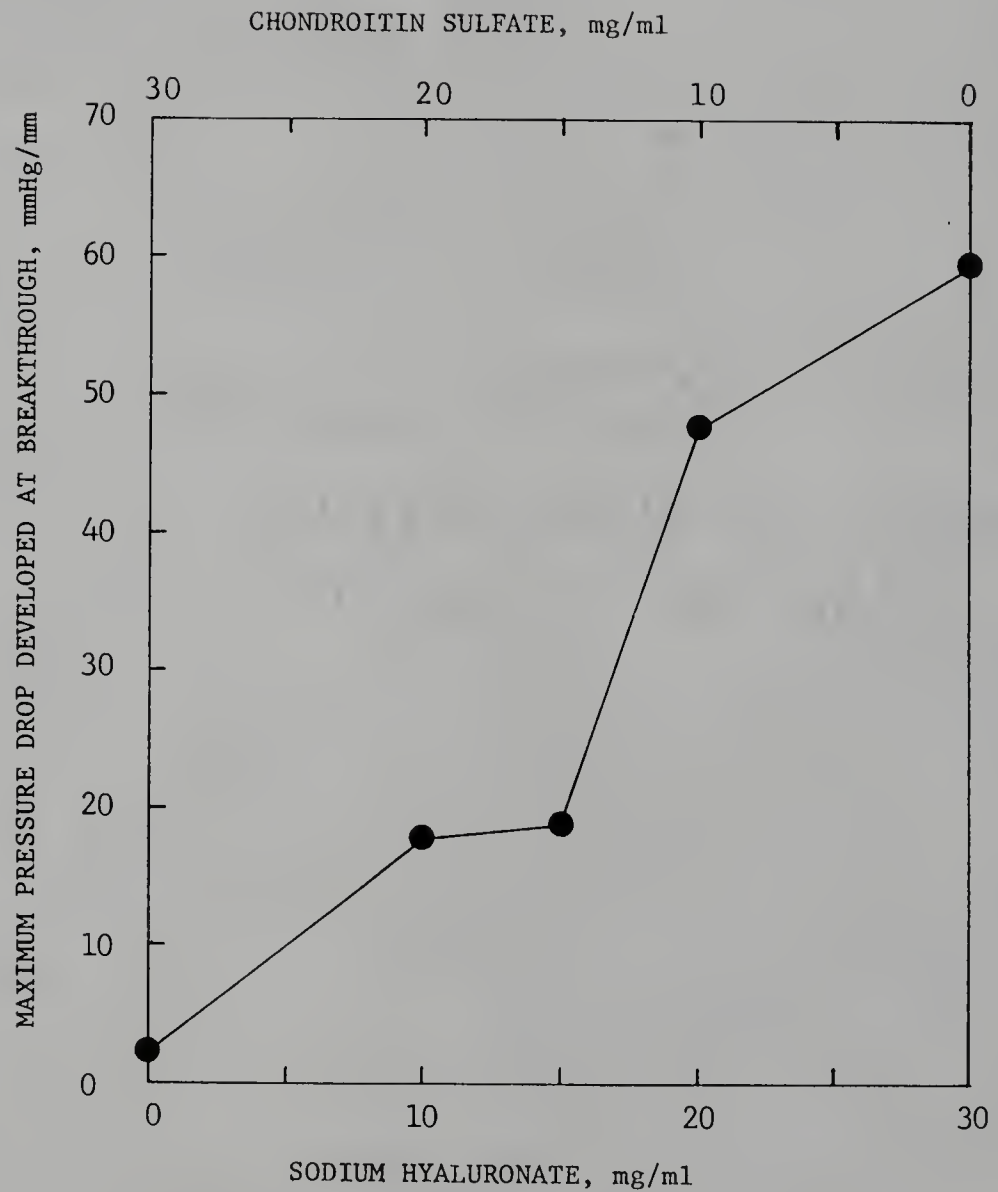

Figure 7.15. Effect of Interaction between Sodium Hyaluronate and Chondroitin Sulfate on the Maximum Pressure Drop Developed at Breakthrough.

concentration. A sharp increase in peak pressure is approximated at the concentration of 60% (vol./vol.) of sodium hyaluronate and 40% (vol./vol.) of chondroitin sulfate. Referring to Figures 7.14 and 7.15, the mixture of 60% (vol./vol.) sodium hyaluronate and 40% (vol./vol.) chondroitin sulfate produces a significant pressure drop compared to the polymer containing 60% (vol./vol.) sodium hyaluronate only. The high pressure drop is due to the large molecular weight and structure as well as the high viscosity resulted from a cross-linking interaction between the two polymers.

CHAPTER VIII

CONCLUSIONS AND RECOMMENDATIONS

8.1 Conclusions

In this study the specific interest was to investigate the surface properties of the foam and foam stability in relation to the foam behavior in porous media. Two mathematical models have been developed and can accurately describe the foam flow in porous media. A general solution of the Poisson-Boltzmann equation was obtained and used to predict the stability of foam bubbles. Interactions between similarly charged surfactant and polymer were studied. The effects of adding polymer on the foam properties were also discussed. Finally, two applications of fluid flow through porous media were reported. Based on the investigations conducted in the entire study, the conclusions are stated as follows:

1. With the exception of the rate of drainage, and bubble size distribution, the chain length compatibility affects the surface properties of the mixed foaming systems. All the changes in the surface properties with respect to the chain length compatibility are attributed to the thermal motion of the terminal

segment of the hydrocarbon chains. The exceptional cases can be explained by the surfactant molecules' packing pattern at the liquid/air interface, adsorption/desorption of the surfactant molecules at the interface, and the rheology of the liquid films.

2. The foam behavior in porous media was well correlated to the surface properties of the foaming agent without adding any alcohol. However, for the mixed foaming agents (e.g., SDS + C_nOH and Stepanflo 40 + C_nOH, n = 8, 10, 12, 14, and 16), there is no strong correlation between the foam behavior in porous media and the surface properties of the foaming agent measured outside porous media. But, the latter can elucidate tremendous useful information for the interpretation of the foam behavior in porous media. For a given mixed foaming agent, the fluid displacement depends on the stability of in-situ foam, the amount of in-situ foam generated, and the bubble size relative to the pore size.
3. The model of foam displacing fluid can accurately predict the system behavior of the fluid displacement by foam. It can also be used to predict the pressure distributions and velocity profiles for any foam flooding process if the average volume flow rate at the producing site is provided. The model of foam flow through porous media is useful when the foam is considered as a homogeneous fluid with constant

density and viscosity. It may be used to estimate the foam viscosity in porous media.

4. The foam stability is theoretically studied by employing the DLVO theory. A general numerical solution of the Poisson-Boltzmann equation is obtained. It is believed that the method used here is the most general approach so far. The results of this work can also be applied to predict the aggregation behavior of particles in liquid media. It has great potential in application of many products and processes such as pharmaceutical preparations, mineral flotation, paints, pigments, dyestuffs, drilling muds for oil, etc.
5. The improvement of surface activity of the anionic surfactant (e.g., SDS and Stepanflo 40) by adding the anionic polymer (e.g., xanthan) is mainly due to the effect of excluded polymer volume and electrical double layers. Foam stability and viscosity can be improved by adding a small amount of polymer. For a given foaming agent, there is an optimum polymer concentration such that the highest apparent foam viscosity and the minimum average bubble size are obtained.

8.2 Recommendations

8.2.1 Effect of Temperature

All the experiments mentioned in this study are carried out at room temperature. In practice, temperature is a very important factor which can change the foam properties, foam stability, and foam life. Therefore, the effects of temperature on the surface properties of foam, foam stability, fluid displacement efficiency, breakthrough time, etc., need to be systematically investigated in future work.

8.2.2 Mean Bubble Size in Porous Media

The ratio of the bubble size to the pore size plays an important role for the fluid displacement by foam in porous media. For a porous medium of a given permeability, it seems that there exists a specific mean bubble size corresponding to the maximum fluid displacement. In Chapter II, the mean bubble size was measured outside porous media, which was difficult to relate to the pore structures. More work is needed to correlate the mean bubble size of foam with the permeability of the porous media. The foam can be photographed after its passage through porous media and analyzed using a digital image analysis system. The results will be very helpful to explain the relationship between the foam properties and the foam behavior in porous media.

8.2.3 Rate of Loss of Interfacial Area

The rate of loss of interfacial area is a fundamentally significant parameter for the foam stability. It gives a measure of the ability of adsorption of the surfactant molecules at the liquid/gas interface. Since the reduction of surface area, consequent to rupture of the lamellae, requires that adsorbed surfactant molecules return to the bulk solution. A slower rate of loss of interfacial area corresponds to a higher foam stability. Ross [118] proposed an equation of state for a foam.

$$P_e V_f + (2/3)\gamma A = n_f RT \qquad (8.1)$$

where P_e = the pressure external to the foam

V_f = total foam volume

γ = the surface tension of the foam lamellae

A = total surface area of the liquid films in foam

n_f = the moles of gas in the foam

R = gas constant

T = absolute temperature of the foam

In differential form Equation (8.1) may be written

$$P_e dV_f + V_f dP_e + (2/3)\gamma dA = n_f R dT$$

For foam degradation at constant volume and temperature, we have

$$V_f dP_e + (2/3)\gamma dA = 0$$

or $$dA/dt = -(3/2)(V_f/\gamma)(dP_e/dt)$$

The measurement of the pressure change gives change of interfacial area. A preliminary experiment has been tested

in the laboratory. It was found that the system temperature must be strictly controlled because of the easily affected pressure. The change of pressure due to the foam degradation is very small, an accurate sensitive pressure transducer is required for the measurement. Since the rate of loss of interfacial area is a direct indicator of foam stability, the study would be very useful for the interpretation of foam stability.

8.2.4 Foam Compressibility

In the derivation of the mathematical model for foam flow through porous media, the equation of state of the foam is essential. For most purposes, the equation (e.g., Equation (4.3)) is expressed as a pressure-dependent density function. Usually, two constant parameters are needed for the equation and they are determined by experiment. Unfortunately, the parameters for the equation of state of the foam are not available in the literature because the foam itself has no unique composition and is affected by many factors. A systematic study on the foam compressibility, which is one of the most important but still mysterious properties of the foam, is definitely required. The effect of pressure on foam properties and elasticity of thin film can be revealed by this study. The results will give a clearer understanding of the foam compressibility and stability as well as provide a better description of the equation of state of foam. In

consequence, the mathematical models can be developed and used to simulate the foam behavior in a much more accurate way in porous media.

8.2.5 Applications of the DLVO Theory

In addition to the prediction of the foam stability, DLVO theory is a very powerful and useful tool for an insight into the factors involved in stable dispersions and aggregation of particles in liquid media. In Chapter V, we have developed a general numerical solution of the Poisson-Boltzmann equation. This solution requires experimental validation and theoretical polishing for numerical efficiency. Using quasi-elastic light scattering, electronic particle counters, microelectrophoresis apparatus, and a zetameter, we can study time-dependent particle size distributions, characterization of the particles, and the stability of particles in a liquid medium. In this context, the effects of temperature, ionic strength, the Hamaker constant, and the addition of polymers or surfactants should be investigated for various colloidal systems in future work.

APPENDIX A

Any point P in space (Figure 5.2) can be described by rectangular coordinates (x,y,z) or bispherical coordinates $(\eta,\theta,\varepsilon)$ and the transformation equations from one set of coordinates to the other are given by [97]

$$x = \frac{a\sin\theta\cos\varepsilon}{\cosh\eta-\cos\theta} \tag{A-1}$$

$$y = \frac{a\sin\theta\sin\varepsilon}{\cosh\eta-\cos\theta} \tag{A-2}$$

$$z = \frac{a\sinh\eta}{\cosh\eta-\cos\theta} \tag{A-3}$$

The scale factors, h_1, h_2, and h_3, for bispherical coordinates can be derived using the following formulas [119]

$$h_1 = \left[\left(\frac{\partial x}{\partial \eta}\right)^2 + \left(\frac{\partial y}{\partial \eta}\right)^2 + \left(\frac{\partial z}{\partial \eta}\right)^2\right]^{1/2} \tag{A-4}$$

$$h_2 = \left[\left(\frac{\partial x}{\partial \theta}\right)^2 + \left(\frac{\partial y}{\partial \theta}\right)^2 + \left(\frac{\partial z}{\partial \theta}\right)^2\right]^{1/2} \tag{A-5}$$

$$h_3 = \left[\left(\frac{\partial x}{\partial \varepsilon}\right)^2 + \left(\frac{\partial y}{\partial \varepsilon}\right)^2 + \left(\frac{\partial z}{\partial \varepsilon}\right)^2\right]^{1/2} \tag{A-6}$$

Substituting equations (A-1)-(A-3) into equations (A-4)-(A-6), we have

$$h_1 = \frac{a}{\cosh\eta - \cos\theta} \tag{A-7}$$

$$h_2 = \frac{a}{\cosh\eta - \cos\theta} \tag{A-8}$$

$$h_3 = \frac{a\sin\theta}{\cosh\eta - \cos\theta} \tag{A-9}$$

The Laplacian of Φ is given by [119]

$$\nabla^2\Phi = \frac{1}{h_1 h_2 h_3}\left[\frac{\partial}{\partial\eta}\left(\frac{h_2 h_3}{h_1}\frac{\partial\Phi}{\partial\eta}\right) + \frac{\partial}{\partial\theta}\left(\frac{h_1 h_3}{h_2}\frac{\partial\Phi}{\partial\theta}\right) + \frac{\partial}{\partial\varepsilon}\left(\frac{h_1 h_2}{h_3}\frac{\partial\Phi}{\partial\varepsilon}\right)\right] \tag{A-10}$$

Substituting for h_1, h_2, and h_3 in equation (A-10), we have

$$\nabla^2\Phi = \frac{(\cosh\eta-\cos\theta)^2}{a^2}\left[\frac{\partial^2\Phi}{\partial\eta^2} - \frac{\sinh\eta}{\cosh\eta-\cos\theta}\frac{\partial\Phi}{\partial\eta} + \frac{\partial^2\Phi}{\partial\theta^2} + \left(\cot\theta - \frac{\sin\theta}{\cosh\eta-\cos\theta}\right)\frac{\partial\Phi}{\partial\theta} + \frac{1}{\sin^2\theta}\frac{\partial^2\Phi}{\partial\varepsilon^2}\right] \tag{A-11}$$

From equation (5.6), the Poisson-Boltzmann equation in bispherical coordinates becomes

$$\frac{(\cosh\eta-\cos\theta)^2}{a^2}\left[\frac{\partial^2\Phi}{\partial\eta^2} - \frac{\sinh\eta}{\cosh\eta-\cos\theta}\frac{\partial\Phi}{\partial\eta} + \frac{\partial^2\Phi}{\partial\theta^2} + \left(\cot\theta - \frac{\sin\theta}{\cosh\eta-\cos\theta}\right)\frac{\partial\Phi}{\partial\theta} + \frac{1}{\sin^2\theta}\frac{\partial^2\Phi}{\partial\varepsilon^2}\right]$$

$$= -(e^2/DkT)\sum_i Z_i\left[n^+_{oi}\,\mathrm{EXP}(-Z_i\Phi) - n^-_{oi}\,\mathrm{EXP}(Z_i\Phi)\right]$$

APPENDIX B

From equations (A-1) and (A-3),

$$x(\cosh\eta-\cos\theta) = a\sin\theta\cos\varepsilon \tag{B-1}$$

$$z(\cosh\eta-\cos\theta) = a\sinh\eta \tag{B-2}$$

Equation (B-1) divided by equation (B-2) gives

$$\sin\theta = \frac{x}{z}\,\frac{\sinh\eta}{\cos\varepsilon} \tag{B-3}$$

From equation (B-2),

$$\cos\theta = \cosh\eta - \frac{a\sinh\eta}{z} \tag{B-4}$$

Since $\sin^2\theta + \cos^2\theta = 1$

$$\left(\frac{x}{z}\,\frac{\sinh\eta}{\cos\varepsilon}\right)^2 + \left(\cosh\eta - \frac{a\sinh\eta}{z}\right)^2 = 1 \tag{B-5}$$

Rearranging equation (B-5) and letting $\varepsilon = 0$, we have

$$\frac{x^2}{(a\,\mathrm{csch}\eta)^2} + \frac{(z - a\coth\eta)^2}{(a\,\mathrm{csch}\eta)^2} = 1 \tag{B-6}$$

Equation (B-6) represents a family of circles with center at $(0, a\coth\eta)$, the radii of the circles being $a\,\mathrm{csch}\eta$.

Referring to Figure 5.3 and equation (B-6), equations (5.13)-(5.15) can be easily obtained from geometry. Equations (5.16) and (5.18) are simply the definition of η in bispherical coordinates. Equations (5.17), (5.19), and (5.20) are straightforward relationships between sides and angles of a plane triangle.

REFERENCES

1. Marsden, S.S. and Khan, S.K., Soc. Pet. Eng. J., 17 (March 1966).

2. Sydney, R., Ind. Eng. Chem., 61, 10, 48(1969).

3. Lemlich, R., J. Colloid Int. Sci., 64, 107(1978).

4. Holcomb, D.L., Callaway, E., and Curry, L.L., Soc. Pet. Eng. J., 410(August 1981).

5. Chen, J.D., J. Colloid Int. Sci., 109, 341(1986).

6. Bernard, G.G., Holm, L.W., and Jacobs, W.L., Soc. Pet. Eng. J., 295(Dec. 1965).

7. Patton, J.T., Holbrook, S.T., and Hsu, W., Soc. Pet. Eng. J., 456(June 1983).

8. McEntee, W.R. and Mysels, K.J., J. Phy. Chem., 73, 9, 3018(1969).

9. Frankel, S. and Mysels, K.J., J. Phy. Chem., 73, 9, 3028(1969).

10. Sibree, T.O., Trans. Faraday Soc., 30, 325(1943).

11. Lemlech, R., Ind. Eng. Chem. Fundam., 17, 2, 89(1978).

12. Shaw, D.J., "Introduction to Colloid and Surface Chemistry," Butterworth Inc., Woburn, Massachusetts, 1970.

13. Brown, A.G., Thuman, W.C., and McBain, J.W., J. Colloid Sci., 8, 491(1953).

14. Bikerman, J.J., "Foam," Springer-Verlag, New York, 1973.

15. Miles, G.D., Ross, J., and Shedlovsky, L., J. Am. Oil Chemists Soc., 27, 268(1950).

16. Grundmann, S.R. and Ford, D.L., J. Pet. Tech., 597 (March 1983).

17. Blauer, R.E. and Kohlhaas, C.A., paper SPE 5003 presented at the 1974 SPE Annual Meeting, Houston, Oct. 6-9, 1974.

18. Holcomb, D.L., Drilling, 47(Jan. 1982).

19. Montman, R., World Oil, 171(June 1982).

20. Warnock, W.E., Harris, P.C., and King, D.S., J. Pet. Tech., 80(Jan. 1985).

21. Sharma, M.K., Shah, D.O., and Brigham, W.E., paper SPE 10612 presented at the 1982 SPE Sixth International Symposium on Oilfield and Geothermal Chemistry, Dallas, Texas, Jan. 25-27, 1982.

22. Helfferich, F.G., Soc. Pet. Eng. J., 51(Feb. 1981).

23. Mattax, C.C. and Kyte, J.R., Oil and Gas J., 115 (Oct. 1961).

24. Roof, J.G., Soc. Pet. Eng. J., 85(1970).

25. Eakin, J.L. and Eckard, W.E., Pet. Eng., 71(July 1966).

26. Mast, R.F., paper SPE 3997 presented at SPE-AIME 47th Annual Fall Meeting, San Antonio, Texas, Oct. 8-11, 1972.

27. Minssieux, L., J. Pet. Tech., 100(Jan. 1974).

28. Slattery, J.C., AIChE J., 25, 2, 283(1979).

29. Shelton, J.L. and Yarborough, L., J. Pet. Tech., 1171(Sept. 1977).

30. Dilgren, R.E., Deemer, A.R., and Owens, K.B., paper SPE 10774 presented at the Regional Meeting of the SPE held in San Francisco, California, March 24-26, 1982.

31. Raza, S.H., Soc. Pet. Eng. J., 328(Dec. 1970).

32. Sharma, M.K., Shah, D.O., and Brigham, W.E., Ind. Eng. Chem. Fundam., 23, 2, 213(1984).

33. Sharma, M.K., Shah, D.O., and Brigham, W.E., SPE Reservoir Engineering, 253(May 1986).

34. Goddard, E.D. and Hannan, R.B., J. Colloid Int. Sci., 55, 73(1976).

35. Barkin, S., Frank, H.P., and Eirich, F.R., J. Phys. Chem., 61, 1357(1957).

36. Saito, S., J. Colloid Int. Sci., 15, 283(1960).

37. Maruta, I., J. Chem. Soc. Japan, 83, 782(1962).

38. Jones, M.N., J. Colloid Sci., 23, 36(1967).

39. Botre, C., DeMartiis, F., and Solinas, M., J. Phys. Chem., 68, 3624(1964).

40. Desai, N., Ph.D. Dissertation, University of Florida, Gainesville, Florida, 1983.

41. Huang, D.D., Nikolov, A., and Wasan, D.T., Langmuir, 2, 5, 672(1986).

42. Mark, H.F., Othmer, D.F., Overberger, C.G., Seaborg, G.T., and Grayson, M.,"Encyclopedia of Chemical Technology," 3rd edition, Vol. 11, 127, 1982.

43. Shick, M.J. and Fowkes, F.M., J. Phys. Chem., 61, 1062(1957).

44. Klevens, H.B., J. Am. Oil Chem. Soc., 30, 74(1953).

45. Vold, R.D. and Vold, M.J., "Colloid and Interface Chemistry," Addison-Wesley Publishing Company, Inc., Reading, Massachusetts, 1983.

46. Shiao, S.Y., Ph.D. Dissertation, University of Florida, Gainesville, Florida, 1976.

47. Wilhelmy, L., Ann. Physik, 119, 117(1863).

48. Osipow, L.I., "Surface Chemistry: Theory and Industrial Application," R.E. Krieger Publishers, Huntington, New York, 1977.

49. Shah, D.O., J. Colloid Sci., 32, 570(1970).

50. Shah, D.O., J. Colloid Sci., 37, 744(1971).

51. Bikerman, J.J., Discussion in Proc. Intern. Congr. Surface Activity 2nd, London, 2, 254(1957).

52. Weast, R.C., "CRC Handbook of Chemistry and Physics," 63rd edition, The Chemical Rubber Co., Cleveland, Ohio, 1983.

53. Raza, S.H. and Marsden, S.S., Soc. Pet. Eng. J., 359 (Dec. 1967).

54. Miller, C.A. and Neogi, P., "Interfacial Phenomena: Equilibrium and Dynamic Effects," Marcel Dekker, Inc., New York, 1985.

55. Latil, M., Bardon, C., Burger, J., and Sourieau, P., "Enhanced Oil Recovery," Gulf Publishing Company, Houston, Texas, 1980.

56. Patton, J.T., Watts, R., Belkin, H., Holbrook, S., and Kuntamukkula, M., "Enhanced Oil Recovery CO_2 Foam Flooding," First Annual Report for Department of Energy, New Mexico University, Las Cruces, New Mexico, 1979.

57. Bird, R.B., Stewart, W.E., and Lightfoot, E.N., "Transport Phenomena," John Wiley and Sons, Inc., New York, 1960.

58. Princen, H.M., J. Colloid Int. Sci., 91, 160(1983).

59. Davies, J.T. and Rideal, E.K., "Interfacial Phenomena," Academic Press, New York, 1963.

60. Monsalve, A. and Schecter, R.S., J. colloid Int. Sci., 97, 327(1984).

61. Holcomb, D.L., paper SPE 9033 presented at the SPE Rocky Moutain Regional Meeting, Casper, Wyoming, May 14-16, 1980.

62. Holbrook, S.T., John, T.P., and Hsu, W., paper SPE/DOE 9809 presented at the 1981 SPE/DOE Second Joint Symposium on Enhanced Oil Recovery of the Soc. of Pet. Eng., Tulsa, Oklahoma, April 5-8, 1981.

63. Holm, L.W., Soc. Pet. Eng. J., 359(Dec. 1968).

64. Albrecht, R.A. and Marsden, S.S., Soc. Pet. Eng. J., 51(March 1970).

65. Fried, A.N., U.S. Bureau of Mines, R.I. 5866, 1961.

66. David, A. and Marsden, S.S., paper SPE 2544 presented at the 44th Annual Fall Meeting of Soc. of Pet. Eng. of AIME, Denver, Co., Sept. 28 - Oct. 1, 1969.

67. Egbogah, E.O. and Dawe, R.A., Bulletin of Canadian Petroleum Geology, 28, 2(June 1980).

68. Sharma, S.K., M.S. Report, Stanford University, Stanford, California, Dec. 1965.

69. Bonnet, J., Ph.D. Dissertation, Toulouse University, Toulouse, France, 1978.

70. Owete, S.O., Ph.D. Dissertation, Stanford University, Stanford, California, 1982.

71. Chiang, M.Y., personal communication, Stepan Company, Northfield, Illinois.

72. Malmberg, W.E. and Burtch, W.F., "Large-scale Samples of Sulfonates for Laboratory Studies in Tertiary Oil Recovery, Preparation and Related Studies," Final Report, FE-2605-20, prepared for the US Department of Energy, May, 1979.

73. Shah, D.O. and Shiao, S.Y., "Chain Length Compatibility and Molecular Area in Mixed Monolayers," Advances in Chemistry Series, 144, 153(1975).

74. Shah, D.O. and Dysleski, C.A., J. Am. Oil Chem. Soc., 46, 645(1969).

75. Sharma, M.K., Shah, D.O., and Brigham, W.E., AIChE J., 31, 2, 222(1985).

76. Ling, T.F. and Shah, D.O., paper presented at 6th International Symposium on Surfactants in Solutions, New Delhi, India, August 18-22, 1986.

77. Hirasaki, G.J. and Lawson, J.B., Soc. Pet. Eng. J., 176(April 1985).

78. Moroi, Y., Motomura, K., and Matuura, R., Bulletin of the Chem. Soc. of Japan, 44, 2078(1971).

79. Sharma, M.K., Ling, T.F., and Shah, D.O., paper presented at the 1984 SPE Forum on Foams, Jackson Hole, Wyoming, August 12-17, 1984.

80. Nahid, B.H., Ph.D. Dissertation, University of Southern California, Los Angelas, California, 1971.

81. Bernard, G.G. and Holm, L.W., Soc. pet. Eng. J., 267(Sept. 1964).

82. Craft, B.C. and Hawkins, M.F., "Applied Petroleum Reservoir Engineering," Prentice-Hall, Inc., Englewood Cliffs, New Jersey, 1959.

83. Dietz, D.N., Bruining, J., and Heijna, H.B., J. Pet. Tech., 921(May 1985).

84. Owete, S.O. and Shah, D.O., paper presented at ACS 42nd Annual Southwest Regional Meeting, Houston, Texas, Nov. 19-21, 1986.

85. Marle, C.M., "Multiphase Flow in Porous Media," Gulf Publishing Company, Houston, Texas, 1981.

86. Bretherton, F.P., J. Fluid Mech., 166(1961).

87. Brinkman, H.C., Appl. Sci. Research, A1, 27, 81(1947).

88. Derjaguin, B.V. and Landau, L.D., Zh. Eksp. Teor. Fiz., 15, 662(1945).

89. Verwey, E.J.W. and Overbeek, J.Th.G., "Theory of Stability of Lyophobic Colloid," Elsevier, New York, 1948.

90. Hamaker, H.C., Physica, 4, 1058(1937).

91. Derjaguin, B.V., Discuss. Faraday Soc., 18, 85(1954).

92. Langmuir, I., J. Chem. Phys., 6, 873(1938).

93. Bell, G.M., Levine, S., and McCartney, L.N., J. Colloid Int. Sci., 33, 335(1970).

94. McCartney, L.N. and Levine, S., J. Colloid Int. Sci., 30, 345(1969).

95. Hogg, R., Healy, T.W., and Fuerstenau, D.W., Trans. Faraday Soc., 62, 1638(1966).

96. Ring, T.A., J. Chem. Soc., Faraday Trans., 2, 78, 1513(1982).

97. Morse, P.M. and Feshback, H., "Methods of Theoretical Physics," McGraw-Hill, New York, 1953.

98. Hornbeck, R.W., "Numerical Methods," Quantum Publishers, Inc., New York, 1975.

99. Carnahan, B., Luther, H.A., and Wilkes, J.O., "Applied Numerical Methods," John Wiley & Sons, Inc., New York, 1969.

100. Anderson, D.A., Tannchil, J.C., and Pletcher, R.H., "Computational Fluid Mechanics and Heat Transfer," McGraw-Hill, New York, 1984.

101. Shih, T.I-P., Class Notes from EML 5710, Fall 1986, Mechanical Engineering Department, University of Florida, Gainesville, Florida.

102. Philips, J.C., Miller, J.W., Wernau, W.C., Tate, B.E., and Auerbach, M.H., paper SPE 10617 presented at the SPE 6th International Symposium on Oilfield and Geothermal Chemistry, Dallas, Texas, January 25-27, 1982.

103. Philips, J.C., Miller, J.W., Wernau, W.C., Tate, B.E., and Auerbach, M.H., Soc. Pet. Eng. J., 594(August 1985).

104. Fishman, M.L. and Eirich, F.R., J. Phys. Chem., 75, 3135(1971).

105. Schwuger, M.J., J. Colloid Int. Sci., 43, 491(1973).

106. Lee, H.K., personal communication, Chemical Engineering Department, University of Florida, Gainesville, Florida.

107. Tabor, J.J., "Research on Enhanced Oil Recovery: Past, Present, and Future" in Surface Phenomena in Enhanced Oil Recovery, p.13-53, ed. by D.O. Shah, Plenum Publication Co., New York, 1981.

108. Foster, W.R., J. Pet. Tech., 205(Feb. 1973).

109. Bansal, V.K. and Shah, D.O., in Micellization, Solubilization, and Microemulsions, Vol. I, p.87-113, ed. by K.L. Mittal, Plenum Press, New York, 1977.

110. Sharma, M.K. and Shah, D.O., J. Am. Oil Chem. Soc., 61, 3, 585(1984).

111. Ling, T.F., Lee, H.K., and Shah, D.O., paper presented at ACS 42nd Annual Southwest Regional Meeting, Houston, Texas, Nov. 19-21, 1986.

112. Ling, T.F., Lee, H.K., and Shah, D.O., "Surfactants in Enhanced Oil Recovery" in Industrial Applications of Surfactants, p.126-178, ed. by D.R. Karsa, Royal Society of Chemistry, Burlington House, London W1VOBN.

113. Lee, H.K. and Shah, D.O., paper presented at 6th International Symposium on Surfactants in Solution, New Delhi, India, August 18-22, 1986.

114. Product Monograph: Viscoat from Cilco, Cilco, Inc., 1616 13th Avenue, Huntington, West Virginia.

115. Lang, E., Mark, D., Miller, F.A., Miller, D., and Wik, O., Arch Ophthalmol, 102, 1079(1984).

116. Barron, B.A., Busin, M., Page, C., Bergsma, D.R., and Kaufman, H.E., Am. J. Ophthalmology, 100, 377(1985).

117. Hoopes, P.C., AM Intra-Ocular Implant Soc. J., 8, 148(1982).

118. Ross, S., Ind. Eng. Chem., 61, 48(1969).

119. Spiegel, M.R., "Mathematical Handbook of Formulas and Tables," Schaum's Outline Series, McGraw-Hill Book Company, New York, 1968.

BIOGRAPHICAL SKETCH

Tien-Feng Tyrone Ling was born in 1954 in Kungshan, Taiwan, Republic of China. He attended Kungshan Elementary and Kungshan Junior and Senior High Schools in Taiwan. He received his B.S. degree in chemical engineering from National Central University, Taiwan, Republic of China, in July 1977. After serving in the Chinese Army for two years, he worked for one year as a teaching assistant in the Chemical Engineering Department of the National Central University. In August 1980, he came to the United States and joined the University of Alabama where he received his M.S. degree in chemical engineering. He then transferred to the University of Florida to pursue a Doctor of Philosophy degree in chemical engineering.

He married Miss Ling-Jean Chang on January 1, 1983 and they have one child, Vincent, born on January 12, 1987. He is a member of Tau Beta Pi, Omega Chi Epsilon, Phi Tau Phi, A.I.Ch.E., the American Chemical Society, the American Institute of Chemists, and the Society of Petroleum Engineers.

I certify that I have read this study and that in my opinion it conforms to acceptable standards of scholarly presentation and is fully adequate, in scope and quality, as a dissertation for the degree of Doctor of Philosophy.

Dinesh O. Shah, Chairman
Professor of Chemical Engineering

I certify that I have read this study and that in my opinion it conforms to acceptable standards of scholarly presentation and is fully adequate, in scope and quality, as a dissertation for the degree of Doctor of Philosophy.

Birdwell Finlayson
Professor of Surgery

I certify that I have read this study and that in my opinion it conforms to acceptable standards of scholarly presentation and is fully adequate, in scope and quality, as a dissertation for the degree of Doctor of Philosophy.

Gerald B. Westermann-Clark
Associate Professor of
Chemical Engineering

I certify that I have read this study and that in my opinion it conforms to acceptable standards of scholarly presentation and is fully adequate, in scope and quality, as a dissertation for the degree of Doctor of Philosophy.

Ranganatha Narayanan
Associate Professor of
Chemical Engineering

I certify that I have read this study and that in my opinion it conforms to acceptable standards of scholarly presentation and is fully adequate, in scope and quality, as a dissertation for the degree of Doctor of Philosophy.

John P. O'Connell
Professor of Chemical Engineering

I certify that I have read this study and that in my opinion it conforms to acceptable standards of scholarly presentation and is fully adequate, in scope and quality, as a dissertation for the degree of Doctor of Philosophy.

Gerasimos K. Lyberatos
Assistant Professor of
Chemical Engineering

I certify that I have read this study and that in my opinion it conforms to acceptable standards of scholarly presentation and is fully adequate, in scope and quality, as a dissertation for the degree of Doctor of Philosophy.

Brij M. Moudgil
Professor of Materials Science
and Engineering

This dissertation was submitted to the Graduate Faculty of the College of Engineering and to the Graduate School and was accepted as partial fulfillment of the requirements for the degree of Doctor of Philosophy.

December 1987

Dean, College of Engineering

Dean, Graduate School